To the Graduate Council:

I am submitting herewith a thesis written by Brittany Allison Davis entitled "Tectonic evolution of the southern Appalachian Inner Piedmont: Identification and interpretation of crustal features from aeromagnetic data and detailed geologic mapping in central Georgia." I have examined the final electronic copy of this thesis for form and content and recommend that it be accepted in partial fulfillment of the requirements for the degree of Master of Science, with a major in Geology.

Robert D. Hatcher, Jr., Major Professor

We have read this thesis
and recommend its acceptance:

Theodore C. Labotka

Micah J. Jessup

Accepted for the Council:

Carolyn R. Hodges
Vice Provost and Dean of the Graduate School

(Original signatures are on file with official student records.)

Tectonic evolution of the southern Appalachian Inner Piedmont: Identification and interpretation of crustal features from aeromagnetic data and detailed geologic mapping in central Georgia

A Thesis
Presented for the
Master of Science Degree
University of Tennessee, Knoxville

Brittany Allison Davis
May 2010

DEDICATION

This thesis is dedicated in loving memory of
Helen McMillian and Missy ma'loo

ACKNOWLEDGMENTS

A great thanks to my advisor and mentor Robert D. Hatcher, Jr. for having infinite patience and endless encouragement, while attempting to unlearn me of my bad writing habits, spending many times trucking through the wilderness of central Georgia during mid-summer heat, and constantly making me think critically. I am truly a good geologic mapper, and would not have been able to call myself so without the guidance from Dr. Hatcher. Special thanks to my committee: Dr. Ted Labotka, thank you for taking the time to walk me through things I should already know, and being the metamorphic petrology cherpa; Dr. Micah Jessup, thanks for taking the time to discuss Himalayan geology with me on occasion. Dr. Hap McSween, although you weren't on my committee, I greatly appreciate your help in understanding granitoid geochemistry. Dr. Linda Kah, thank you for always being a friend and mentor; our conversations are priceless. Dr. Greg Baker, thanks for buying my dad's boat and getting some use out of it, I hope it lasts you for years to come! Nancy Meadows, I can't thank you enough for listening to me complain and whine, even when you had problems of your own, and for taking the time to read many of my papers. Chocolate on Nancy's desk…. thank you, that is all. Also, a great thanks to Dr. Alan Patchen for performing the microprobe analysis for my metamorphism chapter. I would also like to thank Ralph Crawford (Geologic Mapping Institute) and John Costello (Georgia Geologic Mapping Program) for taking time out of their lives to participate in my field review. I am also thankful for the grant from the EDMAP component of the National Cooperative Geologic Mapping Program awarded by the U. S. Geological Survey, the University of Tennessee-Knoxville Office of Research (Dr. Greg Reed, Director), and the UTK Science Alliance Center of Excellence, for funding this research. I would also like to thank Bob Hatcher again for the Swingle Award and all of the people that made donations to it. That got me through some rough times!

The Hatchery: Arthur, you are an amazing and wonderful person, and I wouldn't have been able to get through this mess without you: your words were always encouraging and your help was invaluable; Mary and Heather, you two are my best friends, and I'm glad I could be so lucky to have two people to be crazy with. I am no longer ashamed of my weird factor; Matt, you

were a great field partner, keep up the hard work; Phillip, William, and Chris, thank you guys for being your silly selves. Andrew Wunderlich, you are the GIS guru, and there is no way I would have been able to compile my map in GIS without your help. Also, thanks for always taking a second glance at my posters and finding all those tiny mistakes that drive you mad. You are the best at your job, and a funny guy to boot! Everyone else in the department, thank you for words of encouragement and fun times at GSA!

My family, there are no words to express how much my family has helped through grad school. I love you all more than the world itself. At the lowest and greatest times in my life you have been there for me, and never judged. Mom, you are the most kind and considerate woman on the face of this Earth. Dad, you are probably the goofiest one, but that's why I love you. My father is responsible for my love of rocks, blame everything on him. Jennifer, I love you sister. Mamaw and Papaw Davis, I'm so lucky to have you both, a girl couldn't ask for better grandparents. Mamaw and Papaw McMillian, I wish you were here, and yes I'm still your "doll" Papaw! Chuck Beckman, I love you and look forward to our Jamaican wedding! Thanks for going mapping with me all of those times.

ABSTRACT

The Inner Piedmont (IP) is the Neoacadian migmatitic orogenic core of the southern Appalachians, exhibiting the widest area of high-grade metamorphism; regional upper amphibolite facies with isolated pods of granulite grade metamorphism. Peak P-T conditions in central GA reached 4.0-7.6 kbars and 630-715˚C. The Brindle Creek fault (BCf) separates high-grade metasedimentary rocks of the eastern Tugaloo terrane (Tt) and Cat Square terrane (CSt). The Tt consists of the Neoproterozoic to early Paleozoic(?) Tallulah Falls Formation, Chauga River Formation, and the Mid-Ordovician Poor Mountain Formation, intruded by Early to Middle Ordovician granitoids. The CSt consists of Siluro-Devonian metasedimentary rocks, such as sillimanite-schist, biotite gneiss, amphibolite, and minor calc-silicate, intruded by Acadian-Neoacadian plutons.

Original termination of the CSt was mapped by the USGS just south of Athens, GA, against the central Piedmont suture; however, new evidence from aeromagnetic anomalies and detailed geologic mapping revealed that the CSt and BCf extend into central GA. The BCf truncates a suite of curved magnetic anomalies on the aeromagnetic map. The curved anomalies that truncate against the linear feature may represent the Neoacadian deflection of the IP southwestward along the crustally weak Brevard fault zone. Another prominent lineament was identified southeast of the BCf; detailed geologic mapping revealed an additional thrust sheet in the CSt.

Mesozoic brittle reactivation of the late Paleozoic dextral Towaliga fault was also identified striking NE-SW through the field area. Multiple episodes of movement were observed in outcrop and at the micro-scale, defined by crosscutting fracture sets. Low temperature quartz mylonite (350-450˚C) may signify continued shearing of the IP into the late Alleghanian orogeny.

A felsic plutonic suite extends the length of the field area, consisting of three distinct granitoids: (1) an older biotite-rich megacrystic granite with megacrysts of K-feldspar; (2) a weakly foliated medium to coarse grained inequigranular granodiorite; and (3) a younger non-foliated fine-grained granodiorite. Analysis revealed that granitoids from central GA are similar texturally and petrographically with granitoids from NC's CSt. Further whole-rock geochemical

analysis revealed that these rocks share similar REE, trace element, and tectonic discriminate patterns. The most important point garnered from the trace element and REE patterns in spider diagrams, such as similarities in peaks and troughs, is that they must share either a common parent, process, or contaminant.

Table of Contents

Chapter 1: Inner Piedmont Overview 1

Introduction 1

Objectives 4

Location 4

Previous Work 6

Methodology 6

Geologic Background 7

Stratigraphy 8

Metamorphism 9

Structure 10

Chapter 2: Rock Units 14

Introduction 14

Western Inner Piedmont – Eastern Tugaloo terrane 14

Lower Metagraywacke-Schist-Amphibolite Member 19

Eastern Inner Piedmont – Cat Square terrane 19

Metasedimentary Rocks 23

Sillimanite Schist (metapelite) 23

Metagraywacke (metapsammite) 26

Calc-Silicate 30

Metaigneous Rocks 34

Murder Creek Granite 34

Dow's Pulpit granodiorite 41

Rocky Creek granodiorite 43

Cat Square terrane amphibolite 47

Mesozoic Rocks 50

Siliceous Cataclasite 50

Diabase Dikes 50

Chapter 3: Metamorphism 56

Introduction 56

Regional Metamorphism 56
Timing 57
Migmatization 60
Methodology 60
Pelitic Schist 63
Petrogenesis of Assemblages A1, A2, and A3 63
Retrograde metamorphism 65
Zoned Minerals and Diffusion 67
Sample Description 72
F-1236 metagraywacke sample 72
F-1296-amphibolite sample 76
Synthesis and Discussion 76
P-T Paths 83
Conceptual Model 86
Chapter 4: Geochemistry of the Murder Creek granite and Rocky Creek granodiorite, and similarities with other Inner Piedmont granitoids 88
Introduction 88
Sample Collection and Methods 89
Sample Selection 89
Methods 89
Sample description and petrology 93
Granitoid Geochemistry 93
Harker variation diagrams 93
Trace element geochemistry 99
REE geochemistry 100
Tectonic discrimination diagrams 100
Synthesis and Conclusions 104
Chapter 5: Central Georgia Inner Piedmont Kinematics and Structure 108
Introduction 108
Methods 111

Aeromagnetic Data 114
D_1 Deformation 114
D_2 Deformation 116
Foliation 116
Lineations 120
Folds 120
Faults 124
D_3 Deformation 127
D_4 and D_5 Deformation 127
D_5 and D_6 Brittle Deformation 127
Low Temperature Quartz Mylonite 131
Central Piedmont Map Patterns and Farrar and Mansfield Cross Sections 131
Cross Section A-A' 133
Cross Section B-B' 133
Cross Section C-C' 133
Inner Piedmont Tectonic Models and Deformation Synthesis 134
Origins and Evolution of the Cat Square Terrane 138
Chapter 6: Conclusions 140
REFERENCES CITED 142
APPENDICES 158
VITA 222

LIST OF FIGURES

Chapter 1

Figure 1-1. Simplified tectonic map of the southern Appalachians 2
Figure 1-2. Location map. 5
Figure 1-3. Crustal flow in the Inner Piedmont 12

Chapter 2

Figure 2-1. Simplified geologic map of portions of the Farrar and Mansfield 7.5 minute quadrangles. 16
Figure 2-2. Locations of samples collected for detailed petrographic analysis. 17
Figure 2-3. Tallulah Falls Formation. 18
Figure 2-4. Tallulah Falls Formation lower metagraywacke-schist-amphibolite member. 20
Figure 2-5. Simplified tectonic map of part of the Tugaloo and adjacent terranes. 21
Figure 2-6. Photomicrographs of quartz mylonite. 24
Figure 2-7. Saprolite outcrop of sillimanite schist. 25
Figure 2-8. Outcrop of sillimanite schist. 27
Figure 2-9. Photomicrographs of sillimanite schist. 29
Figure 2-10. Saprolite outcrop of metagraywacke. 31
Figure 2-11. QFM diagram comparing compositions of the metasedimentary rocks in the Cat Square terrane. 32
Figure 2-12. Crosscutting relationships of granitoids. 35
Figure 2-13. Pavement outcrop of Murder Creek granite. 36
Figure 2-14. Photomicrographs of Murder Creek granite. 39
Figure 2-15. Saprolite outcrop of Murder Creek granite. 40
Figure 2-16. Dow's Pulpit. 42
Figure 2-17. Photomicrographs of Dow's Pulpit granodiorite. 44
Figure 2-18. IUGS classification of Murder Creek, Dow's Pulpit, and Rocky Creek granitoids. 45
Figure 2-19. Hand sample and outcrop of Rocky Creek granodiorite. 46
Figure 2-20. Photomicrographs of Rocky Creek granodiorite. 48
Figure 2-21. Amphibolite boudins. 49
Figure 2-22. Photomicrographs of hangingwall amphibolites. 52
Figure 2-23. Outcrop and photomicrographs of siliceous cataclasite. 53
Figure 2-24. Diabase photomicrograph and hand sample. 54

Chapter 3

Figure 3-1. Metamorphic isograd map of the southern Appalachian Blue Ridge and Inner Piedmont. 58
Figure 3-2. Simplified geologic map of portions of the 7.5-minute Farrar and Mansfield quadrangles and locations of pelitic schist petrographically analyzed, along with amphibolite and biotite gneiss sample used in electron microprobe analysis. 61
Figure 3-3. Photomicrographs of a sillimanite fish and rotated garnets. 66

Figure 3-4. Retrograde fabrics in sillimanite schist. 68
Figure 3-5. Development of diffusion zoning in garnets with increasing metamorphic grade. 69
Figure 3-6. Garnet zoning profile of sample F-1236: garnet D. 73
Figure 3-7. X-ray maps of Fe, Mg, Ca, and Mn illustrating garnet zoning patterns in garnet B of sample F-1296. 74
Figure 3-8. Garnet zoning profile of sample F-1236: garnet C. 75
Figure 3-9. X-ray maps of Fe, Mg, Ca. and Mn illustrating garnet zoning patterns of garnet B in sample F-1296. 77
Figure 3-10. X-ray maps of Fe, Mg, Ca, and Mn illustrating garnet zoning patterns of garnet C in sample F-1296. 78
Figure 3-11. Garnet zoning profile of sample F-1296: garnet E. 79
Figure 3-12. Garnet zoning profile of sample F-1296: garnet D. 80
Figure 3-13. Peak temperature and pressure for sample F-1236. 81
Figure 3-14. Peak temperature and pressure estimates for sample F-1296. 82
Figure 3-15. Projected P-T path of Farrar and Stewart quadrangles biotite gneiss and amphibolite. 84
Figure 3-16. Retrograde, prograde, and peak metamorphic conditions based on rock assemblage and overprinting relationships. 85
Figure 3-17. Tectonothermal timeline for the Inner Piedmont. 87

Chapter 4

Figure 4-1. Simplified geologic map of the Farrar and Mansfield 7.5-minute quadrangles with locations of samples geochemically analyzed. 90
Figure 4-2. Normative-feldspar classification of Farrar quadrangle granitoids. 95
Figure 4-3. Shand's Index showing both the Rocky Creek granodiorite and Murder Creek granite. 96
Figure 4-4. Harker variation diagram for Cat Square terrane granites. 97
Figure 4-5. TiO_2 variation diagrams of Cat Square terrane granitoids from previous studies and this study. 98
Figure 4-6. Trace element diagrams for the Murder Creek granite and Rocky Creek granodiorite samples. 101
Figure 4-7. Trace element diagrams for Walker Top Granite samples. 102
Figure 4-8. REE diagrams for the Farrar quadrangle granitoids, and Walker Top granites. 103
Figure 4-9. Tectonic discriminant diagrams for eastern Inner Piedmont granitoids. 105

Chapter 5

Figure 5-1. Simplified geologic map of portions of the Farrar and Mansfield quadrangles. 109
Figure 5-2. Grayscale aeromagnetic map, reduced to pole. 113
Figure 5-3. Aeromagnetic map with tectonic map overlay. 115
Figure 5-4. Perserved S_1 foliation in amphibolite boudin. 117
Figure 5-5. S_2 foliation form-line and domain map of portions of the Mansfield and Farrar quadrangles. 118
Figure 5-6. Scatter plots of foliation and schistocity measurements. 119

Figure 5-7. Scatter plots of L_2 mineral stretching lineations measure in the Mansfield and Farrar quadrangles. 121
Figure 5-8. F_2 and F_3 fabric diagrams. 122
Figure 5-9. F_2 and F_3 folds in outcrop. 123
Figure 5-10. Brindle Creek fault in outcrop and float. 125
Figure 5-11. Outcrop located along the Rex Haven fault. 126
Figure 5-12. Outcrop with a upright tight F_3 fold. 128
Figure 5-13. Rose diagram of joint sets. 129
Figure 5-14. Cross sections through the Mansfield and Farrar quadrangles. 132
Figure 5-15. 3-D cross section of Inner Piedmont nappe complex in northwest South Carolina. 135
Figure 5-16. Diagram of W-directed thrusts and SW-directed thrusts of the Inner Piedmont and Chauga Belt. 137
Figure 5-17. Maps representing the tectonic history of the Cat Square terrane. 139

List of Tables

Table 2-1. Point-counted samples of sillimanite schist from the Brindle Creek thrust sheet. 28
Table 2-2. Point-counted samples of metagraywacke from the Brindle Creek thrust sheet. 33
Table 2-3. Point-counted samples of Farrar and Mansfield 7.5-minute quadrangle granitoids. 38
Table 2-4. Point-counted samples of amphibolite from the Brindle Creek thrust sheet. 51
Table 3-1. Modes of pelitic schist from the Brindle Creek thrust sheet..... 64
Table 4-1. Whole-rock major and trace element data for representative granitic samples in the Cat Square terrane. 92
Table 4-2. Granitoid CIPW normative compositions. 94
Table 5-1. Summary and relative timing of deformation events in the central Inner Piedmont, Georgia. 112

List of Attachments

Plate 1: Geologic map of portions of the Farrar and Mansfield quadrangles, Georgia……..Plate 1

Plate 2: Geologic map of the central Georgia Inner Piedmont, including portions of the Farrar, Stewart, Mansfield, Berner, Indian Springs, Worthville, Lloyd Shoals, Covington, and Jackson……Plate 2

Chapter 1: Inner Piedmont Overview

Introduction

The Inner Piedmont comprises more than half of the southern Appalachian Neoacadian orogenic core. Previous work in the Inner Piedmont in South and North Carolina has provided much insight into its tectonic history, mostly attributed to efforts of previous workers and relief of the area, which ranges from 200-2000 ft (Griffin, 1971, 1974; Hopson and Hatcher, 1988; Davis, 1993; Giorgis, 1999; Wilson, 2006; Gatewood, 2007). Previous misconceptions that there was little exposure in the eastern Inner Piedmont led to a large portion of the southern Appalachians remaining unmapped and unstudied. Often, the orogenic core of a mountain chain is highly migmatitic and is a helpful guide when interpreting the geologic history of a region. Studying this portion of the orogen allows insight into the most deep-seated processes that occurred in the geologic past of the southern Appalachians. Polyphase deformation, high-grade metamorphism, and the migmatitic high-grade nature of these rocks, in combination with sometimes poor exposure, results in the near loss or total obliteration of primary lithostratigraphy and rock fabrics.

Aeromagnetic data provided by the USGS has been an important tool used in constructing the current tectonic map of the southern Appalachians (Fig. 1-1) (Daniels, D.L., unpub. data). Many gaps still exist where little detailed geologic mapping has been performed, but aeromagnetic data in combination with other data sets provide further insight into the tectonic history of the southern Appalachians. Previous mapping in the Inner Piedmont suggested that the Brindle Creek fault originally terminated along the Central Piedmont suture, just south of Athens, GA. Newly reprocessed aeromagnetic data provided by the United States Geological Survey (USGS) suggest the Brindle Creek fault extends to west-central Georgia. High-frequency curved magnetic anomalies truncate along an extensive linear boundary. This linear feature can be traced northward into the southern extension of the Brindle Creek fault, and may represent the SW continuation of the Brindle Creek fault into the central Georgia Inner Piedmont. The curved anomalies that truncate against the linear feature may represent the Neoacadian deflection of the Inner Piedmont southwestward along the crustally

Figure 1-1. Simplified tectonic map of part of the Tugaloo, Cat Square, and adjacent terranes. Field area in black. Red bodies–Grenvillian basement. Lime green bodies–mafic rocks. Light green inside Pine Mountain window–Paleozoic cover rocks. Orange inside Dahlonega gold belt–metasandstone and pelitic schist. Yellow inside Tallulah Falls dome–quartzite. Light and dark green in Carolina superterrane–low and high grade rocks, respectively. Lavender in Tugaloo terrane–variously migmatitic metasandstone, pelitic schist, and mafic metavolcanic rocks. Dgb–Dahlonega gold belt. Aa–Alto Allochthon. TFd–Tallulah Falls dome. GRf–Goat Rock fault. BFf–Bartlett's Ferry fault. MSf–Mill Spring fault.SMf–Six Mile fault. DROw–Dog River-Opelika window. BAf–Box Ankle fault.Td–Toxaway Dome. PMf–Pine Mountain fault. Km–Kings Mountain belt. PMw-Pine Mountain window. Wr–Whitmire reentrant. Plutons: Dark purple–Ordovician granitoids. Light purple–Ordovician(?) granitoids. Medium blue–Devonian granitoids. Darker blue-green–Mississippian. (From Hatcher et al., 2007).

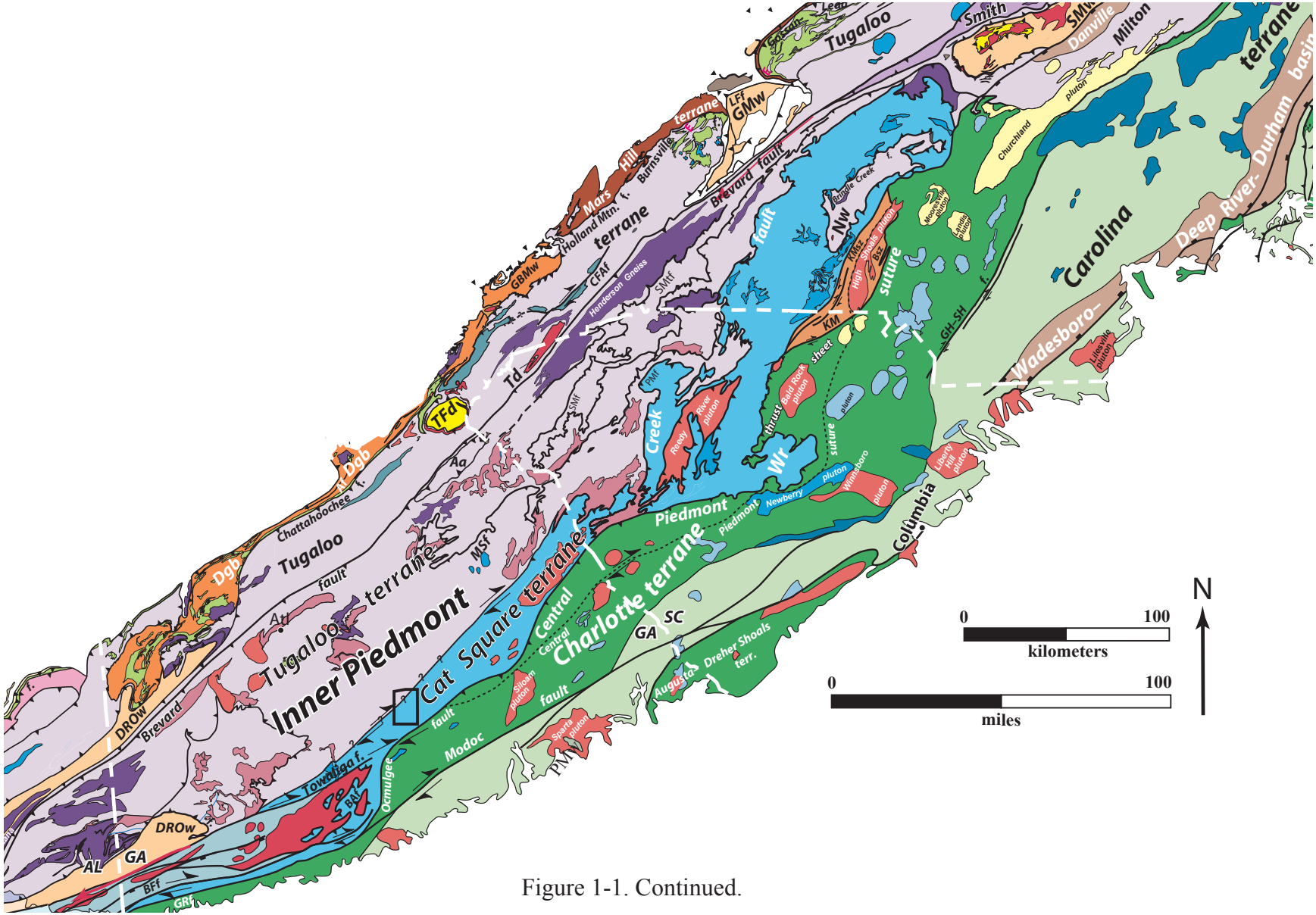

Figure 1-1. Continued.

weak Brevard fault zone (Hatcher et al., 2007). These aeromagnetic data have been the primary motivation in choosing the field area (Hatcher et al., 2007).

Objectives

This study was performed to address current problems regarding the Inner Piedmont, and its southwestern extent.

1. Map and trace the southern extent of the Brindle Creek fault and Cat Square terrane.
2. Create a detailed geologic map and cross sections of the Farrar 7.5-minute quadrangle (60 mi^2) and southern portion of the Mansfield 7.5-minute quadrangle.
3. Identify and sample rocks of the Tugaloo and Cat Square terranes.
4. Interpret bulk-rock geochemistry of the Murder Creek and Rocky Creek granitoids.
5. Determine the nature and relationship of the Mesozoic features that extend through the field area, such as diabase dikes, siliceous cataclasites, and threshold quartz ductility mylonites.
6. Determine peak metamorphic conditions in the central Georgia Inner Piedmont, along with retrograde reactions and fabrics.

Location

The study area is located approximately 64 km (40 mi) southeast of Atlanta, Georgia, and approximately 23 km (14 mi) northeast of Jackson, Georgia (Fig. 1-2). The area is accessible from Interstate 20 via GA Hwy-11 and GA Hwy-142. The majority of the field area is accessible only by using secondary gravel or dirt roads and logging roads. Approximately ¼ of the field area was incorporated into the Charlie Elliott Wildlife Center (State Park), and is located along the western-most portion of the field area.

The central Georgia region is dominated by a relatively low relief ranging from 300-400 ft, thereby limiting exposure. However, exposure in creeks and logging roads is often quite good.

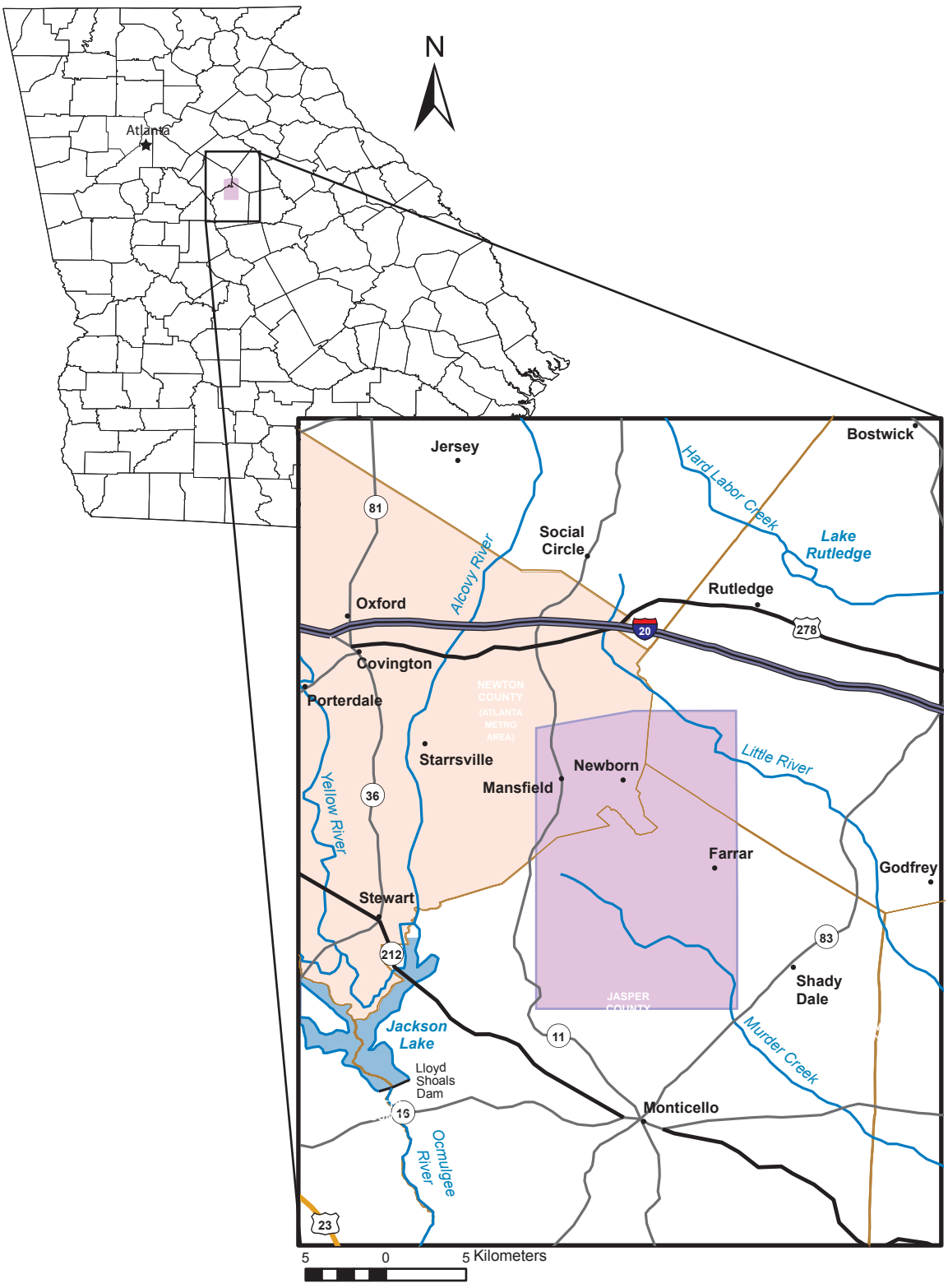

Figure 1-2. Location of field area.

Previous Work

Previous work in the vicinity began in 1960 with mapping performed just north and northwest of the proposed field area by Emory University graduate students followed by completion of the generalized state map by the Georgia Geologic Survey in 1976. These studies involved macro- and microfabric analyses and petrology (Reade, 1960; Gardner, 1961; Schultz, 1961; Jones, 1970; Prowell, 1972). Also, M. W. Higgins conducted generalized reconnaissance mapping (unpublished data, 2007). Lester Williams, a USGS WRD geologist, has created some lithologic maps of the area, but Williams' mapping is not related to his work for the USGS (Hatcher written commun., 2007). In addition to these previous workers, R. J. Hooper and R. D. Hatcher, Jr. (Hooper, R. J., 1989) made detailed geologic maps of the area south and southeast of the field area. Hooper and Hatcher mapped portions of the central Piedmont suture and Pine Mountain window in the Berner, Indian Springs, and Forsyth areas.

Methodology

This work is a compilation of data that was gathered over the course of two field seasons mapping 60 mi^2 in central Georgia. During this investigation, the field area was searched for evidence of the extension of the Brindle Creek fault and Cat Square terrane into central Georgia. Field data, such as structural measurements, lithologic descriptions, and field sketches, were compiled from 1,794 stations.

Samples were taken from each rock unit in the field area, and were made into approximately 30 thin sections. Thin sections of Murder Creek granite, Rocky Creek granodiorite, Dow's Pulpit granodiorite, metagraywacke, sillimanite schist, and amphibolite were point counted. Other thin sections were examined for a visually estimated modal mineralogy. Aside from mineralogy, other features were studied in each thin section, such as microstructures, fabrics, and paragenesis, and this information was used to interpret metamorphism and deformation conditions.

Geologic Background

The Inner Piedmont extends southwestward from the frame of the Sauratown Mountains window in north-central North Carolina, to the Coastal Plain of Alabama. The Inner Piedmont is ~700 km long and 100 km wide at its broadest extent (Hatcher, 2002). It is the Neoacadian migmatitic orogenic core of the southern Appalachians, and contains the largest area of high-grade metamorphism in the southern Appalachians (King, 1955; Griffin, 1971). The Inner Piedmont is bordered to the west by the Brevard fault zone, which separates rocks of the Inner Piedmont (Tugaloo and Cat Square terrane) from the eastern Blue Ridge (Tugaloo terrane) (Hatcher, 2002). The Inner Piedmont is the footwall of the exotic Carolina superterrane along the central Piedmont suture. The Tugaloo and Cat Square terranes are separated by the Neoacadian Brindle Creek fault (Hatcher, 2002).

The rocks of the western Inner Piedmont, Tugaloo terrane, are bound to the west by the Chattahoochee-Holland Mountain fault. The Brevard fault zone is located in the interior of the Tugaloo terrane, and is the western boundary of the Inner Piedmont. During the Neoacadian orogeny, the Brevard fault zone was a point of structural weakness. Due to its structurally weak and suitably oriented nature, there were multiple episodes of reactivation (Hatcher et al., 2007). In the past, the Brevard fault zone has been interpreted as a terrane boundary or suture (Hatcher, 2002). This interpretation indicates that the Inner Piedmont is a suspect or exotic terrane. Similarities between the eastern and western portions of the Tugaloo terrane indicate that it is one terrane. Identical stratigraphic sequences are recognized on both sides of the Brevard fault zone, and detrital zircon age dates reveal that both the eastern and western Tugaloo terrane have a Laurentian affinity. Therefore, the Brevard fault zone is most likely an area of crustal weakness, and not a representative terrane boundary.

The Brindle Creek fault is located between the eastern Tugaloo and Cat Square terranes. It was originally mapped as a contact (not a fault) in the reconnaissance map of the Charlotte 1˚x 2˚sheet (Goldsmith et al., 1988), but was later identified and mapped as a low-angle fault by Giorgis (1999). Giorgis traced it across parts of the Morganton South and Dysartsville quadrangles in the South Mountains, North Carolina. Williams (2000) traced the fault through the remainder of the Dysartsville quadrangle. The Brindle Creek fault has subsequently been

traced northward through the Brushy Mountains (Kalbas, 2003; Merschat, 2003; Wilson, 2006; Gatewood, 2007) and may truncate against a Mesozoic border fault related to the Davie County basin. The southern continuation of the Brindle Creek fault into South Carolina was mapped by Curl (1998) in the Reidville and Wellford 7.5-minute quadrangles, located southeast of Greenville, South Carolina. Nelson et al. (1998) recognized that the fault could be traced between Spartanburg and Greenville, and into Georgia, where it was thought to ultimately truncate against the central Piedmont suture (Hatcher, 2002).

The Brindle Creek fault is one of the most important tectonic boundaries in the southern Appalachians (Bream, 2003), and functions as a structural boundary between the Tugaloo and Cat Square terranes (Hatcher, 2002). The Cat Square terrane is considered an independent terrane based on its zircon age suite, which includes Laurentian, peri-Gondwanan, Paleozoic, and minor Archean ages (Hatcher, 2002; Bream, 2003; Merschat et al., 2005). The Cat Square terrane is further defined by its anatectic Devonian-Mississippian plutons.

Stratigraphy

The Tugaloo terrane consists of the Neoproterozoic to early Paleozoic(?) Tallulah Falls Formation, Chauga River Formation, and the Mid-Ordovician Poor Mountain Formation. All of these formations were intruded by Early to Middle Ordovician granitoids, such as the Dysartsville, Toccoa, Henderson, and Caesars Head (Davis, 1993; Mapes et al., 2002; Bream, 2003). The Tallulah Falls Formation contains three members: 1) an upper metagraywacke-schist member; 2) a middle aluminous schist member; and 3) a lower metagraywacke-schist-amphibolite member. This stratigraphy was first recognized in the eastern Blue Ridge, and was later correlated with the western Inner Piedmont (Davis, 1993). The Poor Mountain Formation lies unconformably above the Tallulah Falls formation, and can be separated into three distinct units (Giorgis, 1999; Hatcher, 2002).

The Cat Square terrane consists of Siluro-Devonian metasedimentary rocks, such as sillimanite-schist, biotite gneiss, and amphibolite (Merschat et al., 2005). These metasedimentary rocks are intruded by Acadian-Neoacadian plutons, such as the Walker Top and Toluca Granites

(Hatcher et al., 2007). Stratigraphic nomenclature has not been established for the Cat Square terrane thus far.

Metamorphism

Increases in temperature from cores to rims in garnets and single continuous garnet zoning profiles suggest that the Inner Piedmont underwent a single prograde metamorphic event (Davis, 1993; Bier et al., 2002; Merschat and Kalbas, 2002; Merschat et al., 2005). U-Pb dating of monazite and zircon metamorphic rims suggests peak metamorphism occurred in the Inner Piedmont during the mid-Paleozoic (360-345 Ma) (Davis, 1993; Bier, 2001; Bream, 2002; Merschat and Kalbas, 2002). The mid-Paleozoic event recorded in the southern Appalachians is referred to as the Neoacadian orogeny (Hatcher, 2002). Monazite and zircon metamorphic rims also yielded age clusters from 325-320 Ma; these ages are thought to represent Alleghanian overprint (Dennis and Wright, 1997; Mirante and Patino-Douce, 2000; Carrigan et al., 2001; Merschat and Kalbas, 2002).

The interior portion of the Inner Piedmont is highly migmatitic, but migmatization decreases toward the flanks, and P-T estimates range from 500-800° C and 3-7 kbar (Bier et al., 2002; Merschat, 2003). Inner Piedmont rocks are regionally metamorphosed to sillimanite II and granulite facies assemblages (Mirante and Patino-Douce, 2000; Bier, 2001; Bream, 2002). The Inner Piedmont has the widest area of high-grade metamorphism in the southern Appalachians. The core of the Inner Piedmont is dominated by sillimanite I and sillimanite II grade metamorphism, and there is a decrease in metamorphic grade from the interior toward the flanks. There is an increase in metamorphic grade eastward from the Brevard fault zone into the core of the Inner Piedmont ranging from garnet-staurolite grade (in northwest South Carolina) to sillimanite I and higher (in North and South Carolina), then decreasing to kyanite grade along the central Piedmont suture (Merschat et al., 2005). Merschat and Kalbas (2002) suggested that the Brindle Creek fault was emplaced while hot, indicated by strong migmatization occurring in the footwall of the fault.

Structure

The Inner Piedmont is the polydeformed, migmatitic crystalline core of the southern Appalachians, with structure characterized by large-scale SW-directed ductile type-F thrust sheets (Griffin, 1971; Hatcher, 2004; Merschat et al., 2005). These thrust sheets later transformed into type C thrusts during emplacement. This allows the thrust sheets to achieve greater strength, considerable size and variable displacement (Hatcher and Hooper, 1992). Transport direction of these thrusts has been determined from sheath folds, asymmetric boudins, winged porphyroclasts, mineral lineations, snowball garnets, S-C fabrics, and vergence of asymmetric folds (Davis et al., 1991; Yanagihara, 1993). The Inner Piedmont has been deformed by early ductile Neoacadian (360-345 Ma) and early Alleghanian (320 Ma) events, and was later deformed and overprinted by several late Alleghanian events (Merschat and Kalbas, 2002; Hatcher et al., 2005). During the early Alleghanian brittle event, structures are characterized by broad open folds, then followed by normal faults and joints related to Mesozoic extension (Merschat and Kalbas, 2002).

At least seven deformational events have been recorded in the Appalachians. D_1 deformation events occurred during recrystallization producing F_1 folds and S_1 foliation, preserved in boudins and xenoliths (Davis, 1993). According to Bream (2003), the D_2 deformation event is described as "the most penetrative polyphase event at or near peak metamorphism forming the dominant foliation (S_2), the most prominent mineral lineation (L_2), reclined to recumbent, tight to isoclinals folds, sheath folds and Type-F thrust faults." Structures recognized from this stage of deformation are the dominant D_2 foliation (S_2) and the curved mineral lineation patterns (L_2), showing a northwestern flow pattern that curves to the southwest along the Neoacadian Brevard fault zone (Hatcher, 2001; Merschat et al., 2005). This pattern was interpreted by Merschat et al. (2005) and Hatcher and Merschat (2006) to represent crustal flow in the orogenic core. Buttressing against the crustally weak Brevard fault zone is believed to have diverted the Inner Piedmont toward the southwest. Final emplacement of coherent thrust sheets marks the D_3 deformation event, occurring toward the end of the Neoacadian orogeny (Davis, 1993). The dominant L_2 mineral lineation, formed during D_2, displays strong orientation throughout the Inner Piedmont. This orientation has been interpreted by Merschat et al. (2004)

to reflect the southwestward deflection of the westward-advancing thrust sheets of the Inner Piedmont against the pre-Alleghanian Brevard fault zone (Fig. 1-3). D_4 deformation corresponds to Alleghanian brittle deformation, producing NE-SW-trending upright open folds; D_5 deformation occurred during the late Alleghanian and appears as joints and broad open folds (Merschat and Kalbas, 2002). During both D_4 and D_5, reactivation occurred along the Brevard fault zone and the central Piedmont suture (Merschat and Kalbas, 2002). D_5 and D_6 mark Mesozoic extension and Cenozoic uplift (Merschat and Kalbas, 2002). Injections of magmas into joints formed during the Mesozoic extension resulted in dike emplacement (diabase dikes). Joints formed during the Late Permian and Early Triassic were most likely filled with these same injections, resulting in the emplacement of diabase dikes. Forming almost simultaneously with the diabase dikes are low temperature siliceous cataclasites. They have a northeast trend, and appear to have multiple episodes of movement. Orthogonal joint sets can be seen in outcrop and thin section. The siliceous cataclasites have similar timing of formation to the diabase dikes, and have been noted to cross-cut one another. These crosscutting relationships complicate exact timing and relationships between the two structures.

Figure 1-3. Simplified tectonic map of part of the Tugaloo and adjacent terranes. Flow lines represent crustal flow in the Inner Piedmont.Red bodies–Grenvillian basement. Lime green bodies–mafic rocks. Light green inside Pine Mountain window–Paleozoic cover rocks. Orange inside Dahlonega gold belt–metasandstone and pelitic schist. Yellow inside Tallulah Falls dome–quartzite. Light and dark green in Carolina superterrane–low and high grade rocks, respectively. Lavender in Tugaloo terrane–variously migmatitic metasandstone, pelitic schist, and mafic metavolcanic rocks. Dgb–Dahlonega gold belt. Aa–AltoAllochthon. TFd–Tallulah Falls dome. GRf–Goat Rock fault. BFf–Bartlett's Ferry fault. MSf–Mill Spring fault.SMf–Six Mile fault. DROw–Dog River-Opelika window. BAf–Box Ankle fault.Td–Toxaway dome. PMf–Pine Mountain fault. Km–Kings Mountain belt. Wr–Whitmire reentrant. Plutons: Dark purple–Ordovician granitoids. Light purple–Ordovician(?) granitoids. Medium blue–Devonian granitoids. Darker blue-green–Mississippian plutons. Orange–Pennsylvanian granitoids.Modified from Hatcher et al. (2007).

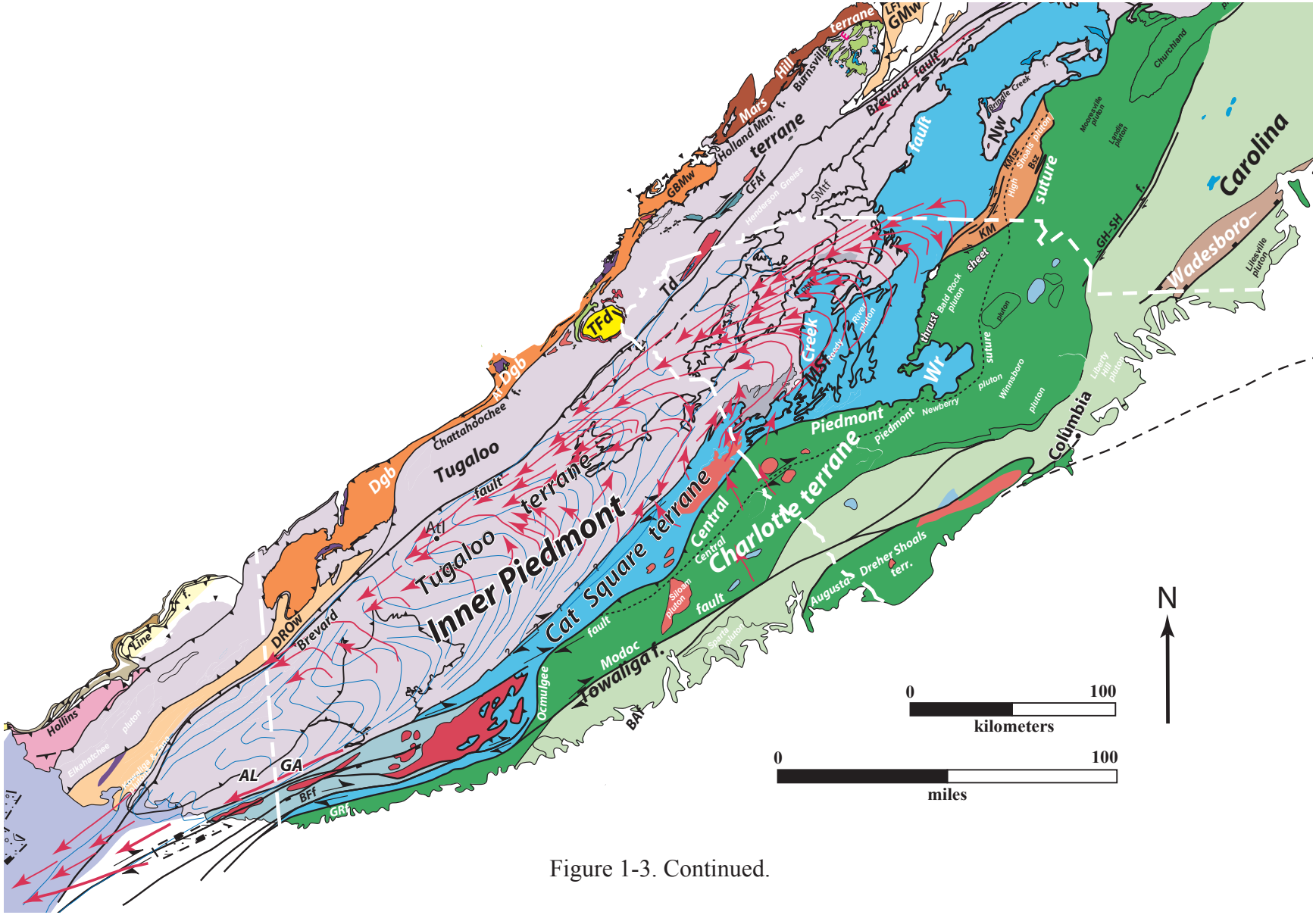

Figure 1-3. Continued.

Chapter 2: Rock Units

Introduction

Rock units present in the field area belong to the Tugaloo and Cat Square terranes, and a felsic plutonic suite located adjacent to and northwest of the Towaliga fault (Fig. 2-1). Representative samples of each rock unit located in the field area were collected and analyzed petrographically (Fig. 2-2). Five amphibolite, three Murder Creek granite, two Rocky Creek granodiorite, two Dow's Pulpit granodiorite, two metagraywacke, and three sillimanite schist thin sections were point counted. Modes of other rock types discussed in this chapter were visually estimated. Plagioclase compositions were determined by using the Michel-Lévy extinction and Carlsbad albite methods.

Western Inner Piedmont – Eastern Tugaloo terrane

In North and South Carolina the Tugaloo terrane is noted to consist of the Neoproterozoic to early Paleozoic(?) Tallulah Falls Formation and the Mid-Ordovician Poor Mountain Formation. Both of these formations are intruded by Early to Middle Ordovician granitoids, such as the Dysartsville, Toccoa, Henderson, and Caesars Head (Davis, 1993; Mapes et al., 2002; Bream, 2003). In the South Mountains, North Carolina, previous workers (Bream, 1999; Hill, 1999) were able to determine a recognizable stratigraphy in the Tugaloo terrane. The distinguishing factor is a greater amount of amphibolite in the lower Tallulah Falls member relative to lesser amounts of amphibolite in the upper Tallulah Falls member, and an aluminous schist member that separates the lower member from the upper (Hatcher, 1971). The Tallulah Falls Formation is a three-part formation consisting of: 1) an upper metagraywacke-schist member; 2) a middle aluminous schist member; and 3) a lower metagraywacke-schist-amphibolite member (Fig. 2-3) (Giorgis, 1999; Hatcher, 2002). The Poor Mountain Formation rests unconformably above the Tallulah Falls Formation and can be separated into three distinct units: (1) a lower metasiltstone; 2) a middle amphibolite-hornblende gneiss; and 3) an upper quartzite with amphibolite and marble (Giorgis, 1999).

Rock Units

Mesozoic rocks

Ŧ Jc Siliceous cataclasite

Ŧ Jd Diabase dikes

Cat Square terrane (?)

Igneous Rocks

rcg Rocky Creek granodiorite

dpg Dow's Pulpit granodiorite

mcg Murder Creek granite

am Amphibolite

Metasedimentary Rocks

bg Biotite gneiss/metagraywacke

ss Sillimanite-mica schist

Tugaloo terrane

ltf Tallulah Falls Formation

Contacts

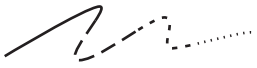

Fault



Shear Zone



*solid line - observed contact, dashed line - approximate contact, dotted line - concealed contact, arrows indicate transport direction

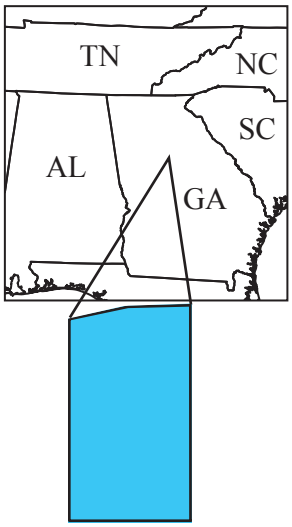

EDMAP, 2008-2009

Figure 2-1. Geologic map explanation.

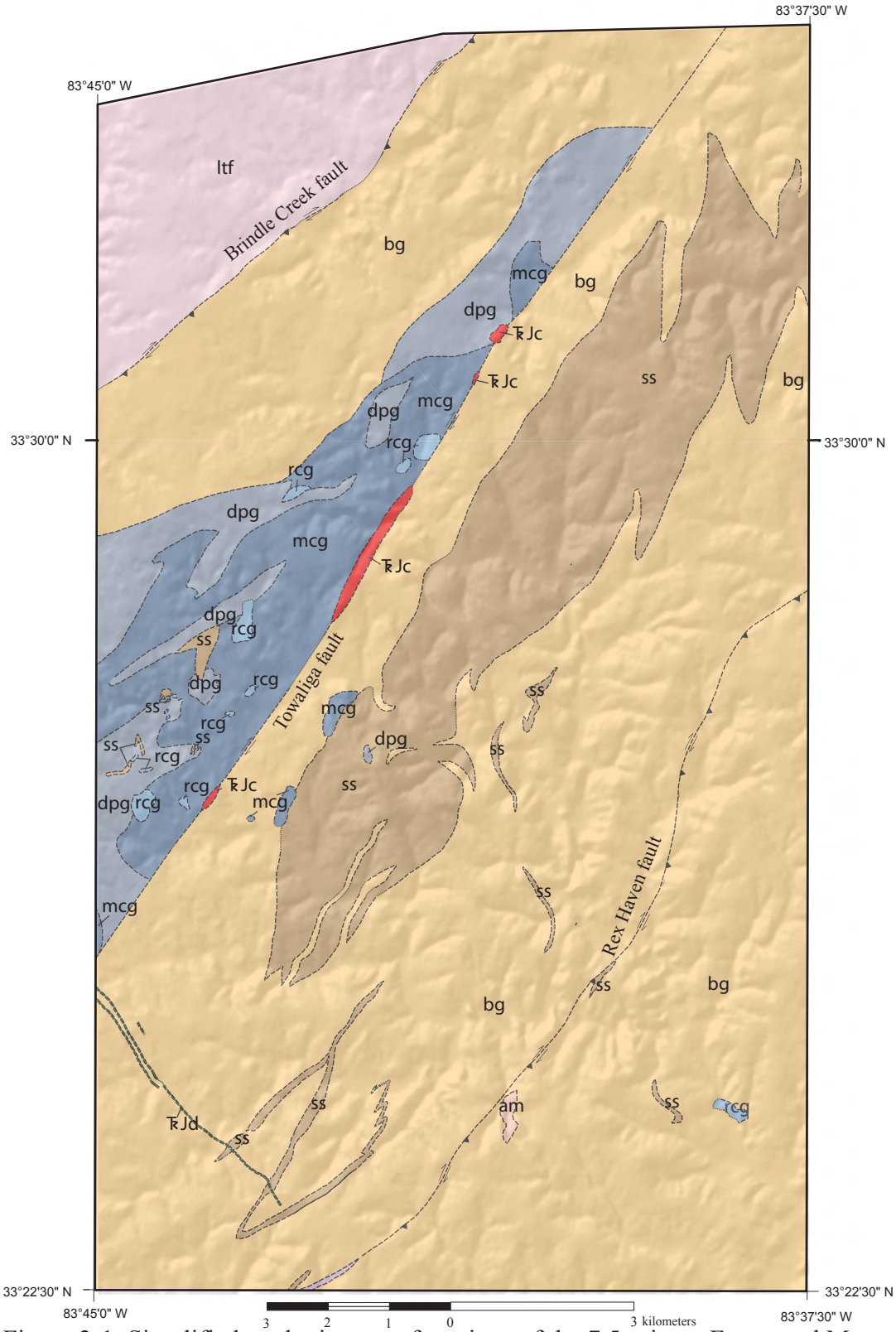

Figure 2-1. Simplified geologic map of portions of the 7.5-minute Farrar and Mansfield quadrangles (See Plate 1 for map unit descriptions).

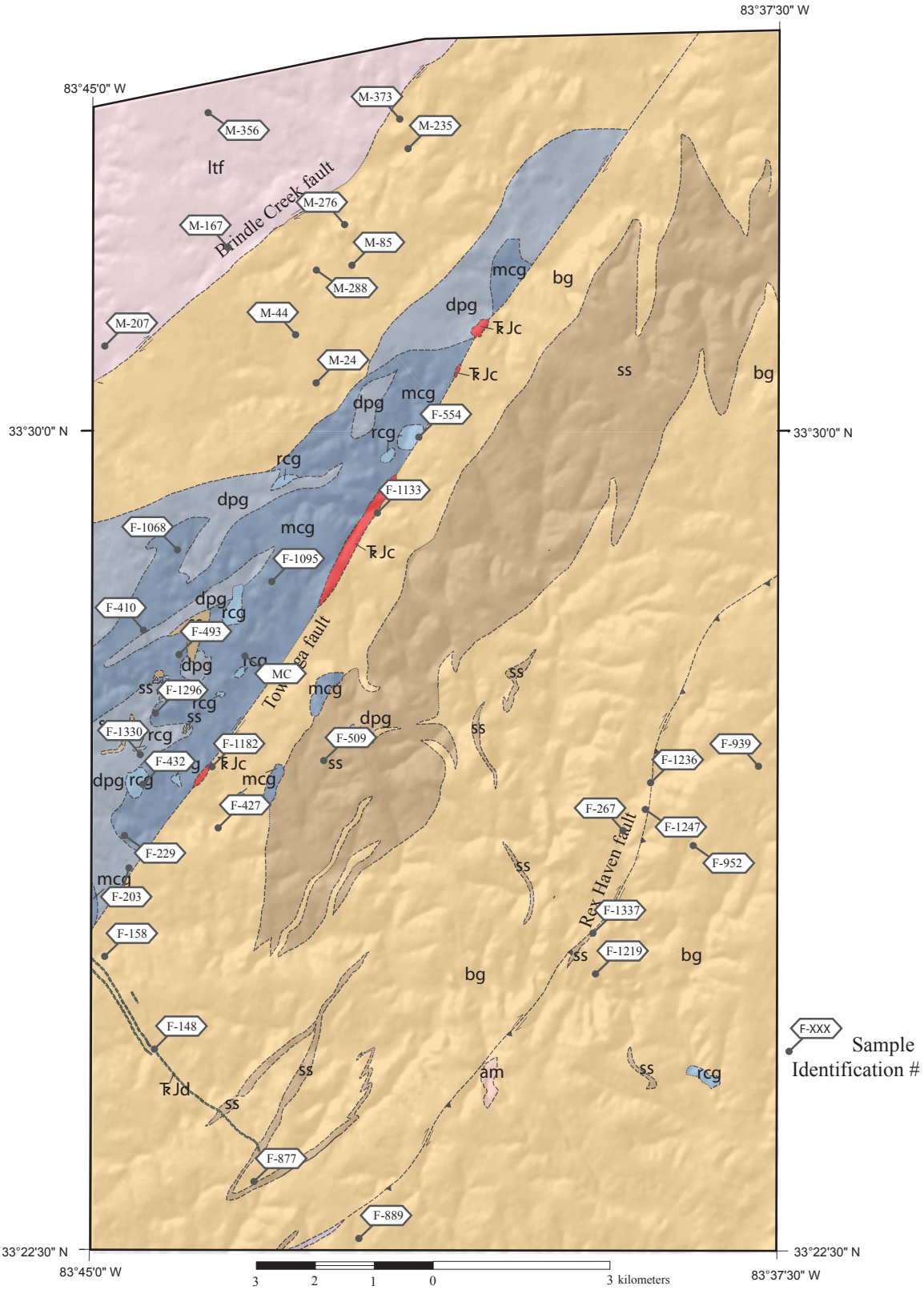

Figure 2-2. Location of samples collected for detailed petrographic analysis. Sample numbers correspond with quadrangle name and station number.

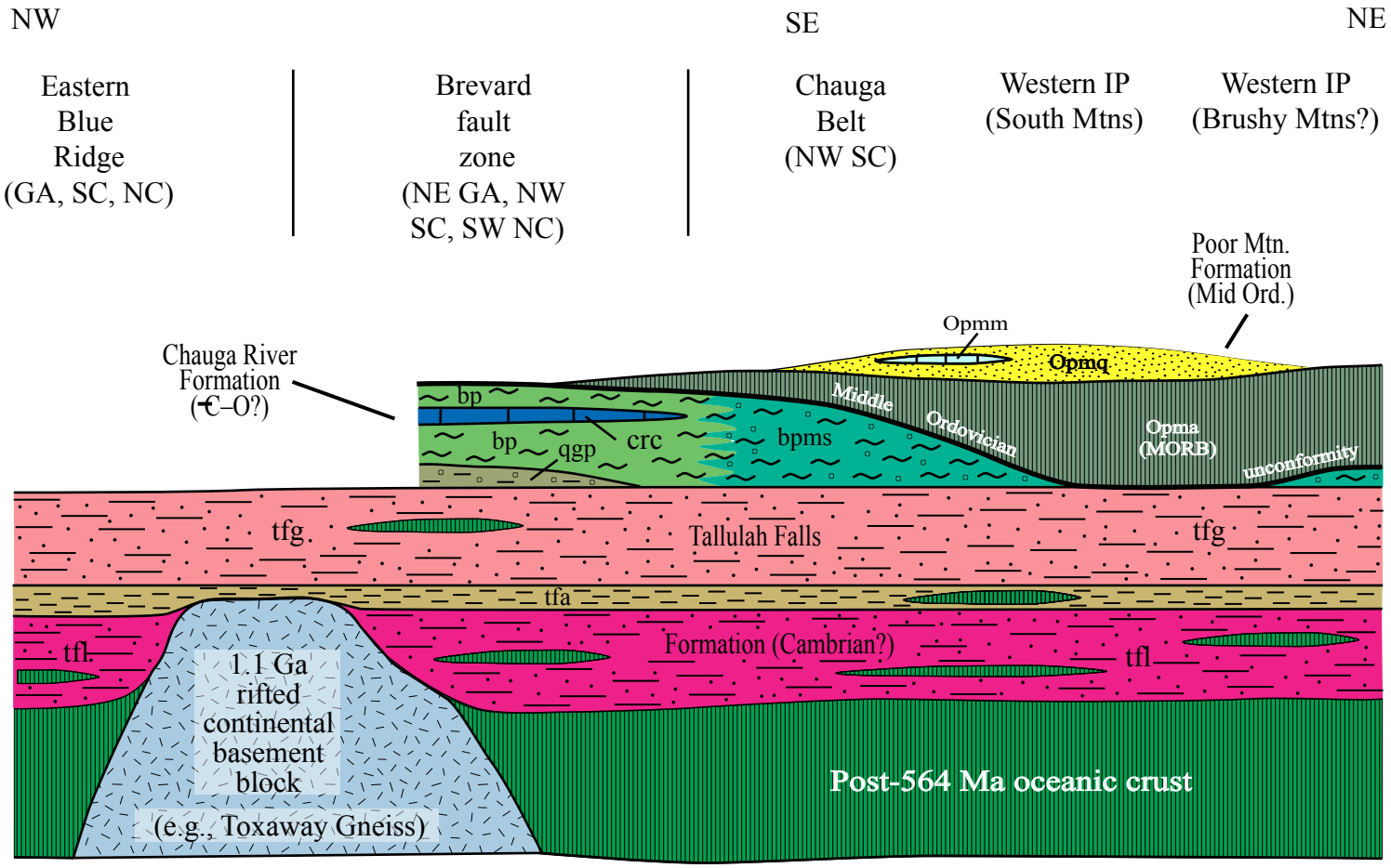

Figure 2-3. tfg, tfa, and tfl are members of the deep-water unit. bp, qgp, bpms, and crc are members of the overlying formation (more fine-grained material and some carbonate). Opmq (quartzite/felsic tuff), and Opmm (marble) are members of the Ordovician unit. Modified from Hatcher, 2002.

Lower Metagraywacke-Schist-Amphibolite Member

Only a small portion of the Tugaloo terrane was identified and mapped. It is located in the northwestern portion of the field area (Fig. 2-1). Based on the abundance of amphibolite, it appears to be the lower metagraywacke-schist-amphibolite member of the Tallulah Falls Formation.

In outcrop, the lower metagraywacke-schist-amphibolite member appears light gray to black, and is consistent of biotite gneiss with a biotite-muscovite interlayer (Fig. 2-4). The lower Tallulah Falls member ranges from fine- to coarse-grained, thinly to thickly layered, strongly foliated, highly migmatitic, and commonly porphyroblastic. Garnets are the dominant porphyroblasts identified. Mineral assemblage includes: muscovite, biotite, alkali feldspar, plagioclase (An_{25-30}), and quartz. Accessory minerals include: epidote, zircon, chlorite, and opaques. Abundant amphibolite occurs throughout the lower Tallulah Falls member, with little calc-silicate noted.

Eastern Inner Piedmont – Cat Square terrane

The Cat Square terrane was originally believed to be part of the Neoproterozoic-Cambrian metasedimentary and metaigneous rocks of the Tugaloo terrane (Bream, 1999; Giorgis, 1999; Hill, 1999; Williams, 2000; Bier, 2001). Changes in thickness of aluminous schist from the western Inner Piedmont to the eastern Inner Piedmont were attributed to complex folding and/or thickening of the metapelite unit eastward. Recent geochronological data provided by Bream (2003) suggested that the eastern Inner Piedmont is a separate terrane. The Tugaloo terrane is dominated by an abundance of 1.1-1.2 Ga Laurentian detrital zircons. While the Cat Square terrane does contain an abundance of Laurentian detrital zircons, it also contains: (1) 600 and 500 Ma zircons; (2) 480 and 430 Ma zircons; and (3) a small amount of Archean zircons (Merschat, 2009). These younger zircons are not found in the Tugaloo terrane (Bream, 2003). A combination of Grenvillian and younger 600 and 500 Ma ages suggests that the source of the Cat Square terrane consisted of a Laurentian and peri-Gondwanan mixed affinity (Bream, 2003). U/Pb zircon TIMS age dating was performed on one detrital zircon sample from the Stewart quadrangle west of the field area, and yielded a suite of ages from 1.3-0.9 Ga (Fig. 2-5)



Figure 2-4. Upper metagraywacke-schist member. Hammer for scale. Note the biotite gneiss with a biotite-muscovite interlayer. This outcrop is located in the creek on the eastern portion of Burge's Plantation. Photo taken facing north.

Figure 2-5. Simplified tectonic map of part of the Tugaloo and adjacent terranes. Red bodies–Grenvillian basement. Lime green bodies–mafic rocks. Light green inside Pine Mountain window–Paleozoic cover rocks. Orange inside Dahlonega gold belt–metasandstone and pelitic schist. Yellow inside Tallulah Falls dome–quartzite. Light and dark green in Carolina superterrane–low- and high-grade rocks, respectively. Lavender in Tugaloo terrane–variously migmatitic metasandstone, pelitic schist, and mafic metavolcanic rocks. Orange star represents location of detrital zircons used for U/Pb zircon TIMS age dating. Modified from Hatcher et al. (2007).

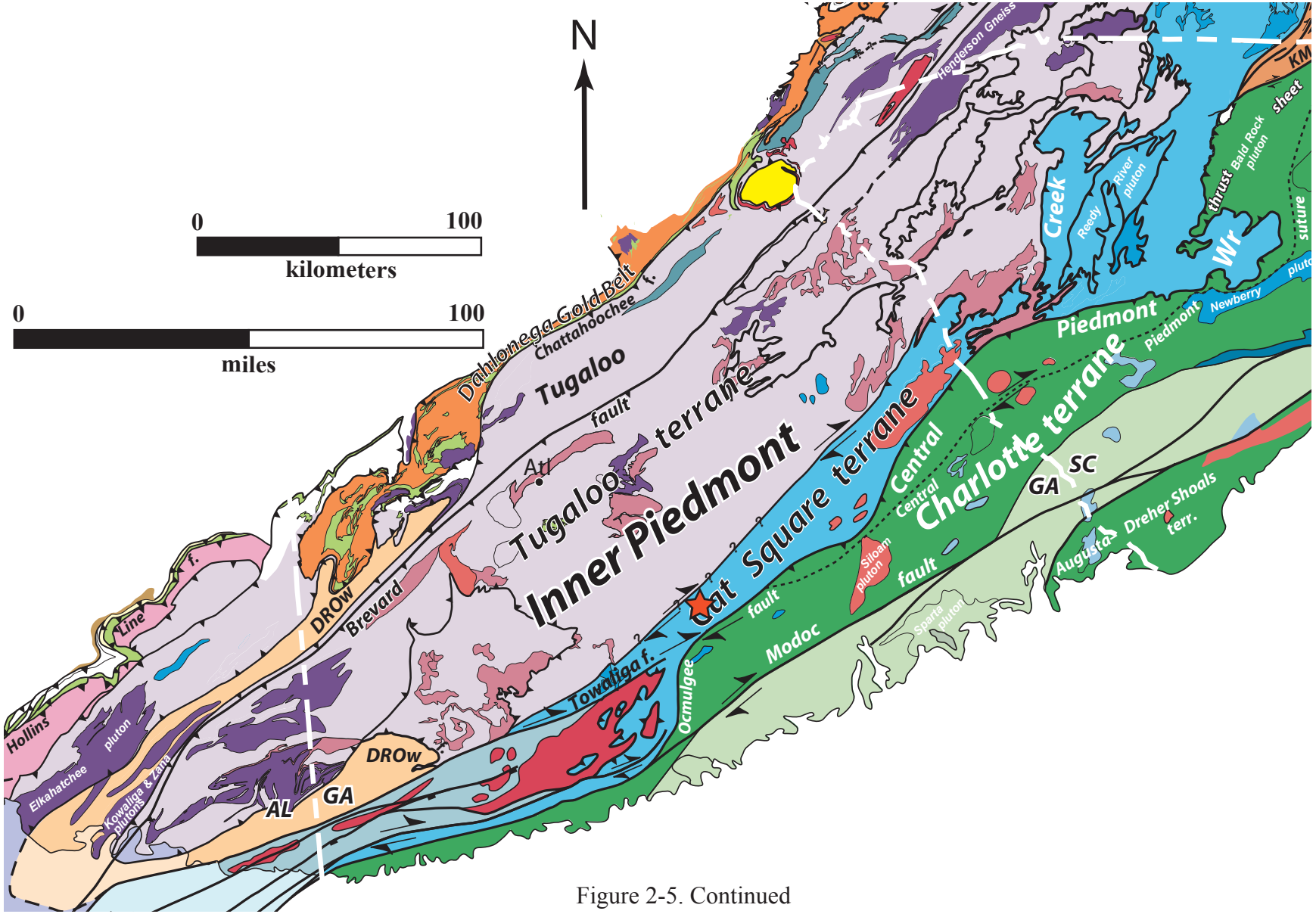

Figure 2-5. Continued

(Merschat, 2009). This sample also yielded three Neoproterozoic ages at ~630 Ma, and a discordant analysis at 1.55 Ga (Merschat, 2009). This is consistent with the detrital zircon age suite of the Cat Square terrane, and provides strong evidence that the Cat Square terrane extends into central Georgia.

The Cat Square terrane in North Carolina consists of Siluro-Devonian metasedimentary rocks, such as sillimanite-schist (metapelite), biotite gneiss (metapsammite), amphibolite, and minor amounts of calc-silicate. These metasedimentary rocks in North Carolina are intruded by peraluminous anatectic Devonian-Mississippian plutons, such as the Walker Top (407, 356, and 325 Ma) and Toluca (378 Ma) Granites (Mapes, 2002; Gatewood, 2007; Byars, 2009). In central Georgia, granitoids of the Cat Square terrane are coined Murder Creek, Dow's Pulpit, and Rocky Creek. The Georgia Inner Piedmont granitoids appear similar to the Inner Piedmont granitoids in North Carolina in texture, fabric, and petrography.

Metasedimentary Rocks

Sillimanite Schist (metapelite)

Sillimanite schist is one of the dominant rock types in the Brindle Creek thrust sheet, and in hand sample, biotite, sillimanite, muscovite, quartz, feldspars, and garnet can readily be seen. Sillimanite schist is generally distinguished by a contrasting soil color from that of other rock units in the field area, and by the abundance of muscovite, garnet, and sillimanite in float. Quartz mylonites are commonly interlayered with the sillimanite schist, and appear to be transposed quartz veins (Fig. 2-6). The residual soil of the sillimanite schist varies from light brown to dark red to an almost iridescent purple (Fig. 2-7). The drastic change in soil color makes tracing contacts between the metagraywacke/granitoids and the sillimanite schist relatively easy. Rock and/or saprolite outcrops of sillimanite schist are usually limited to roadcuts, ditches, and logging roads. If soil is not readily visible, contacts can easily be traced by schist float commonly found at the base of trees. Felted masses of sillimanite are readily recognizable in hand samples, and align with the foliation. Sillimanite schist is strongly foliated, displays S-C fabric, tight-to-isoclinal folds, sheath folds, uncommon interlayered quartz

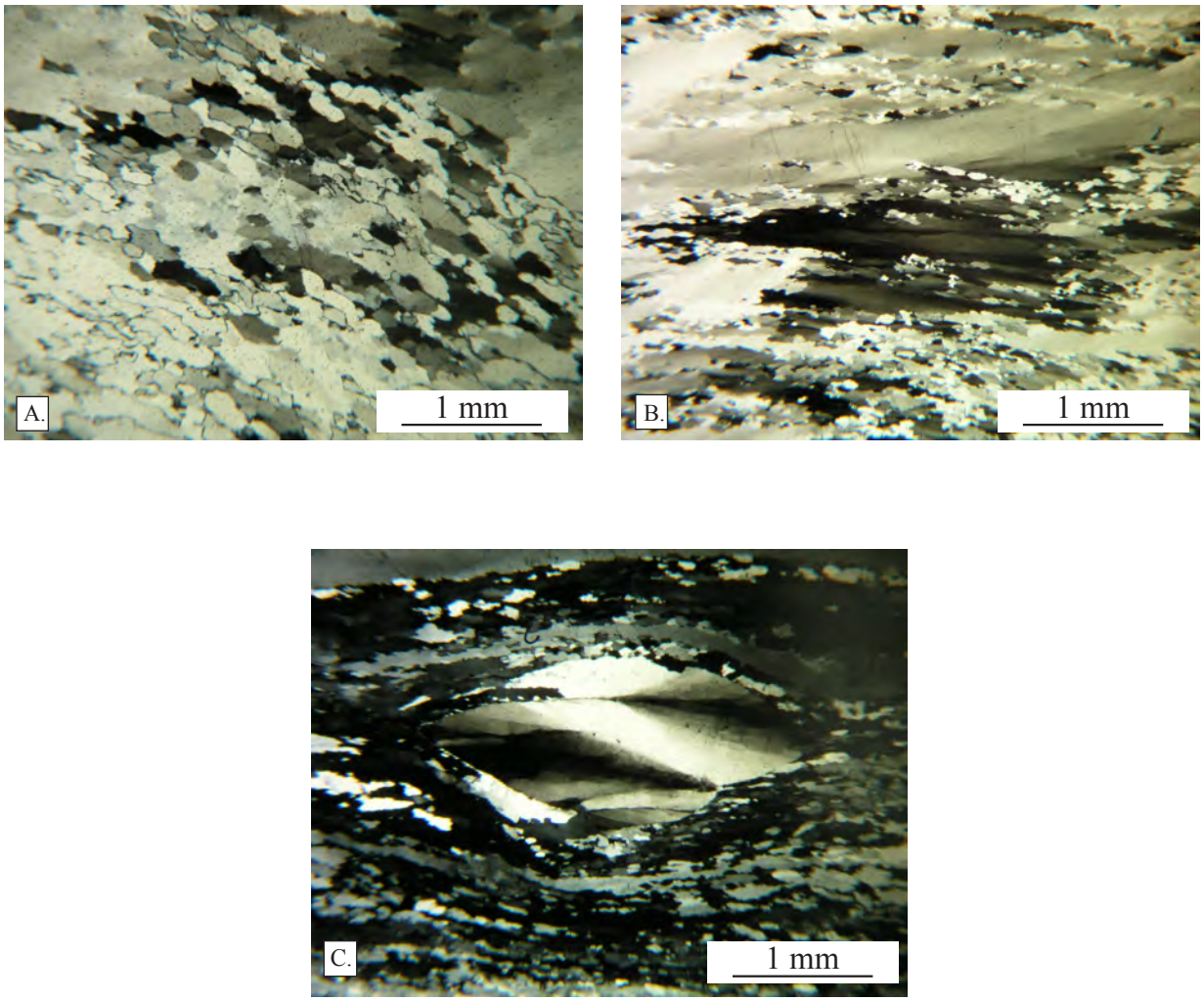

Figure 2-6. Photomicrographs of quartz mylonite. A. Triple points of quartz represent recovery in the quartz mylonite. B. Quartz ribbons displaying minor amounts of recovery and subgrain rotation. C. Quartz ribbons displaying recovery surrounding a large quartz porphyroclast. Samples taken from near the intersection of Concord Rd. and Alfred Ln.

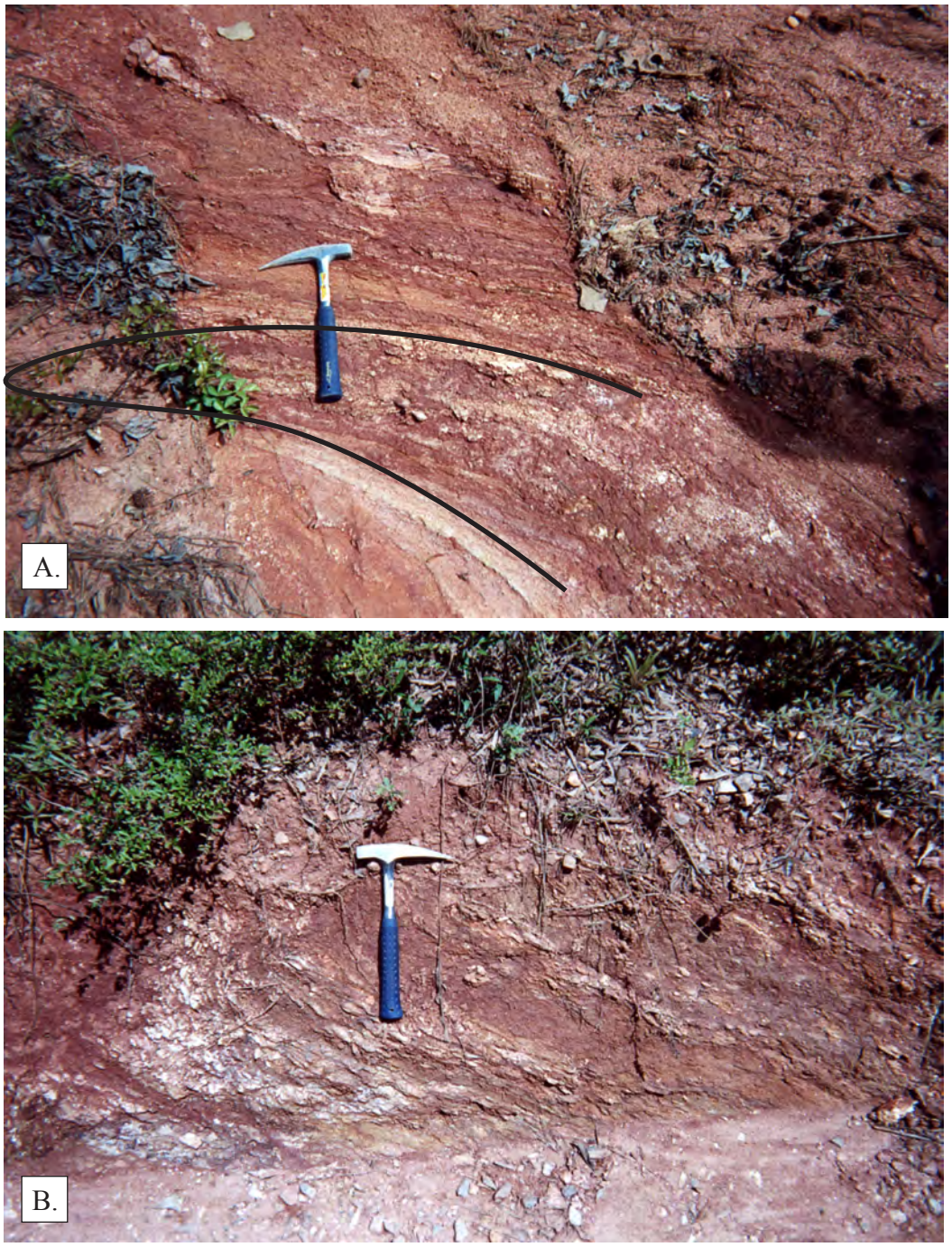

Figure 2-7. A. Saprolite outcrop of sillimanite schist (dark red to dark brown) with a recumbent tight fold and interlayered amphibolite. This outcrop is located at the intersection of Marben Farm Rd. and Concord Rd. Photo taken facing northeast. B. Outcrop of sillimanite schist with visible felted masses of sillimanite (white). This outcrop is located at the intersection of Aldridge Rd. and Murder Creek Church Rd. Photo taken facing northeast. Rock hammer for scale.

mylonite, rotated garnet porphyroblasts, proto- to ultramylonitic texture, and overprinted crenulation cleavage (Fig. 2-8). Blocky muscovite crystals commonly occur as pseudomorphs after sillimanite. In some parts of the Inner Piedmont, sillimanite schist has been noted to be devoid of muscovite, where sillimanite replaces muscovite (Merschat, 2003; Bier, 2001; Gatewood, 2007; Wilson, 2006). Sillimanite schist has an overall lepidoblastic and/or nematoblastic texture, and is generally thinly to thickly layered, mostly garnetiferous; feldspar alteration to sericite is commonly present in thin-section and hand specimen.

The mineral assemblage of the sillimanite schist in the Brindle Creek thrust sheet includes sericite, ilmenite, chlorite, biotite, muscovite, sillimanite, quartz, and plagioclase (An_{15-25}), with trace amounts of epidote, apatite, zircon, and tourmaline. Zircon occurs as an accessory mineral (Table 2-1). Two types of sillimanite were noted in thin section, both fibrolite and elongate prismatic crystals. The sillimanite ranges in size from ~ 1 mm (fibrolitic) to 3 mm (prismatic). Fibrolitic sillimanite is generally located on the interior of muscovite crystals, and prismatic sillimanite is seen in all samples. In thin section, the sillimanite is commonly located close to muscovite crystals, unless muscovite is absent in that particular thin section. In one sample devoid of muscovite, fibrolitic and prismatic sillimanite are wrapped around garnet porphyroblasts (Fig. 2-9). Muscovite crystals have two distinct orientations: one that reflects the dominant S_2 foliation, and one that is oriented perpendicular to the dominant foliation. Porphyroblastic garnets are generally fractured and rotated. Subhedral to anhedral garnets contain inclusions of biotite, sillimanite, quartz, and plagioclase, and reflect an overall poikilitic texture. In some instances, the garnets have been so severely deformed that portions of the original porphyroblasts are included in the dominant foliation.

Metagraywacke (metapsammite)

Metagraywacke is the other of the two dominant rock types in the Brindle Creek thrust sheet, and is primarily composed of biotite, quartz, plagioclase (An_{15-25}), and K-feldspar. There are two distinct northeast-trending bands of metagraywacke that outcrop adjacent to the zone of granitoids and the sillimanite schist (Fig. 2-1). Generally, metagraywacke has a greater quartz

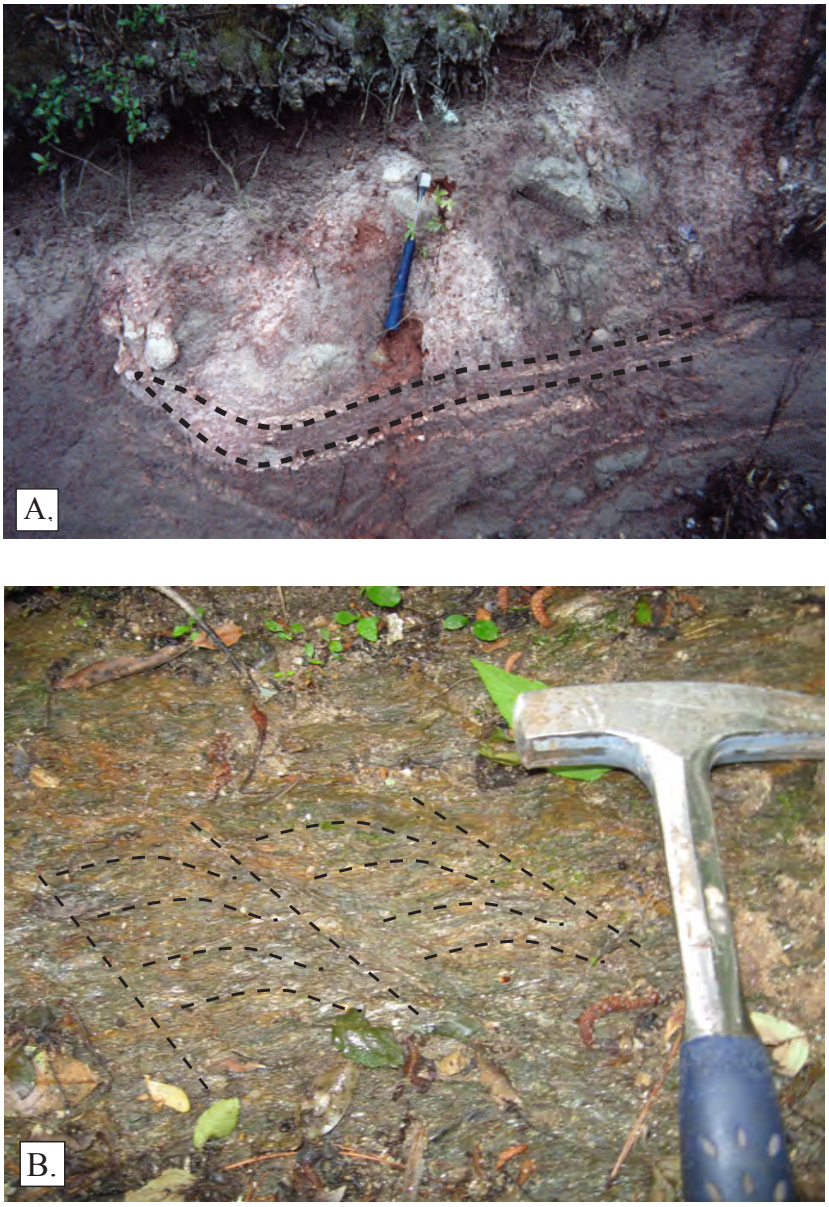

Figure 2-8. A. Leucocratic layer in sillimanite schist outcrop. Sillimanite weathers to a silvery-blue color and the leucosome layer weathers to a popcorn texture. This outcrop can be seen at the intersection of Murder Creek Church Rd. and Clybell Rd. Photo taken facing east. B. S-C fabric in sillimanite schist. This outcrop can be seen east of Jeffries Rd. in a tributary of Pittman Creek. Photo taken facing north. Rock hammer for scale.

Table. 2-1. Point-counted samples of sillimanite schist from the Brindle Creek thrust sheet.

Sample ID	M-24	F-229	F-1219
Unit	Sillimanite Schist	Sillimanite Schist	Sillimanite Schist
Tectonic Unit	EIP	EIP	EIP
Points Counted	1000	1000	1000
Plagioclase	27.5	30.9	30.4
Quartz	8.1	4.2	7.9
Microcline	0	0	4
Biotite	0.9	14.6	4.6
Muscovite	36.4	32.5	0
Chlorite	0.2	0.2	0.1
Sillimanite	14.7	14.8	25.3
Apatite	0.2	0	0.9
Epidote	0.4	0.1	0.6
Tourmaline	0.1	0.1	0
Garnet	10.8	0	22.5
Sericite	0.1	2	2.4
Zircon	0	0	0.1
Opaques	0.6	0.6	1.2
Total	100	100	100

Note: Trace represents <0.1% of mode. Stage step size was 0.1 mm for all of the thin sections listed above.

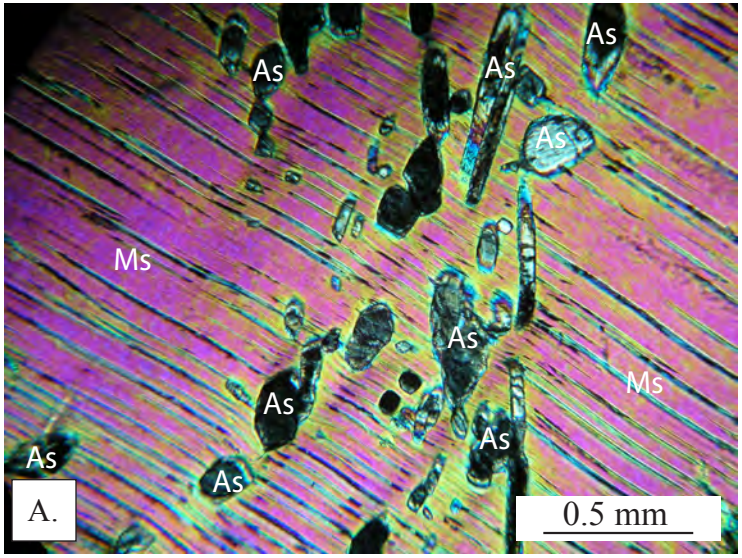

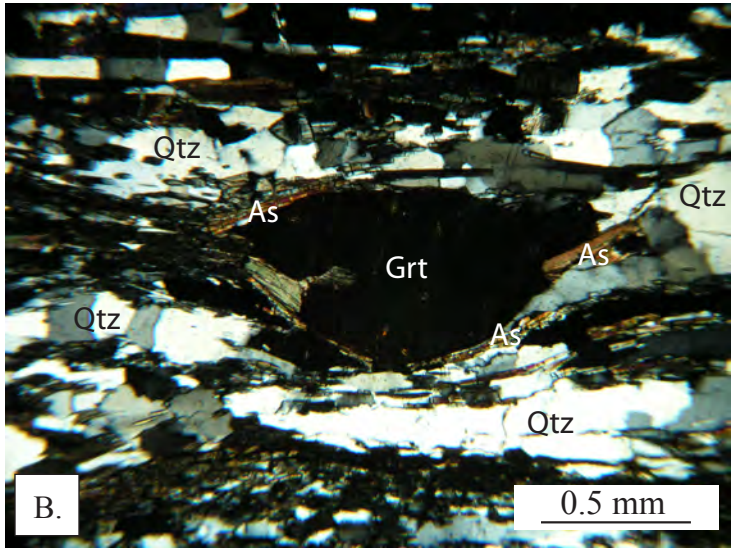

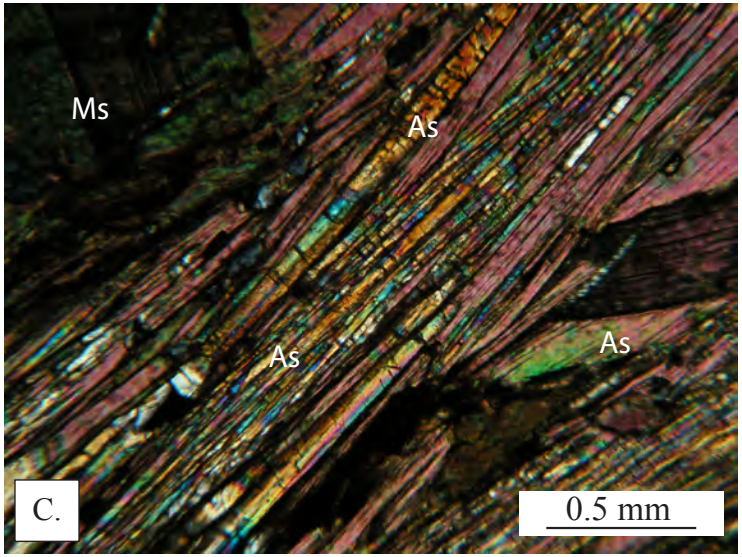

Figure 2-9. Photomicrographs of sillimanite schist (cross-polarized light). A. Prismatic sillimanite in a muscovite grain. Sample F-229. B. Garnet, surrounded by prismatic sillimanite. This sample contains little <0.1% muscovite and minor amounts of K-feldspar, suggesting sillimanite II grade metamorphism. Sample M-24. C. Prismatic sillimanite surrounded by muscovite grains. Interference colors appear to be third-order pink to orange. Sample F-1219. As-Sillimanite. Ms-Muscovite. Qtz-Quartz. Grt-Garnet.

content than biotite orthogneiss. Metagraywacke ranges from thinly to thickly layered, appears light gray to dark gray in fresh outcrop, and is gradational into and interlayered with the sillimanite schist. Depending on iron content, this unit generally weathers from a light to dark reddish brown color (Fig. 2-10). Farrar quadrangle metagraywacke appears to be compositionally similar to Cat Square terrane metagraywacke located in the Brushy Mountains, North Carolina that plots as a graywacke-feldspathic sandstone-quartzose sandstone (Merschat and Kalbas, 2002; Gatewood, 2007) (Fig. 2-11). Mineral assemblage includes plagioclase, biotite, microcline, ± hornblende, opaques, ± garnet, chlorite, and muscovite (Table 2-2). Zircon and apatite are accessory minerals.

There is ubiquitous migmatization; however, migmatization increases with proximity to the Brindle Creek and Rex Have faults. The quartzofeldpathic melt in the metagraywacke degrades to a light tan to a white colored saprolite, with a popcorn texture. Also dependent on proximity to shear zones is the grain size in the rock unit, which can range from fine- to coarse-grained, and it is generally inequigranular and porphyroblastic. Large tailed porphyroclasts of K-feldspar and plagioclase are commonly present in this unit, due to intense and pervasive simple shear.

Calc-Silicate

Calc-silicate generally occurs as boudins in the field area, and is commonly found as float. It is mostly found interlayered with the metagraywacke and sillimanite schist units, and does not appear at map-scale. The lack of calc-silicate provides some clue to the depositional environment of this particular area of the Cat Square terrane. Since calc-silicate is a metamorphosed carbonate rock, therefore, the depositional environment was most likely not a shallow environment.

In outcrop it is generally green, dark green, or gray in color. Foliation is commonly weakly to strongly developed.







Figure 2-10. A. Saprolite outcrop in metagraywacke unit. Sillimanite schist is the irredescent purple, metagraywacke is red to pink, leucosome is white, and amphibolite is orange. This outcrop can be seen at the intersection of Shepard Pond Rd. and Shepard Creek, in the Charlie Elliott Wildlife Center. Photo taken facing south. B. Amphibolite boudin and recumbent tight to isoclinal folds in metagraywacke outcrop; rock hammer for scale. Photo taken facing west. This outcrop can be seen in a tributary of Pittman Creek, just off Sewell Rd. C. Isoclinal fold in float; rock hammer for scale. This sample is at the same locality as B.

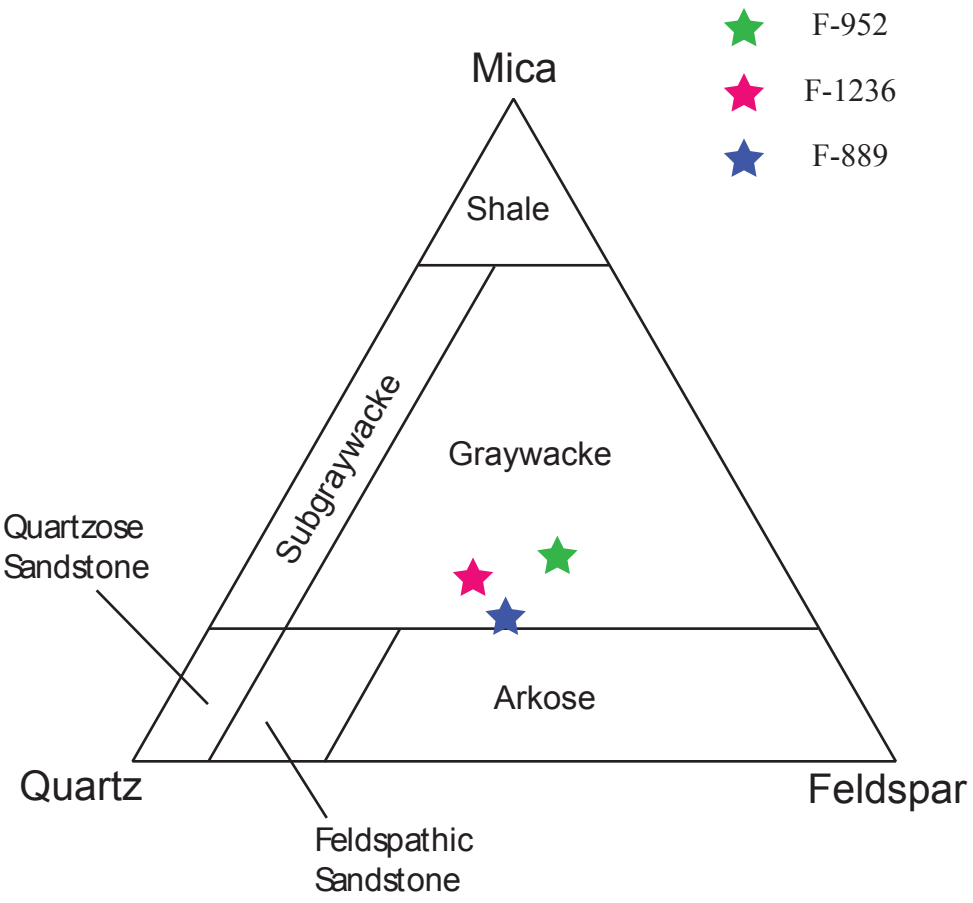

Figure 2-11. QFM diagram (Pettijohn, 1954) comparing the compositions of the metasedimentary rocks in the Cat Square terrane.

Table. 2-2. Point-counted samples of metagraywacke from the Brindle Creek thrust sheet.

Sample ID	F-952	F-1236	F-889
Unit	Metagraywacke	Metagraywacke	Metagraywacke
Tectonic Unit	EIP	EIP	EIP
Points Counted	1000	1000	1000
Plagioclase	28	30.2	26
Quartz	33.4	41.8	42.7
Microcline	11.4	0.4	2.8
Biotite	25	25.2	13.2
Muscovite	0.2	0.5	0.4
Chlorite	0.2	0.1	0.1
Epidote	0	0	4
Hornblende	0.4	0	8
Garnet	0	1.2	1.6
Opaques	1.4	0.6	1.2
Total	100	100	100

Note: Trace represents <0.1% of mode. Stage step size was 0.1 mm for all of the thin samples listed above.

Metaigneous Rocks

A felsic plutonic suite extends from the west edge to the north-central portion of the Farrar and Mansfield quadrangles (Fig. 2-1). They appear as discontinuous elongate bodies in the Brindle Creek thrust sheet, trending northeast-southwest. Three separate granitoid units have been recognized within this zone. The level of migmatization in the field area suggests near-melt conditions during prograde metamorphism and melt conditions in the case of the granitoids (Merschat, 2003; Wilson, 2006; Gatewood, 2007). The metamorphic conditions in this area indicate that, like the North Carolina Walker Top and Toluca granites, the granites in the Georgia Inner Piedmont may be anatectic in origin, originating from *in situ* melting of metasedimentary rocks of the Cat Square terrane (see Chapter 5). From field observations, it is believed that there is: (1) an early, strongly foliated, coarse-grained megacrystic granitoid (Murder Creek); (2) a later, weakly foliated, coarse-grained granitoid (Dow's Pulpit); and (3) a weakly foliated, fine-grained granitoid that appears to be the youngest of the three granitoids (Rocky Creek). Plutons in the field area have not been age dated, but detailed descriptions of thin sections and field observations are provided (Fig. 2-12). Two samples of the Murder Creek granite and two samples of the Rocky Creek granodiorite were geochemically analyzed (see Chap. 5).

Murder Creek Granite

The Murder Creek granite was named after Murder Creek, which runs northwest to southeast through the field area, and empties into the Little River along the Putnam and Baldwin counties border. According to local representatives, Murder Creek was so named for a series of murders that took place during the early 1800s. The history of the area is somewhat sketchy, and the names of the victims are unknown, although it is thought to have involved a family by the name of Findley.

The Murder Creek granite is a moderately to strongly foliated megacrystic granite. It contains both subhedral to euhedral K-feldspar (microcline) megacrysts that range in size from 1.0 to 6.0 cm and anhedral to subhedral plagioclase megacrysts that range from 1.0 to 2.0 cm in size (Fig. 2-13). Microcline megacrysts display carlsbad twinning and irregular cross-hatch twinning. Both albite and carlsbad twinning can be seen in the plagioclase crystals, along with

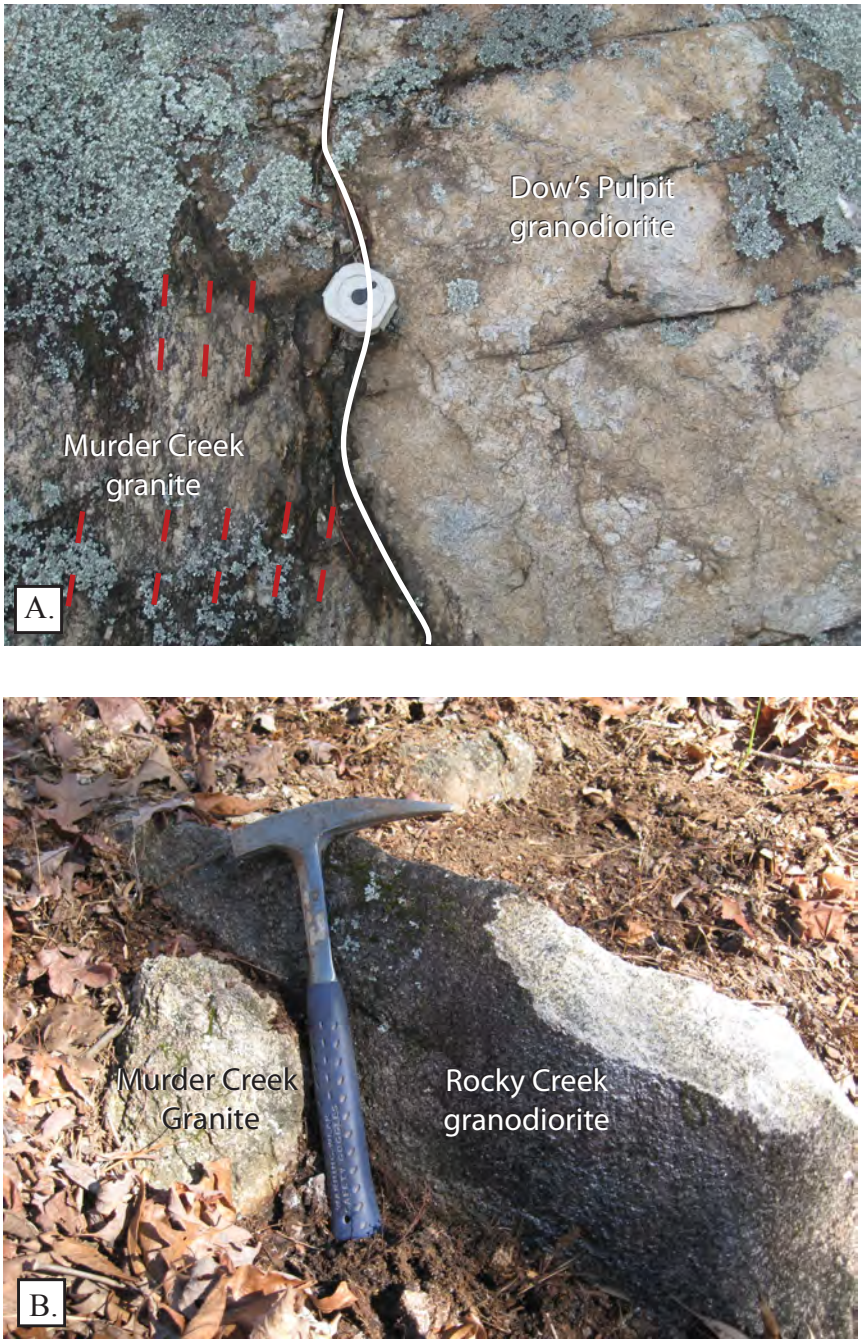

Figure 2-12. A. Dow's Pulpit granodiorite crosscutting Murder Creek granite. Dashed red lines represent foliation. Brunton for scale. B. Rocky Creek granodiorite crosscutting Murder Creek granite. Brunton for scale. These outcrops can be seen along a trail that heads west from the Charlie Elliott Wildlife Center. Eastern portion of the Farrar quadrangle.

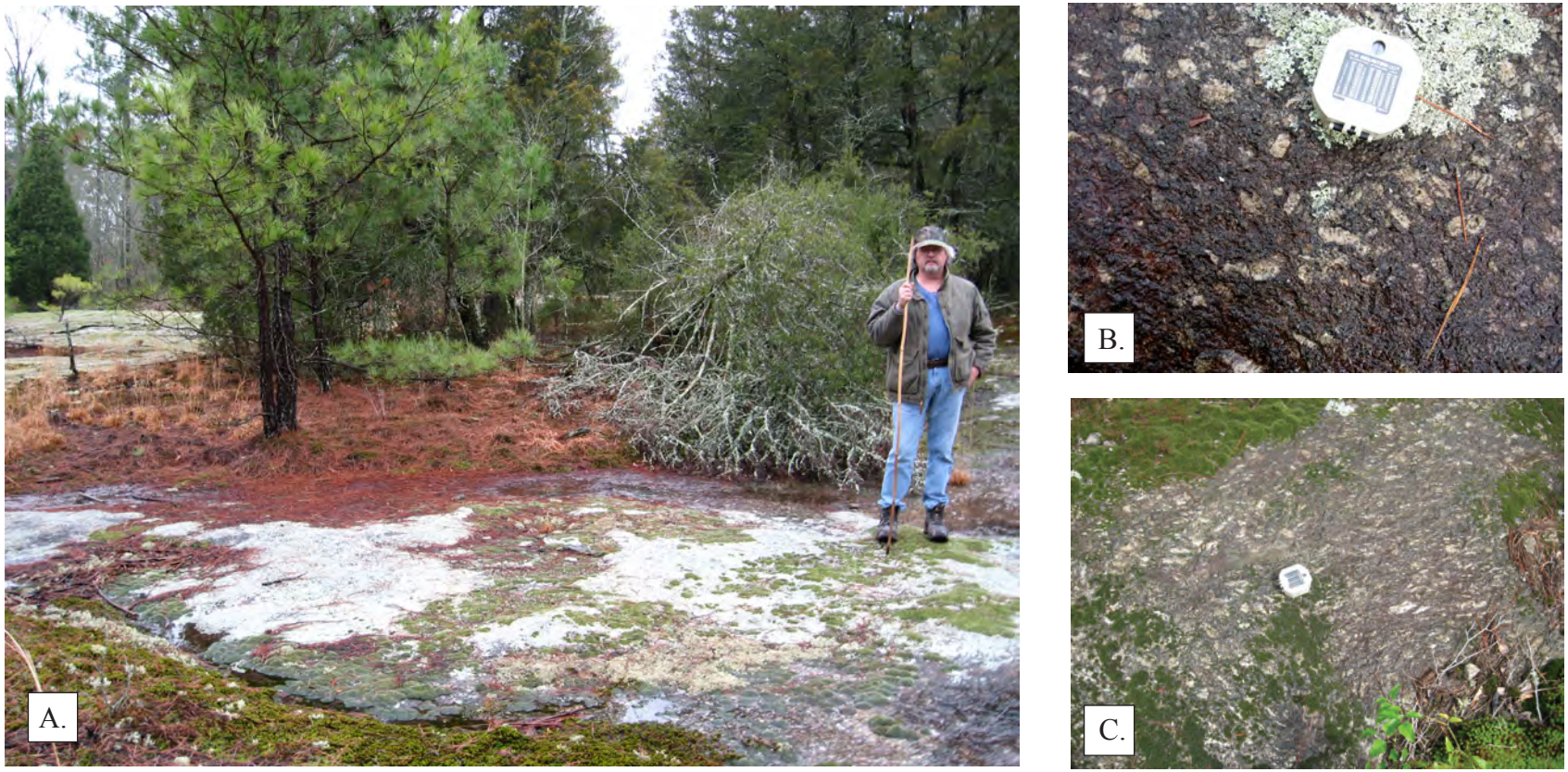

Figure 2-13. A. Pavement outcrop of Murder Creek granite. Some species of pine, shrubs, and moss live specifically on these pavement outcrops. Philip Davis for scale (6 ft. 1 in.). B. Poorly foliated Murder Creek granite with poorly aligned megacrysts. Megacrysts are K-feldspar grains with Carlsbad twinning. C. Well-foliated Murder Creek granite with strongly aligned megacrysts. All of the above can be found along a trail that leads directly west from the Charlie Elliott Wildlife Visitors' Center. Eastern portion of the Farrar quadrangle.

undulatory extinction. Many of the plagioclase crystals in thin section appear to be untwinned as well, and have a dusty appearance. These megacrysts are surrounded by an equigranular matrix that contains amounts of opaques, ± chlorite, ±hornblende, epidote, muscovite, sericite, biotite, microcline, quartz, and plagioclase (An_{35-43}). Trace minerals include zircon, myrmekite, perthite, and apatite (Table 2-3). Myrmekite of quartz in plagioclase can readily be seen in thin section (Fig. 2-14).

Murder Creek granite commonly outcrops as pavement and weathered boulders, and exposure is very good in this unit. Depending on biotite content, this rock appears light to dark gray in outcrop. Saprolitic outcrops of Murder Creek Granite weather to a dark red color, and appear very similar to weathered metagraywacke. Megacrysts of microcline and/or plagioclase are commonly well perserved in saprolite, allowing distinction to be made between the granite and metagraywacke (Fig. 2-15).

The Murder Creek granite shares many similarities (such as texture, mineralogy, and tectonic setting) with the Walker Top Granite of North Carolina, and the Anderson's Mill Gneiss, in Spartanburg, South Carolina (Curl, 1998; Kalbas, 2003; Wilson, 2006; Merschat, 2003). The Murder Creek and Walker Top granites are located in the Brindle Creek thrust sheet. In North Carolina, the Walker Top Granite was originally correlated with the Ordovician Henderson Gneiss (~492 Ma, U-Pb SHRIMP) (Goldsmith et al., 1988; Vinson, 1999). This original correlation was based on both granites containing K-feldspar megacrysts; however, recent geochronological data refute this original concept. U-Pb SHRIMP age dating of Walker Top Granite from various localities in North Carolina yielded ages of ~407, 406, 356, and 325 Ma, indicating an Early Devonian to late Mississippian formation (Mapes, 2002; Gatewood, 2007; Byars, 2009). An ion microprobe U/Pb zircon crystallization Neoacadian age of 366±3 Ma was reported by Mapes (2002). The variation in ages from Early Devonian to late Mississippian of the Walker Top Granite most likely indicates that there was diachronous *in situ* melting of the Walker Top protolith and/or that the zircons were reset during Neoacadian metamorphism (Wilson, 2006).

When first documented, Walker Top Granite was described as a non-mylonitic orthogneiss that contained weakly aligned plagioclase (5%) and microcline (95%) megacrysts

Table. 2-3. Point-counted samples of Murder Creek granite, Rocky Creek granodiorite, and Dow's Pulpit granodiorite from the Brindle Creek thrust sheet.

Sample ID	MC	F-410	F-1095	F-1337	F-435	F-1330	F-554
Unit	Murder Creek	Murder Creek	Murder Creek	Rocky Creek	Rocky Creek	Dow's Pulpit	Dow's Pulpit
Tectonic Unit	EIP	EIP	EIP	EIP	EIP	EIP	EIP
Points Counted	1000	1000	1012	1090	1048	1000	1000
Plagioclase	23.6	18.8	34.4	33.9	40.8	36.5	33.9
Quartz	32.4	42.4	22.5	27.5	34.7	31.0	28.6
Microcline	29.6	22.6	19.8	15.6	5.7	19.0	14.4
Biotite	7.6	6.4	19.4	9.2	8.4	4.8	5.6
Muscovite	1.6	1	0.8	2.8	1.1	2.4	9.6
Chlorite	0	1.2	0	1.7	0.4	0	0
Apatite	0.6	0.2	0	2.0	0.4	0.8	0.4
Sphene	0	0	0	2.8	2.3	0.4	2.4
Epidote	1	2.4	2.0	0	5	0.8	1.2
Hornblende	0	1.4	0	1.4	0.4	0.8	0.8
Garnet	0	0	0	0	0.1	0	0
Sericite	2.2	1.8	0	1.1	0.3	3.2	1.6
Zircon	0	0.2	0.4	0.8	0.2	0.3	0.3
Myrmekite	0.7	0	0	0	0.2	0	0
Perthite	0.3	0	0	0	0	0	0
Opaques	0.4	1.6	0.8	1.1	0.3	0	1.2
Total	100.0	100.0	100.1	99.9	100.3	100.0	100.0

Note: Trace represents <0.1% of mode. Stage step size was 0.1 mm for all of the thin samples listed above.

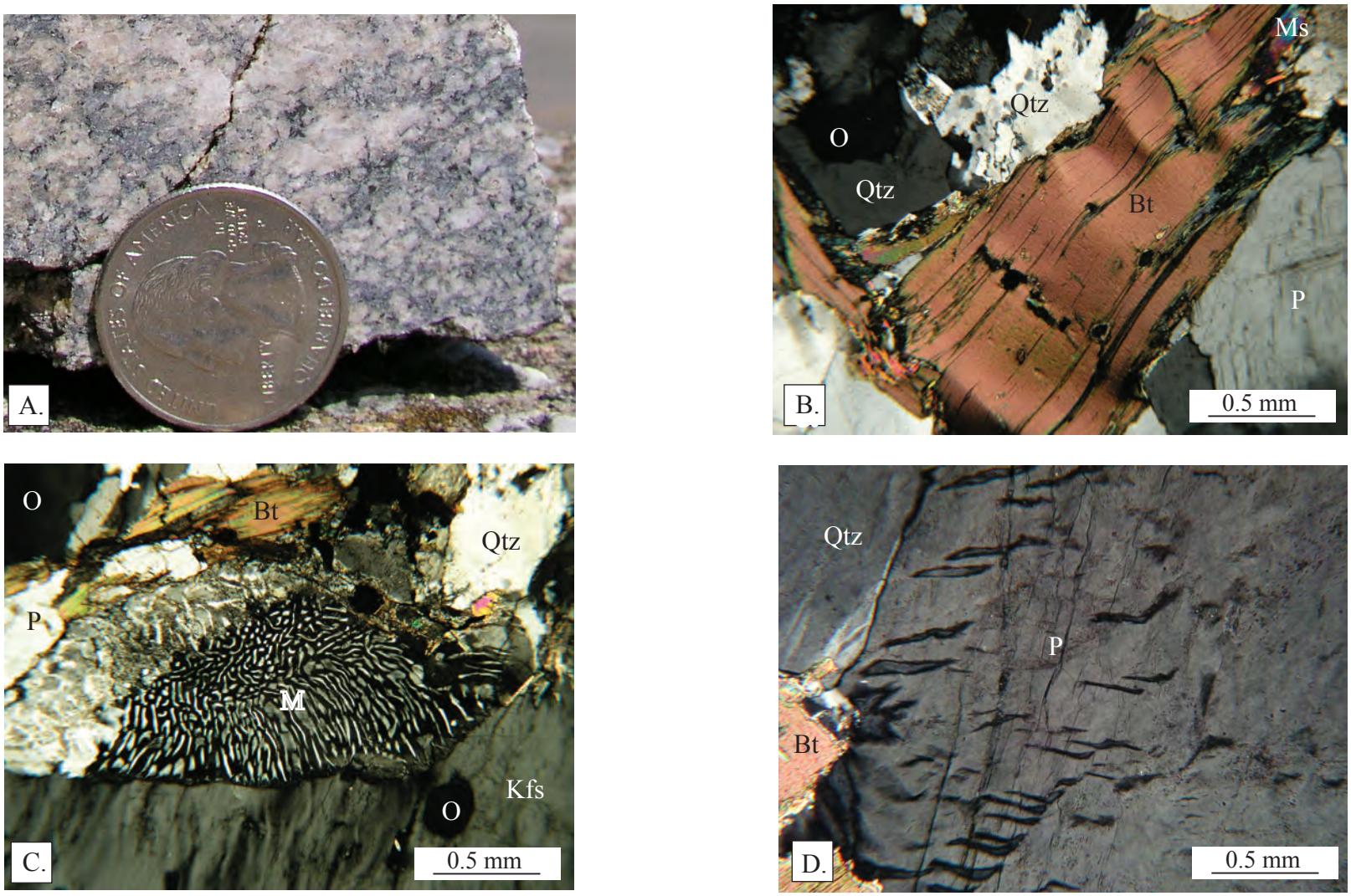

Figure. 2-14. A. Murder Creek Granite. Photomicrographs of Murder Creek Granite (cross-polarized light). B. Note kinked biotite crystal. Sample F-410. C. Myrmekitic intergrowth. Sample F-410. D. En echelon tension gashes in plagioclase grain filled with quartz. Sample - MC. Qtz-Quartz. P-Plagioclase. O-Opaques. M-Myrmekite. Bt-Biotite. Ms-Muscovite. Kfs-K-

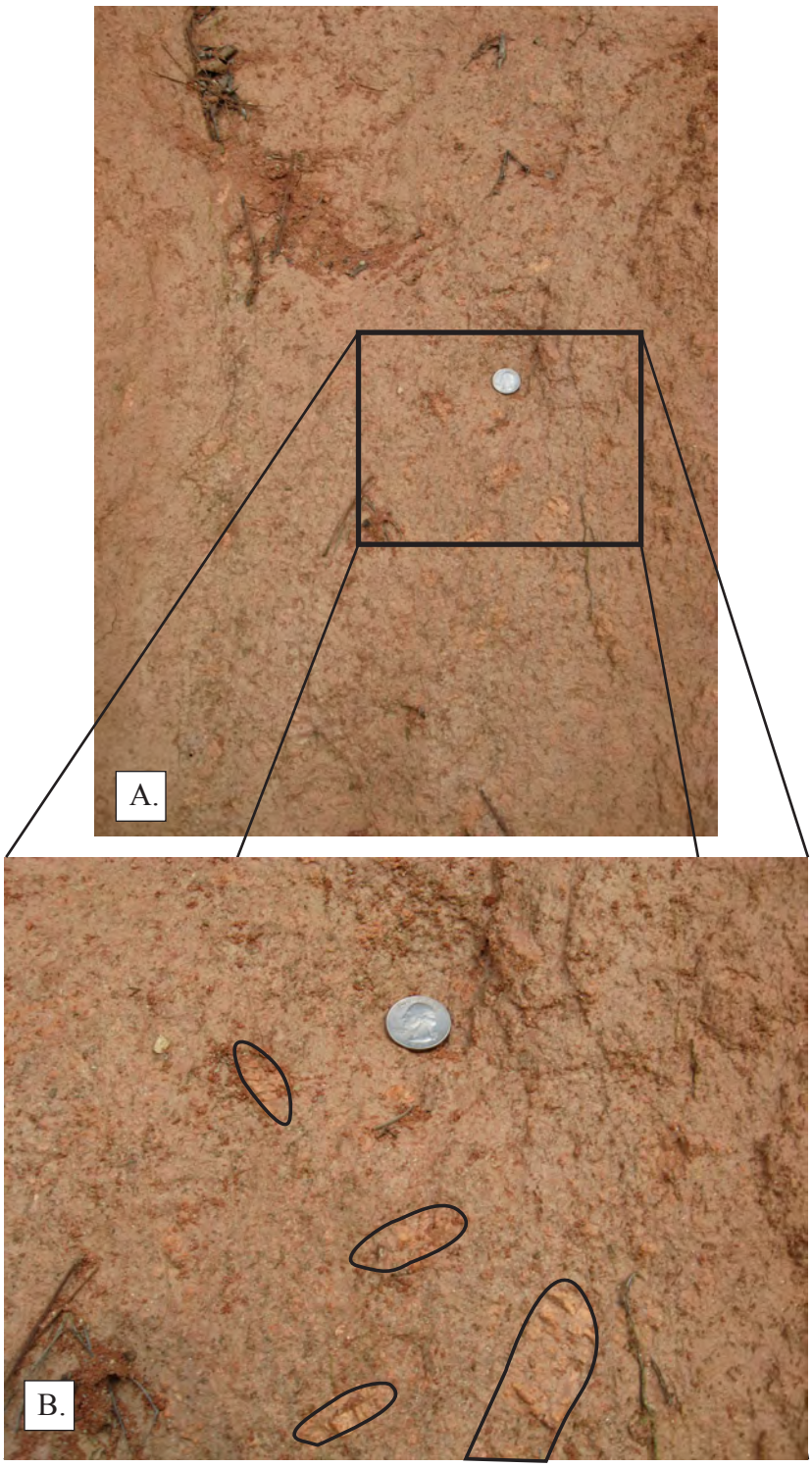

Figure 2-15. Note quarter for scale. A. Saprolite outcrop of Murder Creek Granite. B. Close up of a., note the outlined mega-crysts in saprolite. This outcrop is located on Church Road in Jasper Count, north of Murder Creek. Eastern portion of the Farrar quadrangle.

(Giorgis, 1999; Vinson and Miller, 1999; Bier, 2001; Mapes, 2002). This poorly developed alignment of megacrysts was attributed to original flow pattern in the pluton (Goldsmith et al., 1988). Discontinuous and continous northeast-southwest striking bodies of Murder Creek granite have been mapped through a portion of central Georgia. Areas containing both weakly and strongly aligned megacrysts are present in the Farrar and Mansfield quadrangles. Strongly aligned megacrystic Murder Creek granite generally correlates with the northeast-southwest regional foliation. Protomylonitic and mylonitic Murder Creek granite have been identified southwest of the Farrar and Mansfield quadrangles, in the Stewart and Lloyd Shoals Dam quadrangles. Where they contain more flattened and rounded K-feldspar megacrysts, some displaing well-developed tails (Huebner, unpub). The intensely deformed Murder Creek granite is located closer to the northeastern extension of the Towaliga fault (Huebner, 2009).

Dow's Pulpit granodiorite

The Dow's Pulpit granodiorite was so named from a monument erected for Lorenzo Dow, an evangelical minister. The same boulder from which Lorenzo Dow preached is displayed along Highway 11, just west of the Charlie Elliott Wildlife Center (Fig. 2-16).

Just as the Murder Creek granite resembles the Walker Top Granite identified in North Carolina, the Dow's Pulpit granodiorite resembles the Toluca Granite. Bier (2001) and Wilson (2006) described the Toluca Granite as a moderately to strongly foliated, fine- to coarse-grained, equigranular granite with occasional phases displaying a porphyritic texture with garnet or K-feldspar megacrysts (Bream, 2002; Kalbas, 2003). At map scale, the Toluca Granite appears as elliptical bodies that lie parallel with regional foliation. Foliation of the Toluca Granite does not always lie parallel to contacts, but instead appears to display some relict magmatic foliation (Bier, 2001; Wilson, 2006). Dow's Pulpit granodiorite appears within the same zone of granitoids as the Murder Creek granite, and has a less elongated shape. Dow's Pulpit granodiorite has a more bulbous form and from map and outcrop pattern, appears less deformed than the Murder Creek granite. Like the Toluca Granite, the Dow's Pulpit granodiorite displays both regional foliation and what may be a relict magmatic foliation. Similarities between the



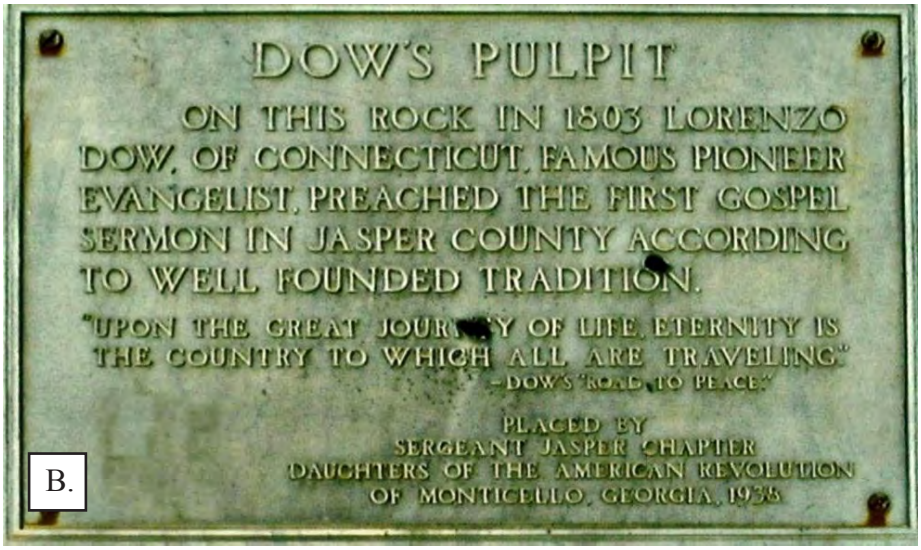

Figure 2-16. A. Dow's Pulpit. Bottom. Photo by Dr. Robert D. Hatcher, Jr. B. Close-up of plaque mounted on Dow's Pulpit.

Toluca Granite in North Carolina and the Dow's Pulpit granodiorite in central Georgia, namely the texture, mineralogy, and tectonic setting, suggest that they may be related.

The Dow's Pulpit granodiorite ranges from medium- (0.5-1.0 mm) to coarse-grained (1.0–4.0 mm) and weakly to strongly foliated, displaying tight to isoclinal folding in areas with strong foliation. It ranges from equigranular to inequigranular with a local porphyritic texture. Megacrysts of K-feldspar are most common, and microcline megacrysts display myrmekite rims. The mineral assemblage includes opaques, sphene, sericite, myrmekite, biotite, muscovite, microcline, quartz, and plagioclase (An_{10-14}), with trace amounts of epidote, apatite, and hornblende (Fig. 2-17) (Table 2-3). Zircon is an accessory mineral. According to the Streckeisen IUGS classification system, the Dow's Pulpit granodiorite is granitic to granodioritic in composition, but mostly granodioritic (Fig. 2-18). More often than not, Dow's Pulpit granodiorite is weakly foliated. Outcrops generally consist of exfoliated boulders or pavement outcrops. The Dow's Pulpit weathers to a tan colored sand or soil, and is readily distinguishable from metagraywacke, schist, and Murder Creek granite soils. Saprolite outcrops of Dow's Pulpit granodiorite are only useful for determining rock type, based on lack of a well-developed foliation.

Rocky Creek granodiorite

The Rocky Creek granitoid was named after Rocky Creek that runs adjacent to Rocky Creek Church outside of Mansfield, Georgia.

In the Farrar and Mansfield quadrangles the Rocky Creek appears mostly as dikes; however, in the adjacent Stewart quadrangle it occurs as massive discontinuous bodies (Fig. 2-19). Gatewood (2007) described an intrusive granitic body that crosscuts a body of Walker Top Granite that appears relatively undeformed in outcrop; however, closer examination reveals myrmekitic rims on K-feldspar, indicating a varying amount of strain, also crosscuts the penetrative S_2 foliation. Unfortunately, there are no photo pictures or a more detailed petrographic analysis of this particular intrusive body. According to Hatcher (personal commun., 2009), this granitoid is a fine-grained granitoid, much like the Rocky Creek granitoid. Sensitive

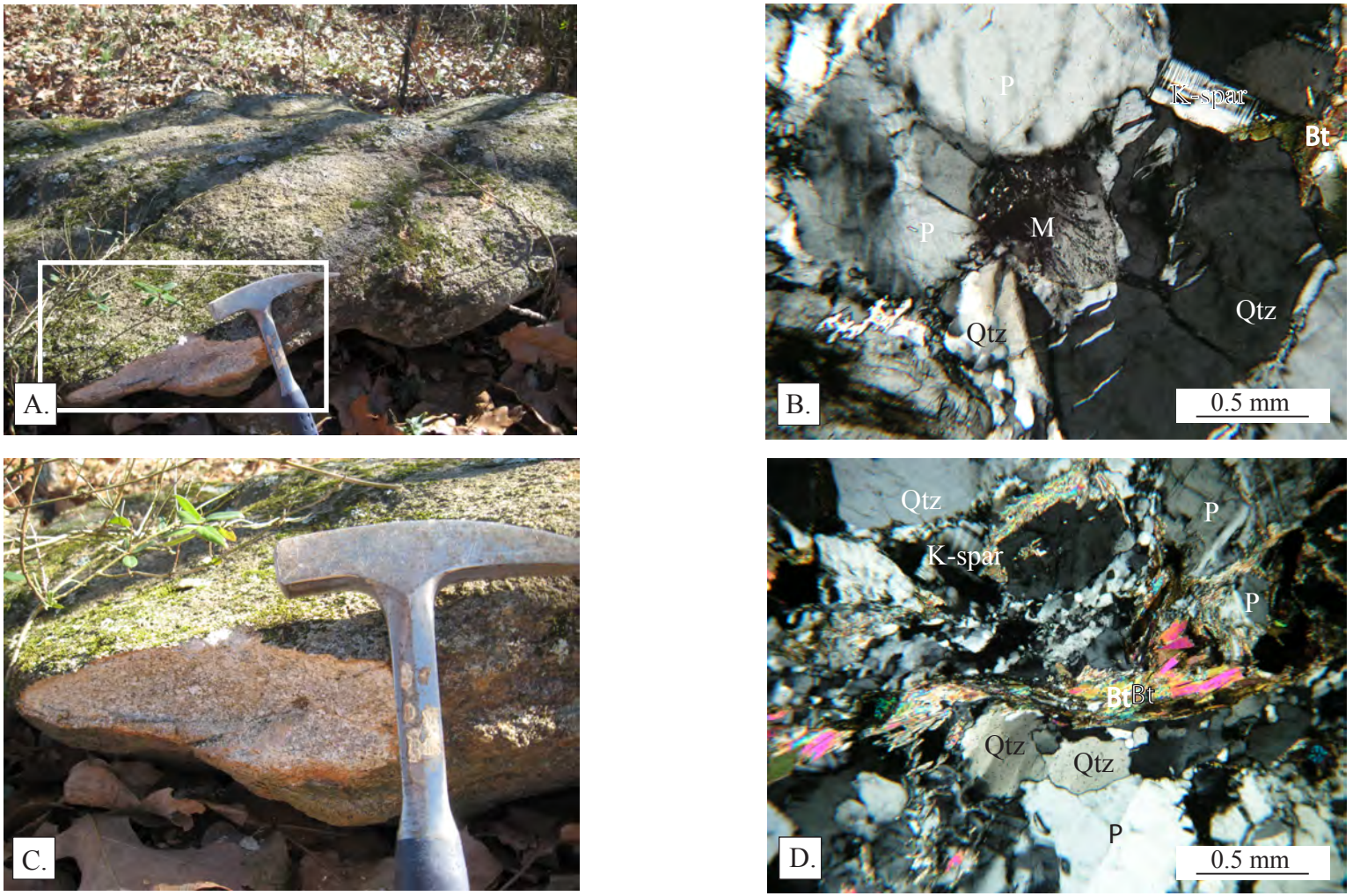

Figure 2-17. A. Dow's Pulpit granitoid B. Myrmekite C. Detail of (A). Coarse-grained and weakly foliated granitoid. D. Note weakly-developed foliation. Photomicrographs of Dow's Pulpit granitoid (cross-polarized light). Sample F-554. A and B are located at the intersection of Henderson and Benton Roads. Qtz-Quartz. K-spar-K-feldspar. P-Plagioclase.

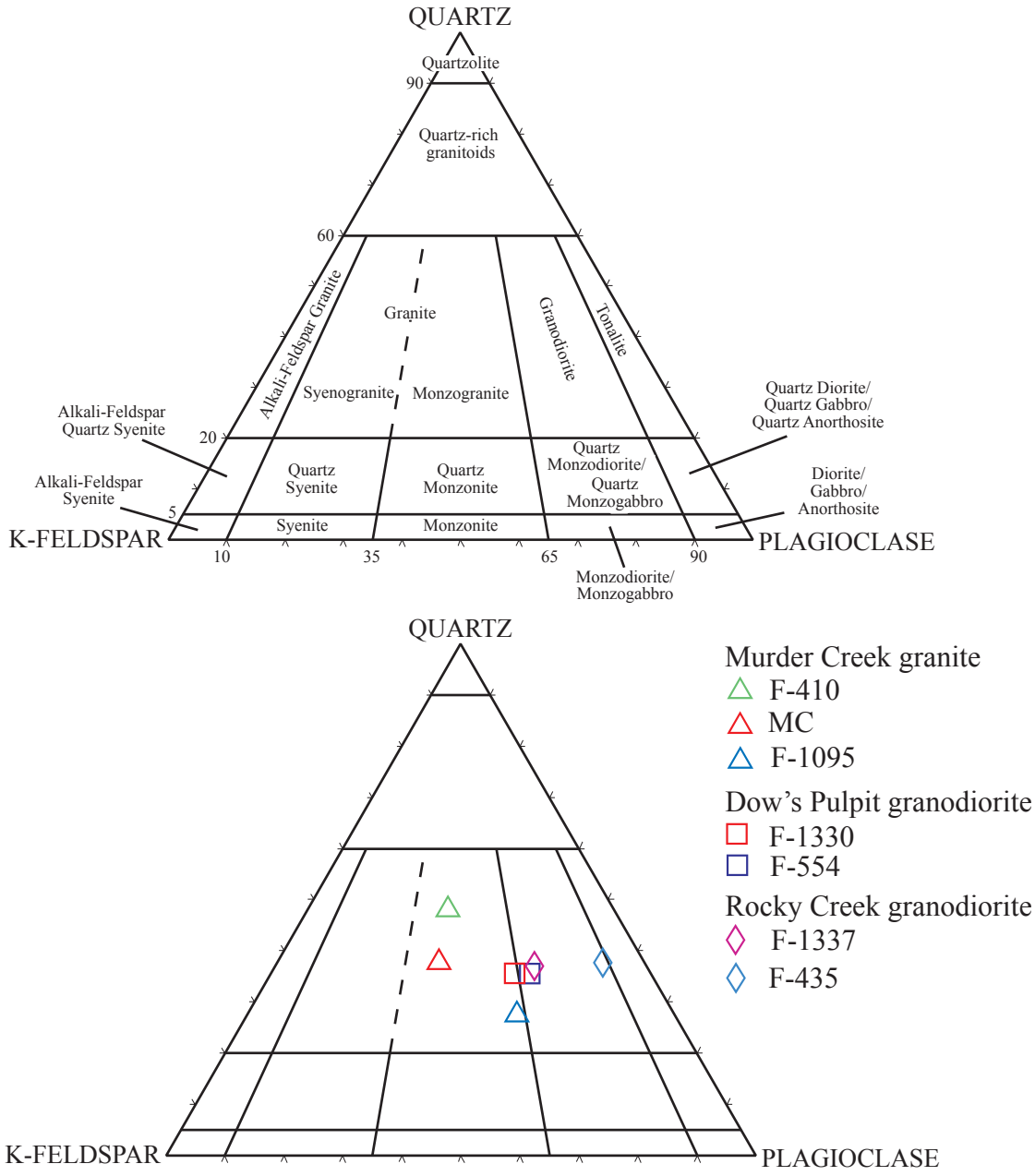

Figure 2–18. IUGS classification (Streckeisen, 1976) of Murder Creek, Dow's Pulpit and Rocky Creek samples.



Figure 2-19. A. Hand sample of Rocky Creek granodiorite. B. MC-Murder Creek. Large opaques are ilmenite with reaction rims of sphene. RC-Rocky Creek. Rocky Creek granodiorite in outcrop, here shown as a dike, intruding Murder Creek granite. Located along the eastern portion of the Farrar quadrangle.

high-resolution ion microprobe U-Pb analyses performed on this sample yielded an age range of 320-330 Ma.

Rocky Creek granodiorite is fine-grained and varies from weakly to moderately foliated. Mineral assemblage includes opaques, sericite, hornblende, chlorite, apatite, myrmekite, sphene, muscovite, biotite, microcline, quartz, plagioclase (An_{15-19}), and trace amounts of zircon (Table 2-3). Myrmekite also occurs along boundaries of K-feldspar (Fig. 2-20). Recognized commonly as dikes, the Rocky Creek granodiorite has been noted to cross-cut both Murder Creek and Dow's Pulpit plutons. Rocky Creek weathers to a tan-colored soil, making it difficult to trace contacts in saprolite exposures.

Cat Square terrane amphibolite

Amphibolite is common in the western Inner Piedmont where it occurs as pods, lenses, and as map-scale units in the lower metagraywacke-schist-amphibolite member of the Tallulah Falls Formation (Wilson, 2006). Amphibolite is ubiquitous in the Cat Square terrane, and occurs as small pods and boudins and, in some rare cases, as map-scale bodies. The amphibolite occurs most often in the migmatitic metagraywacke, and rarely in the Murder Creek and Dows Pulpit granitoids, where it is sometimes interlayered and other times found on the surface as float, because of its resistance to weathering. It is generally black to dark green in color. Amphibolite can often be seen in saprolite outcrops throughout the field area as light to dark orange, layers and boudins which can easily be distinguished from the interlayered leucosome, metagraywacke, and sillimanite schist saprolite (Fig. 2-21). Five samples of amphibolite from the eastern Inner Piedmont (Brindle Creek thrust sheet) portion of the field area were analyzed petrographically and geochemically (see Chap. 4). All of these samples were collected in the metagraywacke and sillimanite schist units of the Cat Square terrane.

The texture, fabric, and grain size of the amphibolite varies drastically from one sample to another: from fine to medium-grained, weakly to strongly layered amphibolite that exhibits tight to isoclinal folding, to coarse-grained amphibolite that exhibits more of a granoblastic texture. The varying textures can be attributed to localized deformation, protolith mineralogy, and grain size. Modal analyses of five amphibolite samples, which were also geochemically

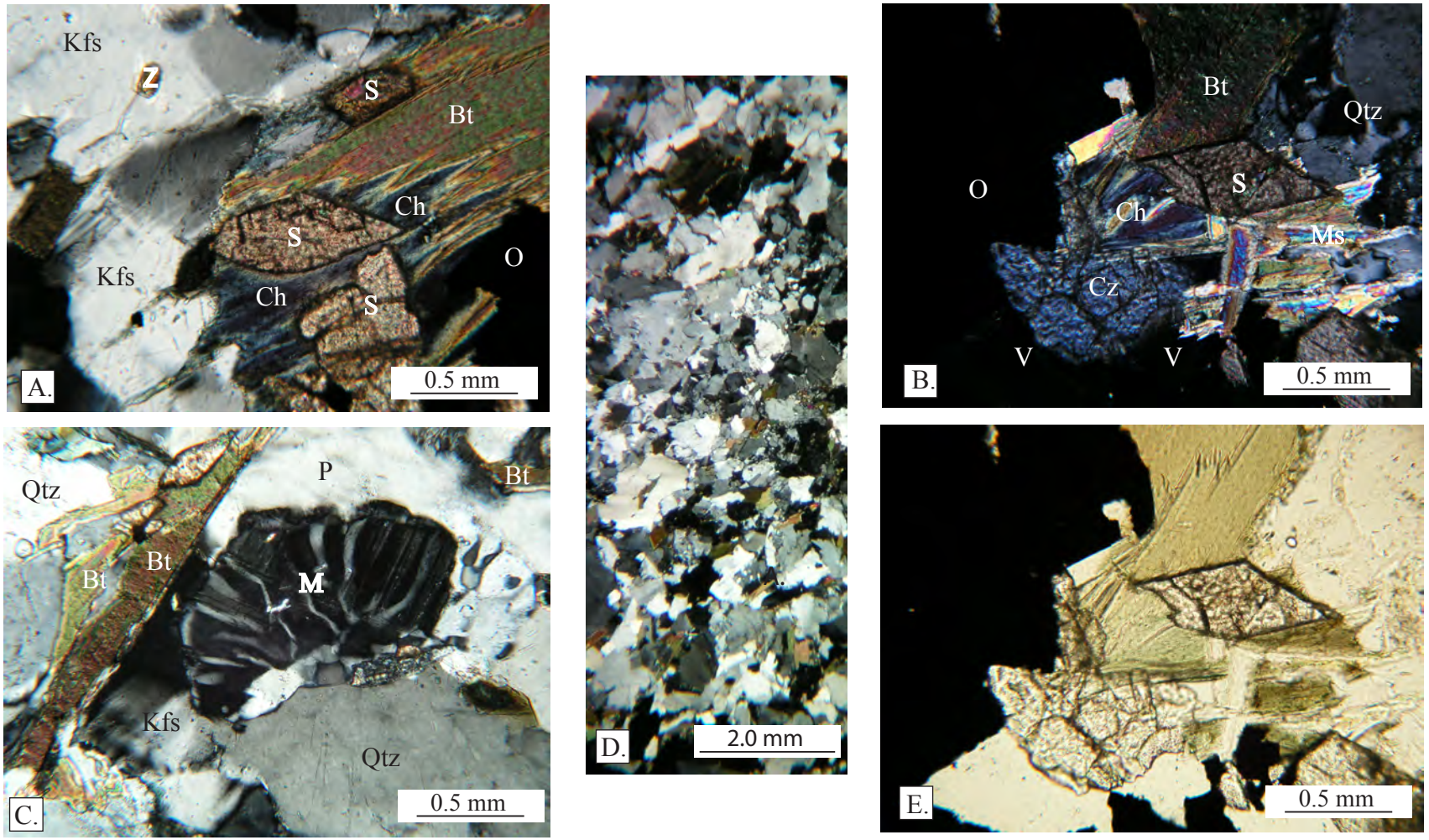

Figure 2-20. Photomicrographs of Rocky Creek Granite (Sample F-1337) (cross-polarized light). A. Note the euhedral sphene crystal and poikiloblastic texture. B. Myrmekite intergrowth. C. Low-power view of Rocky Creek granitoid in thin section. D. cross-polarized image of E. Plane light of D. Note euhedral sphene crystal partially enclosed by chlorite and biotite. Also, note large opaque mineral. S-Sphene. Qtz-Quartz. P-Plagioclase. O-Opaques. M-Myrmekite. Ch-Chlorite. Bt-Biotite. Ms-Muscovite. Kfs-K-feldspar. Z-Zircon. Cz-Clinozoisite. V-Void.



Figure 2-21. A. Amphibolite boudin. Rock hammer for scale. B. Amphibolite outcrop displaying tight to isoclinal folds. Vergence is toward the northeast. Rock hammer for scale. These outcrops can be found along Aldrige Road in the Farrar quadrangle.

analyzed, exhibit hornblende (10-53%) and plagioclase (An_{30-45}) (11-64%), with trace amounts of quartz, garnet, clinozoisite, sphene, opaques, and sillimanite (Table 2-4). Sample F-1296 exhibited the greatest garnet content (23%), with porphyroblastic garnets ranging in size from .5-4 mm in size. Samples M-235 and M-237 display minor amounts of clinozoisite with metamorphosed plagioclase grains around them (Fig. 2-22).

Mesozoic Rocks

Siliceous Cataclasite

Siliceous cataclasite extends 30˚NE-SW from the western edge of the Farrar quadrangle to the eastern edge of the Mansfield quadrangle (Fig. 2-1). It separates the zone of granitoids from metagraywacke located in the Brindle Creek thrust sheet. It is primarily composed of fine- to medium-grained quartz, with trace amounts present of feldspar, sericite, diopside, clinozoisite, and opaques. In outcrop, this unit appears white to tan in color, and often has a pink to red staining. Multiple episodes of deformation can be noted from the various sets of jointing and extensive brecciation (Fig. 2-23).

Siliceous cataclasite is very resistant to weathering and can be traced from topographic maps as a relatively linear structural feature. In the field, siliceous cataclasite is readily identifiable, and can be traced relatively easily from its northeastern trend. Siliceous cataclasite that has experienced multiple episodes of deformation appear to have a web pattern in hand sample. The joints are mostly filled with quartz. Younger cataclasite does not appear to have the web pattern, but is still pervasively jointed. In thin section, quartz crystals appear to have very little recovery and retain a mostly undulous texture.

Diabase Dikes

Three diabase dikes are located in the southwestern portion of the field area, and trend from northwest to southeast (Fig 2-24). They occur as small to large (<0.3 to >1 m in diameter) sized boulders, and generally occur as float. They appear black in boulder form and, when broken, display an orange weathering rind and are black on the interior. Diabase dikes are holocrystalline mafic rocks with a fine-grained ophitic texture. Diabase typically contain large

Table. 2-4. Point-counted samples of amphibolite from the Brindle Creek thrust sheet.

Sample ID	F-158	M-235	M-276	F-1296	M-288
Unit	Amphibolite	Amphibolite	Amphibolite	Amphibolite	Amphibolite
Tectonic Unit	EIP	EIP	EIP	EIP	EIP
Points Counted	1014	1019	1070	100	1004
Hornblende	66.1	64.2	47.3	60.6	25.9
Plagioclase	26.6	24.3	36.4	10.7	63.7
Quartz	2.6	1.0	2.4	1.6	2.0
Garnet	1.0	1.2	2.6	23.8	1.7
Epidote	1.4	0.1	1.4	0	0
Sphene	0.6	5.3	4.3	1.8	0.5
Microcline	0.7	3.1	0.6	0.2	2.4
Opaques	0.3	0.1	2.8	1.1	3.2
Sericite	0.4	0	0.2	0	0.4
Zircons	0.1	0.5	0.4	0	0
Zoesite	0.3	0.2	1.6	0.2	0.2
Total	100.0	100.0	100.0	100	100.0

Note: Trace represents <0.1% of mode. Stage step size was 0.1 mm for all of the thin samples listed above.

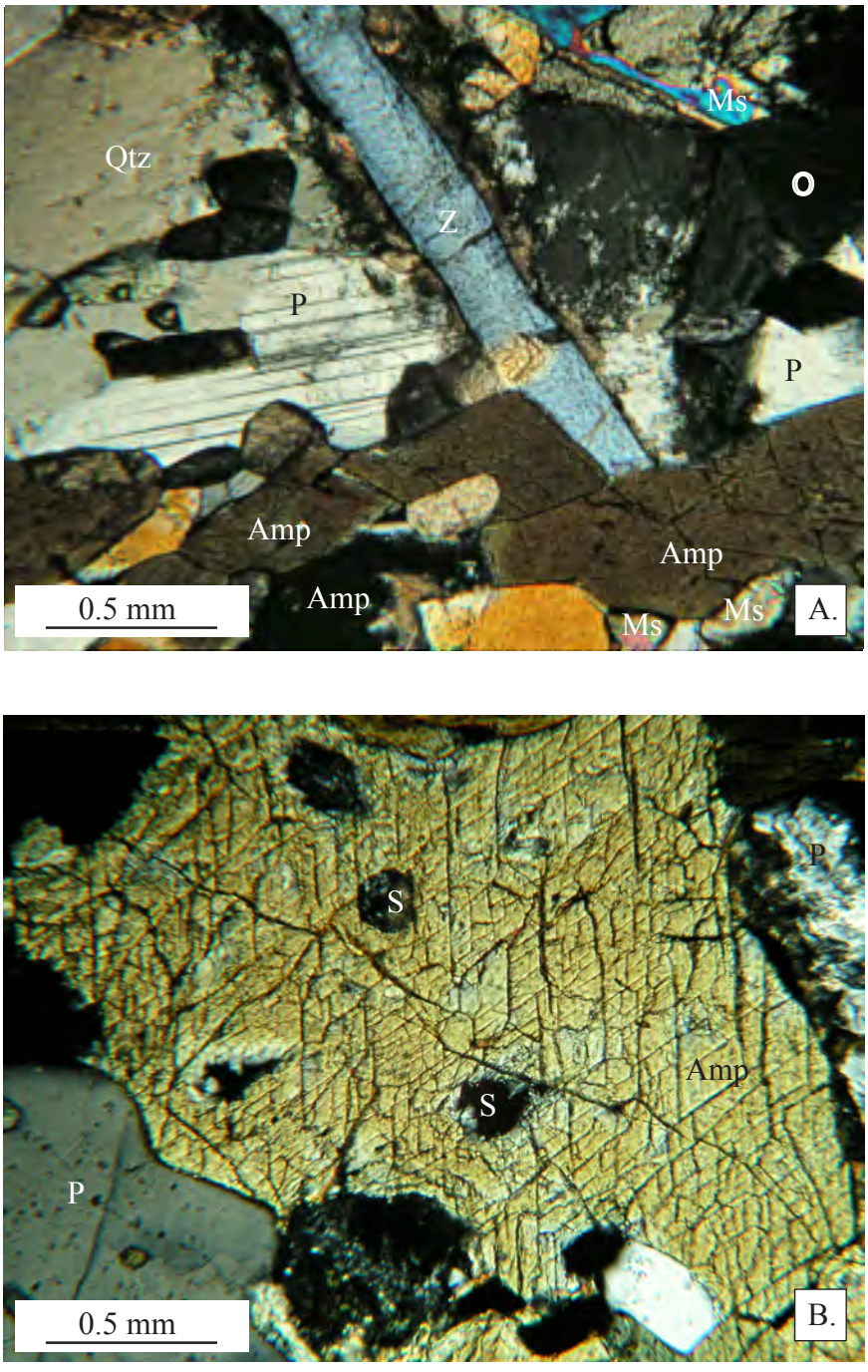

Figure 2-22. Photomicrographs of hanging wall amphibolites (Sample M-235) (cross-polarized light). A. Note zoisite surrounded by unidentified mineral. B. Note poikilitic texture, sphene inside hornblende crystal. S-Sphene. Qtz-Quartz. P-Plagioclase. O-Opaques. Ms-Muscovite. Amp-Hornblende. Z-Zoisite. U-Unidentified.

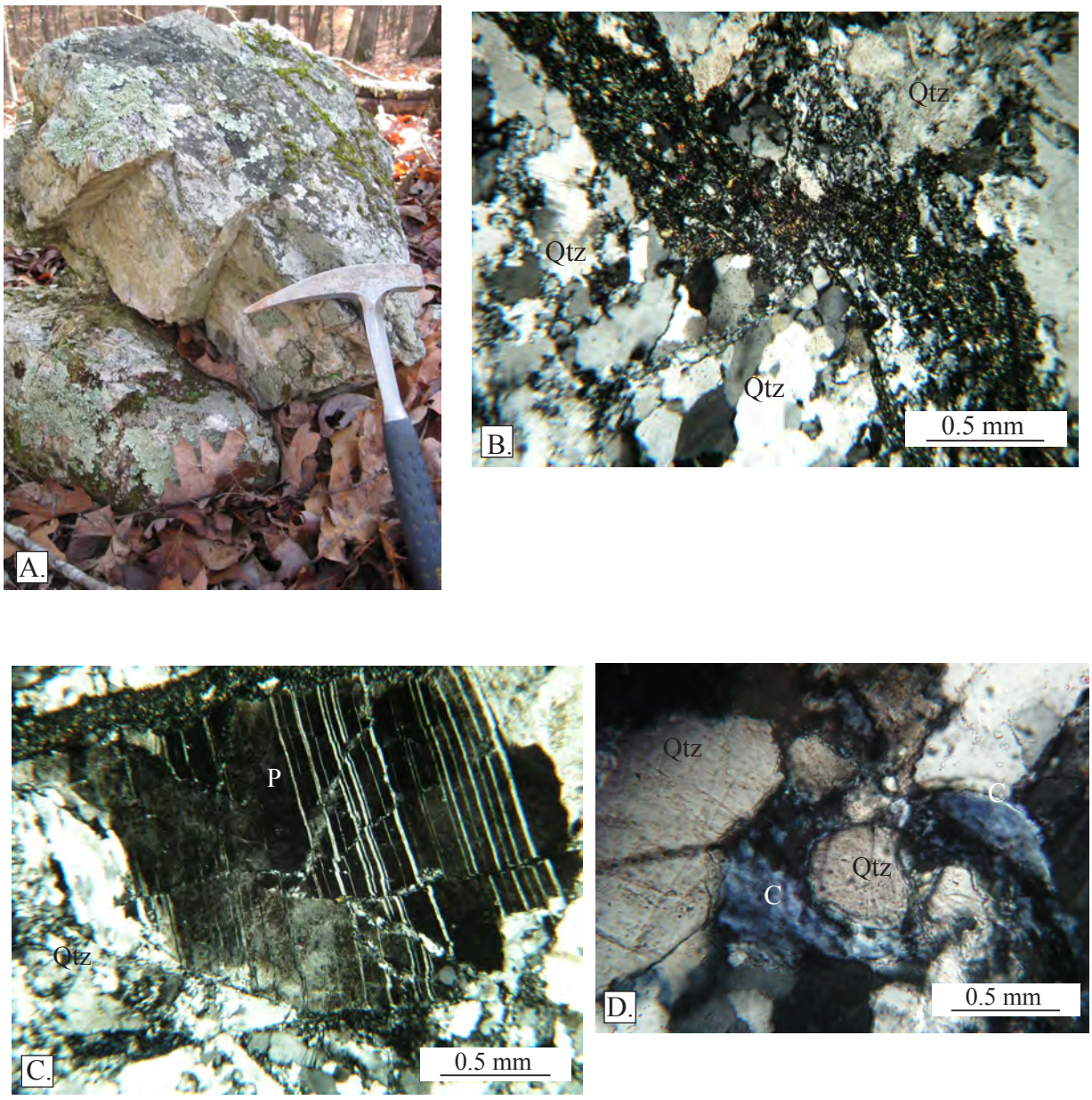

Figure 2-23. A. cataclasite exhibiting steeply dipping orthogonal jointing. Location is just south from Pittman Branch Creek, and west of Pitts Chapel Road. Photomicrographs are cross-polarized. Sample F-1182. B. Photomicrograph of quartz-filled fractured quartz vein. C. photomicrograph of quartz-filled fractured plagioclase crystal. D.Photomicrograph of clinozoisite. P-Plagioclase. Qtz-Quartz. C-Clinozoisite.

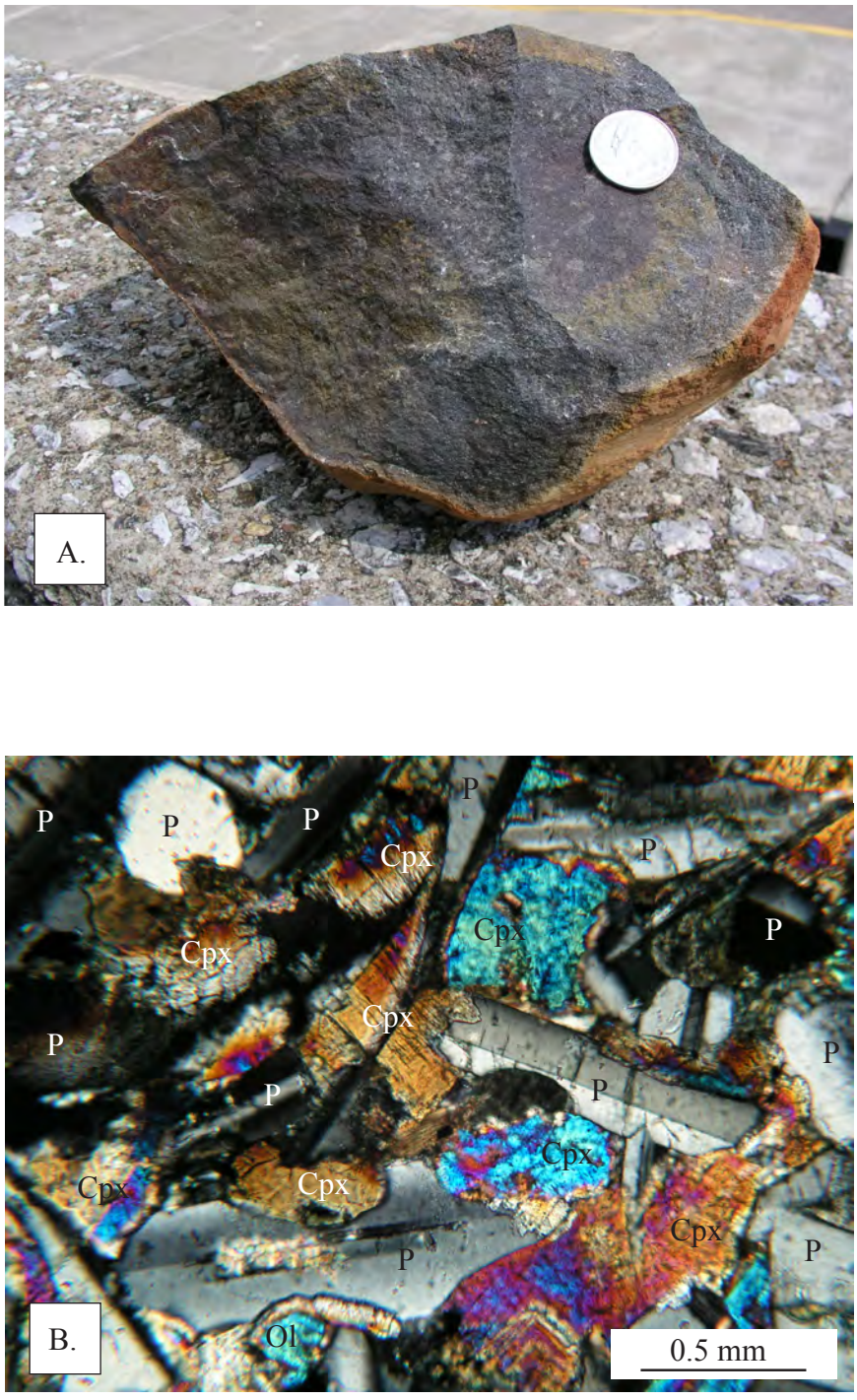

Figure 2-24. A. Boulder of diabase dike. Quarter for scale. B. Photomicrograph of laths of plagioclase and clinopyroxene crystals (cross-polarized light). Located in southwestern portion of the Farrar quadrangle. Note the subpoikilitic and ophitic texture. P-Plagioclase. Ol-Olivine.

amounts of euhedral plagioclase laths, and are surrounded by clinopyroxene (augite), olivine and opaques. Accessory minerals include: biotite, chlorite, and apatite.

Chapter 3: Metamorphism

Introduction

Mineral assemblages change drastically as rocks undergo solid-state reactions during progressive deformation and increasing P-T conditions. These reactions produce entirely new mineral assemblages that mostly erase original assemblages. Therefore, identifying mineral assemblages, index minerals, petrographic textures, and zoned minerals are keys to understanding the metamorphic history of an orogen, particularly in high-grade rocks located in the metamorphic core.

Identifying index minerals is important for determining metamorphic isograds in the field, but determining whole-rock assemblages plus index minerals is the first step in characterizing metamorphic grade and facies in an area. Metamorphic conditions can be refined to a P-T-t path through the use of phase-equilibria geothermobarometry, apatite fission tracks, radiogenic isotopes, zircon saturation temperatures, and thermochronology (Spear, 1993).

The combination of detailed geologic mapping and structural analysis, petrographic analysis, and geochronologic data has delimited the existence of the mid-Paleozoic (360-350 Ma) Neoacadian high-temperature orogenic event (Merschat et al., 2005). The purpose of this chapter is to present mineral assemblages and P-T estimates from biotite gneiss and amphibolite samples to further refine metamorphic conditions for the Cat Square terrane proposed by Merschat (2003), Wilson (2006), and Hatcher and Merschat (2006).

Regional Metamorphism

The majority of the southern Appalachian metamorphic core is dominanted by medium- to high-grade Neoacadian metamorphism with occasional inliers of Grenvillian granulite grade rocks east of the Brevard fault zone. The Inner Piedmont consists of southwest-vergent polydeformed antiformal Type-F thrust sheets or plastic nappes that are bound to the west by the Brevard fault zone and to the east by the Carolina superterrane (Hatcher, 2002).

The Inner Piedmont has the widest area of high-grade metamorphism in the southern Appalachians, and the core is dominated by sillimanite I grade metamorphism, along with muscovite-absent K-feldspar schist, indicative of sillimanite II grade metamorphism (Eq. 3-1). Inner Piedmont rocks are regionally metamorphosed to upper amphibolite facies assemblages (Bier, 2001; Bream, 2003).

$$KAl_3Si_3O_{10}(OH)_2 + SiO_2 = Al_2SiO_5 + KAlSi_3O_8 + H_2O \quad (3\text{-}1)$$

Muscovite + Quartz = Sillimanite + K-feldspar + Water

There is a decrease in metamorphic grade from the interior toward the flanks of the Inner Piedmont. Metamorphic grade increases eastward from the Brevard fault zone into the core of the Inner Piedmont ranging from garnet grade (in northwest South Carolina) to sillimanite I and higher (in North Carolina and South Carolina), then decreases to kyanite grade along the central Piedmont suture (Butler, 1991; Fig. 3-1). Sillimanite often occurs as pseudomorphs after muscovite, is ubiquitous throughout the field area, and is commonly found in both fibrolitic and prismatic form.

Timing

U-Pb dating of monazite and zircon metamorphic rims suggests peak metamorphism occurred in the Inner Piedmont during the mid-Paleozoic (360-345 Ma) (Bier, 2001; Bream, 2003; Merschat and Kalbas, 2002). Increases in temperature from cores to rims in garnets and single continuous garnet zoning profiles suggest that the Inner Piedmont underwent a single prograde metamorphic event (Davis, 1993; Bier et al., 2002; Merschat and Kalbas, 2002). Monazite and zircon metamorphic rims, however, yielded age clusters from 325-320 Ma; these ages most likely represent an early Alleghanian overprint (Dennis and Wright, 1997; Mirante and Patino-Douce, 2000; Carrigan et al., 2001; Merschat and Kalbas, 2002).

Figure 3-1. Metamorphic isograd map of the southern Appalachian Blue Ridge and Inner Piedmont compiled from various studies including (e. g., Hadley and Goldsmith, 1963; Carpenter, 1970; Hadley and Nelson, 1971; Rankin et al., 1972; Espenshade et al., 1975; Goldsmith et al., 1988; Merschat and Wiener, 1988; Eckert et al., 1989; Hopson et al., 1989; Butler, 1991; Hatcher and Goldberg, 1991; Quinn, 1991; Nelson et al., 1998; Settles, 2002; Higgins et al., 2003; Merschat, 2003; Tull and Holm, 2005; Hatcher and Merschat, 2006; Hatcher et al., 2007; Tull, 2007; Merschat et al., 2008). BCf–Brindle Creek fault. Bf–Burnsville fault. GLf–Gossan Leed fault. GMw–Grandfather Mountain window. CHMf–Holland Mountain fault. BFZ–Brevard fault zone. PMw–Pine Mountain window. SMw–Sauratown Mountains window. Modified from Merschat et al., 2008.

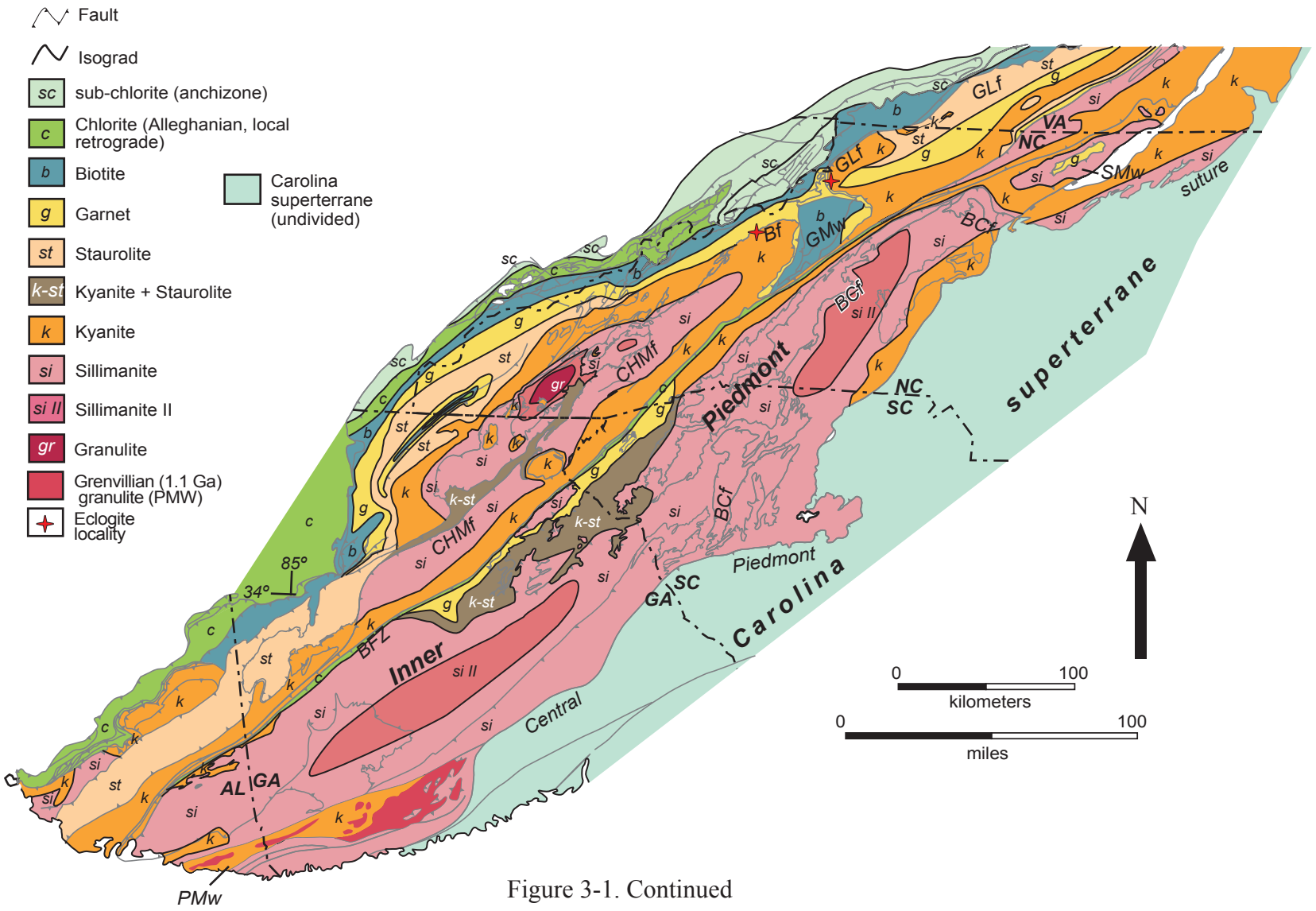

Figure 3-1. Continued

Migmatization

The Inner Piedmont has long been recognized as an area of widespread migmatization (Griffin, 1971; Hatcher, 2002). The interior portion of the Inner Piedmont is highly migmatitic, and migmatization decreases toward the flanks (Bier et al., 2002; Merschat, 2003). In the Brushy Mountains, North Carolina, increased migmatization in the footwall occurs closer to the Brindle Creek fault, suggesting that the Brindle Creek thrust sheet was emplaced hot (Williams, 2000; Merschat and Kalbas, 2002). Griffin (1974) also noted this trend in South Carolina. Migmatization also increases closer to the Brindle Creek fault in central Georgia.

Methodology

Three pelitic schist samples from the hanging wall were petrographically analyzed, and the mineral assemblage was recorded for each sample. One garnet-bearing biotite gneiss (sample F-1236) and one garnet-bearing amphibolite sample (sample F-1296) were collected from the Farrar quadrangle to obtain P-T estimates using an electron microprobe (Fig. 3-2). The biotite gneiss sample was collected along the trace of the Rex Haven (Kinnard Creek) fault. The amphibolite sample was collected from the interior portion of the Brindle Creek thrust sheet. Chips for the thin sections were prepared for both samples, and the final polished thin sections were prepared by Idaho Petrographics in Grangeville, Idaho.

Compositional analyses were performed by Allan Patchen at the University of Tennessee with the CAMECA SX 100 fully automated electron microprobe (EMP). All EMP data are reported in Appendix 1. Calibration of the EMP was performed with the use of both synthetic and natural materials, and analysis was conducted with a beam diameter from 1-5 microns along mineral transects. The EMP is also equipped with a wavelength dispersive spectrometer, which was used to obtain X-ray maps of both samples. These maps display variations in mineral chemistry and zoning in garnets.

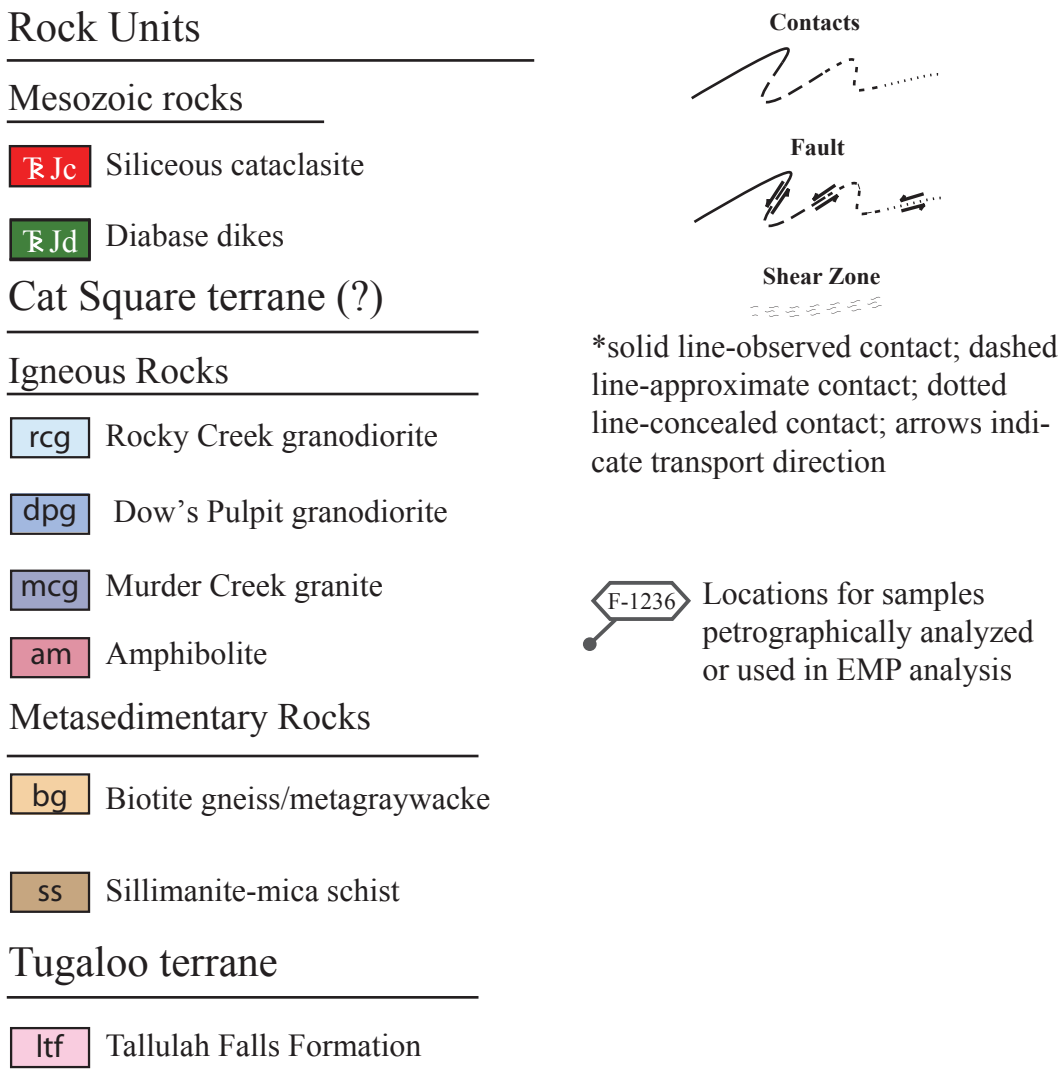

Figure 3-2. Simplified geologic map of portions of the 7.5-minute Farrar and Mansfield quadrangles and locations of pelitic schist petrographically analyzed, along with the amphibolite and biotite gneiss sample used in electron microprobe analysis.

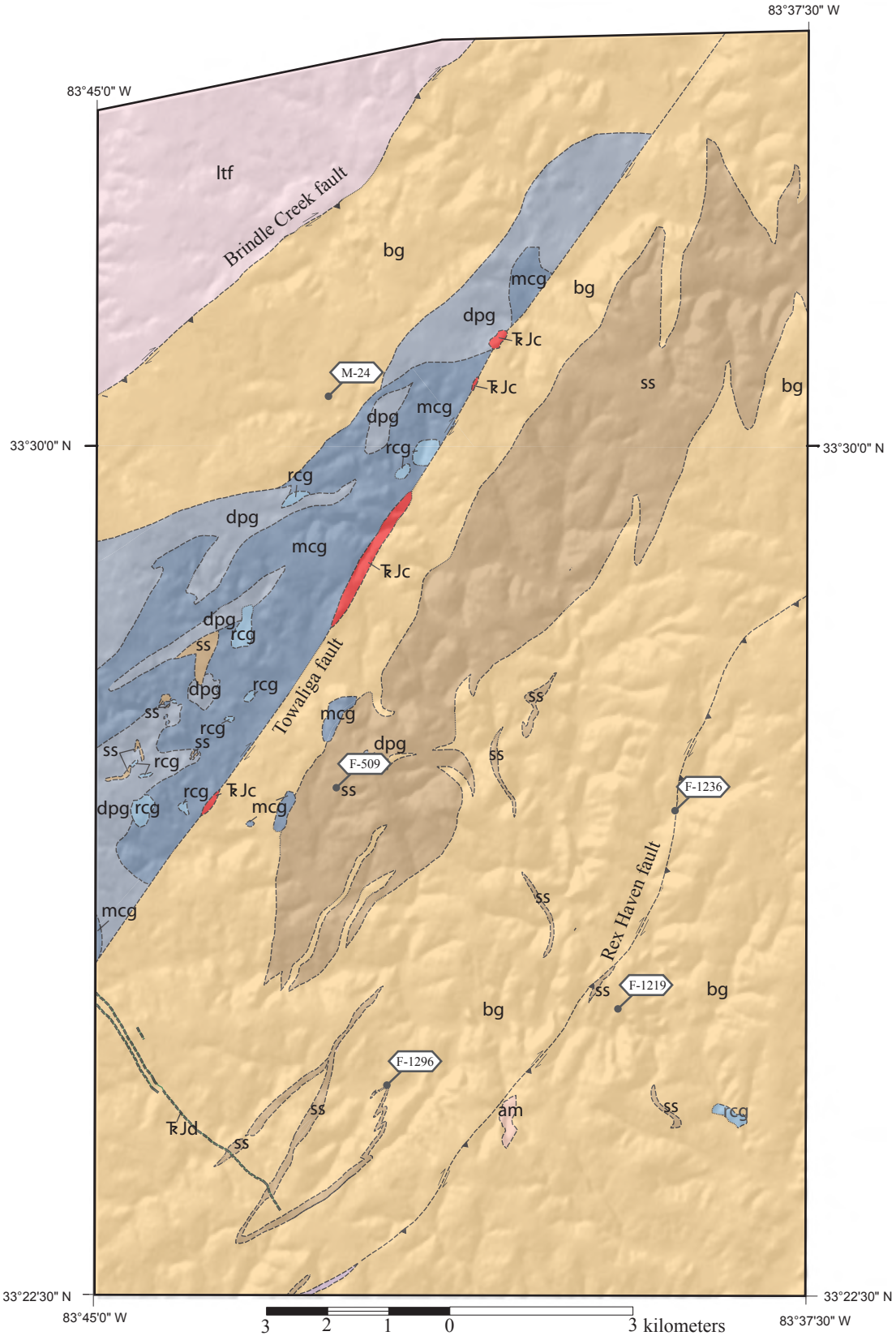

Figure 3-2. Continued

Pelitic Schist

Examination of mineral assemblages in thin section, combined with field observations reveal that there are three mineral assemblages in pelitic schists (Table 3-1). Assemblage A1 contains both muscovite and biotite.

Muscovite + plagioclase + sillimanite + biotite + quartz ± chlorite ± opaques (A1)

A2 assemblage is dominated by muscovite, possibly two generations, with little biotite present (biotite-quartz-garnet-sillimanite-plagioclase-muscovite schist). The first generation of muscovite appears to define the dominant S_2 foliation and is fine- to medium-grained, while the second generation crosscuts the foliation, is coarse-grained, and poikiloblastic. The later muscovite is postkinematic.

Muscovite + plagioclase + sillimanite + garnet + quartz + biotite ± chlorite ± apatite ± epidote ± opaques (A2)

The third assemblage contains the greatest amount of sillimanite and is devoid of muscovite (K-feldspar-biotite-quartz-garnet-sillimanite-plagioclase schist).

Plagioclase + sillimanite + garnet + quartz + biotite + K-feldspar ± opaques (A3)

Petrogenesis of Assemblages A1, A2, and A3

Assemblages A1 and A2 are typical of the first sillimanite zone upper amphibolite facies metamorphism. The majority of the field area lies in this zone. Assemblage A1 and A2 display a continuous reaction of:

Garnet + muscovite = biotite + sillimanite (3-2)

Table. 3-1. Modes of pelitic schist from the Brindle Creek thrust sheet.

Sample ID	M-24	F-229	F-1219
Unit	Sillimanite Schist	Sillimanite Schist	Sillimanite Schist
Tectonic Unit	EIP	EIP	EIP
Points Counted	1000	1000	1000
Plagioclase	27.5	30.9	30.4
Quartz	8.1	4.2	7.9
Microcline	0	0	4
Biotite	0.9	14.6	4.6
Muscovite	36.4	32.5	0
Chlorite	0.2	0.2	0.1
Sillimanite	14.7	14.8	25.3
Apatite	0.2	0	0.9
Epidote	0.4	0.1	0.6
Tourmaline	0.1	0.1	0
Garnet	10.8	0	22.5
Sericite	0.1	2	2.4
Zircon	0	0	0.1
Opaques	0.6	0.6	1.2
Total	100	100	100

Note: Trace represents <0.1% of mode. Stage step size was 0.1 mm for all of the thin sections listed above.

where garnet and muscovite are being consumed to produce biotite and sillimanite (Fig. 3-3a). This reaction is continuous with increasing metamorphic grade. Consumption of garnet can be seen in subhedral garnet grains that contain inclusions of quartz and biotite (Fig. 3-3b). Both fibrolitic and prismatic sillimanite were noted in thin section, although there appears to be a dominance of prismatic sillimanite in all samples petrographically studied. Prismatic sillimanite generally defines the S_2 foliation in sillimanite schist; however, it also has grown orthogonal to the regional foliation. In muscovite-bearing assemblages, prismatic sillimanite markedly occurs close to the muscovite grains, but in muscovite-absent assemblages, sillimanite occurs close to garnets or along planes where muscovite defines the foliation. Sillimanite tends to have difficulty nucleating; therefore, in many cases it will grow along muscovite [001] cleavage planes (Bruce, 1977).

Assemblage A3 is also representative of sillimanite I grade metamorphism although this sample is devoid of muscovite. Muscovite has been replaced by sillimanite in sample F-1219, and also forms sillimanite fish with a dextral shear sense, indicating that the Rex Haven (Kinnard Creek) fault formed during very high temperatures. If K-feldspar was abundant in this assemblage, as well as being in contact with the prismatic sillimanite, this sample would represent sillimanite II-grade metamorphism. No evidence of sillimanite II-grade metamorphism was noted in the field area.

The different mineral assemblages in the pelitic schist in the hanging wall most likely reflect original bulk rock composition, widespread variable metamorphic conditions, or multiple episodes of metamorphism. The latter of the three explanations is least likely.

Retrograde metamorphism

Along with prograde assemblages, retrograde fabrics and assemblages were also noted in the biotite gneiss, pelitic rocks, granitoids, and amphibolite samples:

$$\text{Quartz + chlorite + sericite} \quad \text{(R1)}$$

$$\text{Muscovite} \quad \text{(R2)}$$

$$\text{Zoisite + quartz = anorthite + } H_2O \quad \text{(R3)}$$

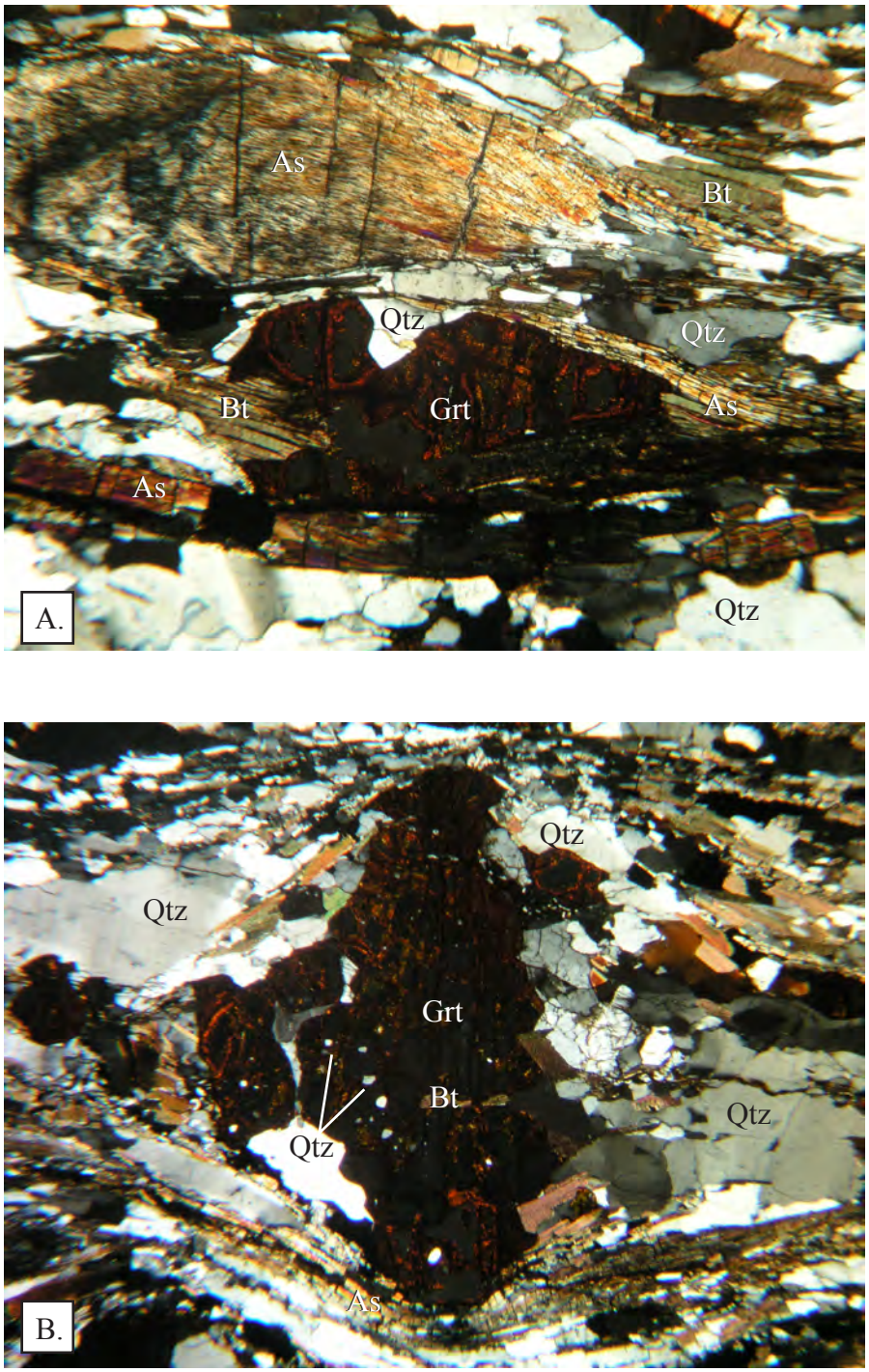

Figure 3-3. A. Anhedral garnet next to prismatic and fibrolitic sillimanite. Sillimanite defines the regional S_2 foliation. B. Anhedral garnet next to prismatic sillimanite with inclusions of quartz and biotite. Abbreviations: Grt-garnet; Qtz-quartz; Bt-biotite; As-aluminum silicate (sillimanite).

Both R1 and R2 crosscut the earlier S_2 foliations, and chlorite is present inside biotite grains (Fig. 3-4). In amphibolite, zoisite, and quartz form at the expense of anorthite and H_2O (R3) (see Figure 2-22 in Chapter 2).

Zoned Minerals and Diffusion

Metamorphic minerals generally display chemical zoning: garnets are the prime example, aside from feldspars (Spear, 1993). Chemical zoning records changes in the P-T-t path; understanding and documenting zoning is essential for interpreting the metamorphic evolution of a rock mass. Two major types of zoning are: growth zoning and diffusion zoning. Both are typically affected by external changes, such as changes in P and T (Spear, 1993). Growth zoning occurs as a new compositional layer is added to the rim of a mineral; whereas, diffusion zoning is a modification in the previously existing mineral composition through volume diffusion (Spear, 1993). Volume diffusion is a thermally driven process, and thus more prevalent in higher grade metamorphic rocks (Spear, 1993). As growth and diffusion zoning occur, chemical composition changes over a traverse from the core to the rim of a mineral, in this case garnets. The rims of garnets frequently record peak metamorphic conditions, but rims can become modified by re-equilibrating at lower temperatures through diffusion (Spear 1991, 1993). Net transfer and exchange reactions occur during diffusion, although each reaction occurs independently and can either change modal proportions within a rock or consume one mineral while producing another. Each reaction produces chemical gradients in crystals that produce distinct zoning patterns. These gradients are related to the presence or absence of certain mineral phases within the rock (Spear, 1993).

Garnets were chosen for analysis in both amphibolite and biotite gneiss samples, and are ubiquitously zoned in the major cations Fe, Mg, Mn, and Ca, trace elements, and oxygen isotopes, making garnet a very important geothermobarometer. Growth zoning displays a varying profile attributed to the bell-shaped curve that occurs for Mn in garnets that grow in amphibolite and lower facies (Fig. 3-5a-c). Volume diffusion profiles do not display this distinctive Mn bell-curve across the mineral traverse, but instead display a relatively flat profile

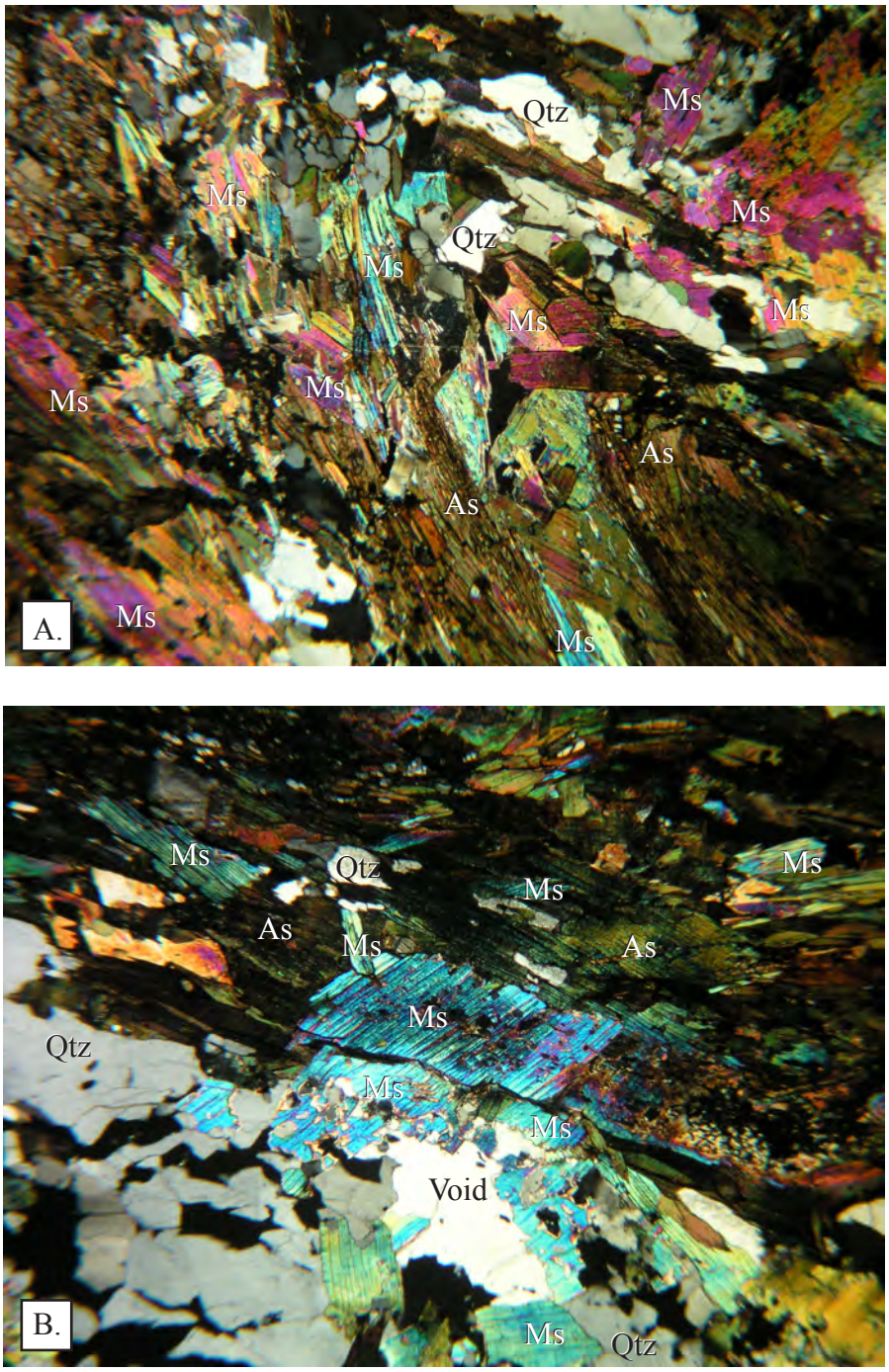

Figure 3-4. Photomicrographs of sillimanite schist (cross-polarized light). Retrograde fabrics. A. Retrograde muscovite crosscutting the regional foliation. Sample M-24. B. Retrograde muscovite replacing sillimanite and crosscutting the foliation. Sample M-24. Abbreviations: Ms-muscovite; As-sillimanite; Qtz-quartz.

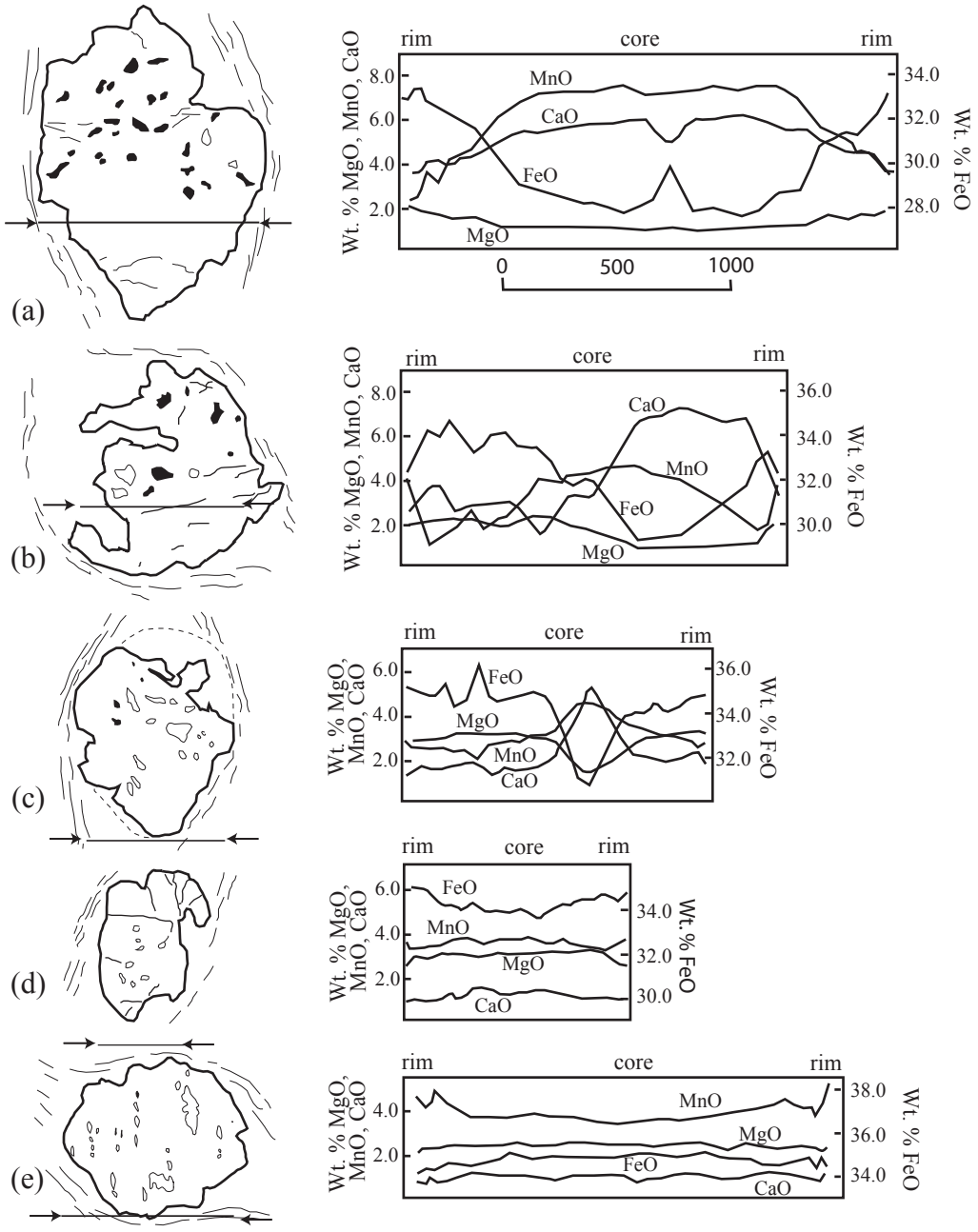

Figure 3-5. Development of diffusion zoning in garnets with increasing metamorphic grade (a-e) from Connemara, Ireland. (a-c) Steeper zoning and "bell-shaped" Mn curve occur in profiles of lower metamorphic grade garnets. (d-e) High-grade metamorphic profiles display a homogeneous core and rims modified by diffusion. (a) Staurolite zone. (b) Lowermost part of staurolite-sillimanite transition zone. (c) Upper part of the staurolite-sillimanite transition zone. (d) Lower sillimanite zone. (e) Upper sillimanite zone. Lines and arrows show location of garnet traverse. From Spear (1993), modified from Yardley (1977).

(Fig. 3-5d-e). Homogenization occurs in garnets at higher metamorphic grades, due to rapid diffusion rates, leading to flatter core to rim profiles (Spear, 1993).

Formation of diffusion zoning is solely based on the chemical species and minerals present during the time of diffusion. Also factored into the diffusion process is the location of minerals relative to one another. Exchange of Fe and Mg between garnet and biotite will only occur when they are in contact with one another, or within close proximity (Spear, 1993). Exchange reactions are considered good geothermometers because they typically have a small $^{\circ}V_{reaction}$. Fe and Mg exchange rates are a direct result of the T and P to which they have been subjected; therefore, the geothermometer best suited for the sample of biotite gneiss is Eq. 3-2 (Hodges and Spear, 1982). This thermometer is based on the exchange of elements (Fe and Mg) between phases. This exchange results in the change of overall mineral composition, but does not decrease nor increase the abundance of the mineral.

$$Fe_3Al_2Si_3O_{12} + KMg_3AlSi_3O_{10}(OH)_2 = Mg_3Al_2Si_3O_{12} + KFe_3AlSi_3O_{10}(OH)_2 \quad (3\text{-}2)$$

Almandine + Phlogopite = Pyrope + Annite

With mineral assemblages taken into consideration, the best geobarometer to use with the metagraywacke sample is garnet-plagioclase-quartz-Al_2SiO_5 (GASP) (Eq. 3-3, Hodges and Spear, 1982). Each geobarometer has its advantages and disadvantages, and GASP is no exception. It is an extremely temperature-sensitive barometer, dependent on the activities of anorthite and grossular. K_{eq} lines that have a moderate slope, in combination with errors in temperature estimates, result in larger errors in pressure estimates. Another problem with GASP is that it only calculates prograde paths, and does not account for retrograde paths. This can also result in large errors in P estimates.

$$3CaAl_2Si_2O_8 = Ca_3Al_2Si_3O_{12} + 2Al_2SiO_5 + SiO_2 \quad (3\text{-}3)$$

Anorthite = Grossular + Aluminum silicate + Quartz

Plagioclase and biotite were identified in the interiors of garnets, sillimanite was not; however, sillimanite is ubiquitous throughout the field area, their activities are set to 1.0. They are nearly pure phases.

$$\Delta\mu^{\circ} = -RTln\left(a_{qtz}\ \ a_{sil^2}\ a_{grs}^{Grt}/(a_{an}^{Pl})3\right) = -RTln\left(a_{grs}^{Grt}/(a_{an}^{Pl})3\right) = -RTlnK_{eq}$$

Like the Mg/Fe exchange that occurs between biotite and garnet, the same exchange occurs in hornblende and garnets. This exchange rate is also a direct result of the T and P, the geothermometer best suited for the sample of amphibolite is (Eq. 3-4; Graham and Powell, 1984).

$$4Mg_3Al_2Si_3O_{12} + NaCa_2Fe_4Al_3Si_6O_{22}(OH)_2 = 4Fe_3Al_2Si_3O_{12} + 3NaCa_2Mg_4Al_3Si_6O_{22}(OH)_2 \quad (3\text{-}4)$$

Pyrope + Fe-hornblende = Almandine + Mg-hornblende

A net-transfer reaction was used to calculate peak metamorphic P in the amphibolite sample: hornblende-garnet-plagioclase geobarometer (Eq. 3-5, Dale et al., 2000). The hornblende-garnet-plagioclase geobarometer also contains pressure estimation drawbacks. According to Dale et al. (2000), there are two aspects of geothermobarometry with respect to amphibole-bearing assemblages that remain unsatisfactory: "firstly, the lack of adequate mixing properties for amphibole and, secondly, the poor correspondence between the empirical constants used in thermobarometers and known entropies and enthalpies of reaction."

$$3Ca_2(Mg, Fe)_5Si_8O_{22}(OH)_2 + 6CaAl_2Si_2O_8 = 3Ca_2(Mg, Fe)_4Al_2Si_7O_{22}(OH)_2 \quad (3\text{-}5)$$
$$+ 2Ca_3Al_2Si_3O_{12} + (Fe, Mg)_3Al_2Si_3O_{12} + 6SiO_2$$

Sample Description

F-1236 metagraywacke sample

Sample F-1236 is from an outcrop located along the Rex Haven (Kinnard Creek) fault in the west-central portion of the Farrar quadrangle. Petrographic analysis revealed that this sample displays an equigranular matrix composed of quartz, plagioclase, biotite, K-feldspar, muscovite, chlorite, and opaques with euhedral to subhedral, fractured, embayed porphyroblasts of garnet (1.0-2.0 mm). Accessory minerals include apatite and rutile. Garnets contain inclusions of plagioclase and biotite along with other accessory phases. The garnets contain almandine cores and show minor variability from core to rim in x-ray maps.

Garnet profiles that have undergone volume diffusion typically contain homogenous almandine cores ($Al_{70}Py_{11}Sp_{6}Gr_{13}$), which transition to diffused outer rims. Subsequent patterns in garnet profiles are generally asymmetric W- and M-shaped profiles, and are a result of net transfer and exchange reactions with the surrounding matrix or inclusions inside the garnet (Spear, 1991). There is a net transfer of Mg and Fe between the garnet crystal and embayed biotite grains, exhibited by a slight zoning in the vicinity of biotite grains in the garnet crystal.

As is the case with many high-grade metamorphic rocks, the garnets in this sample show little variability along zoning profiles, with the exception of CaO, which decreases along the rims and increases in the core of garnet-D in sample F-1236 (Fig. 3-6). There is a MnO curve, with an increase toward the rim and a decrease in the core. This same pattern can also be seen in an X-ray map taken of garnet-D in the metagraywacke (Fig. 3-7). Minor zoning is noted in CaO, again with increase of CaO toward the interior and decrease toward to the rims.

Garnet-B (Fig. 3-8) displays a distinctly different profile compared to garnet-D. There is a gradual increase of MgO in the core of the garnet and a decrease toward the rims, and a similar MnO curve as that observed in garnet-B, where MnO increases with proximity to the rim and decreases in the core. CaO does not display the same variability in garnet-B as in garnet-D, and displays a relatively flat trend. FeO also appears to remain consistent across the traverse of the crystal.

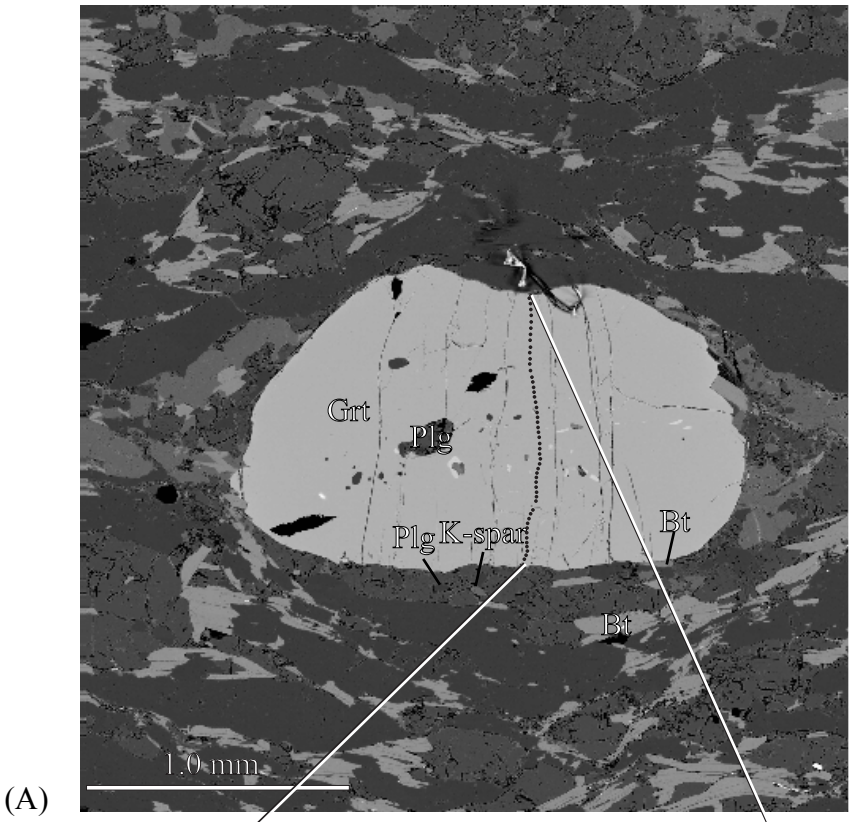

(A)

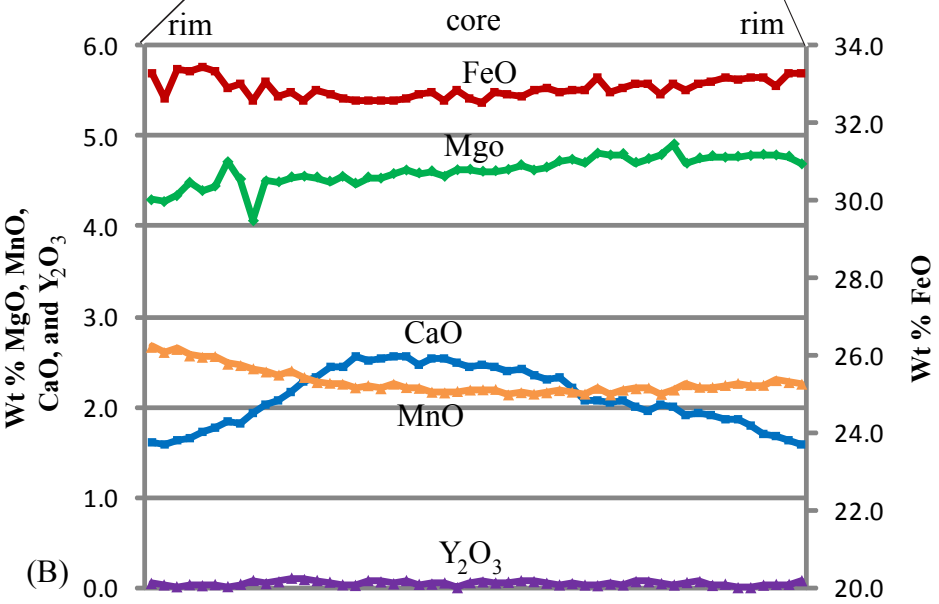

(B)

Figure 3-6. Garnet zoning profile of sample F-1236 from: garnet D. (A). Back-scattered electron image and locations analyzed. (B) Zoning profile. Grt-garnet. K-spar-K-feldspar. Plg-plagioclase. Bt-biotite.

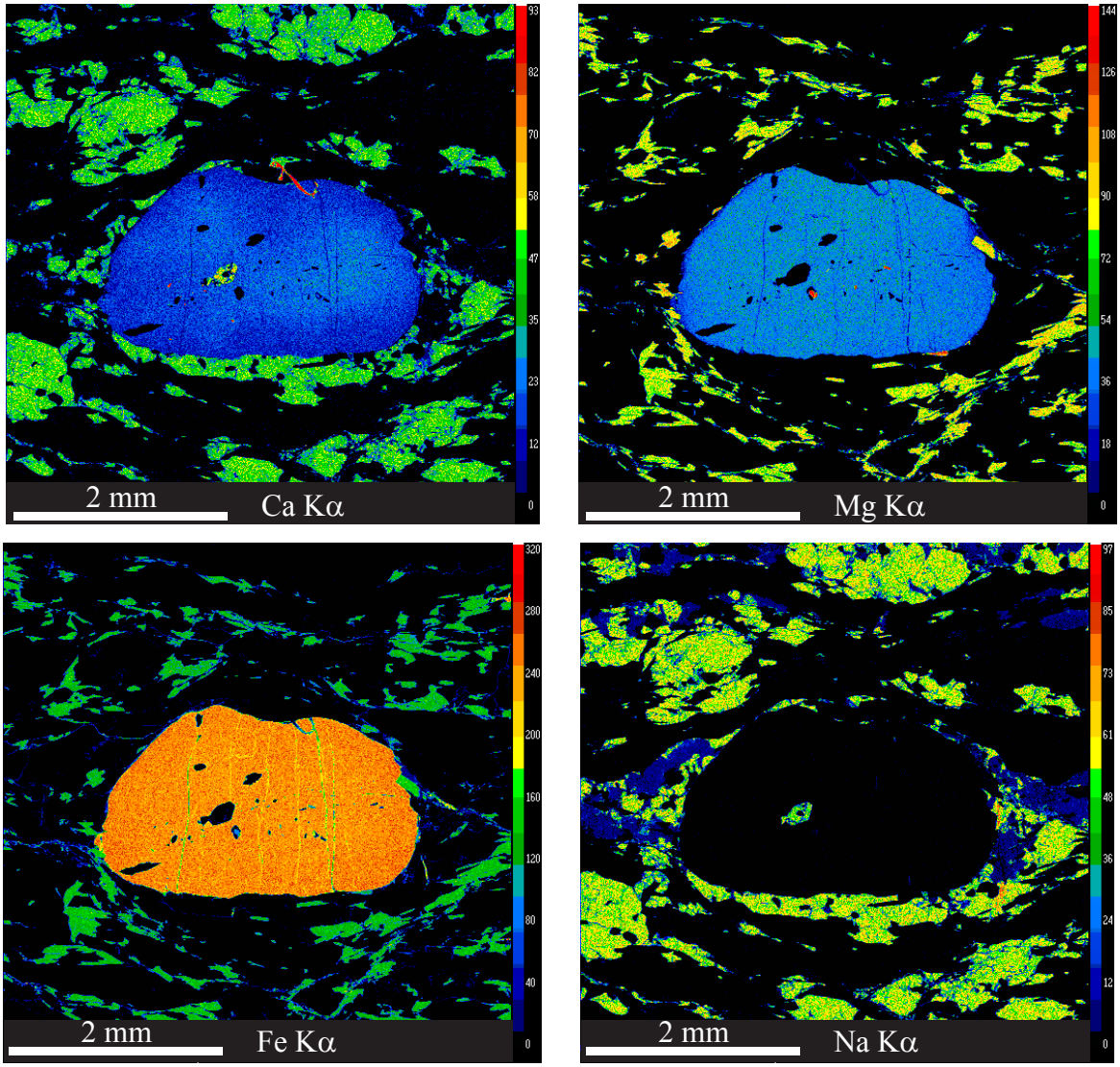

Figure 3-7. X-ray maps of Fe, Mg, Ca, and Mn illustrating garnet zoning patterns in garnet B of sample F-1296.

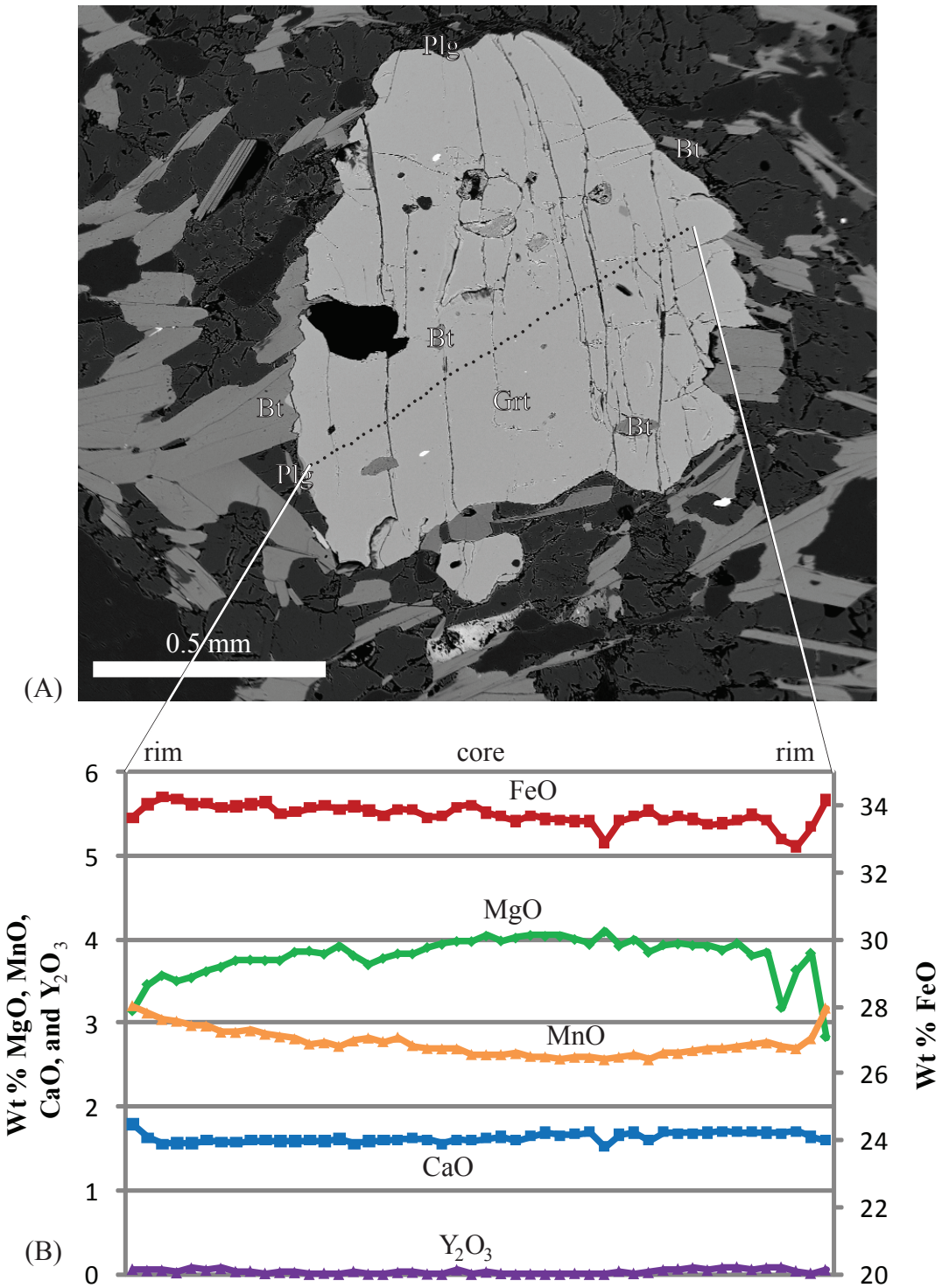

Figure 3-8. Garnet zoning profile of sample F-1236 garnet C. (A). Back-scattered electron image and locations analyzed. (B) Zoning profile. Grt-garnet. Bt-biotite. Plg-plagioclase.

F-1296-amphibolite sample

Sample F-1296 is from an outcrop located along Aldridge Road in the central portion of the Farrar quadrangle. Petrographic analysis revealed that this sample displays an equigranular matrix composed of hornblende and plagioclase along with minor amounts of quartz and opaques. Garnets are typically subhedral to euhedral, with inclusions of plagioclase, hornblende and quartz. Inclusions are typically located on the interior portions of the garnets and do not occur as often along the rims, and range from 2-15 μm. S_1 is preserved in garnets throughout the sample, but the garnets themselves are surrounded by the dominant S_2 foliation. The primary foliation in this sample is composed of hornblende.

Garnets in this sample are dominantly almandine with considerable pyrope and grossular components. Optical zoning of garnets was not identfied; however, in X-ray maps distinct chemical zoning is noted in two of the garnets analyzed (Figs. 3-9 and 3-10). Both the grossular and pyrope components decreases in the interior of the garnet, increases toward the inner rim, and then decreases along the outer rim (Figs. 3-11 and 3-12). The almandine component increases in the core of the garnet, decreases in the inner rim, and then increases along the outer rim. Spessartine decreases in the core and decreases toward the rims of the garnets.

Synthesis and Discussion

Peak pressure estimates were obtained by combining rim garnet with matrix biotite (sample F-1236) phases and core garnet with matrix hornblende (sample F-1296). Originally, garnet cores were combined with hornblende inclusions to obtain a temperature estimate; however, the results plotted in the granulite facies. Field relationships do not support this conclusion. Therefore, garnet core was combined with matrix hornblende instead of using a garnet rim and matrix hornblende combination. The cores of the amphibolite garnets are homogenous almandine, and the rims of the garnets appeared to have been extensively modified by diffusion. The garnet-bearing biotite gneiss sample (sample F-1236) yields pressure estimates of 4.6-7.6 kbars using GASP barometry (Fig. 3-13) (Hodges and Spear, 1982). The garnet-bearing amphibolite sample (sample F-1236) yields pressure estimates of 4-5.3 kbars using hornblende-garnet-plagioclase barometry (Fig. 3-14) (Kohn and Spear, 1990). Peak temperature

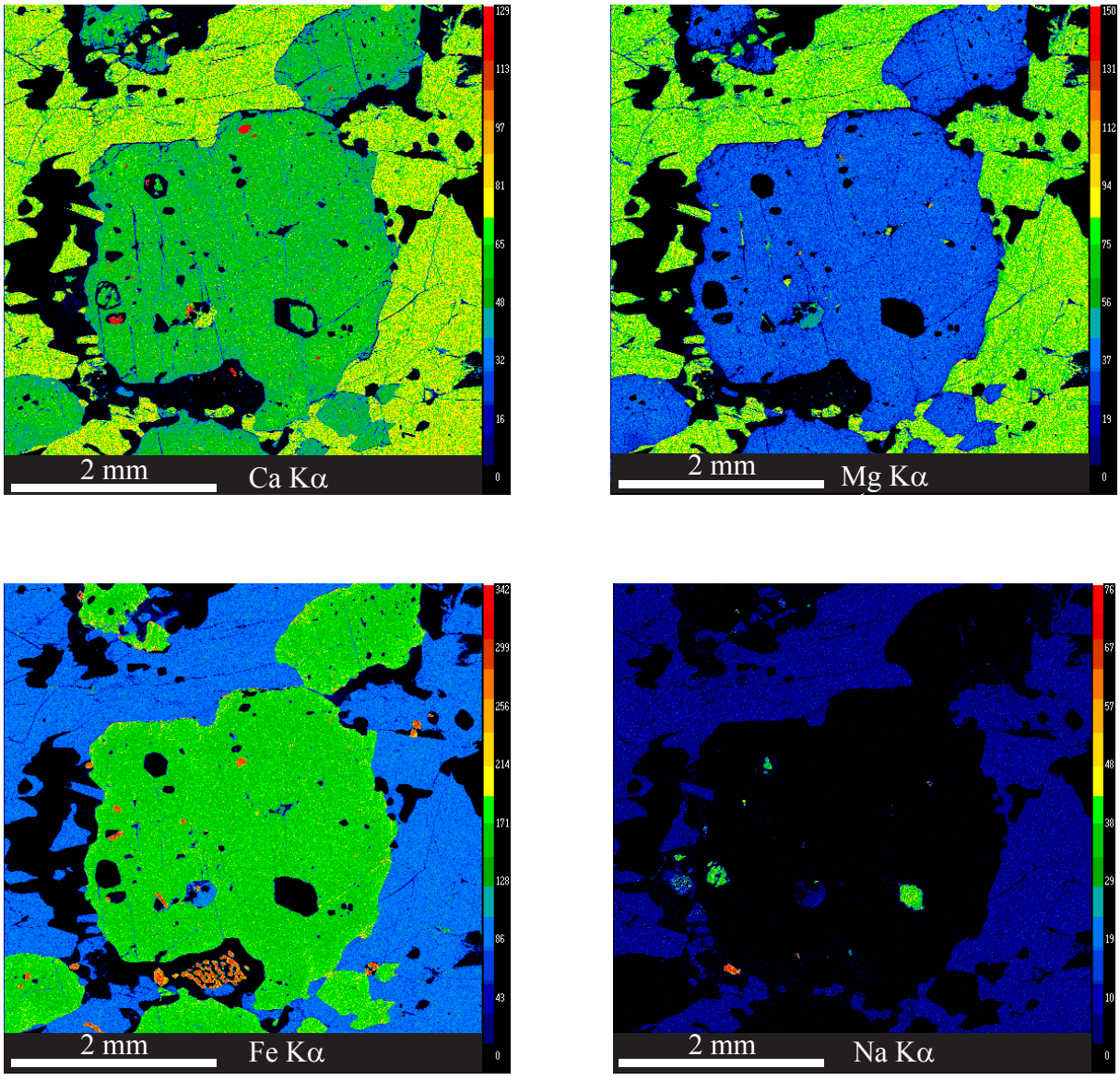

Figure 3-9. X-ray maps of Fe, Mg, Ca, and Mn illustrating garnet zoning patterns of garnet B in sample F-1296.

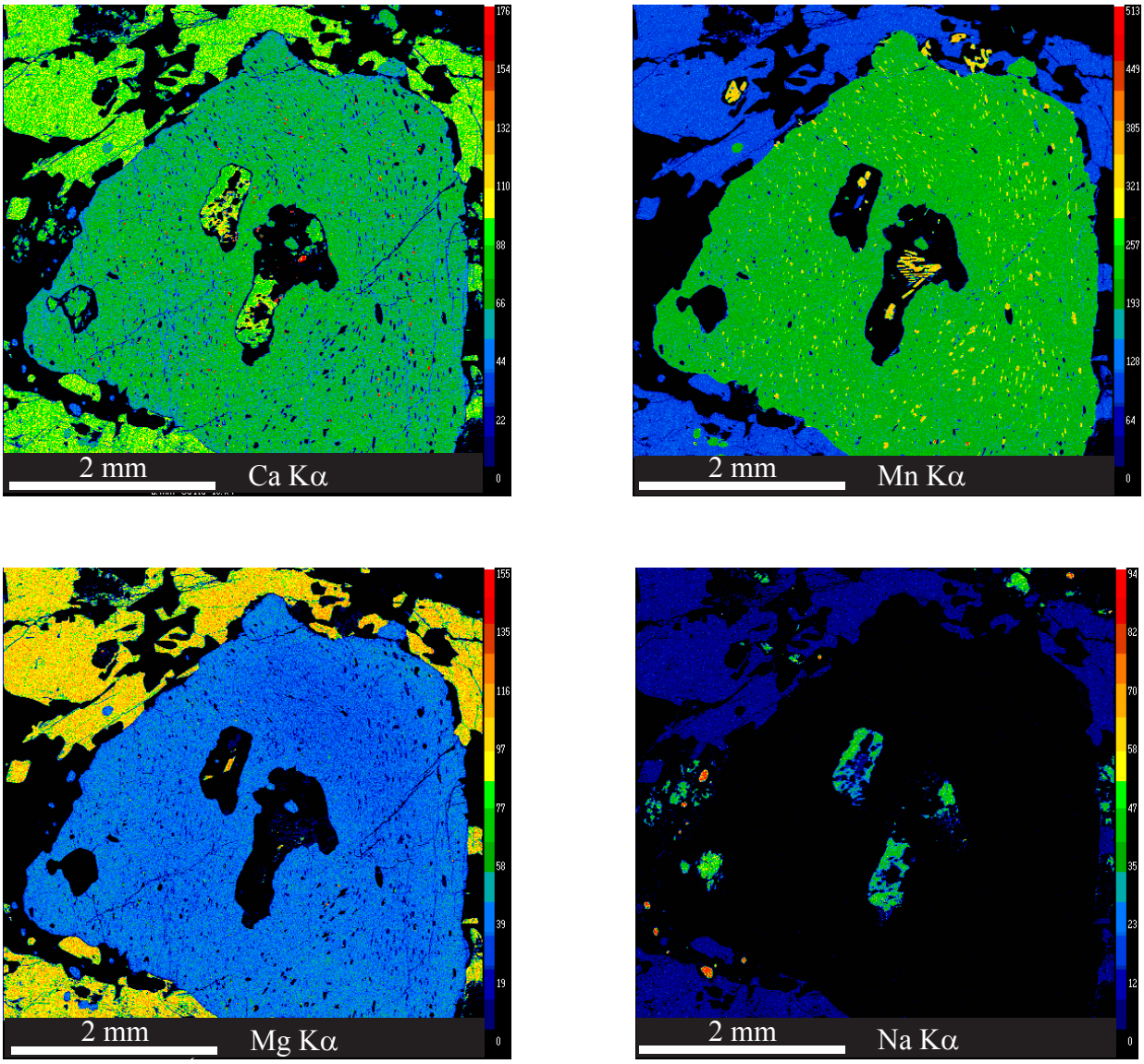

Figure 3-10. X-ray maps of Fe, Mg, Ca, and Mn illustrating garnet zoning patterns of garnet C in sample F-1296.

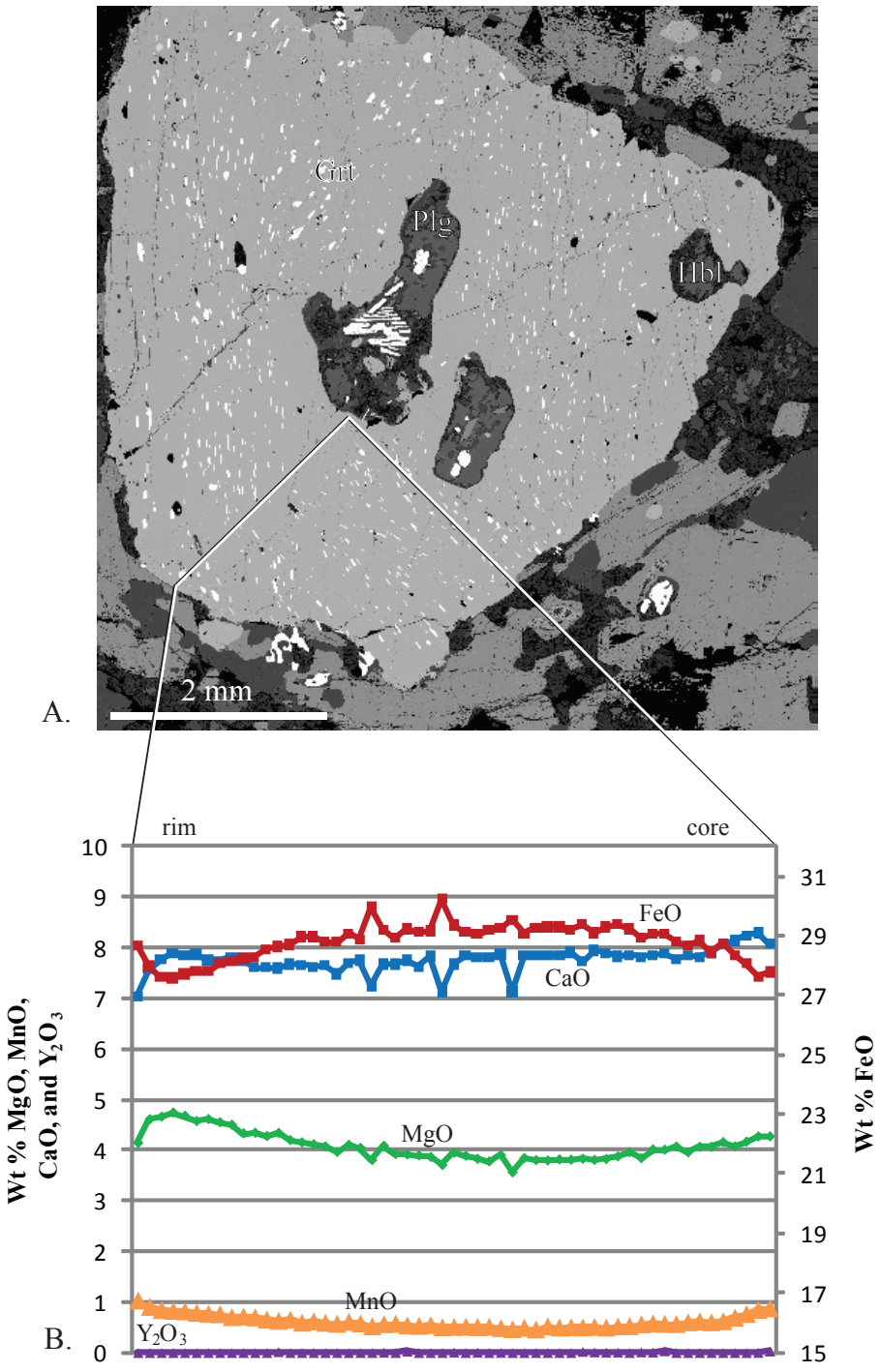

Figure 3-11. Garnet zoning profile of sample F-1296: garnet E. (A). Back-scattered electron image and locations analyzed. (B) Zoning profile. Grt-garnet. Hbl-hornblende. Plg-plagioclase. Note the earlier foliation (S) preserved in this garnet.

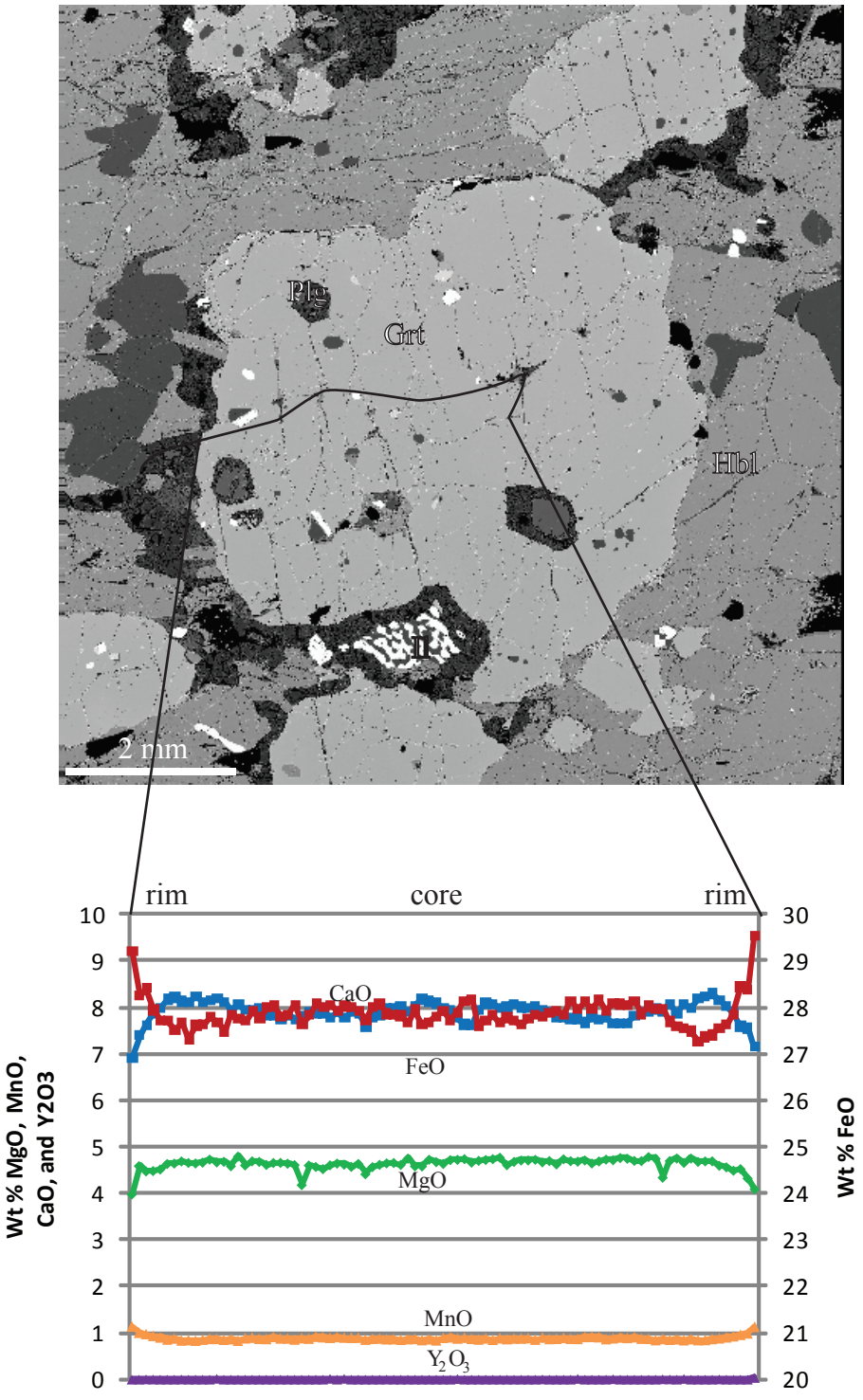

Figure 3-12. Garnet zoning profile of sample F-1296: garnet D. (A). Back-scattered electron image and locations analyzed. (B) Zoning profile. Grt-garnet. Hbl-hornblende. Plg-plagioclase. Il-ilmenite.

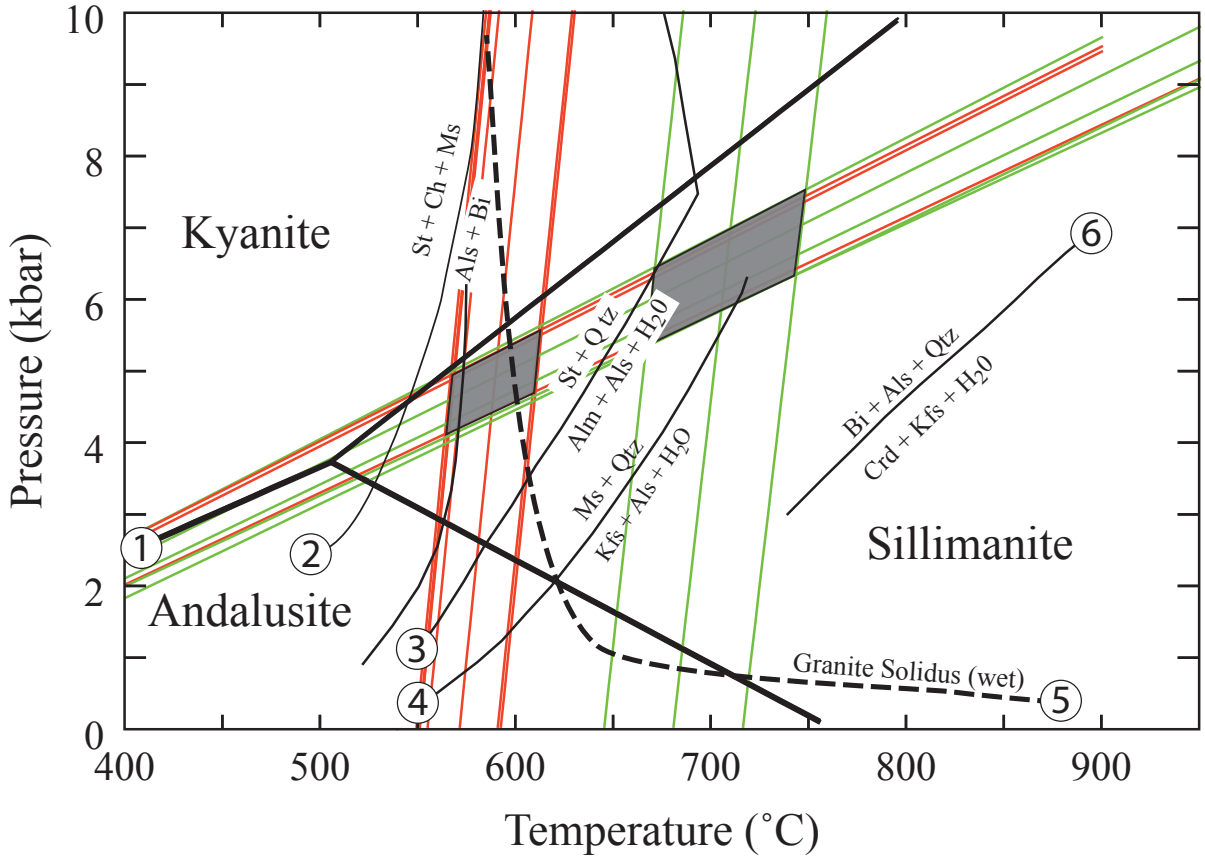

Figure 3-13. Estimates of peak and prograde conditions for F-1236. Steeply inclined lines are temperature estimates. calculated with garnet-biotite thermometry (Ferry and Spear, 1978). Shallow dipping lines are pressure estimates using GASP barometry (Hodges and Spear, 1982). Different line colors represent location within garnet crystals. Green lines are rim and red lines are core. Reactions plotted: (1) Holdaway (1971); (2) Albee (1965); (3) Pigage and Greenwood (1982); (4) Chatterjee and Johannes (1974); (5) Luth et al. (1964); and (6) Holdaway and Lee (1977). Alm-almandine. Bi-biotite. Ch-chlorite. Crd-cordierite. Kfs-potassium feldspar. Ms-muscovite. Qtz-quartz. St-staurolite. Als-aluminum silicate.

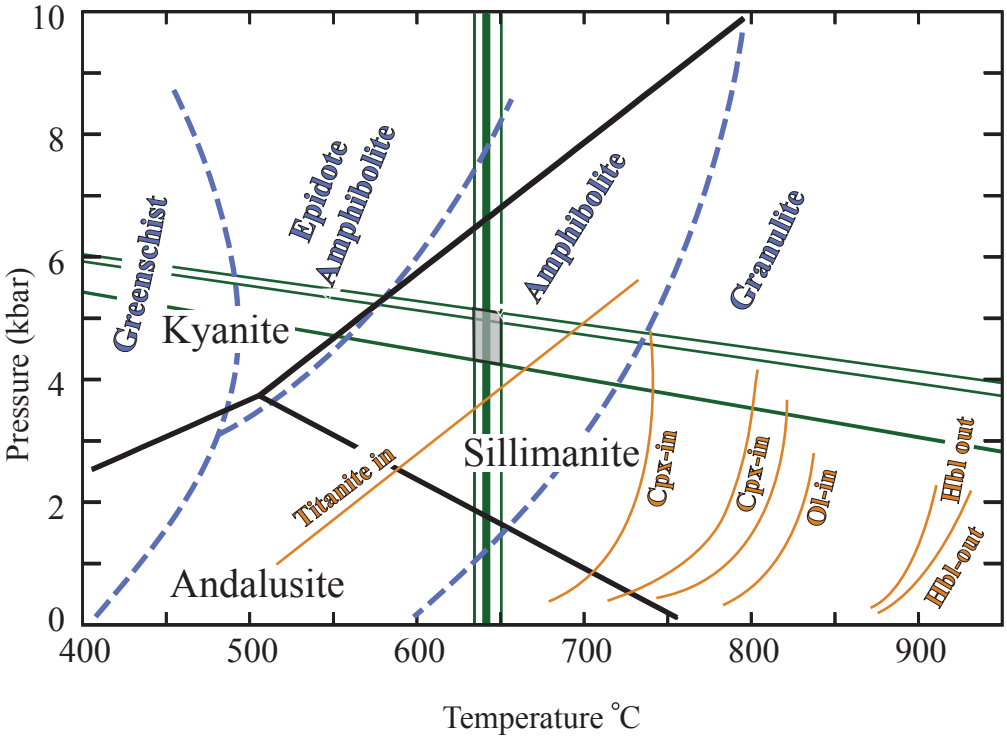

Figure 3-14. Estimates of peak and prograde conditions for F-1296. Steeply inclined lines are temperature estimates, calculated with garnet-hornblende thermometry (Ferry and Spear, 1978). Shallow dipping lines are pressure estimates using hornblende-garnet-plagioclase thermo-barometry (Dale et al., 2000). Orange lines correspond to reaction boundaries pertinent to granulite and amphibolite facies (Spear, 1991). Blue lines correspond to facies changes (after Holdaway, 1971). Green and red colored lines represent location within garnet crystals. Reactions plotted: (1) Holdaway (1971); (2) Albee (1965); (3) Pigage and Greenwood (1982); (4) Chatterjee and Johannes (1974); (5) Luth et al. (1964); and (6) Holdaway and Lee (1977). Cpx-clinopyroxene. Opx-orthopyroxene. Hbl-hornblende.

estimates yield 645-715˚C for the biotite gneiss sample, utilizing the garnet-biotite thermometer (Hodges and Spear, 1982) and 630-650˚C for the amphibolite sample, by applying garnet-hornblende thermometry (Graham and Powell, 1984).

P-T Paths

Previous work in the eastern Inner Piedmont Cat Square terrane in North Carolina revealed a well-constrained P-T path for the Brindle Creek thrust sheet (Fig 3-15). This P-T path revealed two paths of retrograde metamorphism along with peak metamorphic conditions. A partial prograde P-T path has been constructed as a result of this study and continuing work in the eastern Inner Piedmont Cat Square terrane in central Georgia. Both the hornblende-garnet-plagioclase and GASP barometers and garnet-hornblende and garnet-biotite thermometers plot one prograde path. Despite the fact that mineral assemblages from the andalusite stability field were not observed in the field, these estimates may document early metamorphic conditions within the Brindle Creek thrust sheet. Alternatively, it is more likely related to an error associated with the GASP barometer. This path reaches 6.5 to 7.3 kbars of pressure at 775˚C. Assuming error in P-T estimates, and that equilibrium phases are not always identified properly, it is then necessary to compare the mineral reactions seen in the field and petrographically. Prograde and retrograde, continuous and discontinuous reactions aid in delineating a correct P-T path (Fig. 3-16).

New evidence, in combination with previous studies, suggests that the Neoacadian orogeny was one single, prolonged event based on evidence such as: (1) ubiquitous migmatization throughout the Inner Piedmont; (2) optically unzoned garnets; (3) similarities in geochemistry between matrix assemblages and garnet inclusions; (4) presence of prismatic sillimanite; and (5) areas of sillimanite II grade metamorphism throughout the core of the Inner Piedmont (Wilson, 2006).

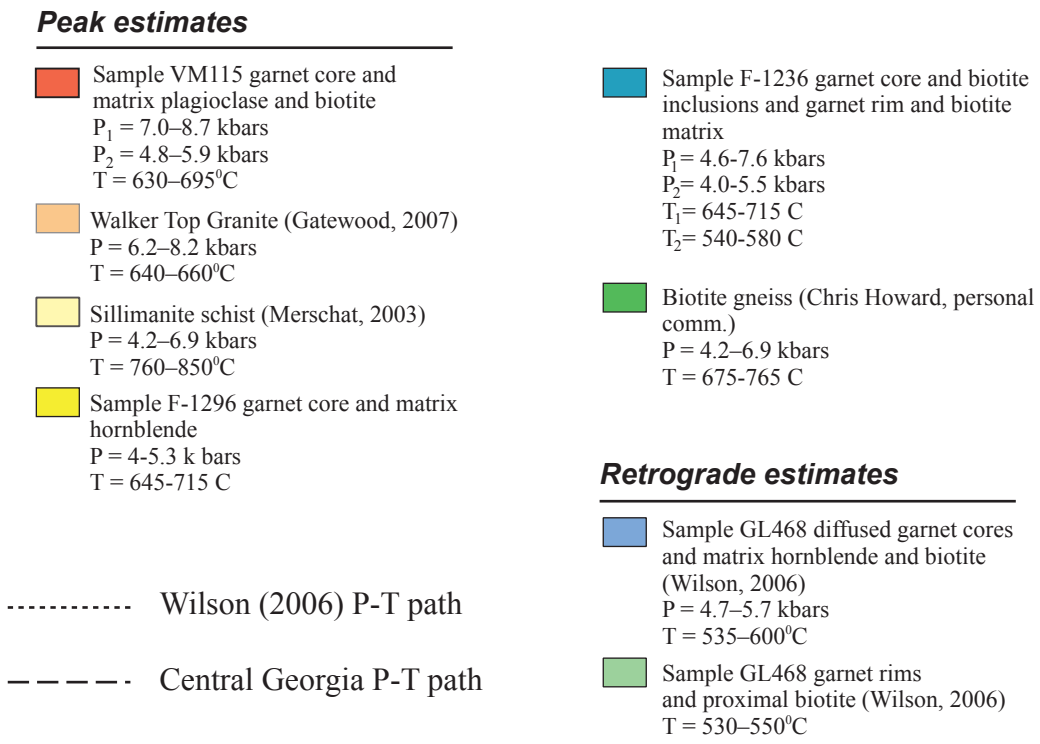

Figure 3-15. Projected P-T path of Farrar and Stewart quadrangles biotite gneiss and amphibolite. (A) Cat Square terrane P-T path from central Georgia samples. (B) Possible P-T path for eastern Inner Piedmont estimated from samples in North Carolina. KFMASH petrogenetic grid univariant reaction curves (Spear and Cheney, 1989). Granite solidus reaction line from Luth et al. (1964). Abbreviations: Als-aluminum silicate; Bt-biotite; Crd-cordierite; Grt-garnet; Kfs-K-feldspar; Ms-Muscovite; St-staurolite; and Qtz-quartz.

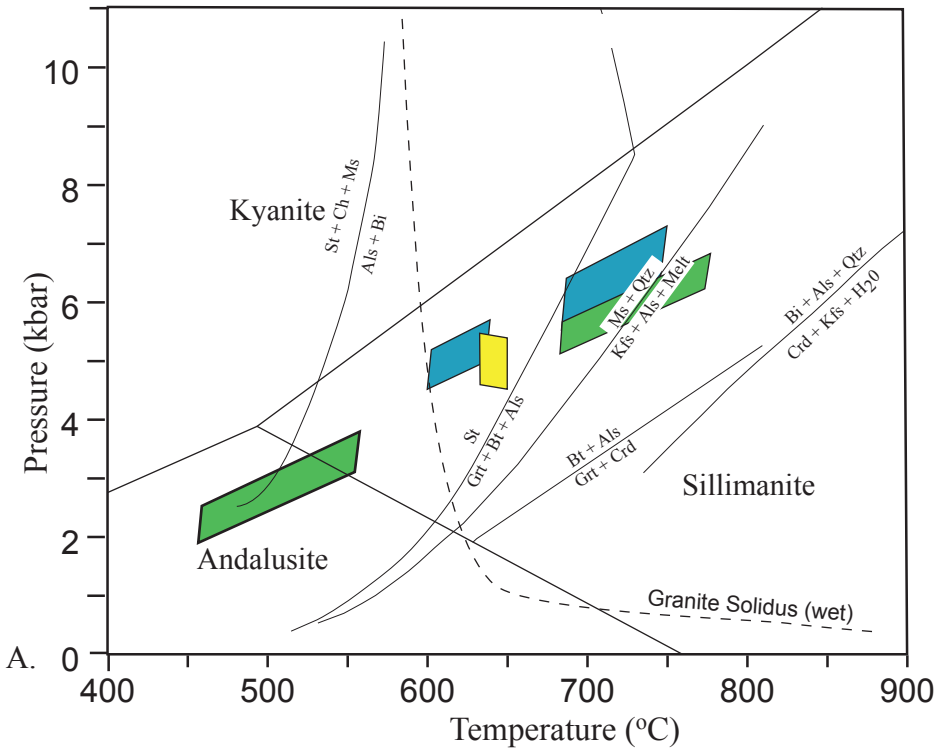

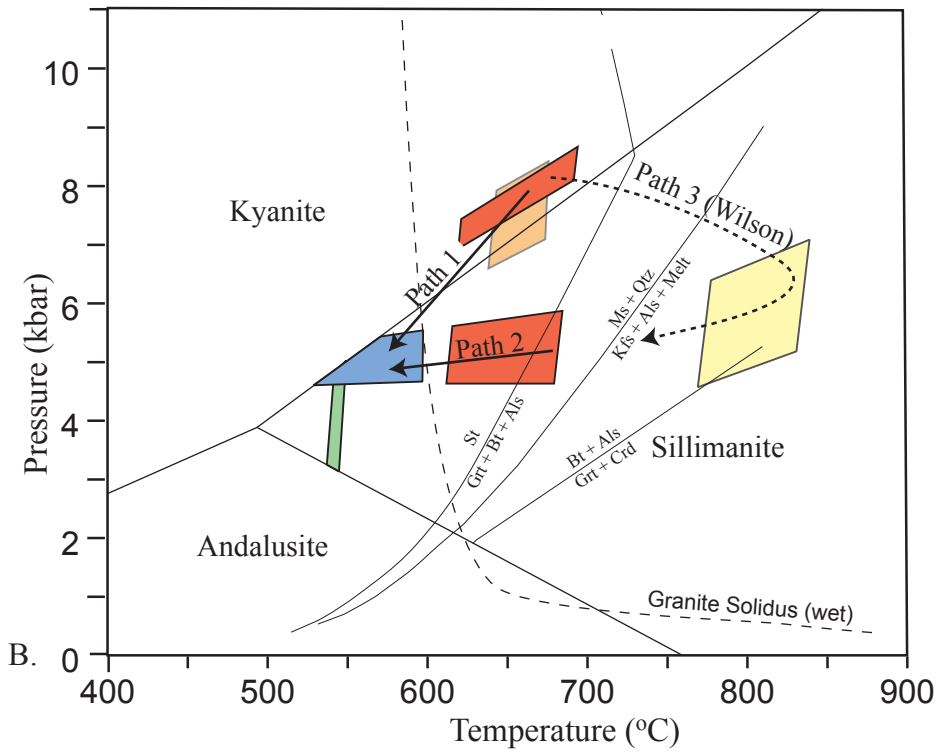

Figure 3-15. Continued

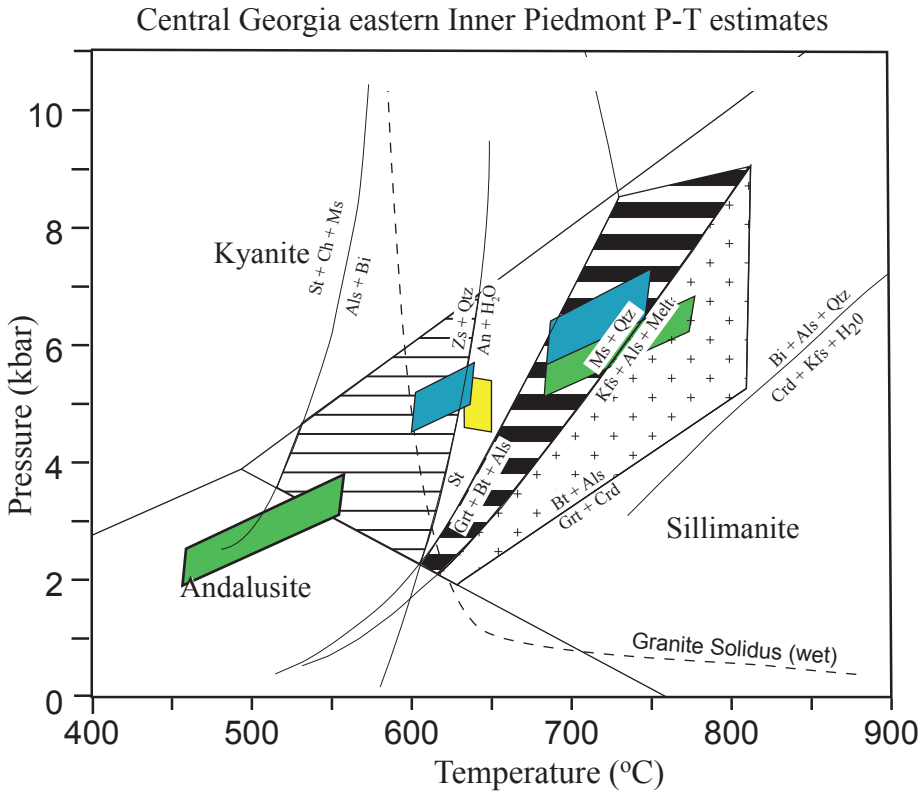

Figure 3-16. Swatches indicate path probability for retrograde, prograde and peak metamorphic P-T conditions based on rock assemblage and overprinting relationships between mineral phases. Refer to Figure 3-15 caption for explanation of abbreviations.

Conceptual Model

New evidence provided from this study reinforces concepts by Merschat (2003), Wilson (2006), and Merschat and Hatcher (2007), regarding the tectonic history of the southern Appalachian Inner Piedmont (Fig. 3-17). The Cat Square terrane began as the Siluro-Devonian Rheic ocean basin, accumulating sediment from both Laurentia and the approaching Carolina superterrane (Bream, 2003; Merschat and Hatcher, 2007). Timing of deposition of the Cat Square terrane was constrained by the youngest detrital zircon (~430 Ma) age along with the oldest age from the anatectic Walker Top (~407 Ma). Therefore, deposition of the Cat Square terrane occurred prior to ~407 Ma. Models proposed by Gatewood (2007) suggest that there was an eastward-dipping subduction zone, leading to magmatism in the Carolina superterrane. The oldest metamorphic rims observed in the Cat Square terrane are ~400 Ma, suggesting that subduction of the Rheic ocean basin occurred from 430-400 Ma, achieving a depth of ~18 km (Bream et al., 2002, 2003). At this depth anatectic melting occurred along with catazonal intrusion, recording the oldest plutonism in the Inner Piedmont. With increasing temperatures that occur with progressive burial, the Cat Square terrane rocks reached sillimanite I and sillimanite II zone conditions, and were later intruded by Devonian-Mississippian anatectic granitoids (Mapes, 2002). At 360-350 Ma the Inner Piedmont reached temperature conditions that peaked above zircon and monazite closure temperatures (>700˚C) (Dennis and Wright, 1997; Mapes, 2002; Bream, 2003), marking peak deformation within the Inner Piedmont and emplacement of the Brindle Creek and Rex Haven thrust sheets. Younger age dates of 330-320 Ma mark the younger Alleghanian orogen (Dennis and Wright, 1997; Bream, 2003).

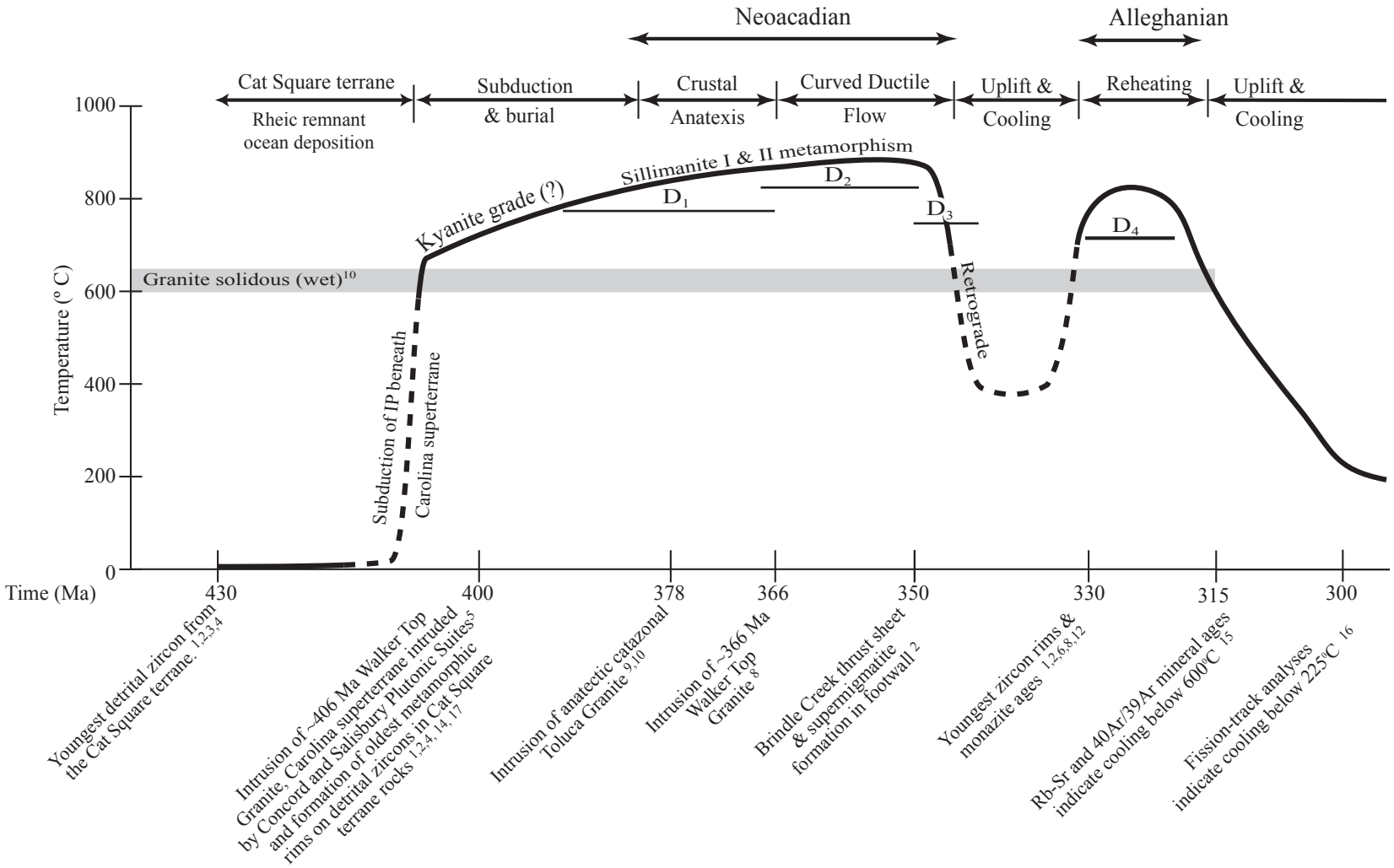

Figure 3-17. Tectonothermal timeline for the Inner Piedmont. Data Sources: Merschat (2003). 1-Bream (2002). 2-Bream (2003). 3-Bream et al. (2001). 4-Bream et al. (2004). 5-McSween et al. (1984, 1991). 6-Carrigan et al. (2001). 7-Davis (1993). 8-Dennis & Wright (1997). 9-Girogis et al. (2002). 10-Luth et al. (1964). 11-Mapes (2002). 12-Mapes et al. (2001). 13-Mirante and Patino-Douce (2000). 14-Gatewood (2006). 15-van Breemen and Dallmeyer (1984). 16-Naeser et al. (2001). 17-Butler and Fullagar (1978). From Wilson (2006).

Chapter 4: Geochemistry of the Murder Creek granite and Rocky Creek granodiorite, and similarities with other Inner Piedmont granitoids

Introduction

Polyphase deformation, coupled with thermal events, increases the complexity of southern Appalachian geology and obscures the geologic relationships, structures, petrology, and chemistry of rocks therein. Gathering and interpreting petrologic and geochemical data is integral to understanding the southern Appalachians complicated geologic history. Like many granitoids in the southern Appalachians (Speer et al., 1980), three distinct facies or pulses of granitoids are present in the field area. They are most likely a product of segregated pulses of the same parental source.

Metaigneous rocks occur in abundance throughout the Inner Piedmont. There are, however, important distinctions in their occurrences and origins. For example, Inner Piedmont granitoids often exhibit different characteristics than those of eastern Blue Ridge granitoids, such as REE trends, isotopic variations, and overall geochemical differences (Mapes, 2002). Further examination of Inner Piedmont granitoids shows a variation between eastern Inner Piedmont and western Inner Piedmont granitoids as well. Wilson (2006) determined that these two terranes retain distinguishing geochemical characteristics. Western Inner Piedmont granitoids tend to have lower K_2O/Na_2O_3, higher SiO_2, and flatter REE patterns relative to eastern Inner Piedmont granitoids. Both the eastern and western Inner Piedmont granitoids share a negative Eu anomaly, as well as volcanic-arc signatures; there is overlap in within-plate signatures for western Inner Piedmont granitoids, but eastern Inner Piedmont granitoids overlap with the syn-collisional field (Wilson, 2006).

This study builds upon previous research, and will ultimately aid in distinguishing the origins of the granitoids in the field area.

Sample Collection and Methods

Sample Selection

Geochemical analyses of southwestern Cat Square terrane granitoids had not been performed prior to this study. Three distinct granitoids were identified in the field area; see Chapter 2 (Rock Units) for a petrographic description of each. Two of the three granitoids were geochemically analyzed, with the exception of the Dow's Pulpit granodiorite, which displays large amounts of sericitic alteration. These granitoids share many textural and petrological similarities with the granitoids previously analyzed in the South Mountains, North Carolina. The Murder Creek granite shares petrologic and textural similarities with the Walker Top Granite of North Carolina. The Rocky Creek granodiorite has no defined counter-component in North Carolina; and the Dow's Pulpit shares petrologic and textural similarities with the Toluca Granite in North Carolina. Two representative Murder Creek granite and two Rocky Creek granodiorite samples were collected from the Farrar quadrangle for geochemical analysis, based on the lack of weathering and locality representation of the field area (Fig. 4-1).

Methods

Slabs of the samples were cut from the freshest portions by a rock tile saw. Thin sections of each sample were prepared by cutting slabs of the rock perpendicular to foliation, and smaller 1-2 cm slabs were prepared for geochemical analysis. These samples were washed with isopropyl alcohol and deionized water; then slabs were crushed into smaller sizes by the Chipmunk™, and finally powdered in a Shatterbox™, using a ceramic mill. At least 20 g of each sample was sent for whole-rock analyses to Activation Laboratories in Ancaster, Ontario. Methods for testing include a combination of: inductively coupled plasma-mass spectrometry (ICP-MS); instrumental neutron activation analysis (INAA); total-digestion inductively coupled plasma (TD-ICP); and lithium metaborate/tetraboarate fusion-inductively coupled plasma emission spectroscopy (FUS-ICP) (Table 4-1).

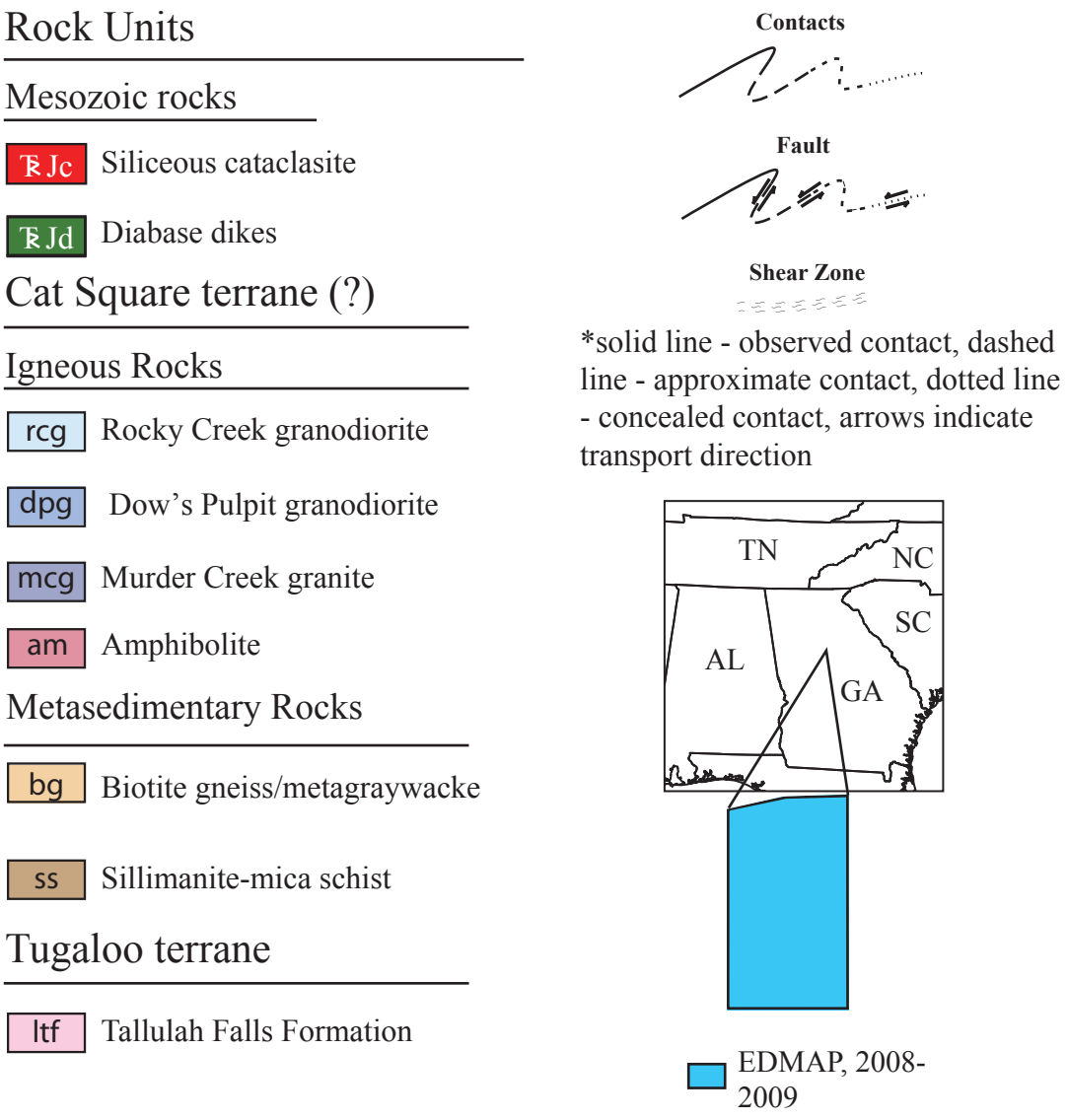

Figure 4-1. Simplified geologic map of portions of the 7.5-minute Farrar and Mansfield quadrangles (See Plate 1 for map unit descriptions). Map showing locations of granitoids sampled for geochemical analyses.

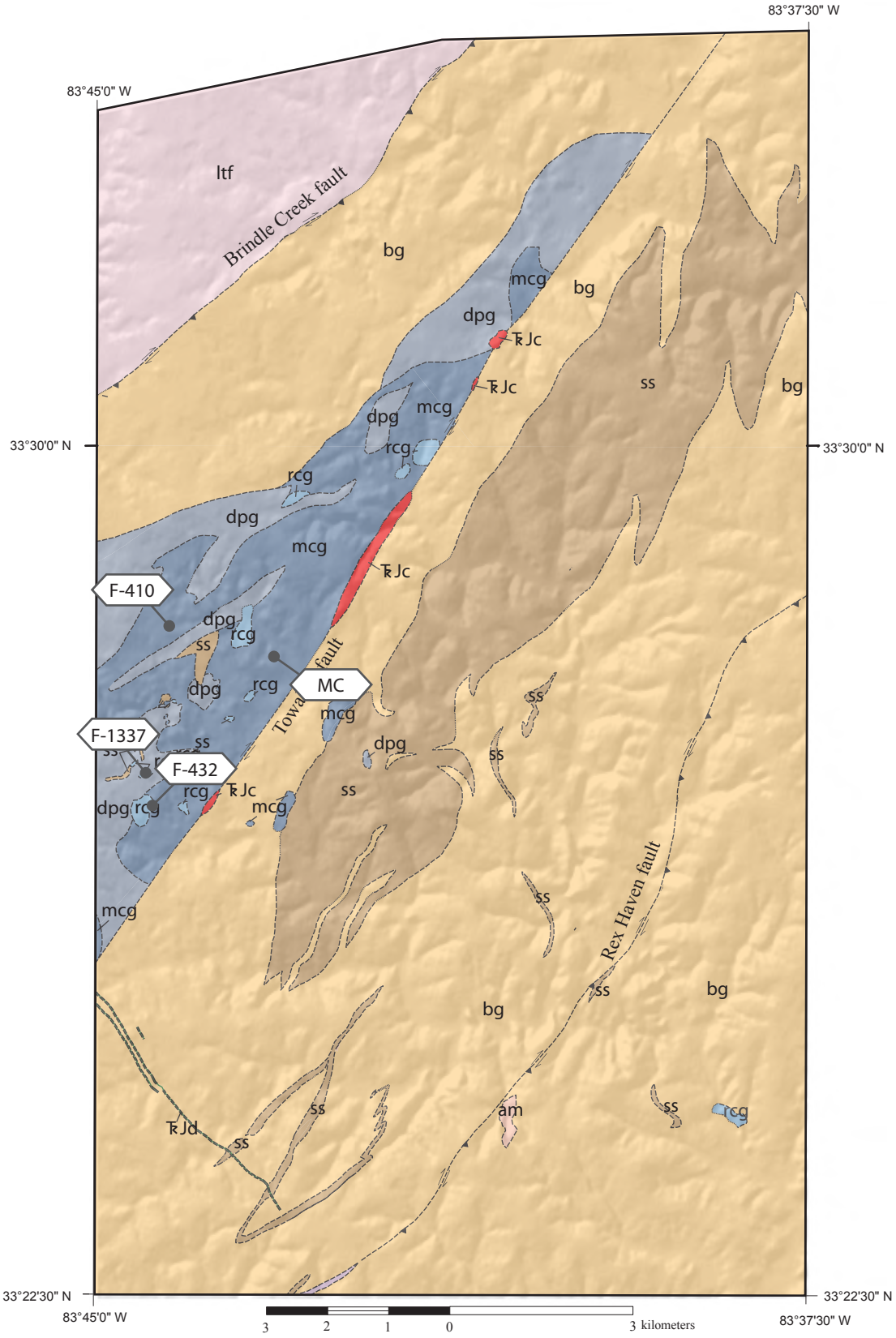

Figure 4-1. Detailed geologic map.

Table 4-1. Whole-rock major and trace element data for representative granitic samples in the Cat Squaret errane.

	Sample ID	F-1337	F432	F-410	MC
	Unit	Rocky Creek granodiorite	Rocky Creek granodiorite	Murder Creek granite	Murder Creek granite
	Tectnoic Unit	EIP	EIP	EIP	EIP
Analysis Type	**Detection Limit**				
FUS-ICP					
Major Oxides (wt%)					
LOI		0.68	0.67	0.22	0.54
SiO_2	0.01	66.05	67.2	68.3	67.6
$Al2O_3$	0.01	17.18	16.45	15.38	15.31
Fe_2O_3(T)	0.01	3.17	3.22	2.86	3.07
MnO	0.001	0.045	0.046	0.062	0.07
MgO	0.01	1.31	1.18	0.9	0.94
CaO	0.01	2.93	2.96	2.28	2.35
Na_2O	0.01	4.22	4.49	3.68	3.87
K_2O	0.01	3.41	3.51	4.76	4.19
TiO_2	0.001	0.525	0.58	0.471	0.482
P_2O_5	0.01	0.16	0.21	0.19	0.24
Total %		99.68	100.5	99.1	98.67
FUS-ICP					
Trace Elements (ppm)					
Ba	1	1185	1226	1066	706
Be	1	3	3	6	7
Sr	2	981	986	337	309
V	5	63	66	44	49
Y	1	10	11	11	10
INAA					
Trace Elements (ppm, -ppb)					
As	1	< 1	< 1	< 1	< 1
Au	1	< 1	< 1	< 1	< 1
Br	0.5	0.6	0.6	<0.5	<0.5
Co	0.1	4.7	7.7	4.7	5.5
Cr	0.5	6.2	6.6	13.3	14
Hg	1	< 1	< 1	< 1	< 1
Ir	1	< 1	< 1	< 1	< 1
Mo	2	<2	<2	<2	<2
Sb	0.1	0.1	0.1	0.2	0.1
Sc	0.01	3.63	5.6	6.82	7.29
Se	0.5	<0.5	<0.5	<0.5	<0.5
W	1	< 1	< 1	< 1	< 1

Table 4-1. Continued.

Sample ID	F-1337 Rocky Creek	F432 Rocky Creek	F-410 Murder Creek	MC Murder Creek
Unit	granodiorite	granodiorite	granite	granite
Tectnoic Unit	EIP	EIP	EIP	EIP
Analysis Type	**Detection Limit**			
MULT INAA / TD-ICP				
Trace Elements (ppm)				
Ag	0.5	0.7	1	<0.5	<0.5
Zn	1	57	57	61	67
TD-ICP				
Trace Elements (ppm)				
Cd	0.5	< 0.5	< 0.5	< 0.5	< 0.5
Cu	1	21	24	4	2
Ni	1	5	6	5	5
Pb	5	11	13	32	27
S	0.001	0.013	0.012	0.006	0.009
FUS-MS				
Trace Elements (ppm)				
Bi	0.1	0.2	<0.1	<0.1	<0.1
Cs	0.1	2	2.1	6.7	8.7
Ga	1	20	21	20	22
Ge	0.5	1	0.6	1	1.4
Hf	0.1	5.2	5.4	4.6	6.4
In	0.1	<0.1	<0.1	<0.1	<0.1
Mo	2	<2	<2	<2	<2
Nb	0.2	4.9	5.4	10	11.7
Rb	1	107	111	194	214
Sn	1	2	2	7	8
Ta	0.01	0.55	0.57	0.88	0.88
Th	0.05	15.8	18.7	22.5	22.3
U	0.01	3.36	3.01	1.53	1.69
Zr	1	230	222	186	244
La	0.05	56.3	55.6	65.4	59.2
Ce	0.05	105	102	130	113
Pr	0.01	11.6	10.6	14.1	11.9
Nd	0.05	39	38.2	47	42
Sm	0.01	5.86	5.74	6.89	6.44
Eu	0.005	1.34	1.32	1.19	1.14
Gd	0.01	3.53	3.48	4.06	3.76
Tb	0.01	0.42	0.42	0.5	0.5
Dy	0.01	2.1	2.09	2.38	2.38
Ho	0.01	0.36	0.38	0.4	0.43
Er	0.01	0.99	0.98	1.05	1.1
Tl	0.05	0.33	0.49	0.34	0.56
Tm	0.005	0.125	0.141	0.141	0.16
Yb	0.01	0.75	0.79	0.89	0.99
Lu	0.002	0.105	0.109	0.128	0.146

Compilation and comparison of eastern Inner Piedmont granitoid geochemistry to western Inner Piedmont granitoid geochemistry in North Carolina was made by Wilson (2006). Byars (2009) later incorporated her data with Wilson's (2006) previously compiled data from the Inner Piedmont, North Carolina. Comparison between the geochemical data from North Carolina and this study are compiled in this chapter.

Sample description and petrology

Barker's 1979 granitoid normative classification for feldspar compositions of the Mansfield and Farrar granitoids agrees with Streckeisen's IUGS classification and modal abundances (Table 4-2) (Fig. 4-2) (Streckeisen, 1976). This agreement in classifications plots the Rocky Creek granitoid as granodiorite and the Murder Creek granitoid as granite in both classification systems. The Murder Creek granite and Rocky Creek granodiorite are meta- to peraluminous (Fig 4-3).

Granitoid Geochemistry

Harker variation diagrams

Harker variation diagrams for Inner Piedmont rocks exhibit a decreasing linear trend for compatible elements, whereas, incompatible elements tend to exhibit an increasing linear trend (Fig. 4-4). With increasing silica content the following trends manifest: (1) TiO_2, FeO, MgO, Na_2O, and CaO decrease in abundance; (2) K_2O increases; and (3) Al_2O_3 does not display a strong variation. The four samples from the field area seem to mirror the Inner Piedmont trend with the exception of Na_2O, where it appears to decrease in a linear trend. Both the eastern Inner Piedmont granitoids from central Georgia and the North Carolina, appear to contain similar amounts of SiO_2.

Covariation diagrams plotted against TiO_2 were compiled for all eastern Inner Piedmont granitoids (Fig. 4-5). These diagrams were constructed to determine if there is a similar geochemical signature between the Murder Creek and Walker Top granites. All samples

Table 4-2. Granitoid CIPW normative compositions. Norms calculated using a pre-formatted Excel spreadsheet courtesy of H. Y. McSween.

Sample ID	F432	F-1337	F-410	MC
Unit	Rocky Creek granitoid	Rocky Creek granitoid	Murder Creek granite	Murder Creek granite
Tectonic Unit	EIP	EIP	EIP	EIP
Normative Mineralogy				
Quartz	20.14	20.67	22.98	23.29
Corundum	0.39	1.61	0.49	0.71
Orthoclase	20.74	20.15	28.13	24.76
Albite	37.99	35.71	31.14	32.75
Anorthite	13.31	13.49	10.07	10.09
Hypersthene	2.94	3.26	2.24	2.34
en	2.94	3.26	2.24	2.34
Hematite	3.22	3.17	2.86	3.07
Ilmenite	0.10	0.10	0.13	0.15
Rutile	0.53	0.47	0.40	0.40
Apatite	0.50	0.38	0.45	0.57
Total	99.86	95.84	98.89	98.13

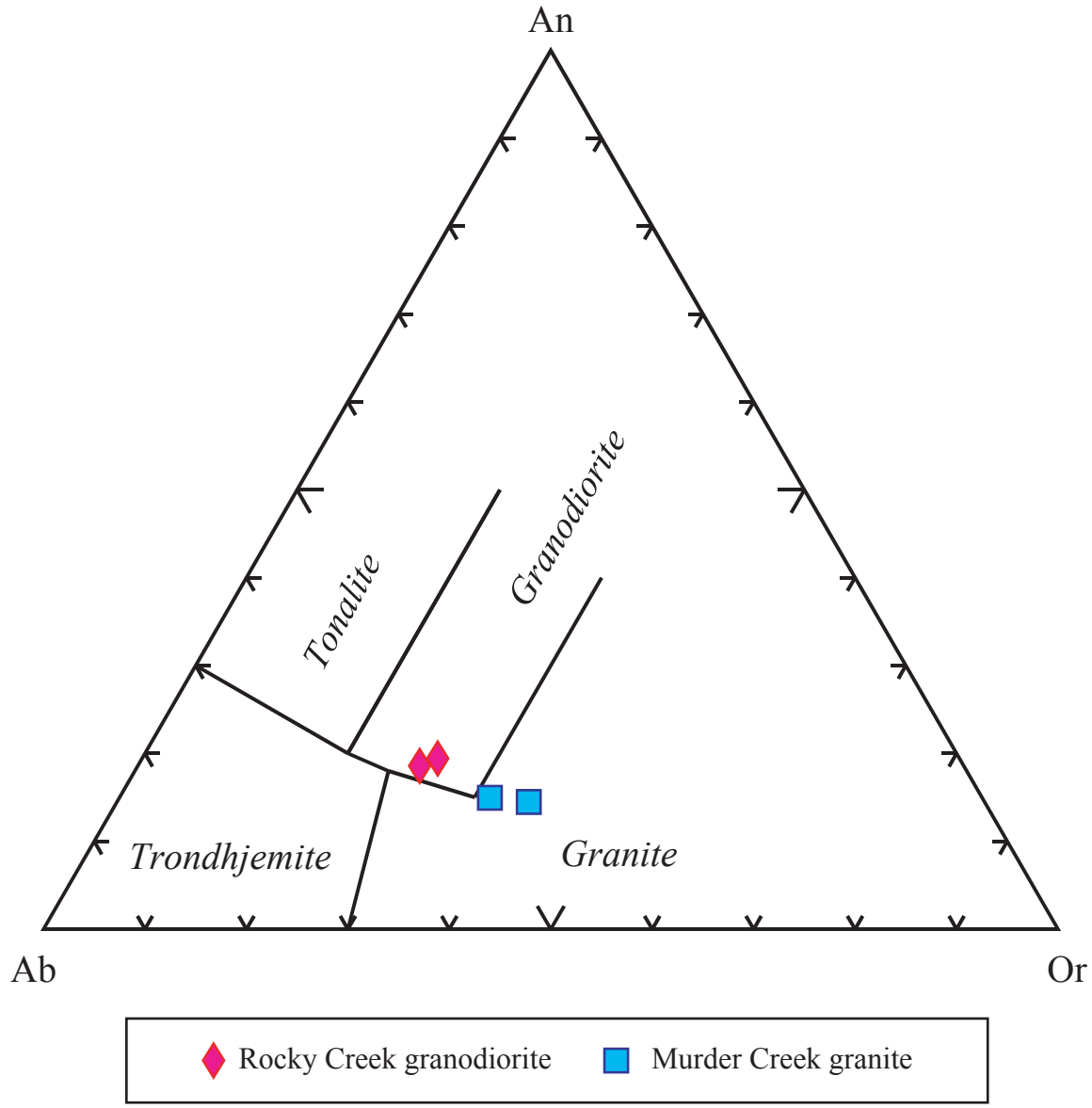

Figure 4-2. Normative-feldspar classification (Barker, 1979) of Farrar quadrangle granitoids.

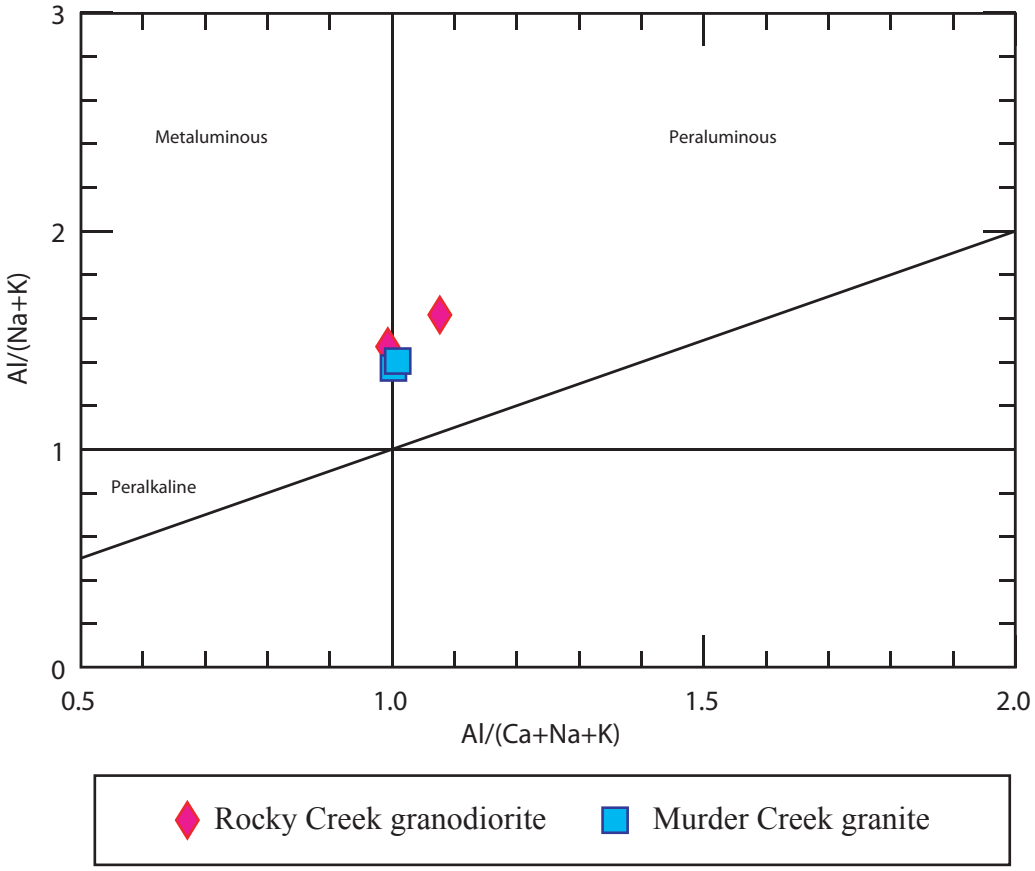

Figure 4-3. Shand's Index (Maniar and Piccoli, 1989) showing both the Rocky Creek granodiorite and Murder Creek granite.

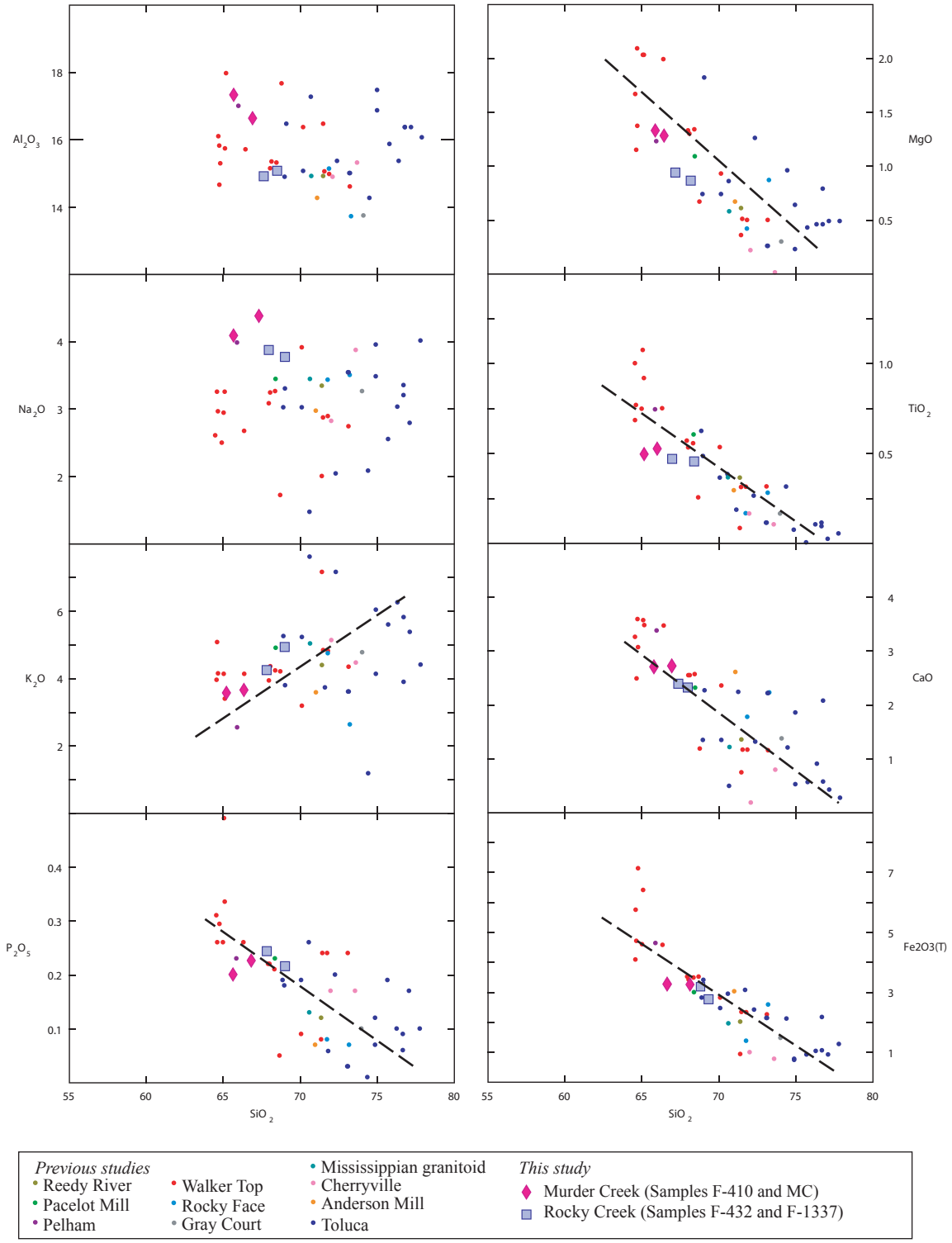

Figure 4-4. Harker variation diagram for Cat Square terrane granites (Wilson, 2006; Gatewood, 2007; Byars, 2010).

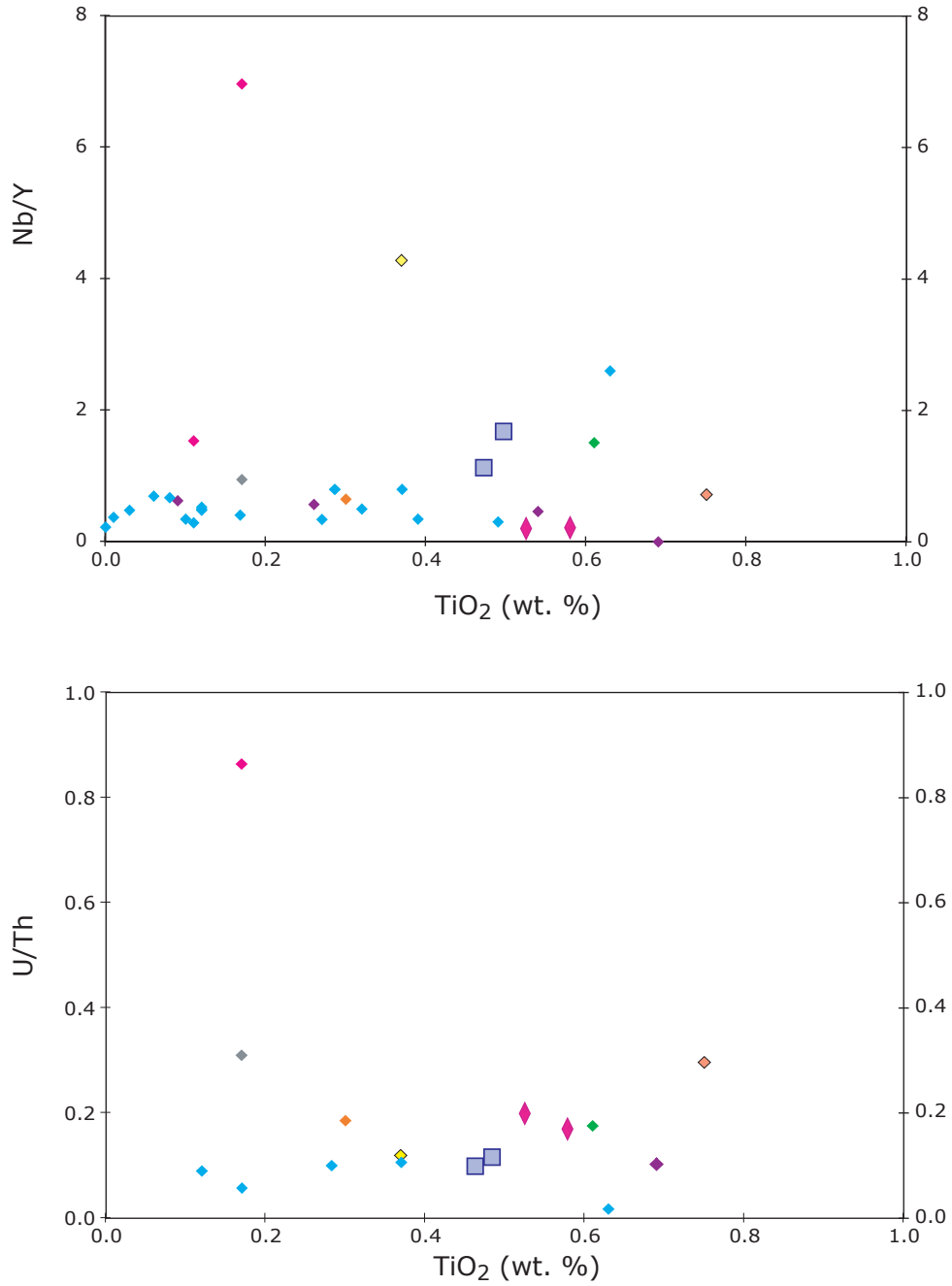

Figure 4-5. TiO_2 variation diagrams of Cat Square terrane granitoids from previous studies and this study (Wilson, 2006; Gatewood, 2007; Byars, 2010).

combined exhibit a varying range of TiO_2 (0.11-1.21 wt.%), a low U/Th (0.07-0.26) value, and a varying range of Nb/Y (0.25-1.32) values. The geochemical signatures are similar to those of the Walker Top Granite in the Brushy and South Mountains, North Carolina, with the exception of higher Nb/Y (0.92-1.32) values. Given similar overall geochemistry, petrographic similarity, tectonic setting, and apparent similarities in trace element geochemistries, the Murder Creek granite may be the southwestern equivalent to the Walker Top Granite. Geochronologic data to be acquired will address this problem.

Trace element geochemistry

Identifying cogenetic relationships and trends in trace-element geochemistry is particularly important when rocks have undergone multiple episodes of deformation and metamorphism. Discerning the way that elements interact with one another as magmas are generated, and how they evolve in their particular tectonic settings, permits us to examine their evolution more closely (McBirney, 1993). Major elements are generally highly mobile in rocks that have undergone metamorphism, but trace elements are rather useful due to their decreased mobility during these events. The decreased mobility of trace elements indicates that, of all elements, they will retain their protolith signatures best; these signatures can be indicative of certain petrogenetic processes (Pearce and Cann, 1973; Pearce, 1982; Rollinson, 1993). Trace elements have a preference for either the melt phase or the solid (mineral) phase (Rollinson, 1993). Elements that prefer the mineral phase are referred to as compatible elements, and have a high ionic potential; elements that prefer the melt phase are incompatible elements, and have a low ionic potential (Rollinson, 1993). As is true with many of Earth's systems, this is not cut and dry; many elements vary in their behavior based on melt composition, although links can be made by recognizing these behaviors and identifying patterns that emerge in systems (McBirney, 1993).

Six normalized multi-element diagrams were compiled in IgPet™; these diagrams are sometimes referred to as incompatible element diagrams or spider diagrams. In these diagrams, light ion lithophile elements (LILE) are plotted on the left side of the diagram, and high field strength elements (HFSE) are plotted on the right side. Presence of LILE elements are more

easily influenced by the fluid phase, so they occur in a greater abundance; HFSE are more immobile, and are therefore generally more depleted than LILE elements. Three of the spider diagrams (Fig. 4-6) contain compiled data from the granitoids of the Farrar and Mansfield quadrangles, and the other three (Fig. 4-7) contain compiled data from granitoids of the eastern Inner Piedmont in the South Mountains, North Carolina.

There is an apparent similarity in trends of the central Georgia Inner Piedmont granitoids, and those of the North Carolina Inner Piedmont. Each diagram exhibits enrichment in LILE elements and a gradual depletion in HFSE elements. Each diagram also exhibits a Nb-Ta depletion trough and a Ti depletion, and the Murder Creek sample, much like the samples from the South Mountains, North Carolina, displays a negative Sr anomaly. The most distinct difference between the trends is a non-deviating trend in Sr that occurs in the Rocky Creek granodiorite. From field relationships and petrographic analyses, this granitoid appears to be the youngest pulse or facies of the three granitoids located in the field area. Generally this granitoid is found as dike intrusions, and commonly intrudes both the Murder Creek and Dow's Pulpit granitoids.

REE geochemistry

A similar trend between the central Georgia granitoids and the North Carolina Inner Piedmont granitoids is observed in the rare earth element (REE) plots as Inner Piedmont granitoids appear to have lower concentrations of light rare earth elements (LREE) resulting in a flat REE pattern (Fig. 4-8). The Rocky Creek samples mirror the trend of the other eastern Inner Piedmont granitoids, with the exception of the absence of a negative Eu anomaly. Wilson (2006) reported that the eastern Inner Piedmont granitoids of the Brushy Mountains, North Carolina, generally display a strongly depleted Sr and negative Eu anomaly, and rarely display an absent to slightly positive Eu anomaly.

Tectonic discrimination diagrams

Tectonic discrimination diagrams reveal that the Farrar quadrangle granitoids retain volcanic-arc signatures, much like that of other eastern Inner Piedmont granitoids, with overlap

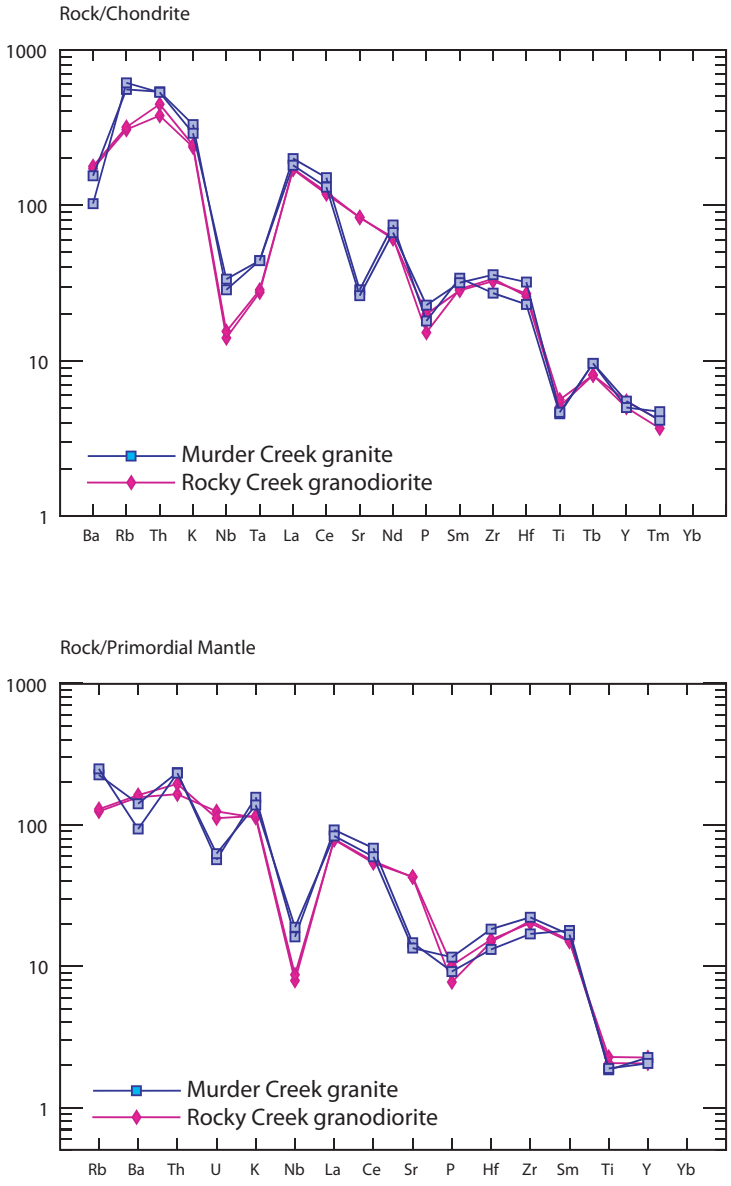

Figure 4-6. Trace-element diagrams for the Murder Creek granite and Rocky Creek granodiorite samples (Thompson, 1982; Holm, 1985).

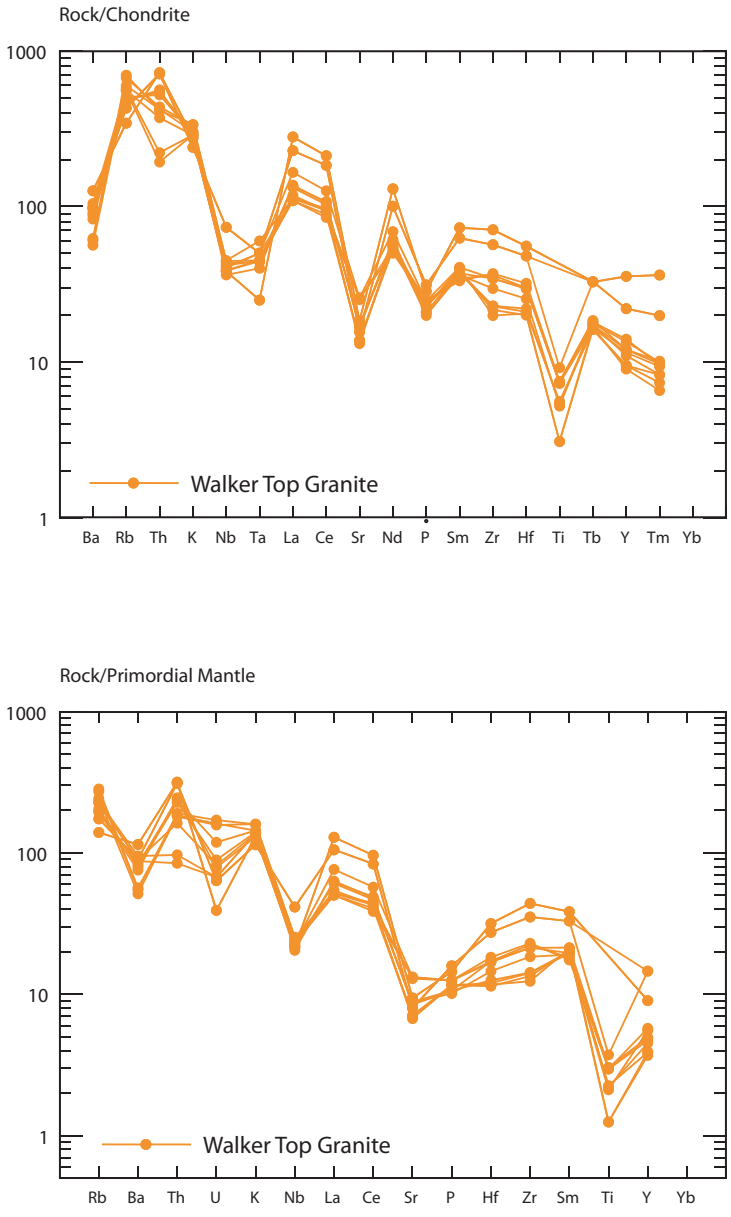

Figure 4-7. Trace-element diagrams for Walker Top Granite samples (Gatewood, 2007; Thompson, 1982; Holm, 1985).

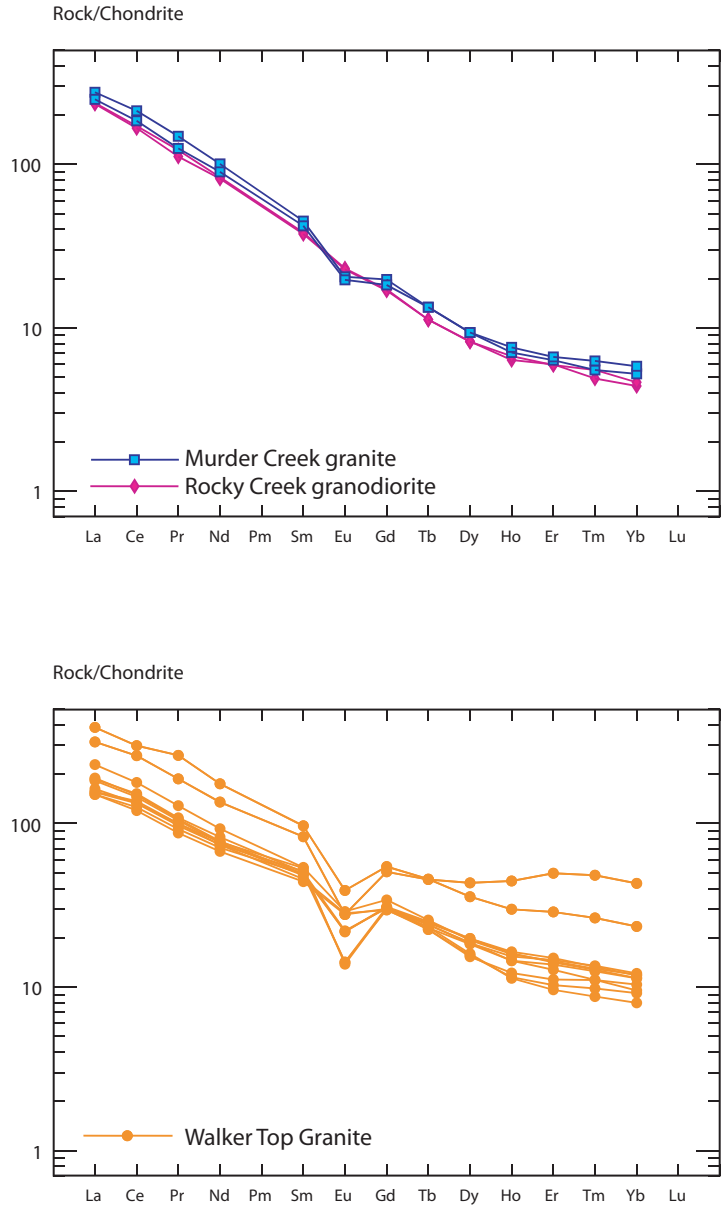

Figure 4-8. REE diagrams (Sun and McDonough, 1989) for the Farrar quadrangle granitoids, and Walker Top Granite (Gatewood, 2007).

in the syn-collisional field (Fig. 4-9). The Rocky Creek granodiorite is restricted to the volcanic-arc field, with exception of the Nb to Y ratios, where it lies in the volcanic-arc + syn-collision field. The Murder Creek granite is more enriched in Ta, Nb, and Rb, with respect to the Rocky Creek granodiorite, and tends to plot on the boundary between the syn-collisional and volcanic arc fields.

Synthesis and Conclusions

Eastern Inner Piedmont granitoids retain distinguishing geochemical signatures, and petrologic and textural similarities across the span of the Cat Square terrane. Similarities in geochemical characteristics, such as trace element and REE patterns suggest that, although separated by a great distance, these granitoids formed from similar geologic conditions, and most likely shared a common anatectic origin. Their signatures are most likely a direct reflection of the surrounding metasedimentary rocks.

Although there have been extensive geochemical analyses performed on the rocks in the Inner Piedmont, many workers have failed to explain specific geochemical signatures seen in trace and REE diagrams in granitoids. Inner Piedmont rocks typically display negative Nb and Ta troughs, along with Ti depletion. These patterns have also been recognized in calc-alkaline basalts, and are generally indicative of the formation of the continental crust through geologic time (Winter, 2001). Applied to granitic rocks, these signatures imply fractional crystallization of sphene, rutile, or ilmenite. This trough is recognized in many trace element plots, and is most likely representative of the evolution of continental crust through time. It gives further credibility that these plutons are most likely anatectic in origin.

Other granitoids of the eastern Inner Piedmont, such as the Walker Top Granite tend to display a negative Sr anomaly, but the Rocky Creek granitoid normative to chondrite shows no variability and mirrors the slope of the diagram. Normative to primitive and primordial mantle Sr displays a negative anomaly. This variability in the Sr value more commonly resembles the Toluca Granite; this may be attributable to the fractionation of plagioclase in earlier granitoid pulses, and accumulation or lack of fractionation of plagioclase in this later granitoid. This hypothesis is reconfirmed from REE plots. The Murder Creek granite and other eastern Inner

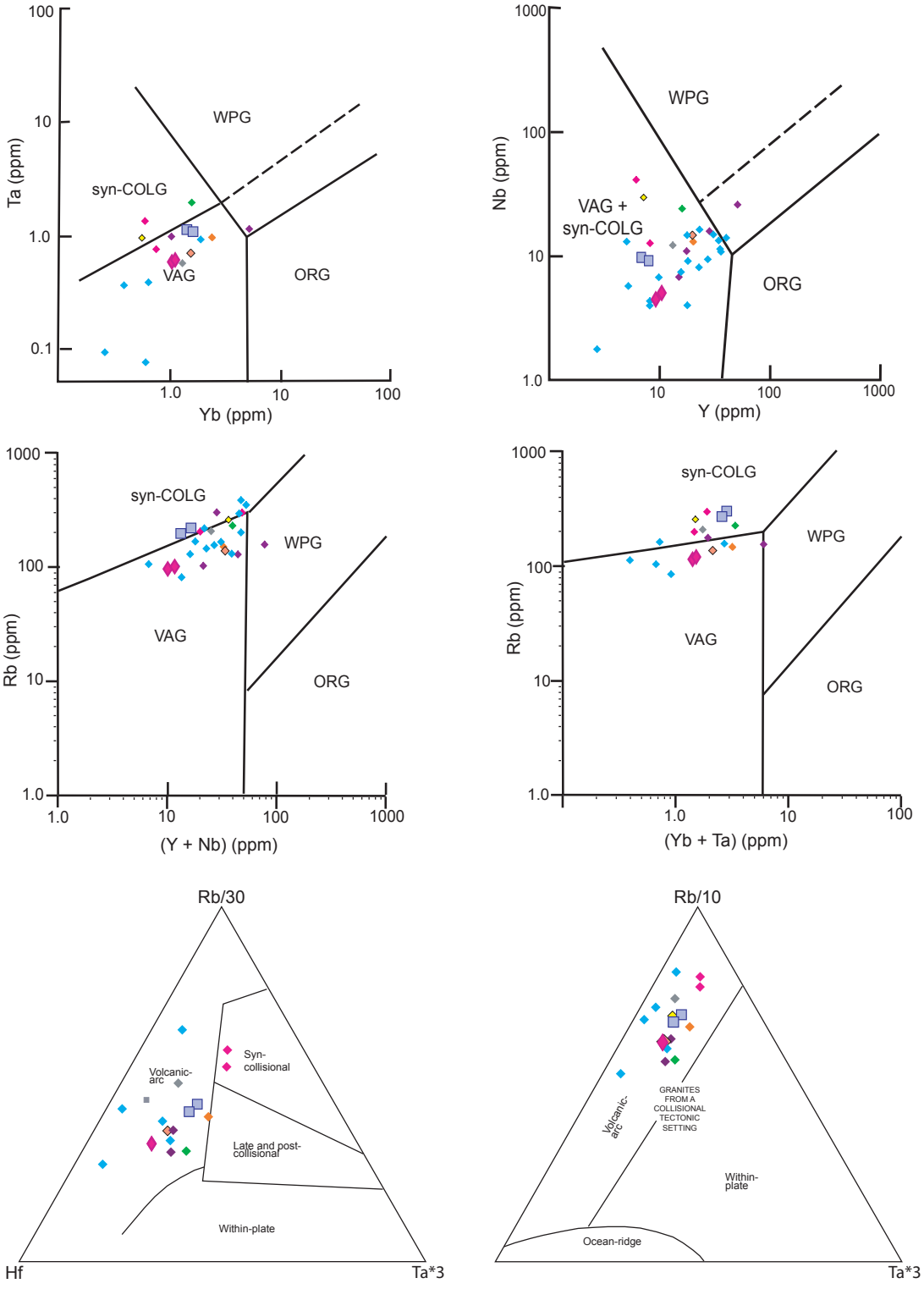

Figure 4-9. Tectonic discriminant diagrams for eastern Inner Piedmont granitoids (Pearce et al., 1984). Abbreviations ORG - orogenic granite; syn-COLG - syn-collisional granite; VAG - volcanic-arc granite; and WPG - within-plate granite. See Figure 4-4 for sample names.

Piedmont granitoids, such as the Walker Top and Toluca Granites, display a negative Eu anomaly, whereas the Rocky Creek granite slope declines gradually. Sr, being a LIL element, is easily mobilized by a hydrous fluid phase, and may be the result of metasomatism; however, this is unlikely based on the K, Rb, and Ba values. The absence of a negative Sr anomaly is most likely a reflection of unfractionated plagioclase from the melt. Anomalies in these diagrams are hard to discern due to other minor or accessory minerals present, such as apatite, zircon, monazite, and allanite, which all have a very high REE distribution coefficients.

The most important point garnered from the trace element and REE patterns in spider diagrams, such as similarities in peaks and troughs, is that they must share either a common parent, process, or contaminant (Winter, 2001). From these patterns, it is likely that the Murder Creek granite is the southwestern equivalent of the Walker Top Granite. The Rocky Creek granodiorite shares similar geochemical characteristics with the Toluca Granite, although they are different both petrographically and texturally. Many granitoids in the southern Appalachians often display three facies or pulses; the first pulse is generally a megacrystic granitoid with megacrysts of either K-feldspar or plagioclase; the second pulse is usually consistent with a medium-grained inequigranular granitoid; and the third is generally a very fine-grained poorly-foliated granitoid (Spear, 1997). The Rocky Creek most likely the represents the third pulse of magmatism, but there appears to be no geochemical analysis for this third facies of granitoid in North Carolina.

Previous isotopic work on granitoids performed by Vinson (1999) and Mapes (2002) revealed that eastern Inner Piedmont granitoids have a high initial $^{87}Sr/^{86}Sr$ (0.705–0.717) and a low ε_{Nd} (-1.6 to -6.4) values, much like the metasedimentary rocks that they intrude (Bream et al., 2004; Bream, 2003; and Mapes et al., 2002). Despite the lack of isotopic work performed on the rocks of the central Georgia Inner Piedmont, it is most likely that these rocks also have an anatectic origin. Overlap of Farrar quadrangle granitoids into the volcanic-arc field may be a relict of anatectic melting of the metapsammite and pelitic rocks of the Cat Square terrane. The sediments of these rocks were derived from a volcanic-arc terrane. Therefore, derivation of Farrar quadrangle granitoids is a result of anatexis of local metasedimentary rocks, induced by collision and burial, as supported by similar REE and trace element geochemical signatures and

patterns along with high normative corundum values. According to Gatewood (2007), melt conditions of metasedimentary units occurred into the Alleghanian, as indicated by a 322 Ma crystallization U-Pb SHRIMP age date of a medium-grained granitoid.

Chapter 5: Central Georgia Inner Piedmont Kinematics and Structure

Introduction

Identifying lithologies along with metamorphic grade is necessary in interpreting P-T paths. These components in combination with structural data, such as foliation, fold, and lineation measurements provide critical information for understanding the tectonic evolution of a region and its deformational history (Fig. 5-1 and Plate 1). The southern Appalachians are a product of three Paleozoic accretionary orogenic events, completing a Wilson cycle, followed by Mesozoic rifting and early Cenozoic uplift (Hatcher, 2002). Multiple orogenies, in combination with polyphase deformation, complicate southern Appalachians tectonic history.

The Inner Piedmont is the polydeformed, migmatitic crystalline core of the southern Appalachians, with structure characterized by large-scale SW-directed ductile, type-F, lobate plastic thrust sheets (Hatcher, 2002). During emplacement and after appreciable cooling, Inner Piedmont faults were transformed into a series of type-C thrust sheets (Hatcher and Hooper, 1992; Hatcher, 2004; Merschat et al., 2005). The transformation from a type-F thrust sheet to type-C allows the thrust sheet to gain strength, cohesiveness, and displacement (Hatcher and Hooper, 1992). Transport direction of Inner Piedmont thrusts was determined from sheath folds, asymmetric boudins, winged porphyroclasts, mineral lineations, snowball garnets, S-C fabrics, and vergence of asymmetric folds (Davis et al., 1991; Yanagihara, 1993). Detailed geologic mapping performed in the northern Inner Piedmont revealed eight major thrusts: the west-bounding Brevard fault zone and the east-bounding Brindle Creek fault. Other internal thrust sheets identified in the Tugaloo terrane in ascending order southeastward from the Brevard fault zone include: the Marion thrust sheet, Tumblebug-Stumphouse Mountain thrust sheet, Walhalla nappe, Sugarloaf Mountain and Six-Mile-Seneca thrust sheet, Mill Spring thrust sheet, and Anderson thrust sheet (Hatcher, 2002; Merschat et al., 2005). No thrust sheets other than the Brindle Creek thrust sheet had been identified in the eastern Inner Piedmont Cat Square terrane

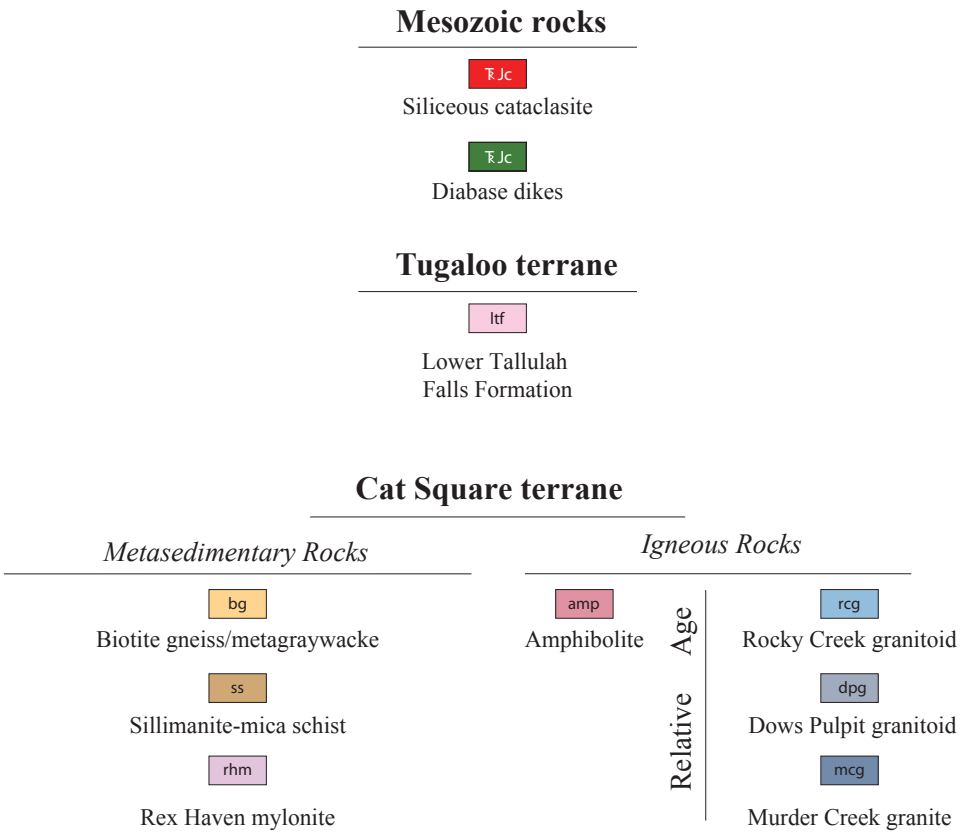

Figure 5-1. Geologic map of portions of the Farrar and Mansfield quadrangles. For rock unit descriptions, see Fig. 2-1 in Chapter 2 or Plate 1.

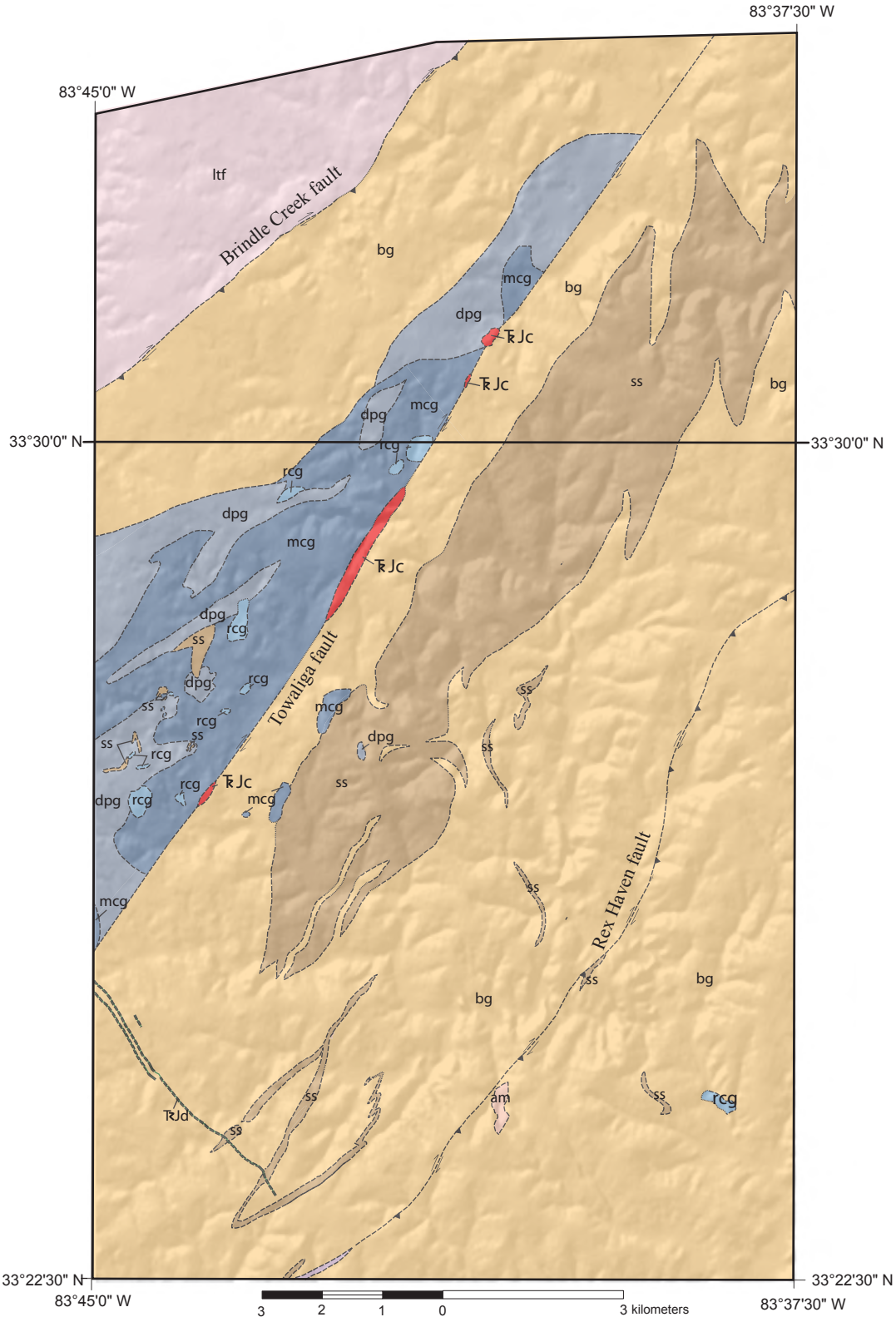

Figure 5-1. Continued.

prior to this study; however, as a result of detailed geologic mapping the Rex Haven (Kinnard Creek) thrust sheet was identified in the central Georgia eastern Inner Piedmont.

Large-scale outcrops**,** such as Woodall Shoals in the South Carolina and Georgia Blue Ridge, became Rosetta Stones to identify the deformational events that occurred in the Inner Piedmont (Hopson et al., 1989; Hatcher et al., 1995). Multiple generations of early ductile flow folds are recognized by orientation, overprinting relationships, and style. Meso- and macroscale structures parallel, normal, and oblique to the orogen are recognized from detailed geologic mapping (Hatcher, 1972; and Griffin, 1974). Six deformational events are recorded in the Inner Piedmont, including five or more major folding events and two brittle events related to extension (Table 5-1) (Davis, 1993, Yanagihara, 1994; Bream, 1999; Giorgis, 1999; Hill, 1999; Williams, 2000; Bier, 2001; Kalbas, 2003; Merschat, 2003; Gatewood, 2007).

Timing of deformation is delimited from granitoid crystallization ages, U/Pb monazite and zircon rim ages, along with meso- and macroscale relationships. The Inner Piedmont was deformed by early ductile Neoacadian (360-345 Ma) and early Alleghanian (320 Ma) events, and was later deformed and overprinted by several late brittle Alleghanian events (Merschat and Kalbas, 2002; Hatcher et al., 2005).

Methods

The motivation for this project lies in the aeromagnetic data that was reprocessed and provided by the USGS (Fig. 5-2) (Daniels, D. L., unpub. data). These aeromagnetic data were used to identify structural features, such as faults and mineral stretching lineations (Hatcher et al., 2007).

A detailed geologic map of portions of the Farrar and Mansfield quadrangles was constructed during two field seasons that spanned early January until mid-July in 2008, and early January to August in 2009. Additional trips were made to the field in order to collect samples, photos, and to conduct a field review during August 2009. A Trimble™ unit was used to record structural measurements, lithologic descriptions, and petrographic information. The Trimble™ unit was also used as a GPS navigation system. 1:24,000 USGS topographic maps were also utilized in the field. All information stored in the Trimble™ unit was transferred daily to a

Table 5-1. Summary and relative timing of deformation events in the central Inner Piedmont, Georgia*.

DEFORMATION EVENTS		STRUCTURES			METAMORPHIC CONDITIONS	REGIONAL EVENTS	OROGENY & TIMING
		FABRICS	FOLDS	FAULTS			
D_1	D_{1wIP}	S_1 local foliation preserved in boudins	F_{1wIP}: intrafolial, rootless folds; folds preserved in boudins; map-scale folds in TCFZ footwall	TCFZ emplacement	moderate pressure and temperature	arc accretion to Laurentian margin and deposition of western IP Ordovician bimodal volcanics	Taconian orogeny 480-450 Ma
	D_{1eIP}	S_1 regional axial planar foliation	F_{1eIP}: intrafolial and rootless folds; folds preserved in boudins; refolded recumbent, and isoclinal folds	initial development of the CPS	high pressure, upper amphibolite, kyanite-grade; above minimum melt conditions	initial subduction of Cat Square terrane sediments beneath Carolina terrane	Acadian orogeny intrusion of ~407 Ma Walker Top Gneiss in eIP
D_2		S_2: penetrative foliation; L_2: mineral lineation	F_2: reclined, tight to isoclinal, and recumbent folds; meso- and macroscale SW-vergent passive flow sheath folds	emplacement of ductile IP thrust sheets of BCFZ, TCFZ, MSFZ, RHFZ; early movement and deflection along Neoacadian BFZ	high temperature, upper amphibolite (granulite?) facies; sillimanite I and II grade; first shared thermal event between eIP and wIP	transpressional accretion of eastern IP and Carolina terrane; SW-directed ductile extrusion and crustal flow of IP	Neoacadian orogeny 360-340 Ma
D_3		S_3: rare mesoscopic foliation L_3: mineral and intersection lineation	F_3: folding of BCFZ and the RHFZ; reclined, open to tight, NW and SW vergent	continued movement along ductile fault zones; further SW-deflection of IP thrust sheets	high temperature, lower pressure conditions; sillimanite I grade	continued emplacement of eastern IP and Carolina terrane; uplift, unroofing, and cooling of IP	Late Neoacadian orogeny
D_4		dextral S-C and shear-related fabrics in MSFZ, TCFZ, BCFZ, BFZ, RHFZ, and CPS sheared quartz veins	F_4: inclined to upright, tight to closed, NW-SE trending, SW-vergent folds, and well developed crenulations	ductile reactivation of BFZ; dextral oblique-slip motion on MSFZ and BCFZ in northeastern IP	moderate to low pressure and temperature brittle conditions	emplacement of composite Blue Ridge-Piedmont type C thrust sheet; regional dextral strike-slip motion along large faults	Alleghanian orogeny 330-300 Ma
D_5		joints	F_5: regional open, broad, trend NE & NW, formation of Newton antiform	brittle reactivation and dextral strike-slip motion along BFZ	low temperature conditions	continued emplacement and exhumation of type C thrust sheet unroofing, and cooling followed by rifting	late Alleghanian uplift; Mesozoic extension
D_6		filled joints unfilled joints	F_6: regional broad, open folds, trend NE	brittle reactivation and dextral strike-slip motion along the Towaliga fault	low pressure and temperature brittle conditions	continued rifting and uplift	Cenozoic uplift

*Modified from Davis, 1993; Yanagihara, 1994; Bream, 1999; Giorgis, 1999; Hill, 1999; Williams, 2000; Bier, 2001; Kalbas, 2003; Merschat, 2003; Merschat et al., 2005; Gatewood, 2007, and Byars, 2009. BCFZ=Brindle Creek fault zone; BFZ=Brevard fault zone; CPS=Central Piedmont suture; MSFZ=Mill Spring fault zone; RHFZ=Rex Haven fault zone. TCFZ=Tumblebug Creek fault zone. eIP-eastern Inner Piedmont. wIP-western Inner Piedmont.

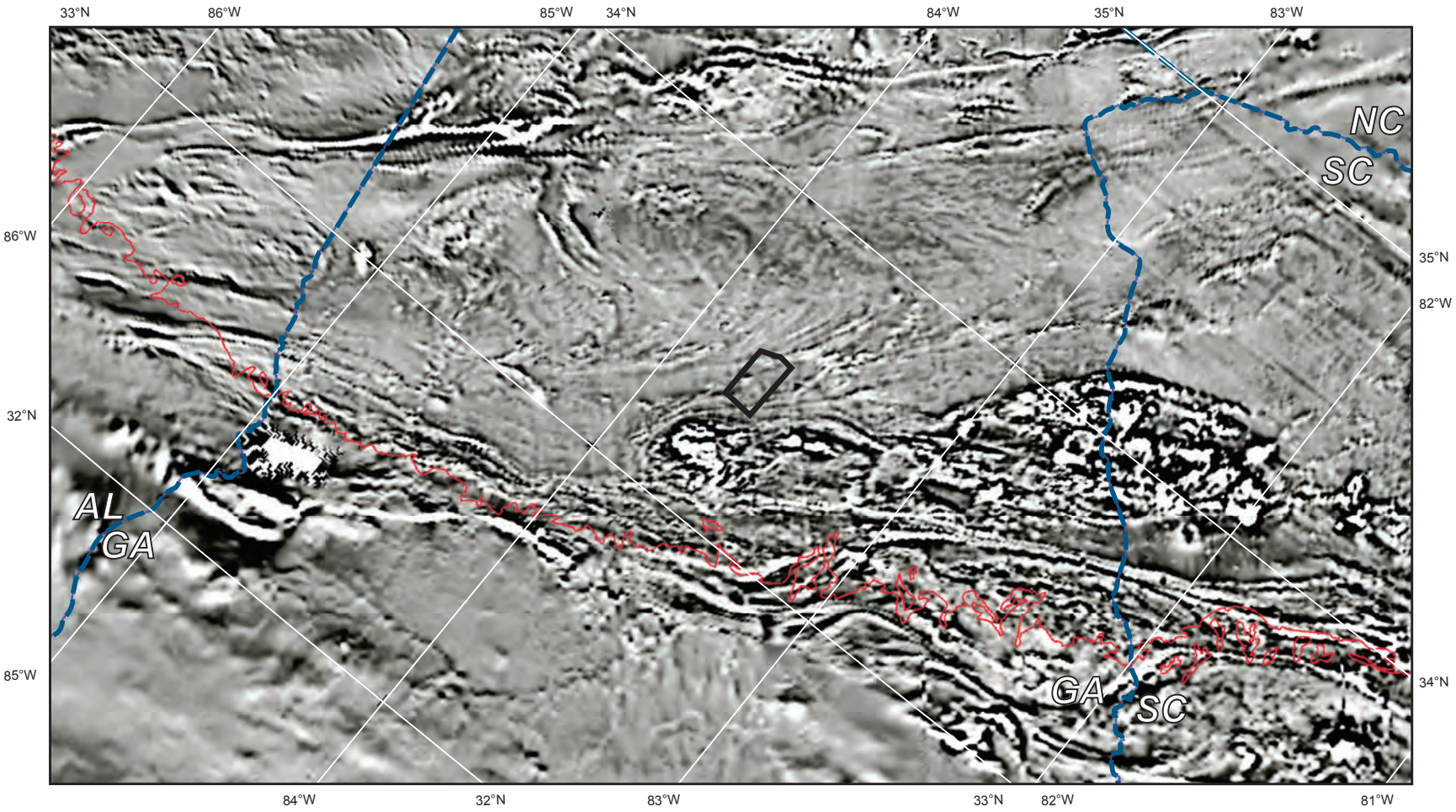

Figure 5-2. Grayscale aeromagnetic map, reduced to pole. Field area is highlighted in black and state lines are in blue. Red line represents the Fall Line (D. L. Daniels, unpub. data).

computer, and compiled in ArcMap GIS™ software. The geologic map and station ID maps were constructed using Arc Map GIS™.

Aeromagnetic Data

Aeromagnetic data provided by the USGS is an important tool used in constructing the current tectonic map of the southern Appalachians (Hatcher et al., 2007), and in deciphering potential areas of interest for further detailed geologic mapping (Fig. 5-3) (Daniels, D.L., unpub. data). Several major structural features were identified in the central Georgia Inner Piedmont, including three prominent lineaments and a suite of curved anomalies. The suite of high-frequency curved magnetic anomalies is truncated along the northernmost linear feature. This prominent linear feature is the southern continuation of the Brindle Creek fault, the suture between the Tugaloo and Cat Square terranes. Other prominent lineaments were identified just south of the Brindle Creek fault. The lineament just southeast of the Brindle Creek fault is the brittlely reactivated Towaliga fault. In aeromagnetic data it appears to extend over 200 km from the Pine Mountain Window into northeastern Georgia. The southernmost lineament identified in the area was confirmed to be another thrust sheet based on new field evidence and detailed geologic mapping.

D_1 Deformation

D_1 deformation occurred prior to the dominant and most pervasive deformational event, producing F_1 folds and S_1 foliation (Davis, 1993). Later more pervasive deformational events overprinted D_1, obscuring the first phase of deformation (Hopson et al., 1989). According to Hopson et al. (1989), D_1 most commonly occurs as isoclinal recumbent folds (F_1). S_1 foliation is characterized by alternating biotite-rich and quartzofeldspathic layers. In a small window of the Tumblebug Creek thrust sheet, Davis (1993) recognized preserved compositional layering in the Poor Mountain Formation in F_1 folds. F_1 is commonly preserved as intrafolial flowage rootless folds. Folds of similar style located inside of amphibolite boudins probably belong to this generation of deformation as well. The orientation of F_1 varies considerably from subsequent episodes of deformation, leading to transposition and overwriting of previous folds.

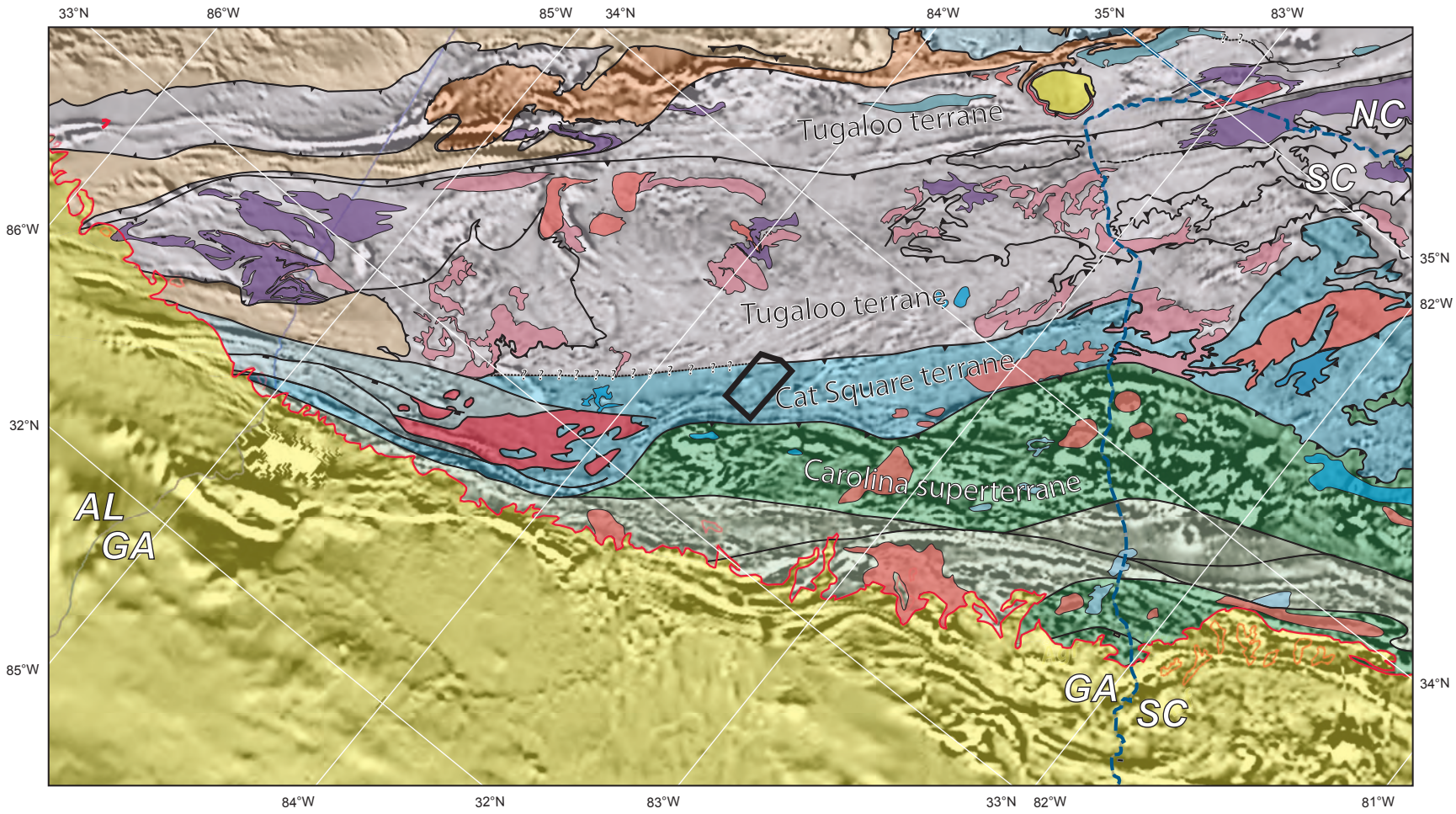

Figure 5-3. Aeromagnetic map (D. L. Daniels, unpub. data) with tectonic map overlay. Field area is highlighted in black and state lines are in blue. Red line represents the Fall Line (Hatcher et al., 2007 and Davis et al., 2009). For a more detailed explanation refer to Fig 1-3.

One D_1 truncated refolded fold was identified in domain II. The penetrative axial planar foliation (S_1) was noted to occur in amphibolite boudins (Fig. 5-4). S_1 was also observed in the interior of garnets in amphibolites. The foliation is defined by opaques. No D_1 deformation was identified at the macroscopic scale.

D_2 Deformation

D_2 deformation formed during the Neoacadian orogeny, and produced a penetrative fabric throughout the Eastern Blue Ridge and Inner Piedmont. Structures related to D_2 deformation include; the dominant S_2 foliation along with a prominent mineral lineation (L_2), tight folds, sheath folds, and type-F thrust faults. According to Bream (2003), the D_2 deformation event is described as, "the most penetrative polyphase event at or near peak metamorphism." Timing of this deformational event was constrained by U-Pb zircon age dating of intensely migmatized footwall rocks, suggesting emplacement of the Brindle Creek thrust sheet occurred ~342 Ma (Mapes, 2002; Merschat et al., 2005). Also, U-Pb monazite and zircon metamorphic ages of 360-350 Ma indicate that peak metamorphism and the Neoacadian orogeny were synchronous (Bream, 2003).

Foliation

The pervasive S_2 foliation parallels the axial surface of the F_2 folds, suggesting coeval timing. S_2 is the dominant foliation in the field area, and is defined by the alteration of muscovite-biotite-rich and quartzofeldspathic layers. S_2 formed as a result of transposition of S_1, and the recrystallization and alignment of biotite and muscovite parallel to the F_2 fold axial surface. Hill (1999) described D_2 as "a progressive episode, in which heterogeneous and slightly diachronous deformation occurred as a continuum."

A compiled form-line map (Fig. 5-5) of portions of the Mansfield and Farrar quadrangles exhibits at least three distinct domains, identified by their S_2 orientations. Equal-area fabric diagrams were constructed using 1,112 foliation and schistocity measurements from the field area (Fig. 5-6). Domain I is dominated by NE-SW-striking foliations. Domain I mirrors the trend of the orogen, and encompasses the lower Tallulah Falls Formation. Domain II greatly varies in



Figure 5-4. Saprolite outcrop with interlayered biotite gneiss (rust red), amphibolite (mustard), and leucosome (white). An amphibolite boudin perserving S_1 foliation, surrounded by the dominant S_2 foliation. Rock hammer for scale. This outcrop is located at the intersection Shepard Pond Creek and Shepard Pond Road. Photo taken facing southeast.

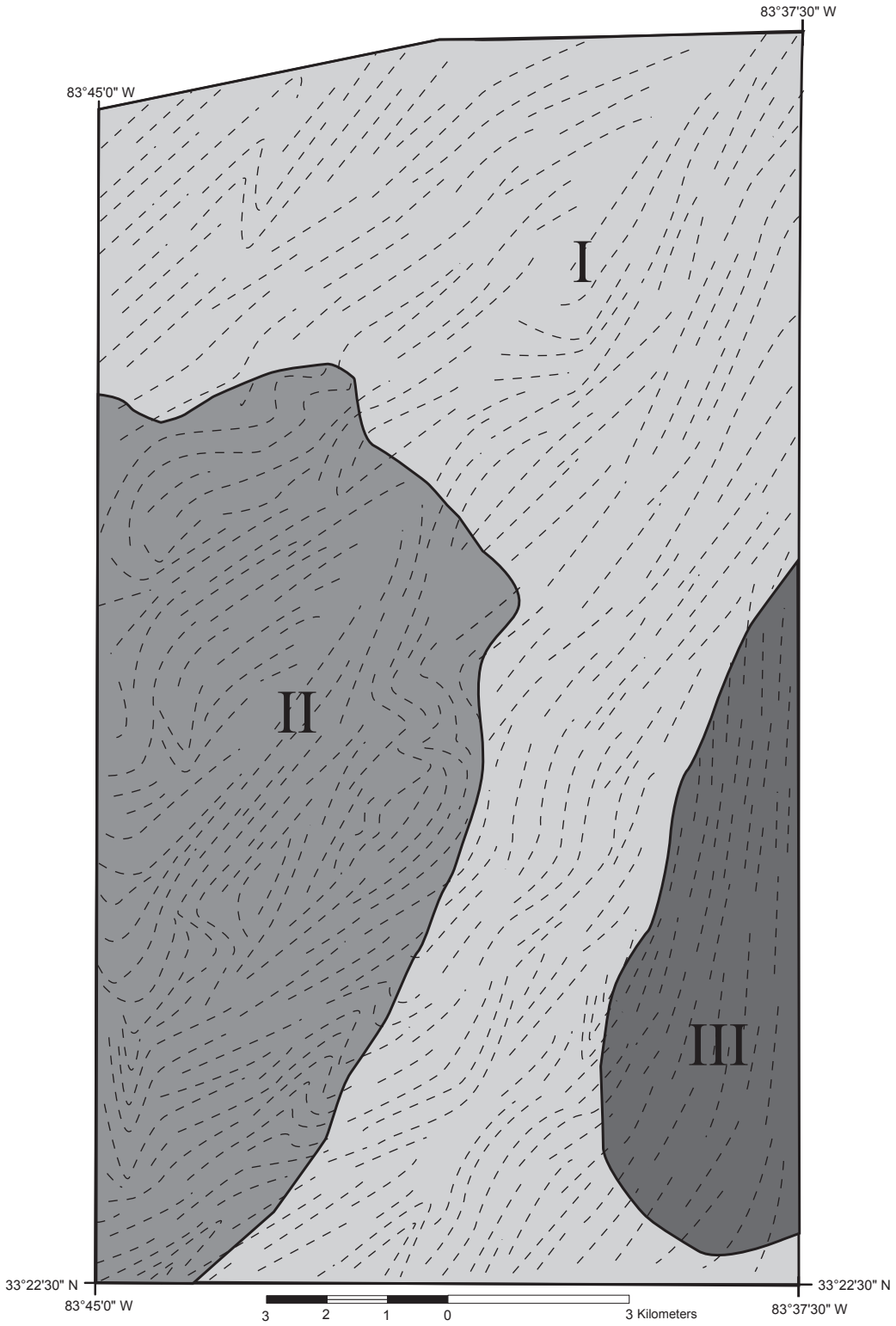

Figure 5-5. S_2 foliation form-line and domain map of portions of the Mansfield and Farrar quadrangles.

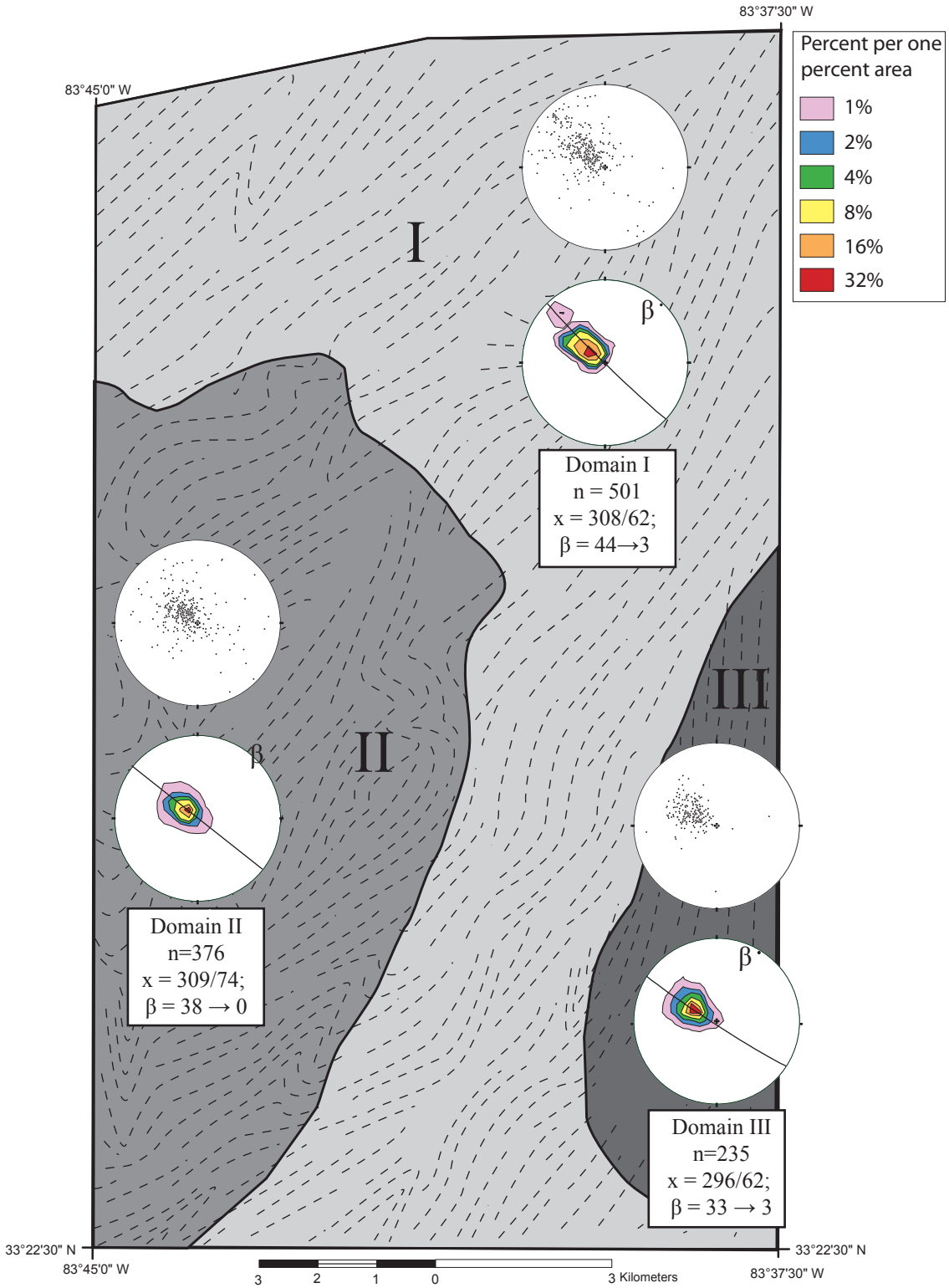

Figure 5-6. Scatter plots and lower hemisphere equal-area contoured diagrams of poles to 1,112 foliation and schistocity measurements in the Mansfield and Farrar quadrangles. S_2 changes from a strong NE-SW alignment in Domain I to more randomly oriented foliation in Domain II, and then to a N-S dominated orientation in Domain III.

overall foliation trend, and encompasses the plutonic suite that spans the length of the field area. In Domain III the foliation becomes increasingly N-S oriented. Domains II and III exhibit relatively shallow dipping foliations, whereas domain I contains a greater variability in shallow- and steeply dipping foliations.

Lineations

In metasedimentary rocks the L_2 mineral lineation is generally defined by quartz, feldspar, muscovite, biotite, and sillimanite, in amphibolite by hornblende, and in granitic rocks by quartz, feldspar(s), and biotite (Fig. 5-7). Of the three granitic rocks units in the field area, L_2 was only identified and measured in the Murder Creek Granite, and only in areas where there is a well-developed foliation. Sillimanite-defined lineations indicate that D_2 deformation occurred synchronously with or prior to regional upper amphibolite-grade metamorphism. L_2 lies within the plane of foliation and parallels NE-SW and NW-SE trends of asymmetric fold hinges, rotated porphyroclasts, and asymmetric boudins. L_2 is interpreted to be a mineral stretching lineation based on parallel alignment with shear sense indicators.

Folds

The prominent S_2 foliation is axial planar to and coeval with inclined to recumbent, tight-to-isoclinal, passive and flexural flow F_2 folds, suggesting that these folds formed during D_2 deformation (Fig. 5-8). Mapping in the Brushy and South Mountains of North Carolina further delimited fold relationships in the Inner Piedmont. Bream (1999) recognized regional-scale sheath folds in the Henderson Gneiss based on the map pattern at both the southern and northeast terminations, and suggested that the prominent NE-SW-oriented mineral stretching lineation provided supporting evidence for these large-scale sheath folds. Wilson (2006) recognized that the tight-to-isoclinal folding and sheath folds formed coevally based on the parallel nature of their axial trends.

Tight-to-isoclinal folds occur at meso- and macro-scales; at the macro-scale they most notably occur in Domain II. D_2 tight-to-isoclinal folds generally verge toward the NE and NW: inconsistencies in vergence direction may be attributed to refolding (Fig. 5-9). Sheath folds

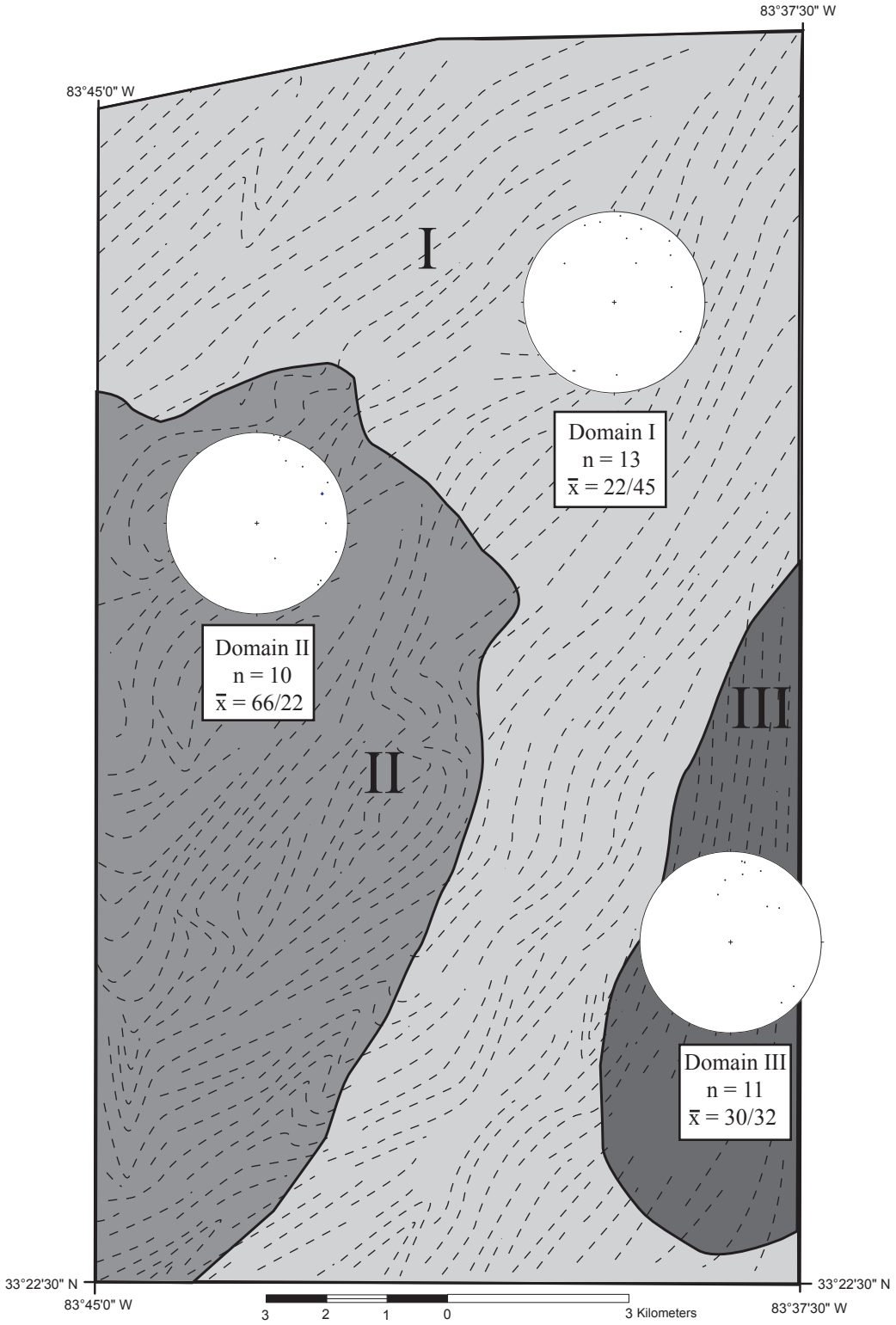

Figure 5-7. Scatter plots of L_2 mineral stretching lineations measured in the Mansfield and Farrar quadrangles. Mean vector orientations are noted below each diagram.

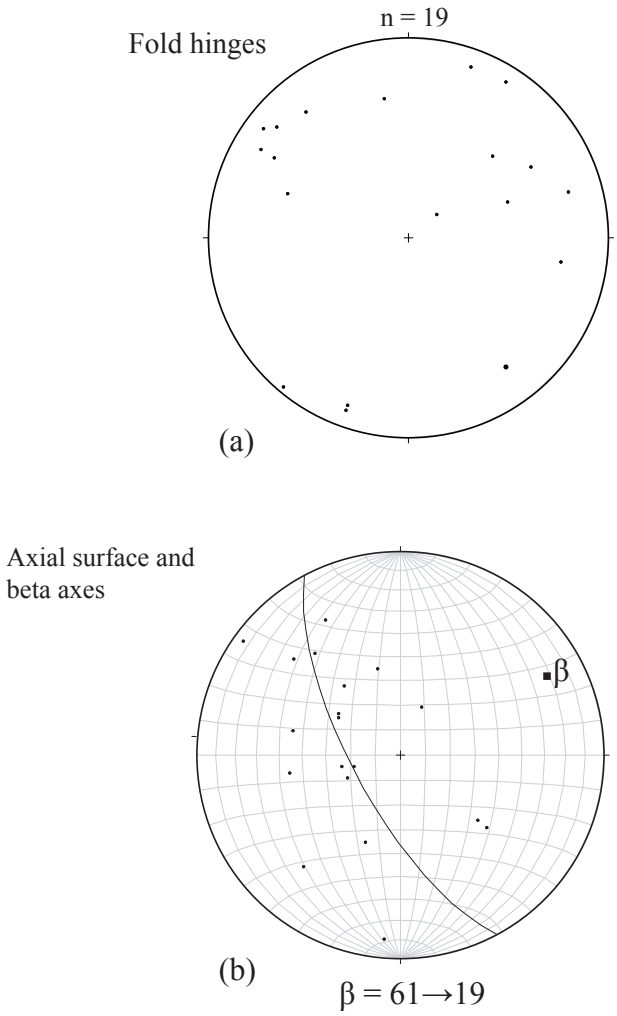

Figure 5-8. F_2 and F_3 fabric diagrams. (a) Scatter plots of F_2 and F_3 fold hinges. (b) Scatter plots of F_2 and F_3 fold axial surfaces. β is about which F_2 and F_3 folds are folded.

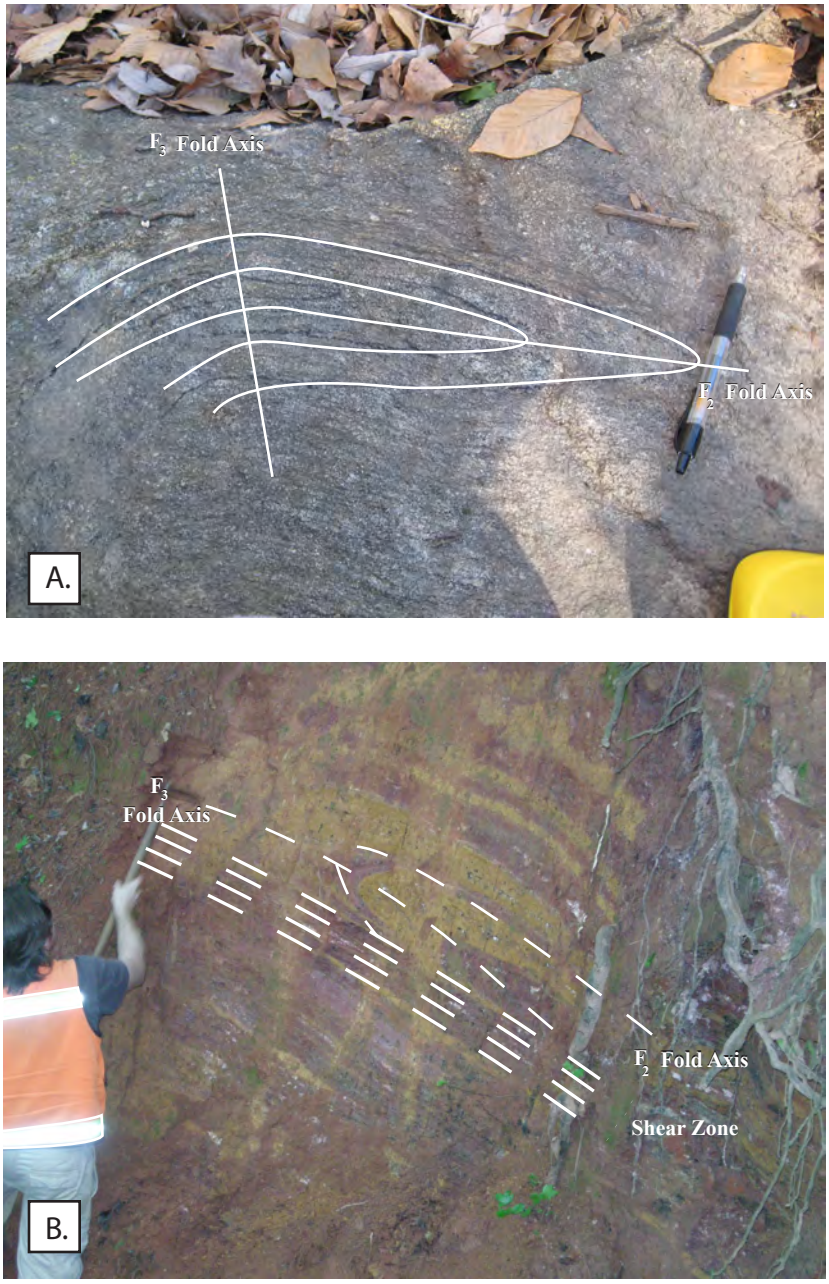

Figure 5-9. A. Outcrop of metagraywacke with F_2 and F_3 folds. Foliation is S_2 with alteration of biotite-rich and plagioclase-quartz-rich layers. Photo taken facing east. B. Saprolitic outcrop of interlayered amphibolite, biotite gneiss, and leucosome. Refolded fold cut by a shear zone and the dominant foliation. F_3 is verging toward the northeast and F_2 is verging toward the south-west. Matt Huebner for scale. This outcrop is located at the intersection of Shepard Pond Creek and Shepard Pond Rd. Photo taken facing southeast.

found in the field area appear to have formed coevally with D_2 deformation, share parallel axial trends with the tight-to-isoclinal folds, and display the characteristic eye or anvil shape.

Faults

Two D_2 faults are identified in the field area: the Brindle Creek fault, located in the northwestern portion of the field area, and the Rex Haven (Kinnard Creek) fault, located in the southeastern portion of the field area (Fig. 5-1 or Plate 1). These faults are defined by mylonitized S_2 foliation. From map patterns the Brindle Creek fault appears to transition from a low-angle thrust fault in North Carolina to a high-angle (70-88˚) strike-slip fault in central Georgia. This transition could be a direct result of the proximity of the fault to the Central Piedmont suture, suggesting that the tectonic setting is in the root zone of the orogen. In North Carolina the Brindle Creek fault is less prominent in aeromagnetic data, possibly due to its low-angle nature; however, farther south it is a strongly defined lineament that extends from northeastern Georgia into central Georgia. Field evidence supporting existence of a fault include: (1) increased migmatization with proximity to the fault, and (2) a well-developed mylonitic fabric (~20 m). Shear-sense indicators include well-developed S-C fabrics, rotated porphyroclasts, and sheath fold axes that indicate SW transport along the entirety of the fault (Fig. 5-10).

Aside from the Brindle Creek thrust sheet, no other large faults had been identified in the Cat Square terrane prior to this research. As a result of this study the low-angle (15-45˚) Rex Haven (Kinnard Creek) thrust fault was identified in the southeastern portion of the field area. The Rex Haven fault was identified by development of an ultramylonitic fabric and well-developed S-C fabric (Fig. 5-11). The ultramylonite has been annealed, suggesting very high-temperature emplacement of the Rex Haven thrust sheet. A variety of lithologies are located along the length of this fault, including sillimanite schist and metagraywacke. Porphyroclasts consist of garnets and feldspars, and display a dextral shear-sense. Based on S-C fabric, rotated porphyroclasts, and boudins, the Rex Haven (Kinnard Creek) fault appears to have a SW-directed transport.



Figure 5-10. A. Quartz-rich float block with S-C fabric located along the trace of the Brindle Creek fault. Rock hammer for scale. B. Biotite gneiss with S-C fabric along the Brindle Creek fault. Pencil for scale. These samples are located near the intersection of Sewell Road and Georgia Highway 142.



Figure 5-11. Garnetiferous biotite gneiss mylonite located along the Rex Haven fault. Tailed porphyroclasts and S-C fabric display a dextral shear sense. Photo was taken from an overhang along a tributary of Murder Creek and the intersection at Post Road. Photo taken facing southeast.

D_3 Deformation

Final emplacement of coherent thrust sheets marks D_3 deformation. D_3 occurred post peak metamorphism, toward the end of the Neoacadian orogeny (Davis, 1993). D_3 structures are defined by upright to inclined, tight-to-open folds with interlimb angles ranging from 20-75˚. Tight F_2 and F_3 folds often appear similar in geometry and orientation; however, F_3 can be distinguished from F_2 in that F_3 folds the penetrative S_2 foliation. D_3 structures also include locally developed S_3 foliation that occurs axial planar to F_3 folds. Many F_3 folds more often maintain limb and hinge thickness (Fig. 5-12). F_3 inclined tight folds are recorded in all three Domains at both meso- and macroscale, and exhibit a general NW vergence.

D_4 and D_5 Deformation

D_4 deformation is marked by the appearance of upright open folds that overprint earlier (F_1-F_3) folds. These folds are upright and have an interlimb angle that ranges from 50-100˚. Due to the lack of F_4 folds identified at mesoscale, a general trend has not been recognized. F_5 folds commonly have greater inner-limb angles than F_4 folds, ranging from 90-180˚. Like F_4 folds, F_5 folds overprint earlier F_1-F_3 folds. F_5 probably formed coevally with joint formation and from sporadic deformation (Whitten, 1966, Bream, 2003). Due to D_4 and D_5 deformations and their perpendicular orientations to previous fold generations, these folds produce dome-and basin and hook fold interference patterns.

D_5 and D_6 Brittle Deformation

A change in temperature and pressure occurred during the transition from D_4 to D_5, most likely attributed to uplift and cooling toward the later part of the Alleghanian orogeny. Brittle structures include filled and unfilled joints and the low temperature brittle reactivation of the Towaliga fault. The dominant joint sets strike N5˚W, and additional joint sets strike N85˚E, N5˚E, and N45˚E (Fig. 5-13).



Figure 5-12. Upright tight F_3 fold with maintained hinge and limb thickness. This outcrop is located along an ephemeral creek between Clifford Circle and County Road 213. Rock hammer for scale. Photo taken facing northeast.

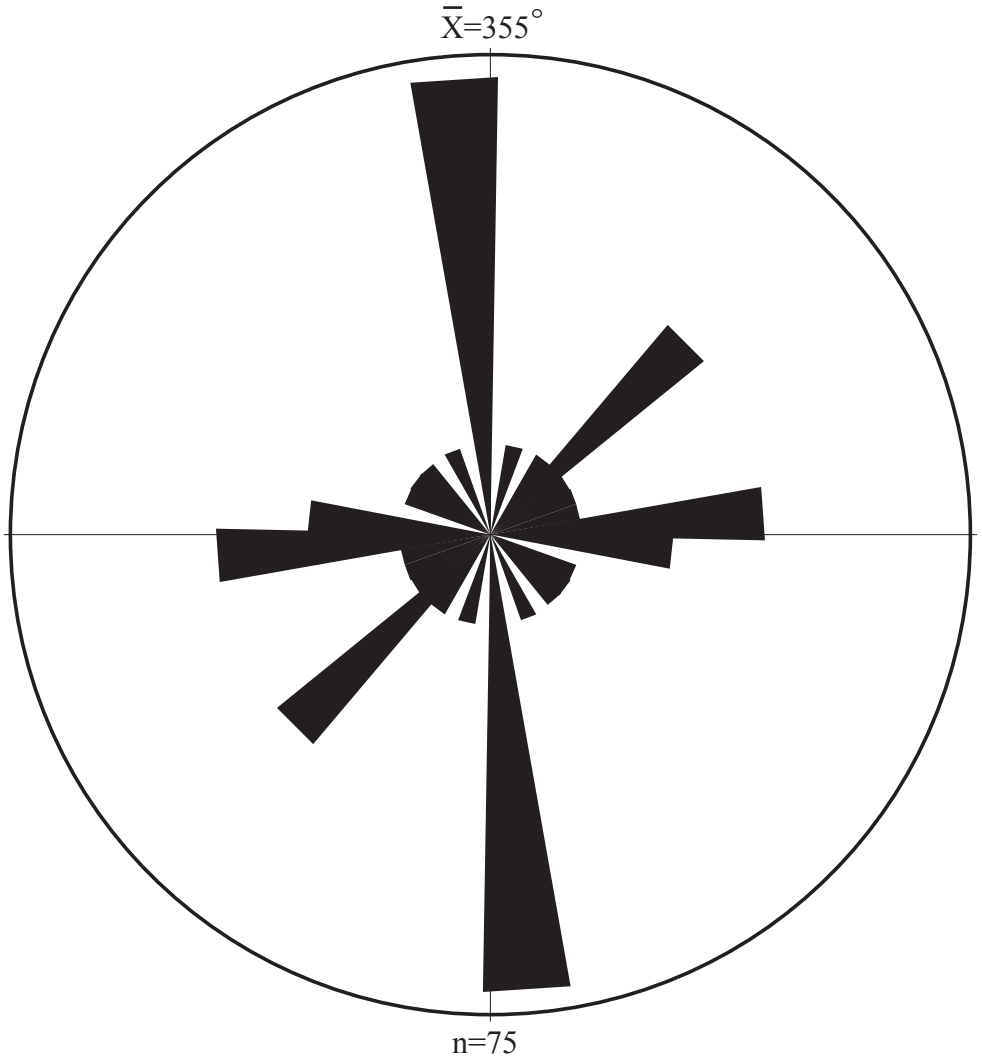

Figure 5-13. Rose diagram of strikes of 75 joints in the Farrar and Mansfield quadrangles. The circle diameter represents 13% of the population.

NW-SE trending diabase dikes are dominant in the southwestern portion of the Farrar quadrangle. Diabase dikes are most likely the product of late Alleghanian, Mesozoic extension and break-up of Pangea. Emplacement of diabase occurred at the Triassic/Jurassic boundary at 200 Ma, forming simultaneously with low temperature siliceous cataclasite. The siliceous cataclasite has similar timing of formation to the diabase dikes, and have been noted to crosscut one another.

Hooper (1989) noted a set of brittle faults located around the Pine Mountain window that display a sinistral shear sense. Hooper (1989) identified the rhomb-shaped geometry of these brittle faults from their topographic signatures, which represent the formation of step-overs and subsequent displacement. The Towaliga fault borders the northern portion of the Pine Mountain Window and truncates the Box Ankle fault, which is dated at 330 Ma, making the Towaliga fault Alleghanian (McBride et al., 2005). The Towaliga fault is a dextral strike-slip fault, determined from shear sense indicators, and contains a garnet-grade mineral assemblage (McBride et al., 2005). Brittle reactivation of the Towaliga fault was traced northeastward from the Pine Mountain window through the Jackson, Lloyd Shoals Dam, Stewart, Farrar and Mansfield quadrangles (Davis et al., 2009; Huebner et al., 2009). At its greatest, the cataclasite reaches ~1/4 kilometer in width in the Stewart quadrangle. To date, its extent has been mapped approximately 30 km; however, in aeromagnetic data it appears to extend from central Georgia to northeastern Georgia. This fault appears to be a very late fault, and displays dextral movement, determined by the shape of the rhombs in topographic maps. Rhombs of cataclasite can be identified from topographic maps (Fig. 5-1). They have a northeast trend, and appear to have multiple episodes of jointing (Refer to Fig. 2-23 in Chapter 2). Determining the amount of displacement should be easily calculated by measuring the length of the rhombs; however, there is a complication. The cataclasite truncates a plutonic suite; however, the southern portion of this suite has not been recognized. The complication in displacement can be explained in four different ways: (1) oblique slip motion could account for the absence of the granitoids, (2) the plutonic suite terminated in close proximity to where the cataclasite formed, (4) this may be the original extent of the plutonic suite, or (3) the displacement along the Towaliga fault is much greater than anticipated, and it has not yet been determined.

Low Temperature Quartz Mylonite

Low-temperature quartz mylonite occurs throughout the field area, and is most common within the sillimanite schist unit. These mylonites contain a definite S-C fabric, rare mica fish, and rare rigid feldspar(s) grains that display a distinct dextral shear sense (see Fig. 2-6 in Chapter 2). In many cases low angle boundary-dominated quartz ribbons will flow around these hard objects (Hatcher et al., 2009). Quartz ribbons will more commonly than not exhibit very little recovery. The samples that display greater amounts of recovery and recrystallization most likely remained at greater depths. Remaining at greater depths would have supplied heat for longer periods of time, allowing for recrystallization. Both subgrain rotation and subgrain bulging are evident in thin section, suggesting a deformation temperature ranging from 350-450° (Hirth and Tullis, 1992; Passchier and Trouw, 2005). The low-temperature mylonites lie in the local S_2 foliation and mineral stretching lineations. This complicates deciphering timing of formation. The quartz mylonites have been interpreted to be related to the siliceous cataclasite; however, there is an absence of a spatial relationship. If these two structures did form coevally, little evidence other than deformation temperature supports this conclusion. Huebner et al., (2009) stated that in some rare instances the quartz mylonites have a jointed appearance similar to the siliceous cataclasite, but this is not always the case, and may be a localized occurrence of crosscutting structures. Explanations for these compelling differences are: (1) stress orientations remained the same after the peak of the Alleghanian orogeny (during D_4), and previously formed quartz veins could have been sheared; or (2) formation of the quartz mylonites and brittle reactivation of the Towaliga fault may have occurred coevally during the breakup of Pangea, explaining similarities in deformation temperature.

Central Piedmont Map Patterns and Farrar and Mansfield Cross Sections

Regardless of complexities from polyphase deformation, overprinting, and transposition, much information can be deciphered from compiled geologic maps and cross sections, such as the sequential nature of deformation in the Inner Piedmont. Three cross sections were constructed through the study area, each was oriented normal to regional foliation, and they were placed to cross major structures in the field area (Fig. 5-14).

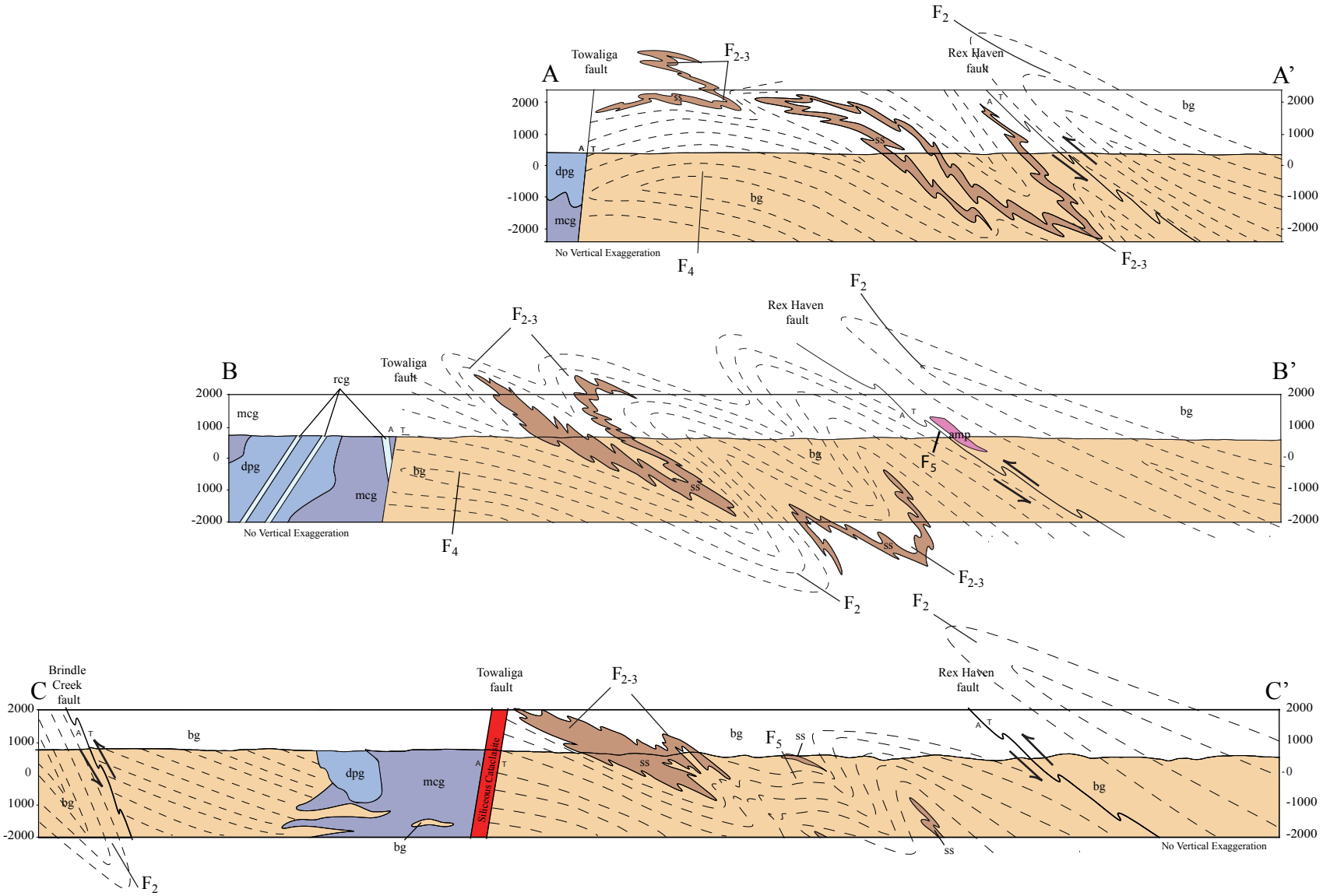

Figure 5-14. Cross sections through the Mansfield and Farrar quadragles. See Figure. 5-1 for explanation of map units and locations of cross sections.

Cross Section A-A'

Cross section A-A' was constructed in the southwestern portion of the map (Plate 1). It crosses two major structures: the Rex Haven (Kinnard Creek) fault and the Towaliga fault. The cross section will be described from east to west. The Rex Haven (Kinnard Creek) thrust sheet is noted as the most eastern structure through this cross section, according to meso- and macro-scale patterns it appears that the fault dips gently. This cross section is dominated by the presence of tight to isoclinal NW-vergent F_2 and F_3 folds. A large z-fold was also recognized from map pattern. One large upright open fold is also illustrated in this cross section. The brittle nature of the steeply dipping Towaliga fault is noted by the absence of folding along the fault.

Cross Section B-B'

Much like cross section A-A', cross section B-B' crosses the Rex Haven (Kinnard Creek) fault and the Towaliga fault; although, there is a transition to a synform/antiform pair that lies stratigraphically above the more southern antiform/synform pair z-fold. The presence of a very large open fold still remains, but there is an overall dominance of F_2 and F_3 folds. On the very northwestern portion of this cross section, note the crosscutting relationships between the granitoids. Rocky Creek granodiorite occurs as intrusive dikes, crosscutting both the Dow's Pulpit granodiorite and Murder Creek granite. This relationship can be seen at both meso- and macro-scales.

Cross Section C-C'

Cross section C-C' also extends across the Rex Haven (Kinnard Creek) and Towaliga faults, and also includes the Brindle Creek fault. In this cross section there is still a dominance of F_2 and F_3 folds, but there are F_5 folds present as well. From map pattern there appears to be a general tightening of the sillimanite schist and subsequently, tightening of the folds. This cross section was drawn through one of the step-overs of the cataclasite. Relationships between the granitoids can also be seen in this cross section.

Inner Piedmont Tectonic Models and Deformation Synthesis

The Inner Piedmont and southern Appalachian tectonic models have varied from regional scale nappes (Hatcher, 1972; Griffin, 1974), stockwork tectonics, tectonic slides (Griffin, 1971, 1974), and oblique convergence (Davis, 1993; Hill, 1999) to tectonic-driven channel flow (Merschat et al., 2005; Hatcher and Merschat, 2006; Hatcher et al., 2007). Each of these models has contributed useful hypotheses to explain the geometry and kinematics of the Inner Piedmont.

Recognizing the geometry of thrust sheets in the Inner Piedmont, Griffin (1971, 1974), applied the stockwork (Haller, 1956, 1971) and tectonic slide models (Hatcher, 1969). These models indicate formation of NW-vergent fold-thrust nappes through the autochthonous emplacement of relatively unmetamorphosed rocks of the Charlotte and Carolina slate belt, thrust over ductile, high-grade rocks of the Inner Piedmont (Fig. 5-15). Applying concepts of the tectonic slide boundary model, this suggested that the Abscherung zone (the detachment zone) was sheared free from the infrastructural (Inner Piedmont), and the suprastructural (Carolina slate belt) during deformation. This model proved to be incorrect, because it failed to incorporate SW-directed transport of the IP. Moreover, Griffin's stockwork-tectonics model suggested that the Inner Piedmont was produced by a single deformation event, Hatcher (1972, 1978) recognized that the nappe-like structures were most likely a product of D_2 deformation.

Hill (1999) applied a two-phase deformation model of Ellis and Watkinson (1987) in an attempt to explain the arcuate trend of the Inner Piedmont. The first phase in this model takes place orogen-parallel, where the footwall reflects relative plate motion. The second phase occurs normal to the orogen, when imbrication take place (Ellis and Watkinson, 1987). Hill (1999) explained that orogen-parallel structures such as the dominant mineral stretching lineation and sheath fold axes in the footwall of the Inner Piedmont were indicative of this first phase of deformation and formed from initial collision of the Inner Piedmont blocks (Hill, 1999). The second phase of deformation is defined by disharmonic map patterns that were formed in the hanging wall during thrust stacking (Hill, 1999). Additional data, along with progression in detailed geologic mapping of the Inner Piedmont have proven this model to be false for three reasons: (1) Orogen-parallel structures such as mineral stretching lineations and sheath folds are not limited to the footwalls; these same structures occur in the Brindle Creek and Rex Haven

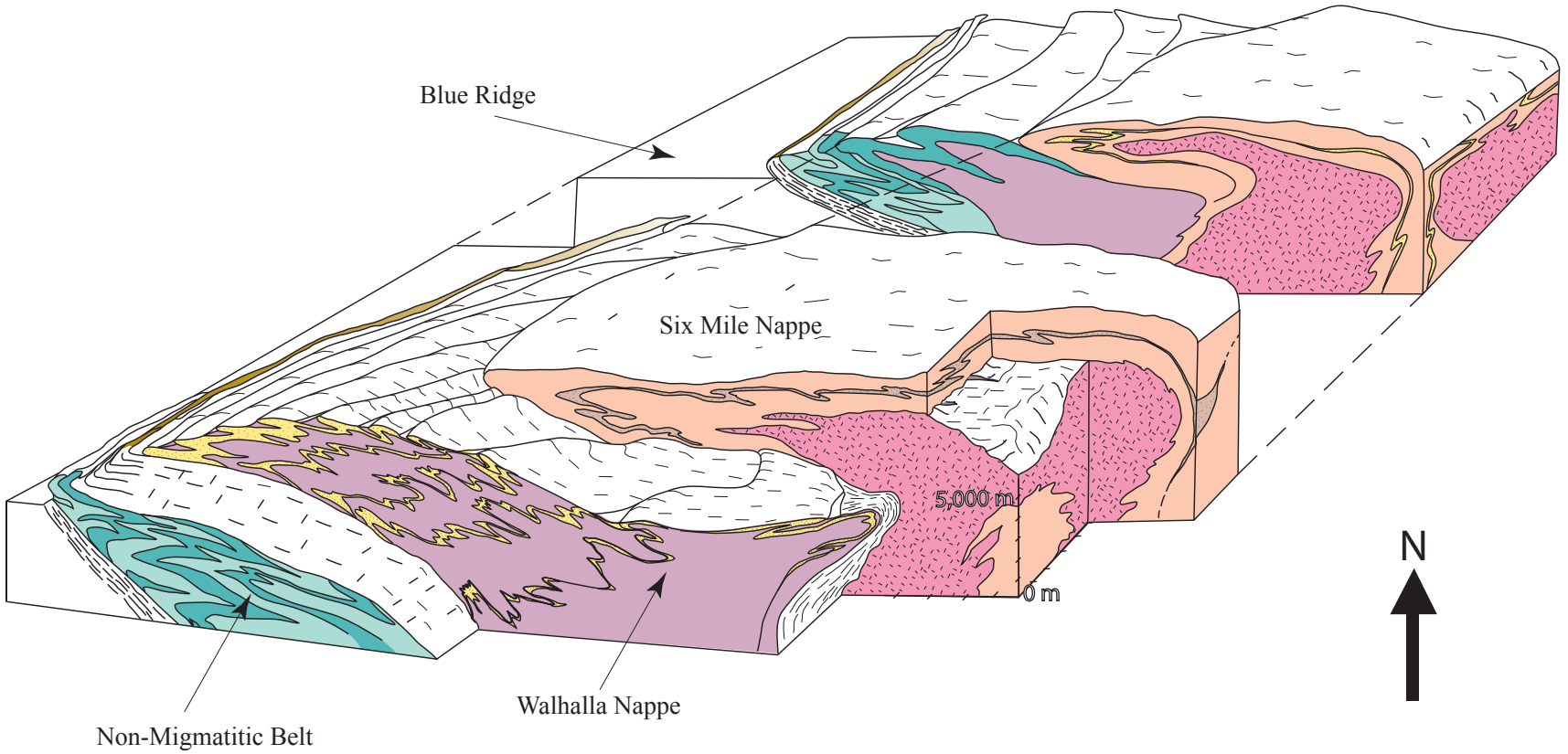

Figure 5-15. 3-D cross section of Inner Piedmont nappe complex in northwest South Carolina (Griffin, 1974).

(Kinnard Creek) thrust sheets (Bier, 2001; Kalbas, 2003; Merschat, 2003; Gatewood, 2007; Wilson, 2006). (2) Metamorphic conditions remain similar throughout the Inner Piedmont. (3) According to this model, structures produced would have a clockwise rotation; this contradicts the counterclockwise, SW-directed structures of the Inner Piedmont.

In the Columbus Promontory, Davis (1993) recognized a change in displacement direction within the Inner Piedmont: from W-directed in the core of the Inner Piedmont to SW-directed along the western portion of the Inner Piedmont. Davis (1993) suggested that changes in the structural orientations could be a result of polyphase deformation, ductile flow, or deformation partitioning during a single event (Fig. 5-16). The continuous change in orientations of structures, similar metamorphic assemblages, and textures across the western Inner Piedmont suggests that this change in displacement direction is the result of a single deformation event during amphibolite faces conditions (Davis, 1993). He suggested that the E-W and NE-SW oriented structures was a result of orogen-normal to orogen-oblique deformation in the central Inner Piedmont, but progressed to orogen-parallel along the Brevard fault zone. Davis (1993) argued that the Inner Piedmont is a crustal-scale shear zone, based on presence of mylonitic structures throughout most of the Inner Piedmont. "The S_2 mylonitic foliation was the common décollement that linked SW-directed transcurrent movement along the primordial Brevard fault zone with E-W contractional movement of Inner Piedmont thrust sheets" (Davis, 1993). Hatcher later added to Davis' crustal flow model by identifying the NW-directed transport of the eastern Inner Piedmont, and recognized the W- and SW-directed transport of the central and western Inner Piedmont. Merschat and Hatcher (2007) recognized that the dominant L_2 mineral stretching lineation displays curved orientation throughout the Inner Piedmont. Merschat and Hatcher (2007) recognized that these mineral lineations appear to mirror curved anomalies in aeromagnetic data. This pattern has been interpreted by Merschat et al. (2004) to represent the southwestward deflection of the Inner Piedmont against the Brevard fault zone (Davis, 1993; Hatcher, 1998; Hill, 1999).

Merschat et al. (2005) and Hatcher et al. (2007), built on Davis' idea of crustal flow, emphasizing the many factors such as *in situ* pluton formation, W- to SW-directed shearing, meso- and macroscale sheath folds, ubiquitous migmatization, and a long tectonothermal history,

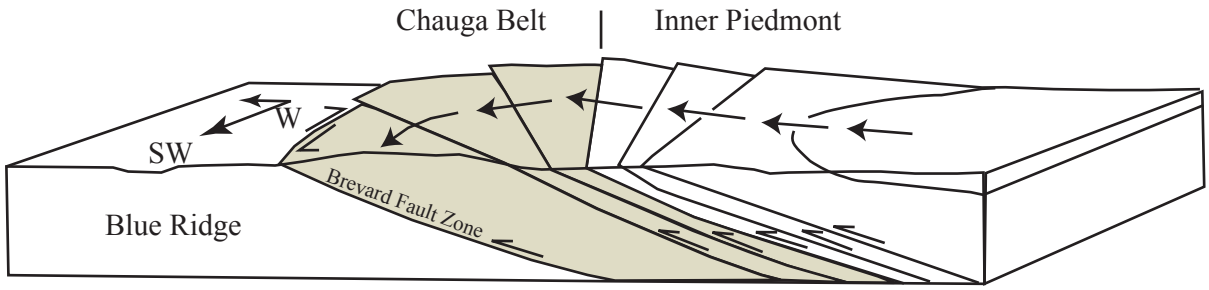

Figure 5-16. diagram of W-directed thrusts and SW-directed thrusts of the Inner Piedmont and Chauga Belt (Modified from Davis, 1993).

which suggest that the Inner Piedmont thrust sheets may have contained enough water to behave as viscous masses in which they could mimic channel flow.

Origins and Evolution of the Cat Square Terrane

Merschat and Hatcher (2007) suggested that the Cat Square terrane is the remnant of the Siluro-Devonian Rheic ocean basin located amid eastern Laurentian terranes and the advancing peri-Gondwanan Carolina superterrane (Fig. 5-17). The origins of the Cat Square terrane are further constrained from palinspastic reconstruction of the Cat Square basin in the Pennsylvania embayment located between the New York and Virginia promontories. As the orogeny evolved and collision continued, the Acadian clastic wedge migrated southwestward. This suggests that there was transpressional convergence of the Carolina superterrane with the Laurentian margin and successive zippering of the Cat Square basin from NE to the SW (Merschat and Hatcher, 2007).

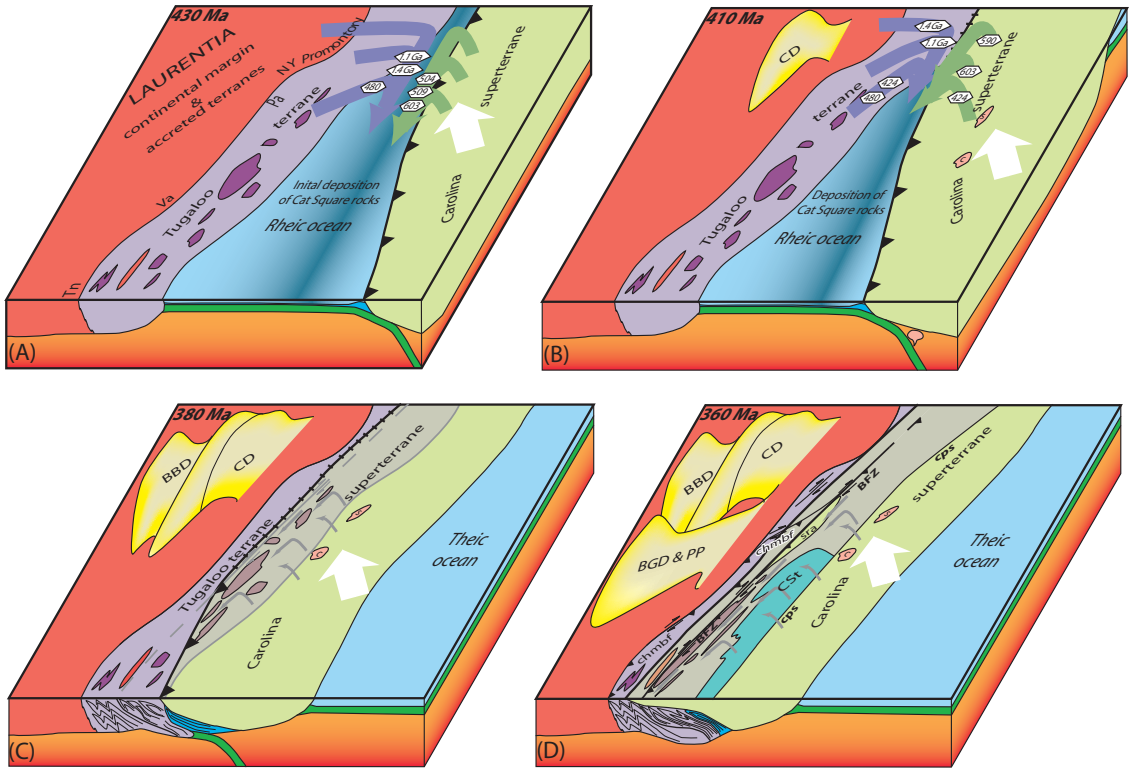

Figure 5-17. Maps representing the tectonic history of the Cat Square terrane. A. Locations of Laurentia and Tugaloo terrane during the Silurian, with mid-Ordovician plutons (dark purple), and the Carolina superterrane separated by the Rheic ocean. B. (Early Devonian) Continued deposition of sediments along with continued closure of the Rheic ocean. Magmatism in the Carolina superterrane, indicated by the Concord and Salisbury plutonic suites, is the product of subduction of the basin beneath the Carolina superterrane. C. ~380 Ma Closure of the Rheic ocean and suturing of Carolina superterrane. Ductile flow of Inner Piedmont material beneath the Carolina superterrane. D. Neoacadian configuration resulting from dextral transpression. BBD-Bedford-Berea delta. BFZ-Brevard fault zone. BGD-Borden-Grainger delta. c-Concord plutonic suite. CD-Catskill delta. chmbf-Chattahoochee-Holland Mountain-Burnsville fault. cps-central Piedmont suture. CSt-Cat Square terrane. PP-Price-Pocono delta. s-Salisbury Plutonic suite. sra-Smith River allochthon (From Merschat and Hatcher, 2007).

Chapter 6: Conclusions

1. The Cat Square terrane is dominated by an abundance of biotite gneiss and sillimanite schist, along with amphibolite and minor calc-silicate.
2. The Tugaloo terrane contains greater abundances of amphibolite than the Cat Square terrane; these commonly occur as mesoscale, so no map-scale bodies were located in the field area.
3. The Murder Creek granite is petrographically and texturally similar to the Walker Top Granite in North Carolina. The Dow's Pulpit granodiorite is texturally similar to the Toluca Granite in North Carolina.
4. Sillimanite occurs ubiquitously throughout the field area, and in thin section it is observed in both prismatic and fibrolitic habits.
5. P-T estimates from biotite gneiss and amphibolite samples suggest that the Inner Piedmont reached peak pressures of 4-7.6 kbars and temperatures of 630-715˚C, suggesting that the central Georgia Inner Piedmont reached upper amphibolite facies metamorphic grade.
6. Trace element and REE patterns in the Murder Creek granite and Rocky Creek granodiorite mirror patterns plotted from the Walker Top Granite in North Carolina.
7. A Nb and Ta trough, in combination with the Ti trough, suggest fractional crystallization of ilmenite, sphene, or rutile in both the Rocky Creek granodiorite and Murder Creek granite samples.
8. Absence of a negative Eu anomaly along with an absence of a negative Sr anomaly suggests that there was no longer fractional crystallization of plagioclase during the crystallization of the Rocky Creek granodiorite.
9. Murder Creek granite, Rocky Creek granodiorite, and Dow's Pulpit granodiorite occur exclusively southeast of the Brindle Creek fault in a linear plutonic complex. This felsic plutonic suite spans the length of the field area and is truncated by the Towaliga fault.
10. The Brindle Creek fault was recognized by correlation of aeromagnetic anomalies and

detailed geologic mapping.

11. Two map-scale shear zones - the Brindle Creek fault zone and the Rex Haven (Kinnard Creek) fault zone - are present in the study area and are orogen parallel, striking northeast-southwest across portions of the Farrar and Mansfield quadrangles.
12. Along the Rex Haven (Kinnard Creek) fault sillimanite fish (dextral shear sense) were observed in annealed ultramylonite, suggesting very high-temperature emplacement of the Rex Haven (Kinnard Creek) fault.
13. Six deformational events are recognized in the central Georgia Inner Piedmont, and correspond to those events identified by previous mappers in the northern Inner Piedmont.
14. This study has provided new evidence disputing the original termination of the Brindle Creek fault near Athens, GA. The Brindle Creek fault and Cat Square terrane have been successfully mapped into central Georgia.
15. Mineral stretching lineations appear to coincide with the curved anomalies recognized in aeromagnetic data. There is a strong NE-SW lineations trend in the southeastern portion of the field area, and a gradual change in trend to N-S toward the northwestern portion of the field area. These lineations parallel F_2 hinges and are also present within the regional foliation, suggesting formation during peak metamorphism.
16. The Murder Creek granitoid displays both regional foliation and relict igneous foliation, suggesting earliest emplacement occurred synchronously with D_2.
17. Structures are overprinted by later D_5 and D_6 jointing and brittle reactivation of the Towaliga fault.
18. Microstructures associated with the Towaliga fault indicate that there were multiple episodes of reactivation along the extent of the fault, evidenced by multiple joint sets.
19. Low temperature quartz mylonites most likely represent later shearing of quartz veins. Microstructures present suggest that quartz mylonites formed prior to D_6 and later than D_4, most likely during D_5.

REFERENCES CITED

Albee, A. L., 1965, A petrogenetic gid for the Fe-Mg silicates of pelitic schists: American Journal of Science, v. 263. p. 512-536. Bier, S. E., 2001, Geology of the southeastern South Mountains, North Carolina [M.S. thesis]: Knoxville, University of Tennessee, 162 p.

Barker, F., 1979, Trondhjemite: Definition, environment and hypotheses of origin, *in* Barker, F., ed., Trondhjemites, dacites and related rocks: Amsterdam, Elsevier, p. 1-12.

Bier, S. E., 2001, Geology of the southeastern South Mountains, North Carolina [M.S. thesis]: Knoxville, University of Tennessee, 162 p.

Bier, S. E., Bream, B. R., Giorgis, S. D., 2002, Inner Piedmont stratigraphy, metamorphism, and deformation in the Marion-South Mountains area, North Carolina, in: Hatcher, Jr., R. D., Bream, B. R. (Eds.), Inner Piedmont geology in the South Mountains, central-western North Carolina. Carolina Geological Society Guidebook, pp. 65-100.

Bream, B. R., 1999, Geology of the Glenwood and Sugar Hill quadrangles, North Carolina, and the structure of the northeast end of the Henderson Gneiss [M.S. thesis]: Knoxville, University of Tennessee, 155 p.

Bream, B. R., 2002, The southern Appalachian Inner Piedmont: new perspectives based on recent detailed geologic mapping, Nd isotopic evidence, and zircon geochronology, *in* Hatcher, R. D., Jr., and Bream, B. R., eds., Inner Piedmont geology in the South Mountains-Blue Ridge Foothills and the southwestern Brushy Mountains, central-western North Carolina: North Carolina Geological Survey, Carolina Geological Society Guidebook, p. 45-63.

Bream, B. R., 2003, Tectonic implications of para- and orthogneiss geochronology and geochemistry from the southern Appalachian crystalline core [Ph.D. dissertation]: Knoxville, University of Tennessee, 296 p.

Bream, B. R., Hatcher, R. D., Jr., Miller, C. F., and Fullagar, P. D., 2004, Detrital zircon ages and Nd isotopic data from the southern Appalachian crystalline core, Georgia, South Carolina, North Carolina, and Tennessee: New provenance constraints for part of the Laurentian margin, *in* Tollo, R. P., Corriveau, L., McLelland, J. M., and Bartholomew,

M. J., eds., Protoerozoic tectonic evolution of the Grenville orogen in North America: Geological Society of America Memoir 197, p. 459-476.

Bruce, W. D., 1977, The nature and significance of the mechanism of sillimanite growth in the Connemara schists, Ireland: Contributions to Mineralogy and Petrology, v. 65. Pp 53-58.

Butler, J. R., and Fullagar, P. D., 1978, Petrochemical and geochronological studies of plutonic rocks in thesouthern Appalachians: III. Leucocratic adamellites of the Charlotte belt near Salisbury, North Carolina: Geological Society of America Bulletin, v. 89, p. 460-466.

Butler, J. R., 1991, Metamorphism, *in* Horton, J. W., Jr., and Zullo, V. A., eds., The geology of the Carolinas, Carolina Geological Society Fiftieth Anniversary Volume: Knoxville, University of Tennessee Press, p. 127-142.

Byars, H., 2010, Tectonic evolution of the west-central portion of the Newton window, North Carolina Inner Piedmont: Timing and implications for the emplacement of the Paleozoic Vale charnockite, Walker Top Granite, and mafic complexes [M. S. thesis]: Knoxville, University of Tennessee, 236 p.

Carpenter, R. H., 1970, Metamorphic history of the Blue Ridge Province of Tennessee and North Carolina: Geological Society of America Bulletin, v. 81, p. 749-762.

Carrigan, C. W., Bream, B. R., Miller, C. F., and Hatcher, R. D., Jr., 2001, Ion microprobe analyses of zircon rims from the eastern Blue Ridge and Inner Piedmont, NC-SC-GA: Implications for the timing of Paleozoic metamorphism in the southern Appalachians: Geological Society of America Abstracts with Programs, v. 33, no. 2, p A-7.

Chatterjee, N. D., Johannes, W., Leistner, H., 1984, The system CaO-Al_2O_3-SiO_2-H_2O: new phase equilibria data, some calculated phase relations, and their petrological applications. Contributions to Mineralogy and Petrology, v. 88. Pp. 1-13.

Curl, D. C., 1998, Stratigraphy and structure of Wellford and Reidville quadrangles in part of the eastern Inner Piedmont, near Spartanburg, South Carolina [unpublished M. S. thesis]: Knoxville, University of Tennessee, 129 p.

Davis, T. L., Hatcher, R. D., Jr., Liu, A., and Tabor, J. R., 1991, Southern Appalachian western Inner Piedmont, U.S.A.: A progressive crustal scale shear zone: Geological Society of America Abstracts with Programs, v. 23, no. 5, p. A138.

Davis, T. L., 1993, Lithostratigraphy, structure, and metamorphism of a crystalline thrust terrane, western Inner Piedmont, North Carolina [Ph.D. dissertation]: Knoxville, University of Tennessee, 245 p.

Dale, J., Holland, T., and Powell, R., 2000, Hornblende-garnet-plagioclase thermobarometry: a natural assemblage calibration of the thermodynamics of hornblende: Contributions to Mineralogy and Petrology, v. 140, p. 353-362.

Dennis, A. J., and Wright, J. E., 1997, Middle and late Paleozoic monazite U-Pb ages, Inner Piedmont, South Carolina: Geological Society of America Abstracts with Programs, v. 29, no. 3, p. 12.

Eckert, J.O., Hatcher, R.D., Jr., and Mohr, D.W., 1989, The Wayah granulite-facies metamorphic core, southwestern North Carolina: High grade culmination of Taconic metamorphism in the southern Blue Ridge: Geological Society of America Bulletin, v. 101, p. 1434-1447.

Eckert, J. O., Jr., 1984, Stratigraphy, structure, and metamorphism of the east half of the Wayah Bald quadrangle, North Carolina: Evidence for Paleozoic granulite facies metamorphism in the southern Appalachians [M. S. thesis]: Columbia, South Carolina, University of South Carolina, 411 p.

Ellis, M., and Watkinson, A. J., 1987, Orogen-parallel extension and oblique tectonics: The relation between stretching lineation and relative plate motions: Geology, v. 15, p. 1022-1026.

Espenshade, G. H., Rankin, D. W., Shaw, K. W., and Neuman, R. B., 1975, Geologic map of the west half of the Winston-Salem quadrangle, North Carolina–Virginia: U.S. Geological Survey Map I–709–B, scale 1:250,000.

Ferry, J. M., and Spear, F. S., 1978, Experimental calibration of the partitioning of Fe and Mg between biotite and garnet: Contributions to Mineralogy and Petrology, v. 66, p. 113-117.

Gardner, C. H., 1961, The geology of central Newton County, Georgia [M. S. thesis]: Atlanta, Georgia, Emory University, 53 p.

Gatewood, M. P., 2007, Tectonics of the northeastern Inner Piedmont from detailed geologic mapping, geochronologic, geochemical, and petrologic studies with macro- and

mesostructural analyses of ductile fault zones. [M.S. thesis]: Knoxville, University of Tennessee, 279 p.

Giorgis, S. D., 1999, Inner Piedmont geology of the northwestern South Mountains near Morganton, North Carolina [M.S. thesis]: Knoxville, University of Tennessee, 191 p.

Giorgis, S. D., Mapes, R. W. and Bream, B. R., 2002, The Walker Top Granite: Acadian granitoid or eastern Inner Piedmont basement?, in Hatcher, R. D., Jr., and Bream, B. R., eds., Inner Piedmont geology in the South Mountains-Blue Ridge foothills and the southwestern Brushy Mountains, central western North Carolina: Carolina Geological Society Guidebook, North Carolina Geological Survey, p. 33-43.

Goldsmith, R., Milton, D. J., and Wright, J. W., Jr., 1988, Geologic map of the Charlotte 1° X 2° quadrangle, North Carolina and South Carolina: U. S. Geological Survey Map I-1251-E, scale 1:250,000.

Graham, C. M., and Powell, R., 1984, A garnet-hornblende geothermometer: calibration, testing and application to the Pelona Schist, southern California: Journal of Metamorphic Geology, v. 2, p. 13-21.

Griffin, V. S., 1971, The Inner Piedmont belt of the southern crystalline Appalachians: Geological Society of America Bulletin, v. 82, p. 1885-1898.

Griffin, V.S., Jr., 1974, Analysis of the Piedmont in northwest South Carolina: Geological Society of America Bulletin, v. 85, p. 1123-1138.

Hadley, J.B., and Goldsmith, R., 1963, Geology of the eastern Great Smoky Mountains, North Carolina: U.S. Geological Survey Map I-654, scale 1:250,000.

Hadley, J. B., and Nelson, A. E., 1971, Geology of the Knoxville quadrangle, North Carolina, Tennessee, South Carolina: U. S. Geological Survey Map I –654, scale 1:250,000.

Haller, J., 1956, Probleme der Tiefentektonik: Bauformen in migmatit-stockwerk der ostgrönländischen Kaledoniden: Geology Rundschau, v. 45, p. 159-167.

Haller, J., 1971, Geology of the East Greenland Calendonides: New York, Interscience Publishers, 358 p.

Hatcher, R. D., Jr., 1972, Developmental model for the southern Appalachians: Geological Society of America Bulletin, v. 83, p. 2735-2760.

Hatcher, R. D., Jr., 1978, Tectonics of the western Piedmont and Blue Ridge: Review and speculation: American Journal of Science, v. 278, p. 276-304.

Hatcher, R.D., Jr., and Goldberg, S.A., 1991, The Blue Ridge Geologic Province, in Horton, J. W., Jr., and Zullo, V. A., eds., The geology of the Carolinas: Knoxville, University of Tennessee Press, p. 11-37.

Hatcher, R. D., Jr., and Hooper, R. J., 1992, Evolution of crystalline thrust sheets in the internal parts of mountain chains, *in* McClay K. R., ed., Thrust Tectonics: London, Chapman and Hall, p. 217-233.

Hatcher, R. D., Jr., Miller, C. F., and Lamb, D. D., 1995, Deformation processes related to emplacement of the Rabun Granite in the eastern Blue Ridge, Georgia and North Carolina *in* Driese, S. G., ed., Guidebook for field trip excursions, Southeastern Section, Geological Society of America: Knoxville, Tennessee, University of Tennessee, Department of Geological Sciences, Studies in Geology 24, p. 39-56.

Hatcher, R. D., Jr., 2001, Rheological partitioning during multiple reactivation of the Paleozoic Brevard fault zone, southern Appalachians, USA, *in* Holdsworth, R. E., Strachan, R. A., Magloughlin, J. F., and Knipe, R. J., eds., The nature and tectonic significance of fault zone weakening: London, Geological Society of London Special Publication 186, p. 255-269.

Hatcher, R. D., Jr., 2002, An Inner Piedmont primer, *in* Hatcher, R. D., Jr. and Bream, B. R., eds., Inner Piedmont geology in the South Mountains–Blue Ridge Foothills and the southwestern Brushy Mountains, central-western North Carolina: Carolina Geological Society Guidebook, p. 1-24.

Hatcher, R. D., Jr., 2004, Properties of thrusts and upper bounds for the size of thrust sheets, *in* McClay, K. R., ed., Thrust tectonics and hydrocarbon systems: American Associated of Petroleum Geologists, Memoir 82, p. 18-29.

Hatcher, R. D., Jr., Merschat, A. J., and Thigpen, J. R., 2005, Blue Ridge primer, *in* Hatcher, R. D., Jr. and Merschat, A. J., eds, Blue Ridge geology geotraverse east of the Great Smoky Mountains National Park, western North Carolina: Carolina Geological Society Guidebook, p. 1-24.

Hatcher, R. D., Jr., and Merschat A. J., 2006, The Appalachian Inner Piedmont: An exhumed strike-parallel, tectonically forced orogenic channel, *in* Law, R. D., Searle, M., and Godin, L., eds., Channel flow, ductile extrusion, and exhumation of lower-mid crust in continental collision zones: London, Geological Society of London Special Publication 268, p. 517-540.

Hatcher, R. D., Jr., Bream, B. R., and Merschat, A. J., 2007, Tectonic map of the southern and central Appalachians: A tale of three orogens and a complete Wilson cycle, *in* Hatcher, R. D., Jr., Carlson, M. P., McBride, J. H., and Martinez Catalan, J. R., eds., The 4D Framework of Continental Crust: Geological Society of America Memoir 200, p. 595.

Hatcher, R. D., Jr., Huebner, M. T., Davis, B. A., and Hooper, R. J., 2009, Initial breakup of Pangea and birth of the Atlantic: A Difficult and complex process comparable to the birth of large animals: Geological Society of America Abstract with Programs, v. 41, p. 693.

Higgins, M. W., Crawford, T. J., Atkins, R. L., and Crawford, R. F., 2003, Geologic map of the Atlanta 30° x 60° quadrangle, Georgia: U.S. Geological Survey, Geologic Investigations Series Map I-2602, scale 1:250,000.

Hill, J. C., 1999, Geology of the Marion East quadrangle, North Carolina, and the stratigraphy of the Tallulah Falls Formation in the Chauga belt [unpublished M.S. thesis]: Knoxville, University of Tennessee, 188 p.

Hirth, G., and Tullis, J., 1992, Dislocation creep regimes in quartz aggregates: Journal of Structural geology, vol. 14, pp. 145-159.

Hodges, K. V., and Spear, F. S., 1982, Geothermobarometry, geobarometry and the Al_2SiO_5 triple point at Mt Moosilauke, New Hampshire: American Mineralogist, v. 67, p. 1118-1134.

Holdaway, M. J., 1971, Stability of andalusite and the aluminum silicate phase diagram: American Journal of Science, v. 271, pp. 97-131.

Holdaway, M. J., and Lee, S. M., 1977, Fe-Mg cordierite stability in high-grade pelitic rocks based on experiemental theoretical and natural observations: Contributions to Mineralogy and Petrology, v. 63. p. 171-198.

Hooper, R. J., 1989, Tectonic implications of a regionally extensive brittle fault system in the Piedmont; evidence from central Georgia: Geological Society of America abstract with programs, v. 21, p. 22.

Hopson, J. L. and Hatcher, R. D., Jr., 1988, Structural and stratigraphic setting of the Alto allochthon, northeast Georgia. Geological Society of America, v. 100. p. 339-350.

Hopson, J. L., Hatcher, R. D., Jr., and Stieve, A. L., 1989, Geology of the eastern Blue Ridge, northeastern Georgia and the adjacent Carolinas, *in* Fritz, W. J., Hatcher, R. D., Jr., and Hopson, J. L., eds., Geology of the eastern Blue Ridge of northeast Georgia and the adjacent Carolinas: Georgia Geological Society Guidebooks, v. 9, p. 1-40.

Huebner, M. T., Davis, B. D., and Hatcher, R. D., Jr., 2009, Triassic-Jurassic reactivation of the Alleghanian (Pennsylvanian-Permian) Towaliga fault, central Georgia, Appalachians: Geological Society of America Abstracts with Programs, v. 41, p. 693.

Jones, D. D., Jr., 1970, Petrofrabric and movement study of faults in Newton and Walton Counties, Georiga [M. S. thesis]: Atlanta, Emory University, 28 p.

Kalbas, J. L., 2003, Geology of part of the southwestern Brushy Mountains, Inner Piedmont, [M. S. thesis]: Knoxville, University of Tennessee, 206 p.

Keith, A. and Sterrett, D. B., 1931, Description of the Gaffney and Kings Mountain quadrangles (South Carolina-North Carolina): United States Geological Survey. Atlas Folio 222, 13 p.

King, P. B., 1955, A geologic cross section across the southern Appalachians: An outline of the geology in the segment in Tennessee, North Carolina, and South Carolina, *in* Russell, R. J., ed., Guides to southeastern geology: Geological Society of America Annual Meeting, p. 332-373.

Kohn, M. J., and Spear, F. S., 1990, Two barometers for garnet amphibolites with applications to southeastern Vermont: American Mineralogist, v. 74, p. 77-84.

Luth, W. D., Jahns, R. H., and Tuttle, O. F., 1964, The granite system at pressures of 4 to 10 kilobars: Journal of Geophysical Research, v. 69, p. 759-773.

Mapes, R. W., Miller, C. F., Fullagar, P. D. and Bream, B. R., 2001, Nature and origin of Acadian plutonism, Piedmont terane, NC-GA: Geological Society of America Abstracts with Programs, v. 33. no. 6, p. A92.

Mapes, R. W., 2002, Geochemistry and geochronology of mid-Paleozoic granitic plutonism in the southern Appalachian Piedmont terrane, North Carolina-South Carolina-Georgia [M. S. thesis]: Nashville, Tennessee, Vanderbilt University, 150 p.

Mapes, R. W., Maybin, A. H., III, Miller, C. F., Fullgar, P. D., and Bream, B. R., 2002, Geochronology and geochemistry of mid-Paleozoic granitic magmatism, central and eastern Inner Piedmont, North Carolina and South Carolina: Geological Society of America Abstracts with Programs (Southeastern Section), v. 34, no. 2, p. A-94.

Maniar and Piccoli, 1989, Tectonic discrimination of granitoids: Geological Society of America Bulletin, v. 101, no. 5, p. 635-643.

McBirney, A. R., 1993, Igneous Petrology, 3rd ed.: Ontario, Canada, Jones and Bartlett Publishers, 508 p.

McBride, J. H., Hatcher, R. D., Jr., Stephenson, W. J., Hooper, R. J., 2005, Integrating seismic reflection and geological data and interpretations across an internal basement massif: The southern Appalachian Pine Mountain window, USA: Geological Society of America Bulletin, v. 117, p. 1-18.

McSween, H. Y., Jr., Sando, T. W., Clark, S. R., Harden, J. T., and Strange, E. A., 1984, The gabbro-metagabbro association of the southern Appalachian Piedmont: American Journal of Science, v. 284, p. 437-461.

McSween H. Y., Jr., Speer, J. A., and Fullagar, P. D., 1991, Plutonic rocks, in Horton, J. W., Jr., and Zullo, V. A., eds., The geology of the Carolinas, Carolina Geological Society Fiftieth Anniversary Volume: Knoxville, University of Tennesse Press, p. 109-126.

Merschat, A. J., and Kalbas, J. L., 2002, Geology of the southwestern Brushy Mountains, *in* Hatcher, R. D., Jr., and Bream, B. R., eds., Inner Piedmont geology in the South Mountains-Blue Ridge Foothills and the southwestern Brushy Mountains, central-western North Carolina: Carolina Geological Society Guidebook, p. 101-126.

Merschat, A. J., 2003, Inner Piedmont tectonics in the southwestern Brushy Mountains, North Carolina: Field and laboratory data revealing 3-D crustal flow and sillimanite I and II metamorphism [M. S. thesis]: Knoxville, University of Tennessee, 198 p.

Merschat, A. J., Hatcher, R. D., Jr., and Davis, T. L., 2004, The northern Inner Piedmont, southern Appalachians, USA: kinematics of transpression and SW-directed mid-crustal flow. Journal of Structural Geology, v. 27, p. 1252-1281.

Merschat, A. J., Hatcher, R. D., Jr., and Davis, T. L., 2005, The northern Inner Piedmont, southern Appalachians, USA: kinematics of transpression and SW-directed mid-crustal flow: Journal of Structural Geology, v. 27, p. 1252-1281.

Merschat, A. J., and Hatcher, R. D., Jr., 2007, The Cat Square terrane: Possible Siluro-Devonian remnant ocean basin in the Inner Piedmont, southern Appalachians, USA, Geological Society of America Memoir, v. 200, pp. 553-556.

Merschat, A.J., Bream, B.R., Hatcher, R.D., Jr., Miller, C., Carrigan, C.W., 2008, Delimiting the spatial extent of superposed metamorphic events of the Blue Ridge and Inner Piedmont with SHRIMP U-PB ages of zircon rims, Geological Society of America Abstracts with Programs, v. 40, no. 4, p. 19.

Merschat, A. J., 2009, Assembling the Blue Ridge and Inner Piedmont: Insights into the nture and timing of terrane accretion in the southern Appalachian orogen from geologic mapping, stratigraphy, kinematic analysis, petrology, geochemistry, and modern geochronology [P.h. D. Dissertation]: Knoxville, University of Tennessee, 453 p.

Merschat, C.E., and Weiner, L.S., 1988, Geology of the Sandymush and Canton quadrangles, North Carolina: North Carolina Geological Survey Bulletin, v. 90, 66.

Mirante, D. C., and Patino-Douce, A. E., 2000, Melting and migmatization in the southern Appalachian Inner Piedmont of northeast Georgia; the Athens gneiss: Geological Society of America Abstracts with Programs, v. 33, no. 1, p. 297.

Naeser, C. W., Naeser, N. D., Kunk, M. J., Morgan, B. A., III, Schultz, A. P., Southworth, C. S., and Weems, R. E., 2001, Paleozoic through Cenozoic uplift, erosion, stream capture, and deposition history in the Valley and Ridge, Blue Ridge, Piedmont, and Coastal Plain provinces of Tennessee, North Carolina, Virginia, Maryland, and District of Columbia: Geological Society of America Abstracts with Programs, v. 33, no. 6, p. A-312.

Nelson, A. E., 1982, Geologic map of the Tray Mountain Roadless Area, northern Georgia: U. S. Geological Survey Miscellaneous Field Studies Map MF – 1347 – A, scale 1:30,000.

Nelson, A. E., Horton, J. W, Jr., and Clarke, J. W., 1998, Geologic map of the Greenville 1° x 2° quadrangle, South Carolina, Georgia, and North Carolina: U.S. Geological Survey Map I-2175, scale 1/250,000.

Passchier C. W., and Trouw, R. A., 2005, Micro-Tectonics, 2nd ed.: Sturtz AG, Wurzburg: Springer-Verlag, 366 p.

Pettijohn, F. J., 1954, Classification of Sandstones, The Journal of Geology, v. 62, pp. 360-365.

Pearce, J. A., 1982, Trace element characteristics of lavas from destructive plate boundaries, *in* Thorpe, R. S., ed., Andesites: orogenic andesites and related rocks: Chichester, Wiley, p. 525-548.

Pearce, J. A., Harris, B. W., and Tindle, A. G., 1984, Trace element discrimination diagrams for the tectonic interpretation of granitic rocks. Journal of Petrology, v. 25, pp. 956-983.

Pearce, J. A., and Cann, J. R., 1973, Tectonic setting of basic volcanic rocks determined using trace element analysis: Earth and Planetary Science Letters, v. 19, p. 290-300.

Pigage, L. C. and Greenwood, H. J., 1982, Internally consistent estimates of pressure and temperature; the staurolite problem. American Journal of Science, v. 282, pp. 943-969.

Prowell, D. C., 1972, Ultramafic plutons in the Central Piedmont of Georgia [M. S. thesis]: Atlanta, Georgia, Emory University, 82 p.

Quinn, M. J., 1991, Two lithotectonic boundaries in western North Carolina: Geologic interpretation of a region surrounding Sylva, Jackson County [M.S. thesis]: Knoxville, University of Tennessee, 223 p.

Rankin, D. W., Espenshade, G. J., and Neuman, R. B., 1972, Geologic map of the west half of the Winston-Salem quadrangle, North Carolina, Virginia, and Tennessee: U.S. Geological Survey Map I-709-A, scale 1:250,000.

Rankin, D. W., Espenshade, G. H., and Shaw, K. W., 1972, Stratigraphy and structure of the metamorphic belt in northwestern North Carolina and southwestern Virginia: A study from the Blue Ridge across the Brevard Fault Zone to the Sauratown Mountains Anticlinorium: American Journal of Science, v. 273, p. 1-40.

Reade, E. H. Jr., 1960, The geology of a portion of Newton and Walton Counties, Georgia [M. S. thesis]: Atlanta, Georgia, Emory University, 65 p.

Rollinson, H., 1993, Using geochemical data: evaluation, presentation, interpretation: Essex, England, Longman Group UK Limited, 352 p.

Schultz, R. S., 1961, The geology of northwestern Newton and southwestern Walton Counties, Georgia [M. S. thesis]: Atlanta, Georgia, Emory University, 46 p.

Settles, D. J., 2002, Defining the Hayesville-Sque River and Allotoona Faults and an Ordovician arc assemblage within the central Blue Ridge northwest of Dahlonega, Georgia [M.S. thesis]: Knoxville, University of Tennessee, 148 p.

Spear, F. S. and Cheney J. T., 1989, A petrogenetic grid for pelitic schists in the system SiO2-Al2O3-FeO-MgO-K2O-H2O. Contributions to Mineralogy and Petrology, v. 101. p. 149-164.

Spear, F. S., 1991, On the interpretation of peak metamorphic temperatures in light of garnet diffusion during cooling: Journal of Metamorphic Geology, v. 9, p. 379-388.

Spear, F. S., 1993, Metamorphic phase equilibria and pressure-temperature-time paths: Chelsea, Michigan, Book Crafters, Inc., 799 p.

Speer, A. J., and Hoff, K., 1997, Elemental composition of the Alleghanian granitoid plutons of the southern Appalachians: Geological Society of America, Memoir 191. p. 297-308.

Streckeisen, A., 1976, To each plutonic rock its proper name: Earth Science Reviews, v. 12, p. 1-33.

Sun, S. S. and McDonough, W. F., 1989. Chemical and isotopic systematic of oceanic basalts: implications for mantle composition and processes. Geological Society, London, Special Publications, v. 42, pp. 313-345.

Thompson, A. B., 1982, Dehydration melting of pelietic rocks and the generation of H2O-undersaturated granitic liquids. American Journal of Science, v. 282, p. 1567-1595.

Tull, J. F., Ausich, W. I., Groszos, M. S., and Thompson, T. W., 1993, Appalachian Blue Ridge cover sequence ranges at least into the Ordovician: Geology, v. 21, p. 215-218.

Tull, J.F., and Holm, C.S., 2005, Structural evolution of a major Appalachian salient-recess junction: consequences of oblique collisional convergence across a continental margin transform fault: Geological Society of America Bulletin, v. 117, no. 3/4, p. 482-499.

Tull, J. F., 2007, Tectonics of the Georgia Blue Ridge: Basement/cover rift architecture,important aspects of overlying drift and clastic wedge facies, and the westernmost accretionary terrane: Georgia Geological Society Guidebook, v. 27, no. 1, 203 p.

van Breeman, O., and Dallmeyer, R. D., 1984, The scale of Sr isotopic diffusion during post-metamorphic cooling of gneisses in the Inner Piedmont of Georgia, southern Appalachians: Earth and Planetary Science Letters, v. 68, p. 141-150.

Vinson, S., 1999, Ion probe geochronology of granitoid gneisses of the Inner Piedmont, North Carolina and South Carolina [M.S. thesis]: Nashville, Tennessee, Vanderbilt University, 84 p.

Vinson, S. B., and Miller, C., F., 1999, Constraints on timing of Inner Piedmont plutonism, N.C. – S.C., from ion microprobe U-Pb zircon analysis: Geological Society of America Abstracts with Programs, v. 31, no. 2, p. A73.

Whitten, E. H., 1966, Structural geology of folded rocks: Chicago, Rand McNally and Company, 663 p.

Williams, S. T., 2000, Structure, stratigraphy, and migmatization in the southwestern South Mountains, North Carolina [M. S. thesis]: Knoxville, University of Tennessee, 111 p.

Wilson, C. G., 2006, Origin and tectonic evolution of the southern Appalachian Neoacadian crystalline core: Evidence from the geology of the Gilreath 7.5-minute quadrangle, North Carolina [M. S. thesis]: Knoxville, University of Tennessee, 200 p.

Winter, John D., 2001, An Introduction to Igneous and Metamorphic Petrology, 3rd ed.: New York : Prentice Hall 698 p.

Yanagihara, G. M., 1993, Evolution of folds associated with D_2 and D_3 deformation and their relationship with shearing in a part of the Columbus Promontory, North Carolina, *in* Hatcher, R. D., Jr., and Davis, T. L., eds., Studies of Inner Piedmont geology with a focus on the Columbus Promontory: Carolina Geological Society Guidebook, North Carolina Geological Survey, p. 45-54.

Yanagihara, G. M., 1994, Structure, stratigraphy, and metamorphism of a part of the Columbus Promontory, North Carolina [M.S. thesis]: Knoxville, University of Tennessee, 214 p.

Yardley, B. W. D., 1977, An empirical study of diffusion in garnet: American Mineralogist, v. 62, p. 793-800.

APPENDICES

Appendix 1A:
Microprobe Analysis of F-1236 - Garnet-D

Oxide Wt. %	GrtDRim1	GrtDRim2	GrtDRim3	GrtDRim4	GrtDRim5	GrtDRim6	GrtDRim7	GrtDRim8	GrtDRim9	GrtDRim10	GrtDRim11	GrtDRim12	GrtDRim13	GrtDRim14
SiO_2	37.33	35.68	37.62	37.40	37.50	37.51	37.81	37.50	38.09	37.76	36.46	37.76	37.85	37.76
TiO_2	0.01	0.09	0.01	0.01	0.00	0.01	0.02	0.03	0.00	0.03	0.01	0.01	0.03	0.02
$Al2O_3$	21.18	20.44	21.59	21.53	21.71	21.63	21.89	21.53	21.82	21.75	21.12	21.65	21.71	21.71
$Y2O_3$	0.05	0.03	0.01	0.03	0.02	0.03	0.01	0.04	0.08	0.04	0.06	0.10	0.09	0.08
MgO	4.29	4.27	4.34	4.48	4.39	4.44	4.71	4.52	4.06	4.50	4.49	4.54	4.55	4.54
CaO	1.61	1.58	1.63	1.66	1.71	1.76	1.84	1.83	1.93	2.01	2.07	2.16	2.28	2.33
MnO	2.67	2.61	2.65	2.57	2.56	2.57	2.48	2.46	2.43	2.39	2.36	2.40	2.33	2.27
FeO	33.28	32.65	33.38	33.31	33.43	33.32	32.89	33.01	32.58	33.08	32.66	32.78	32.60	32.84
Na_2O	0.01	0.05	0.01	0.01	0.02	0.01	0.01	0.02	0.02	0.01	0.03	0.01	0.00	0.03
Total	100.43	97.41	101.24	101.01	101.34	101.27	101.66	100.95	101.01	101.57	99.27	101.43	101.45	101.57
Cation based on 12 oxygens														
Si	2.98	2.95	2.97	2.96	2.96	2.96	2.97	2.97	3.00	2.97	2.95	2.97	2.98	2.97
Ti	0.00	0.01	0.00	0.00	0.00	0.00	0.00	0.00	0.00	0.00	0.00	0.00	0.00	0.00
Al	1.99	1.99	2.01	2.01	2.02	2.02	2.02	2.01	2.03	2.02	2.01	2.01	2.01	2.01
Y	0.00	0.00	0.00	0.00	0.00	0.00	0.00	0.00	0.00	0.00	0.00	0.00	0.00	0.00
Mg	0.51	0.53	0.51	0.53	0.52	0.52	0.55	0.53	0.48	0.53	0.54	0.53	0.53	0.53
Ca	0.14	0.14	0.14	0.14	0.15	0.15	0.16	0.16	0.16	0.17	0.18	0.18	0.19	0.20
Mn	0.18	0.18	0.18	0.17	0.17	0.17	0.17	0.17	0.16	0.16	0.16	0.16	0.16	0.15
Fe	2.22	2.26	2.21	2.21	2.21	2.20	2.16	2.19	2.15	2.18	2.21	2.16	2.14	2.16
OH	0.00	0.00	0.00	0.00	0.00	0.00	0.00	0.00	0.00	0.00	0.00	0.00	0.00	0.00
Na	0.00	0.01	0.00	0.00	0.00	0.00	0.00	0.00	0.00	0.00	0.01	0.00	0.00	0.00
Total	8.03	8.06	8.02	8.03	8.03	8.03	8.02	8.03	7.99	8.02	8.05	8.02	8.02	8.03

Microprobe Analysis of F-1236 - Garnet-D

Oxide Wt. %	GrtDRim15	GrtDRim16	GrtDRim17	GrtDRim18	GrtDRim19	GrtDRim20	GrtDCore1	GrtDCore2	GrtDCore3	GrtDCore4	GrtDCore5	GrtDCore6	GrtDCore7	GrtDCore8
SiO_2	37.76	37.71	37.75	37.83	37.86	37.83	37.76	37.49	37.89	37.82	37.72	37.78	37.76	37.83
TiO_2	0.03	0.01	0.01	0.03	0.03	0.03	0.02	0.03	0.05	0.05	0.07	0.03	0.03	0.01
$Al2O_3$	21.61	21.69	21.62	21.61	21.59	21.59	21.51	21.49	21.44	21.57	21.65	21.60	21.55	21.56
$Y2O_3$	0.06	0.03	0.03	0.08	0.06	0.04	0.08	0.04	0.04	0.05	0.00	0.05	0.06	0.05
MgO	4.49	4.55	4.47	4.54	4.53	4.58	4.62	4.58	4.61	4.55	4.62	4.63	4.60	4.61
CaO	2.45	2.45	2.55	2.50	2.52	2.56	2.57	2.47	2.54	2.53	2.48	2.45	2.46	2.44
MnO	2.27	2.26	2.22	2.24	2.20	2.26	2.22	2.21	2.17	2.16	2.17	2.19	2.19	2.20
FeO	32.75	32.64	32.58	32.58	32.60	32.59	32.63	32.72	32.82	32.58	32.84	32.64	32.50	32.79
Na_2O	0.01	0.01	0.01	0.01	0.01	0.02	0.01	0.01	0.00	0.01	0.02	0.02	0.01	0.02
Total	101.43	101.35	101.23	101.42	101.41	101.50	101.41	101.04	101.56	101.31	101.58	101.38	101.17	101.51
Cation based on 12 oxygens														
Si	2.97	2.97	2.97	2.98	2.98	2.97	2.97	2.96	2.98	2.98	2.96	2.97	2.98	2.98
Ti	0.00	0.00	0.00	0.00	0.00	0.00	0.00	0.00	0.00	0.00	0.00	0.00	0.00	0.00
Al	2.01	2.01	2.01	2.00	2.00	2.00	2.00	2.00	1.99	2.00	2.01	2.00	2.00	2.00
Y	0.00	0.00	0.00	0.00	0.00	0.00	0.00	0.00	0.00	0.00	0.00	0.00	0.00	0.00
Mg	0.53	0.53	0.53	0.53	0.53	0.54	0.54	0.54	0.54	0.53	0.54	0.54	0.54	0.54
Ca	0.21	0.21	0.22	0.21	0.21	0.22	0.22	0.21	0.21	0.21	0.21	0.21	0.21	0.21
Mn	0.15	0.15	0.15	0.15	0.15	0.15	0.15	0.15	0.14	0.14	0.15	0.15	0.15	0.15
Fe	2.16	2.15	2.15	2.14	2.14	2.14	2.15	2.16	2.16	2.15	2.16	2.15	2.14	2.16
OH	0.00	0.00	0.00	0.00	0.00	0.00	0.00	0.00	0.00	0.00	0.00	0.00	0.00	0.00
Na	0.00	0.00	0.00	0.00	0.00	0.00	0.00	0.00	0.00	0.00	0.00	0.00	0.00	0.00
Total	8.02	8.03	8.02	8.02	8.02	8.03	8.03	8.03	8.03	8.02	8.03	8.02	8.02	8.03

Microprobe Analysis of F-1236 - Garnet-D

Oxide Wt. %	GrtDCore9	GrtDCore10	GrtDRim21	GrtDRim22	GrtDRim23	GrtDRim24	GrtDRim25	GrtDRim26	GrtDRim27	GrtDRim28	GrtDRim29	GrtDRim30	GrtDRim31	GrtDRim32
SiO_2	37.74	37.73	37.74	37.67	37.64	37.92	37.71	37.81	37.80	37.84	37.43	37.58	37.68	37.68
TiO_2	0.01	0.03	0.02	0.02	0.01	0.01	0.03	0.00	0.01	0.01	0.01	0.00	0.01	0.01
$Al2O_3$	21.57	21.49	21.51	21.76	21.63	21.70	21.62	21.74	21.74	21.52	21.84	21.65	21.85	21.60
$Y2O_3$	0.06	0.08	0.07	0.05	0.03	0.04	0.03	0.02	0.04	0.03	0.07	0.06	0.04	0.03
MgO	4.62	4.68	4.62	4.65	4.72	4.73	4.70	4.80	4.78	4.80	4.70	4.74	4.79	4.90
CaO	2.39	2.41	2.35	2.31	2.32	2.20	2.07	2.08	2.04	2.07	2.01	1.96	2.03	2.00
MnO	2.14	2.16	2.14	2.16	2.18	2.17	2.14	2.21	2.13	2.19	2.20	2.21	2.14	2.19
FeO	32.74	32.66	32.84	32.91	32.80	32.84	32.85	33.20	32.80	32.90	32.99	33.01	32.76	33.02
Na_2O	0.00	0.00	0.00	0.02	0.02	0.03	0.02	0.01	0.01	0.01	0.02	0.02	0.00	0.00
Total	101.27	101.23	101.29	101.54	101.36	101.64	101.18	101.86	101.35	101.37	101.26	101.24	101.31	101.44
Cation based on 12 oxygens														
Si	2.97	2.97	2.97	2.96	2.96	2.97	2.97	2.96	2.97	2.98	2.95	2.96	2.96	2.97
Ti	0.00	0.00	0.00	0.00	0.00	0.00	0.00	0.00	0.00	0.00	0.00	0.00	0.00	0.00
Al	2.00	2.00	2.00	2.02	2.01	2.01	2.01	2.01	2.01	2.00	2.03	2.01	2.03	2.00
Y	0.00	0.00	0.00	0.00	0.00	0.00	0.00	0.00	0.00	0.00	0.00	0.00	0.00	0.00
Mg	0.54	0.55	0.54	0.55	0.55	0.55	0.55	0.56	0.56	0.56	0.55	0.56	0.56	0.58
Ca	0.20	0.20	0.20	0.20	0.20	0.19	0.18	0.17	0.17	0.17	0.17	0.17	0.17	0.17
Mn	0.14	0.14	0.14	0.14	0.15	0.14	0.14	0.15	0.14	0.15	0.15	0.15	0.14	0.15
Fe	2.16	2.15	2.16	2.16	2.16	2.15	2.17	2.18	2.16	2.17	2.18	2.18	2.16	2.17
OH	0.00	0.00	0.00	0.00	0.00	0.00	0.00	0.00	0.00	0.00	0.00	0.00	0.00	0.00
Na	0.00	0.00	0.00	0.00	0.00	0.01	0.00	0.00	0.00	0.00	0.00	0.00	0.00	0.00
Total	8.02	8.03	8.03	8.03	8.03	8.02	8.02	8.03	8.02	8.02	8.03	8.03	8.02	8.03

Microprobe Analysis of F-1236 - Garnet-D

Oxide Wt. %	GrtDRim33	GrtDRim34	GrtDRim 35	GrtDRim36	GrtDRim37	GrtDRim38	GrtDRim39	GrtDRim40	GrtDRim41	GrtDRim42	GrtDCoreNbte1	GrtDCoreNbte2	GrtDCoreNbte3	GrtDCoreNbte4
SiO_2	37.71	37.77	37.95	37.78	37.60	37.84	37.72	37.91	37.86	37.65	38.28	38.05	37.88	37.53
TiO_2	0.02	0.01	0.00	0.02	0.00	0.01	0.02	0.01	0.02	0.00	0.58	0.61	0.17	0.11
$Al2O_3$	21.81	21.55	21.80	21.67	21.72	21.71	21.78	21.66	21.73	21.86	21.53	21.88	21.55	21.40
$Y2O_3$	0.06	0.07	0.03	0.04	0.00	0.00	0.03	0.04	0.04	0.08	0.00	0.06	0.04	0.04
MgO	4.69	4.75	4.78	4.76	4.77	4.78	4.79	4.78	4.77	4.68	4.20	3.78	4.26	4.44
CaO	1.91	1.93	1.90	1.86	1.86	1.79	1.70	1.67	1.64	1.59	2.17	2.24	2.26	2.27
MnO	2.25	2.22	2.22	2.24	2.26	2.24	2.24	2.30	2.27	2.26	2.08	2.18	2.22	2.22
FeO	32.84	33.03	33.05	33.16	33.14	33.20	33.17	32.95	33.26	33.30	32.01	32.45	32.99	33.20
Na_2O	0.01	0.02	0.01	0.01	0.01	0.02	0.02	0.01	0.03	0.02	0.03	0.02	0.00	0.01
Total	101.29	101.35	101.74	101.54	101.36	101.57	101.47	101.32	101.62	101.44	100.87	101.26	101.37	101.22
Cation based on 12 oxygens														
Si	2.97	2.98	2.97	2.97	2.96	2.97	2.97	2.98	2.97	2.96	3.01	2.99	2.98	2.97
Ti	0.00	0.00	0.00	0.00	0.00	0.00	0.00	0.00	0.00	0.00	0.03	0.04	0.01	0.01
Al	2.02	2.00	2.01	2.01	2.02	2.01	2.02	2.01	2.01	2.03	2.00	2.03	2.00	1.99
Y	0.00	0.00	0.00	0.00	0.00	0.00	0.00	0.00	0.00	0.00	0.00	0.00	0.00	0.00
Mg	0.55	0.56	0.56	0.56	0.56	0.56	0.56	0.56	0.56	0.55	0.49	0.44	0.50	0.52
Ca	0.16	0.16	0.16	0.16	0.16	0.15	0.14	0.14	0.14	0.13	0.18	0.19	0.19	0.19
Mn	0.15	0.15	0.15	0.15	0.15	0.15	0.15	0.15	0.15	0.15	0.14	0.15	0.15	0.15
Fe	2.16	2.18	2.17	2.18	2.18	2.18	2.18	2.17	2.18	2.19	2.11	2.13	2.17	2.20
OH	0.00	0.00	0.00	0.00	0.00	0.00	0.00	0.00	0.00	0.00	0.00	0.00	0.00	0.00
Na	0.00	0.00	0.00	0.00	0.00	0.00	0.00	0.00	0.00	0.00	0.00	0.00	0.00	0.00
Total	8.02	8.03	8.02	8.03	8.03	8.02	8.03	8.01	8.02	8.02	7.96	7.96	8.01	8.03

Microprobe Analysis of F-1236 - Garnet-D

Oxide Wt. %	GrtDCoreNbte5	GrtDNBt2-1	GrtDNBt2-2	GrtDNBt2-3	GrtDNBt2-4	GrtDNBt2-5	GrtDNPlg1	GrtDNPlg1	GrtDNPlg1	GrtDNPlg1	GrtDNPlg1	GrtDNPlg2-1	GrtDNPlg2-2	GrtDNPlg2-3
SiO_2	37.90	38.02	37.87	37.87	37.84	37.46	37.68	37.69	37.86	37.76	37.75	36.75	37.74	37.77
TiO_2	0.05	0.09	0.13	0.03	0.02	0.04	0.05	0.08	0.12	0.27	0.63	0.01	0.01	0.00
$Al2O_3$	21.30	21.86	21.76	21.54	21.50	21.53	21.32	21.50	21.56	21.40	21.36	21.38	21.67	21.67
$Y2O_3$	0.01	0.06	0.07	0.05	0.06	0.03	0.11	0.05	0.05	0.03	0.01	0.08	0.07	0.10
MgO	4.56	4.49	4.48	4.42	4.51	4.39	4.58	4.60	4.59	4.52	4.34	4.78	4.73	4.75
CaO	2.21	2.43	2.47	2.58	2.56	2.56	2.22	2.16	2.23	2.25	2.23	2.12	2.12	2.14
MnO	2.21	2.14	2.11	2.14	2.18	2.16	2.16	2.16	2.16	2.18	2.17	1.99	2.18	2.17
FeO	32.84	32.81	32.56	32.76	32.76	32.92	32.74	32.49	32.75	32.89	32.66	29.19	32.54	32.61
Na_2O	0.01	0.01	0.00	0.01	0.00	0.01	0.01	0.02	0.00	0.01	0.00	0.19	0.02	0.01
Total	101.09	101.91	101.45	101.39	101.43	101.10	100.86	100.76	101.31	101.32	101.15	96.48	101.09	101.23
Cation based on 12 oxygens														
Si	2.99	2.97	2.97	2.98	2.98	2.96	2.98	2.98	2.98	2.98	2.98	3.00	2.97	2.97
Ti	0.00	0.01	0.01	0.00	0.00	0.00	0.00	0.00	0.01	0.02	0.04	0.00	0.00	0.00
Al	1.98	2.02	2.01	2.00	1.99	2.01	1.99	2.00	2.00	1.99	1.99	2.06	2.01	2.01
Y	0.00	0.00	0.00	0.00	0.00	0.00	0.00	0.00	0.00	0.00	0.00	0.00	0.00	0.00
Mg	0.54	0.52	0.53	0.52	0.53	0.52	0.54	0.54	0.54	0.53	0.51	0.58	0.56	0.56
Ca	0.19	0.20	0.21	0.22	0.22	0.22	0.19	0.18	0.19	0.19	0.19	0.19	0.18	0.18
Mn	0.15	0.14	0.14	0.14	0.15	0.15	0.15	0.14	0.14	0.15	0.15	0.14	0.15	0.15
Fe	2.17	2.15	2.14	2.16	2.16	2.18	2.17	2.15	2.16	2.17	2.15	1.99	2.15	2.15
OH	0.00	0.00	0.00	0.00	0.00	0.00	0.00	0.00	0.00	0.00	0.00	0.00	0.00	0.00
Na	0.00	0.00	0.00	0.00	0.00	0.00	0.00	0.00	0.00	0.00	0.00	0.03	0.00	0.00
Total	8.02	8.01	8.01	8.02	8.02	8.03	8.02	8.01	8.01	8.02	7.99	7.986	8.019	8.02

Microprobe Analysis of F-1236 - Garnet-D

Oxide Wt. %	GrtDNPlg2-4	GrtDNPlg2-5	GrtContwbte1	GrtContwbte2	GrtContwbte3	GrtContwbte4	GrtCtwbte1-1	GrtCtwbte1-2	GrtCtwbte1-3	GrtCtwbte1-4	GrtCtwbte1-5	GrtCtwbte1-6	GrtCtwbte1-7	GrtCtwbte1-8
SiO_2	37.72	37.80	37.50	37.26	37.30	37.20	37.57	37.71	37.67	37.52	37.60	37.61	37.49	37.65
TiO_2	0.01	0.01	0.30	0.04	0.02	0.02	0.04	0.04	0.03	0.02	0.02	0.03	0.02	0.01
$Al2O_3$	21.67	21.78	21.75	21.48	21.47	21.46	21.63	21.52	21.56	21.54	21.53	21.58	21.52	21.67
$Y2O_3$	0.06	0.09	0.00	0.07	0.06	0.04	0.08	0.06	0.08	0.06	0.09	0.09	0.07	0.07
MgO	4.73	4.68	11.61	3.26	3.43	3.63	2.49	2.81	3.03	3.25	3.41	3.46	3.64	3.68
CaO	2.15	2.12	0.36	1.56	1.55	1.59	1.94	1.95	1.99	2.05	2.08	2.05	2.04	2.08
MnO	2.16	2.17	0.74	3.06	2.96	2.95	3.63	3.43	3.24	3.12	3.03	2.93	2.87	2.81
FeO	32.80	32.78	17.37	34.33	34.01	34.16	34.46	34.15	34.01	33.80	33.68	33.75	33.74	33.85
Na_2O	0.01	0.02	0.04	0.01	0.03	0.02	0.00	0.01	0.00	0.01	0.01	0.03	0.01	0.01
Total	101.32	101.44	89.67	101.07	100.82	101.08	101.85	101.68	101.59	101.38	101.45	101.53	101.41	101.83
Cation based on 12 oxygens														
Si	2.97	2.97	3.07	2.97	2.98	2.96	2.98	2.99	2.99	2.98	2.98	2.98	2.97	2.97
Ti	0.00	0.00	0.02	0.00	0.00	0.00	0.00	0.00	0.00	0.00	0.00	0.00	0.00	0.00
Al	2.01	2.02	2.10	2.02	2.02	2.02	2.02	2.01	2.01	2.02	2.01	2.01	2.01	2.02
Y	0.00	0.00	0.00	0.00	0.00	0.00	0.00	0.00	0.00	0.00	0.00	0.00	0.00	0.00
Mg	0.56	0.55	1.41	0.39	0.41	0.43	0.30	0.33	0.36	0.39	0.40	0.41	0.43	0.43
Ca	0.18	0.18	0.03	0.13	0.13	0.14	0.17	0.17	0.17	0.17	0.18	0.17	0.17	0.18
Mn	0.14	0.15	0.05	0.21	0.20	0.20	0.24	0.23	0.22	0.21	0.20	0.20	0.19	0.19
Fe	2.16	2.15	1.19	2.29	2.27	2.28	2.29	2.26	2.25	2.24	2.23	2.23	2.24	2.23
OH	0.00	0.00	0.00	0.00	0.00	0.00	0.00	0.00	0.00	0.00	0.00	0.00	0.00	0.00
Na	0.00	0.00	0.01	0.00	0.00	0.00	0.00	0.00	0.00	0.00	0.00	0.01	0.00	0.00
Total	8.024	8.02	7.87	8.02	8.01	8.03	8.00	8.00	8.00	8.01	8.01	8.01	8.02	8.02

Microprobe Analysis of F-1236 - Garnet-D

Oxide Wt. %	GrtCtwbte1-9	GrtRimCtwPlg1	GrtRimCtwPlg2	GrtRimCtwPlg3	GrtRimCtwPlg4	GrtRimCtwPlg5
SiO_2	37.62	37.44	37.36	37.53	37.63	37.28
TiO_2	0.01	0.01	0.01	0.00	0.00	0.00
$Al2O_3$	21.62	21.43	21.55	21.54	21.38	21.67
$Y2O_3$	0.05	0.07	0.04	0.03	0.06	0.05
MgO	3.81	4.67	4.58	4.60	4.54	4.60
CaO	2.11	1.65	1.62	1.60	1.57	1.59
MnO	2.77	2.43	2.46	2.51	2.51	2.47
FeO	33.75	33.07	32.96	33.04	32.84	32.92
Na_2O	0.01	0.01	0.02	0.02	0.01	0.03
Total	101.76	100.78	100.59	100.87	100.56	100.60
Cation based on 12 oxygens						
Si	2.97	2.97	2.97	2.97	2.99	2.96
Ti	0.00	0.00	0.00	0.00	0.00	0.00
Al	2.01	2.00	2.02	2.01	2.00	2.03
Y	0.00	0.00	0.00	0.00	0.00	0.00
Mg	0.45	0.55	0.54	0.54	0.54	0.54
Ca	0.18	0.14	0.14	0.14	0.13	0.14
Mn	0.19	0.16	0.17	0.17	0.17	0.17
Fe	2.23	2.19	2.19	2.19	2.18	2.19
OH	0.00	0.00	0.00	0.00	0.00	0.00
Na	0.00	0.00	0.00	0.00	0.00	0.00
Total	8.03	8.03	8.02	8.02	8.01	8.03

Microprobe Analysis of F-1236 - Mica
near or in garnet-D

Oxide Wt. %	BteNGrt1	BteNGrt2	BteNGrt3	BteNGrt4	BteNGrt5	Bte2NGrt1	Bte2NGrt2	Bte2NGrt3	BteOGrt1	BteOGrt2	BteOGrt3	BteOGrt4	BteOGrt5	BteOGrt6
SiO_2	35.9786	36.1582	36.4181	36.283	36.1547	36.671	36.6298	37.142	35.5674	35.2169	35.7229	35.4489	35.2426	35.3824
TiO_2	2.2179	2.1554	2.2903	2.2677	2.309	4.1341	4.1113	4.1806	4.7609	4.4076	4.57	4.5702	4.5025	4.4103
Al_2O_3	19.018	19.0775	19.4075	19.2987	19.3453	17.0468	17.2287	17.5862	18.7239	19.6565	19.0409	18.7232	18.7823	18.6802
MgO	13.442	13.6619	14.5809	14.2914	14.2872	13.3898	14.3267	14.6409	8.578	8.3777	8.6221	8.666	8.9067	9.0074
CaO	0.0157	0.0204	0.0235	0.0257	0.0253	0.0484	0.0336	0.0493	0.0212	0.0259	0.0398	0.0446	0.0208	0.029
MnO	0.0646	0.0569	0.0462	0.0562	0.0399	0.0708	0.0786	0.0587	0.0813	0.0634	0.0655	0.066	0.0473	0.0637
FeO	13.9696	14.3973	13.3414	13.364	13.1466	13.9682	13.8265	13.9502	18.7182	18.6969	18.7418	18.9446	18.9561	18.707
Na_2O	0.21	0.2108	0.2226	0.2075	0.2088	0.2426	0.2787	0.2792	0.0502	0.0402	0.0675	0.0858	0.0797	0.0692
K_2O	9.2269	9.2694	9.2761	9.2555	9.2638	9.2593	9.2105	9.2387	9.6906	8.8907	9.384	9.4858	9.8183	9.5392
Total	98.1445	99.0388	99.6866	99.1044	98.8267	98.854	99.7877	101.2532	100.1757	99.3481	100.2519	100.0112	100.3357	99.8605
Cation based on 12 oxygens														
Si	5.392	5.379	5.353	5.366	5.358	5.466	5.406	5.396	5.354	5.316	5.359	5.346	5.311	5.341
Ti	0.25	0.241	0.253	0.252	0.257	0.463	0.456	0.457	0.539	0.5	0.516	0.518	0.51	0.501
Al	3.359	3.345	3.362	3.364	3.379	2.995	2.997	3.011	3.322	3.497	3.366	3.328	3.336	3.324
Mg	3.003	3.03	3.195	3.151	3.157	2.975	3.152	3.171	1.925	1.885	1.928	1.948	2.001	2.027
Ca	0.003	0.003	0.004	0.004	0.004	0.008	0.005	0.008	0.003	0.004	0.006	0.007	0.003	0.005
Mn	0.008	0.007	0.006	0.007	0.005	0.009	0.01	0.007	0.01	0.008	0.008	0.008	0.006	0.008
Fe	1.751	1.791	1.64	1.653	1.629	1.741	1.707	1.695	2.356	2.36	2.351	2.389	2.389	2.362
Na	0.061	0.061	0.063	0.059	0.06	0.07	0.08	0.079	0.015	0.012	0.02	0.025	0.023	0.02
K	1.764	1.759	1.739	1.746	1.751	1.761	1.734	1.712	1.861	1.712	1.796	1.825	1.887	1.837
Total	19.591	19.617	19.615	19.603	19.601	19.489	19.546	19.537	19.384	19.296	19.35	19.396	19.467	19.425

Microprobe Analysis of F-1236 - Mica
near or in garnet-D

Oxide Wt. %	BteOGrt7	BteOGrt8	BteOCtwGrt1	BteOCtwGrt2	BteOCtwGrt3	BteOCtwGrt4	Bt2OCtwGrt1	Bt2OCtwGrt2	Bt2OCtwGrt3	Bt2OCtwGrt4	Bt2OCtwGrt5	Bt2OCtwGrt6	Bt2OCtwGrt7	Bt2OCtwGrt8
SiO_2	35.1977	35.6762	35.8429	35.8961	36.0628	36.9215	34.4172	35.045	35.3122	35.5486	35.5053	35.3874	35.57	35.5402
TiO_2	4.378	4.3929	3.0704	2.5323	2.1942	1.0164	1.9862	2.8355	2.7102	2.6792	2.6217	2.624	2.532	2.4184
Al_2O_3	18.5555	19.7127	19.8344	19.0511	19.5746	21.389	20.851	18.7488	19.1442	18.8812	18.6347	18.7212	19.0518	18.8375
MgO	8.9669	8.2832	11.0394	11.7766	12.0156	12.8771	7.6799	9.3311	9.3974	9.356	9.3711	9.592	9.337	9.5046
CaO	0.0186	0.0156	0.0381	0.0728	0.0755	0.0402	0.143	0.0342	0.013	0.0147	0	0.0134	0.0177	0.0216
MnO	0.0605	0.044	0.056	0.0544	0.0529	0.0581	0.2433	0.1313	0.1094	0.0926	0.0833	0.0867	0.091	0.103
FeO	18.559	17.5898	15.9189	16.2823	15.5165	13.3565	17.4717	20.1002	20.0184	19.9756	20.1589	20.3309	20.0333	20.3819
Na_2O	0.0765	0.0425	0.0638	0.0655	0.067	0.0617	0.0834	0.0852	0.0767	0.0689	0.0729	0.0751	0.0793	0.0717
K_2O	9.5209	9.0633	9.5479	9.3208	9.123	8.8856	7.1176	9.4876	9.6093	9.4914	9.609	9.6656	9.2994	9.5835
Total	99.283	98.7929	99.4291	99.0475	98.687	98.6778	93.8017	99.7378	100.3597	100.0707	100.0092	100.4609	99.975	100.4292
Cation based on 12 oxygens														
Si	5.344	5.385	5.35	5.387	5.4	5.438	5.419	5.335	5.335	5.38	5.387	5.353	5.382	5.373
Ti	0.5	0.499	0.345	0.286	0.247	0.113	0.235	0.325	0.308	0.305	0.299	0.298	0.288	0.275
Al	3.321	3.507	3.49	3.37	3.454	3.713	3.869	3.364	3.409	3.368	3.332	3.337	3.397	3.356
Mg	2.03	1.864	2.457	2.635	2.682	2.827	1.803	2.118	2.117	2.111	2.12	2.163	2.106	2.142
Ca	0.003	0.003	0.006	0.012	0.012	0.006	0.024	0.006	0.002	0.002	0	0.002	0.003	0.004
Mn	0.008	0.006	0.007	0.007	0.007	0.007	0.032	0.017	0.014	0.012	0.011	0.011	0.012	0.013
Fe	2.357	2.221	1.987	2.044	1.943	1.645	2.301	2.559	2.529	2.528	2.558	2.572	2.535	2.577
Na	0.023	0.012	0.018	0.019	0.019	0.018	0.025	0.025	0.022	0.02	0.021	0.022	0.023	0.021
K	1.844	1.745	1.818	1.785	1.743	1.67	1.43	1.843	1.852	1.832	1.86	1.865	1.795	1.848
Total	19.429	19.241	19.478	19.544	19.507	19.437	19.139	19.592	19.589	19.558	19.588	19.624	19.541	19.609

Microprobe Analysis
of F-1236 - Feldspar in

Oxide Wt. %	PlgNGrt1	PlgNGrt2	PlgNGrt3	PlgNGrt4	PlgNGrt1	PlgNGrt2	PlgNGrt3	PlgNGrt4	PlgOGrt1	PlgOGrt2	PlgOGrt3	PlgOGrt4	PlgOGrt5	KspWPlgOGrt1
SiO_2	60.3403	59.5748	59.2587	59.5323	59.4835	59.6524	59.6898	58.0723	61.7039	61.7344	61.4476	62.0687	61.7957	63.8964
$Al2O_3$	25.6487	25.705	25.9145	26.0423	25.8581	25.5547	25.7813	25.1313	24.4957	24.147	24.3779	24.5503	24.3185	18.8924
CaO	6.8985	6.9864	7.186	7.1044	7.2578	7.0103	7.1817	6.6519	5.3321	5.3888	5.4873	5.4688	5.5391	0.0136
FeO	0.3662	0.4	0.2921	0.2212	0.236	0.2264	0.265	0.2973	0.2669	0.1155	0.2281	0.132	0.1654	0.0815
Na_2O	7.3155	7.1517	7.1967	7.1931	7.298	7.3523	7.4713	7.5575	8.2629	8.427	8.1062	8.1969	8.1758	0.8993
K_2O	0.3938	0.3844	0.3759	0.379	0.3442	0.3972	0.3617	0.4391	0.2167	0.1931	0.1956	0.2358	0.2431	15.1851
Total	100.963	100.2023	100.2239	100.4723	100.4776	100.1933	100.7508	98.1494	100.2781	100.0057	99.8426	100.6526	100.2377	98.9683
Cation based on 8														
Si	2.666	2.654	2.641	2.644	2.644	2.658	2.648	2.646	2.73	2.739	2.73	2.734	2.735	2.975
Al	1.336	1.35	1.361	1.363	1.355	1.342	1.348	1.35	1.277	1.263	1.277	1.275	1.269	1.037
Ca	0.327	0.333	0.343	0.338	0.346	0.335	0.341	0.325	0.253	0.256	0.261	0.258	0.263	0.001
Fe	0.014	0.015	0.011	0.008	0.009	0.008	0.01	0.011	0.01	0.004	0.008	0.005	0.006	0.003
Na	0.627	0.618	0.622	0.619	0.629	0.635	0.643	0.668	0.709	0.725	0.698	0.7	0.702	0.081
K	0.022	0.022	0.021	0.021	0.02	0.023	0.02	0.026	0.012	0.011	0.011	0.013	0.014	0.902
Total	4.991	4.991	5	4.995	5.002	5	5.01	5.025	4.992	4.998	4.986	4.985	4.988	4.998

Microprobe Analysis
of F-1236 - Feldspar in

Oxide Wt. %	KspWPlgOGrt2	KspWPlgOGrt3	KspWPlgOGrt4	KspWPlgOGrt5	Ksp-Plg1	Ksp-Plg2	Ksp-Plg3	Ksp-Plg4	Ksp-Plg5	Ksp-Plg6	Ksp-Plg7	Ksp-Plg8	Ksp-Plg19	Ksp-Plg10
SiO_2	63.8814	63.2116	63.7547	62.0023	63.8375	63.7383	63.4425	64.1542	63.9606	64.1892	57.2787	59.8265	61.9107	61.8689
$Al2O_3$	18.7539	18.7929	18.7428	24.7383	18.6427	18.6938	18.5112	18.9018	18.703	18.8967	24.0386	24.3028	24.4211	24.2277
CaO	0.0281	0.0245	0.0326	5.6244	0	0.0172	0.0354	0.0336	0.0399	0.0254	3.7594	4.9835	5.5848	5.5046
FeO	0.06	0.0568	0.054	0.0402	0.0639	0.1199	0.05	0.0335	0.1291	0.0518	0.497	0.0451	0.0447	0.0097
Na_2O	0.8541	0.8826	0.7661	8.3239	0.5652	0.5239	0.617	0.8116	0.6793	0.6903	5.6041	7.7622	8.3492	8.4556
K_2O	14.9701	15.3252	15.205	0.1747	15.6278	15.3726	15.363	15.3436	15.4313	15.2401	2.0041	0.1276	0.1948	0.2077
Total	98.5475	98.2935	98.5553	100.9038	98.7372	98.4658	98.0191	99.2783	98.9432	99.0935	93.1819	97.0477	100.5053	100.2742
Cation based on 8														
Si	2.982	2.969	2.98	2.726	2.983	2.983	2.984	2.978	2.981	2.981	2.724	2.726	2.733	2.737
Al	1.032	1.04	1.032	1.282	1.027	1.031	1.026	1.034	1.027	1.034	1.347	1.305	1.27	1.263
Ca	0.001	0.001	0.002	0.265	0	0.001	0.002	0.002	0.002	0.001	0.192	0.243	0.264	0.261
Fe	0.002	0.002	0.002	0.001	0.002	0.005	0.002	0.001	0.005	0.002	0.02	0.002	0.002	0
Na	0.077	0.08	0.069	0.709	0.051	0.048	0.056	0.073	0.061	0.062	0.517	0.686	0.715	0.725
K	0.892	0.918	0.907	0.01	0.932	0.918	0.922	0.909	0.918	0.903	0.122	0.007	0.011	0.012
Total	4.986	5.011	4.992	4.993	4.995	4.984	4.992	4.996	4.995	4.984	4.921	4.969	4.995	4.999

Microprobe Analysis
of F-1236 - Feldspar in

Oxide Wt. %	Ksp-Plg11	Ksp-Plg12
SiO_2	61.8683	61.4644
$Al2O_3$	24.3772	24.4706
CaO	5.4721	5.5945
FeO	0.0174	0.0146
Na_2O	8.3377	8.0324
K_2O	0.2368	0.2413
Total	100.3096	99.8177

Cation based on 8		
Si	2.735	2.73
Al	1.27	1.281
Ca	0.259	0.266
Fe	0.001	0.001
Na	0.715	0.692
K	0.013	0.014
Total	4.994	4.983

Microprobe Analysis
of F-1236 - Garnet-B

Oxide Wt. %	GrtNVoid1	GrtNVoid2	GrtNVoid3	GrtNVoid4	GrtNVoid5	GrtNVoid6	GrtNVoid7	GrtNVoid8	GrtNBte1	GrtNBte2	GrtNBte3	GrtNBte4	GrtNBte5	GrtNBte6
SiO_2	37.3897	37.4013	37.4222	37.4303	36.6297	35.3185	36.5796	36.8552	37.0411	37.2021	36.5072	36.4773	37.3111	35.0949
TiO_2	0.0109	0.0438	0.0175	0.0229	0.3583	0.214	0.0282	0.0265	0.0382	0.0232	0.0702	0.0414	0.0316	0.0257
Al_2O_3	21.2866	21.3281	21.4187	21.3668	20.8403	20.3207	20.8654	21.0024	21.1788	21.2388	20.9608	20.9979	21.3715	20.1248
Y_2O_3	0.0254	0.0058	0.0356	0.0472	0.0301	0.0491	0.0126	0.0458	0	0.038	0.0216	0.0437	0.0311	0.0477
MgO	2.9368	2.9213	2.9185	2.9706	3.0786	2.7176	2.7536	2.873	3.0843	3.3392	3.1896	3.0687	3.676	3.1481
CaO	1.5657	1.6074	1.5772	1.5415	1.5191	1.6841	1.6211	1.5989	1.5308	1.5203	1.5511	1.577	1.5955	1.559
MnO	3.3098	3.2568	3.3117	3.2675	3.0213	3.2034	3.2973	3.3191	2.9336	2.885	2.9352	2.9491	2.8435	2.8361
FeO	34.5939	34.3668	34.4823	34.6325	33.0242	33.8211	34.5112	34.7326	34.7901	34.3073	34.525	34.5688	34.0287	34.2956
Na2O	0.0258	0.004	0.0105	0.0058	0.0004	0.0172	0.0168	0.008	0.0055	0.0171	0.0143	0.0157	0.0015	0
Total	101.1445	100.9354	101.1943	101.2852	98.502	97.3456	99.6857	100.4614	100.6024	100.571	99.7749	99.7396	100.8906	97.1319
Cation based on 12														
Si	2.986	2.989	2.985	2.984	2.989	2.947	2.974	2.973	2.975	2.981	2.96	2.96	2.974	2.939
Ti	0.001	0.003	0.001	0.001	0.022	0.013	0.002	0.002	0.002	0.001	0.004	0.003	0.002	0.002
Al	2.004	2.009	2.013	2.008	2.004	1.999	1.999	1.996	2.005	2.006	2.003	2.008	2.008	1.986
Y	0.001	0	0.002	0.002	0.001	0.002	0.001	0.002	0	0.002	0.001	0.002	0.001	0.002
Mg	0.35	0.348	0.347	0.353	0.375	0.338	0.334	0.345	0.369	0.399	0.386	0.371	0.437	0.393
Ca	0.134	0.138	0.135	0.132	0.133	0.151	0.141	0.138	0.132	0.131	0.135	0.137	0.136	0.14
Mn	0.224	0.22	0.224	0.221	0.209	0.226	0.227	0.227	0.2	0.196	0.202	0.203	0.192	0.201
Fe	2.31	2.297	2.3	2.309	2.254	2.36	2.346	2.343	2.337	2.299	2.341	2.346	2.269	2.402
Na	0.004	0.001	0.002	0.001	0	0.003	0.003	0.001	0.001	0.003	0.002	0.002	0	0
Total	8.013	8.004	8.008	8.01	7.986	8.04	8.026	8.027	8.021	8.016	8.034	8.033	8.019	8.065

Microprobe Analysis

Oxide Wt. %	GrtNBte7	GrtNBte8	GrtRNBte1	GrtRNBte2	GrtRNBte3	GrtRNBte4	GrtRNBte5	GrtNBtePlg1	GrtNBtePlg2	GrtNBtePlg3	GrtNBtePlg4	GrtNBtePlg5	GrtNPlg2-1	GrtNPlg2-2
SiO_2	36.7928	37.2889	36.6183	35.0853	36.6981	37.0947	36.5362	36.6848	36.5847	36.7068	37.0183	36.8315	36.8436	37.1693
TiO_2	0.0391	0	0.051	0.0945	0.0096	0.0964	0.041	0.0197	0.0075	0.0182	0.0144	0.0474	0	0.0047
Al_2O_3	21.128	21.1978	21.0396	20.4517	21.1974	21.1073	21.0875	21.0295	21.179	21.1017	21.0366	20.9805	21.2573	21.3671
Y_2O_3	0.0628	0.0171	0.0645	0.0611	0.0935	0.046	0.0368	0.0516	0.0541	0.0235	0.0268	0.0483	0.075	0.0653
MgO	3.0056	3.5916	2.7302	2.3592	2.9172	2.4175	2.7525	3.4239	3.4242	3.5059	3.3731	3.4394	3.1215	3.4653
CaO	1.5848	1.576	1.5713	1.4988	1.5654	1.5552	1.5571	1.7534	1.7657	1.6707	1.6233	1.6175	1.6693	1.5296
MnO	2.9952	2.9453	3.6541	4.0157	3.5036	3.902	3.5415	3.1184	3.1285	3.0719	3.0921	3.1149	3.2453	3.1381
FeO	34.8453	34.1968	34.3717	33.7201	34.1405	34.4449	34.3507	33.7644	33.5829	33.8985	33.9439	33.9279	33.8085	33.7433
Na2O	0.0022	0.0127	0.0076	0.0128	0.0181	0.0069	0.0138	0.0022	0.0149	0.0054	0	0.0131	0.0098	0.0043
Total	100.4557	100.8262	100.1084	97.299	100.1433	100.6708	99.9171	99.8478	99.7416	100.0028	100.1285	100.0206	100.0303	100.487
Cation based on 12														
Si	2.965	2.979	2.966	2.939	2.965	2.986	2.963	2.965	2.958	2.961	2.98	2.971	2.971	2.976
Ti	0.002	0	0.003	0.006	0.001	0.006	0.003	0.001	0	0.001	0.001	0.003	0	0
Al	2.007	1.996	2.008	2.019	2.019	2.002	2.016	2.003	2.018	2.006	1.996	1.995	2.02	2.017
Y	0.003	0.001	0.003	0.003	0.004	0.002	0.002	0.002	0.002	0.001	0.001	0.002	0.003	0.003
Mg	0.361	0.428	0.33	0.295	0.351	0.29	0.333	0.413	0.413	0.422	0.405	0.414	0.375	0.414
Ca	0.137	0.135	0.136	0.135	0.136	0.134	0.135	0.152	0.153	0.144	0.14	0.14	0.144	0.131
Mn	0.204	0.199	0.251	0.285	0.24	0.266	0.243	0.213	0.214	0.21	0.211	0.213	0.222	0.213
Fe	2.348	2.285	2.328	2.362	2.307	2.319	2.33	2.282	2.271	2.287	2.286	2.289	2.28	2.26
Na	0	0.002	0.001	0.002	0.003	0.001	0.002	0	0.002	0.001	0	0.002	0.002	0.001
Total	8.028	8.024	8.026	8.045	8.025	8.006	8.027	8.032	8.032	8.034	8.02	8.028	8.018	8.014

Microprobe Analysis
of F-1236 - Garnet-B

Oxide Wt. %	GrtNPlg2-3	GrtNPlg2-4	GrtNPlg2-5	GrtRimNBte2-1	GrtRimNBte2-2	GrtRimNBte2-3	GrtRimNBte2-4	GrtRimNBte2-5	GrtRimNBte2-6	GrtRimNBte2-7	GrtRim1	GrtRim2	GrtRim3	GrtRim4
SiO_2	36.8235	36.7438	36.9999	35.6843	37.2271	37.3038	37.1181	36.5904	36.3533	36.6825	35.1622	36.8841	37.1224	37.0445
TiO_2	0.0058	0.0265	0.0071	0.0283	0.0202	0.0126	0.0364	0.0414	0.3996	0.1596	0	0.0049	0	0
Al_2O_3	21.1904	21.2408	21.0933	21.0612	21.2808	21.2654	21.7172	21.0755	21.0946	21.4008	20.1981	21.16	21.1488	21.2742
Y_2O_3	0.0198	0.0363	0.0714	0.0627	0.0522	0.0301	0.0368	0.0189	0.0585	0.0161	0.0592	0.0438	0.0467	0.0191
MgO	3.201	3.0338	3.2954	2.994	2.8061	2.7666	2.3068	2.1963	3.2974	2.6294	3.145	3.4654	3.5705	3.5051
CaO	1.5327	1.5888	1.5553	1.5404	1.5923	1.6122	1.5769	1.5986	1.3986	1.4776	1.7926	1.6342	1.5554	1.5664
MnO	3.2176	3.452	3.2279	3.4378	3.5148	3.4904	3.4932	3.7169	3.1277	3.4568	3.2138	3.1254	3.0476	3.0278
FeO	33.6694	34.3422	34.2166	33.9581	34.3665	34.4552	34.1042	34.5048	32.89	33.9054	33.6457	34.0434	34.2548	34.2045
Na2O	0.0065	0.0066	0.0022	0.0207	0.0185	0.0141	0.0163	0.0208	0.0212	0.0333	0.0194	0.0102	0.0193	0.0138
Total	99.6667	100.4709	100.4689	98.7874	100.8785	100.9503	100.4058	99.7636	98.6409	99.7615	97.2361	100.3715	100.7655	100.6554
Cation based on 12														
Si	2.977	2.96	2.974	2.93	2.983	2.987	2.983	2.976	2.963	2.969	2.939	2.965	2.972	2.968
Ti	0	0.002	0	0.002	0.001	0.001	0.002	0.003	0.024	0.01	0	0	0	0
Al	2.019	2.016	1.998	2.038	2.01	2.007	2.057	2.02	2.026	2.041	1.99	2.005	1.995	2.009
Y	0.001	0.002	0.003	0.003	0.002	0.001	0.002	0.001	0.003	0.001	0.003	0.002	0.002	0.001
Mg	0.386	0.364	0.395	0.367	0.335	0.33	0.276	0.266	0.401	0.317	0.392	0.415	0.426	0.419
Ca	0.133	0.137	0.134	0.136	0.137	0.138	0.136	0.139	0.122	0.128	0.161	0.141	0.133	0.134
Mn	0.22	0.236	0.22	0.239	0.239	0.237	0.238	0.256	0.216	0.237	0.228	0.213	0.207	0.205
Fe	2.276	2.313	2.3	2.332	2.303	2.307	2.292	2.347	2.242	2.295	2.352	2.289	2.293	2.291
Na	0.001	0.001	0	0.003	0.003	0.002	0.003	0.003	0.003	0.005	0.003	0.002	0.003	0.002
Total	8.013	8.03	8.025	8.049	8.012	8.01	7.987	8.012	8	8.003	8.066	8.032	8.031	8.029

Microprobe Analysis

Oxide Wt. %	GrtRim5	GrtRim6	GrtRim7	GrtRim8	GrtRim9	GrtRim10	GrtRim11	GrtRim12	GrtRim13	GrtRim14	GrtRim15	GrtRim16	GrtRim17	GrtRim18
SiO_2	37.0044	37.2089	37.2279	36.8927	37.3118	37.4548	33.6347	21.126	37.0964	37.128	37.3951	37.1551	37.2322	37.4342
TiO_2	0.0135	0	0.0082	0.009	0.0129	0.0282	0.0017	0	0	0.0185	0.0103	0.0037	0.0151	0.0168
Al_2O_3	21.3884	21.335	21.3863	21.31	21.3774	21.2536	23.1957	12.2492	21.1531	21.2758	21.1858	21.2647	21.3537	21.2145
Y_2O_3	0.072	0.049	0.0682	0.0319	0.0379	0.0102	0.0599	0.104	0.0225	0.0211	0	0.0123	0	0.0337
MgO	3.543	3.6186	3.6726	3.7519	3.7594	3.7526	1.9832	2.2427	3.7511	3.8535	3.8676	3.8299	3.9199	3.811
CaO	1.5689	1.6024	1.5853	1.5748	1.6001	1.5951	1.1173	23.4401	1.5879	1.59	1.6023	1.5911	1.6123	1.5558
MnO	2.9755	2.9694	2.8958	2.8936	2.912	2.87	2.1708	1.6774	2.8399	2.8151	2.753	2.7677	2.7257	2.7902
FeO	34.0354	34.0676	33.9289	33.9842	34.0487	34.106	33.6584	20.4144	33.7586	33.8131	33.9365	33.9955	33.9	33.9842
Na2O	0.0182	0.0134	0.0116	0.0312	0	0.0185	0.0525	0.0312	0	0.0127	0.0138	0.0069	0.0156	0.0091
Total	100.6192	100.8645	100.7848	100.4795	101.06	101.089	95.8743	81.2849	100.2094	100.5277	100.7644	100.6268	100.7746	100.8494
Cation based on 12														
Si	2.963	2.971	2.971	2.958	2.971	2.98	2.832	2.284	2.977	2.97	2.982	2.97	2.969	2.983
Ti	0.001	0	0	0.001	0.001	0.002	0	0	0	0.001	0.001	0	0.001	0.001
Al	2.018	2.008	2.012	2.014	2.006	1.993	2.302	1.561	2.001	2.006	1.991	2.003	2.007	1.993
Y	0.003	0.002	0.003	0.001	0.002	0	0.003	0.006	0.001	0.001	0	0.001	0	0.001
Mg	0.423	0.431	0.437	0.448	0.446	0.445	0.249	0.362	0.449	0.459	0.46	0.456	0.466	0.453
Ca	0.135	0.137	0.136	0.135	0.136	0.136	0.101	2.716	0.137	0.136	0.137	0.136	0.138	0.133
Mn	0.202	0.201	0.196	0.196	0.196	0.193	0.155	0.154	0.193	0.191	0.186	0.187	0.184	0.188
Fe	2.279	2.275	2.265	2.279	2.267	2.27	2.37	1.846	2.266	2.262	2.263	2.273	2.261	2.265
Na	0.003	0.002	0.002	0.005	0	0.003	0.009	0.007	0	0.002	0.002	0.001	0.002	0.001
Total	8.027	8.026	8.022	8.037	8.025	8.023	8.02	8.935	8.022	8.027	8.022	8.028	8.028	8.019

Microprobe Analysis
of F-1236 - Garnet-B

Oxide Wt. %	GrtRim19	GrtRim20	GrtCore1	GrtCore2	GrtCore3	GrtCore4	GrtCore5	GrtCore6	GrtCore7	GrtCore8	GrtCore9	GrtCore10	GrtCore11	GrtRim21
SiO_2	36.8417	36.9869	37.1505	37.0585	37.4274	37.3147	37.2196	37.0568	37.1794	37.1568	37.2713	37.2541	37.1363	37.343
TiO_2	0.0163	0.0181	0.0037	0.0247	0.0082	0.0034	0.0185	0.0161	0.006	0.0009	0.0183	0.0028	0.0166	0.0009
Al_2O_3	21.1646	21.1278	21.1001	21.258	21.1958	21.2809	21.1719	21.1171	21.0524	21.3228	21.1314	21.1441	21.1403	21.1417
Y_2O_3	0.0018	0	0.0214	0.0246	0.0038	0	0.0519	0	0.0262	0.0096	0	0.0036	0	0
MgO	3.7002	3.7792	3.835	3.8331	3.9107	3.9484	3.9839	3.983	4.05	3.9903	4.0259	4.0572	4.0465	4.0452
CaO	1.5866	1.6027	1.6115	1.6275	1.6037	1.5574	1.6094	1.5985	1.6246	1.6382	1.6022	1.6452	1.6894	1.6552
MnO	2.8247	2.7819	2.8354	2.7353	2.6993	2.6951	2.6958	2.6275	2.6238	2.6259	2.6386	2.6049	2.5986	2.5732
FeO	33.8481	33.7079	33.8954	33.8825	33.6539	33.693	33.9574	34.0174	33.7968	33.6845	33.5408	33.7152	33.5989	33.5811
Na2O	0.0138	0.0054	0.0149	0.0058	0.0119	0.0177	0.0156	0.021	0.0076	0.0239	0.0029	0.0109	0.0174	0.0076
Total	99.9978	100.0099	100.4679	100.4501	100.5147	100.5106	100.7239	100.4375	100.3667	100.4529	100.2313	100.438	100.2439	100.3478
Cation based on 12														
Si	2.966	2.974	2.975	2.967	2.988	2.979	2.972	2.968	2.977	2.97	2.983	2.978	2.974	2.985
Ti	0.001	0.001	0	0.001	0	0	0.001	0.001	0	0	0.001	0	0.001	0
Al	2.008	2.002	1.992	2.006	1.994	2.003	1.992	1.994	1.987	2.009	1.993	1.992	1.996	1.992
Y	0	0	0.001	0.001	0	0	0.002	0	0.001	0	0	0	0	0
Mg	0.444	0.453	0.458	0.458	0.465	0.47	0.474	0.476	0.483	0.475	0.48	0.483	0.483	0.482
Ca	0.137	0.138	0.138	0.14	0.137	0.133	0.138	0.137	0.139	0.14	0.137	0.141	0.145	0.142
Mn	0.193	0.189	0.192	0.186	0.183	0.182	0.182	0.178	0.178	0.178	0.179	0.176	0.176	0.174
Fe	2.279	2.266	2.27	2.269	2.247	2.25	2.267	2.279	2.263	2.252	2.245	2.254	2.25	2.245
Na	0.002	0.001	0.002	0.001	0.002	0.003	0.002	0.003	0.001	0.004	0	0.002	0.003	0.001
Total	8.03	8.025	8.029	8.028	8.016	8.02	8.031	8.036	8.03	8.028	8.019	8.027	8.028	8.02

Microprobe Analysis

Oxide Wt. %	GrtRim22	GrtRim23	GrtRim24	GrtRim25	GrtRim26	GrtRim27	GrtRim28	GrtRim29	GrtRim30	GrtRim31	GrtRim32	GrtRim33	GrtRim34	GrtRim35
SiO_2	37.319	37.2878	38.6175	36.9389	37.3919	29.7525	34.1593	37.075	37.0517	37.1207	37.8312	37.1396	37.1865	37.1492
TiO_2	0.0261	0.0259	0.0236	0.0142	0.0101	0.0146	0.0092	0.0254	0.0211	0.0211	0.0017	0.0108	0.0185	0.0151
Al_2O_3	21.2604	21.1737	22.4602	21.2632	21.071	21.07	19.7793	21.0975	21.1387	21.1979	22.1172	21.1367	21.2296	21.0298
Y_2O_3	0.011	0	0	0.0368	0.0102	0.0056	0.0218	0.0502	0.0626	0.0748	0.0474	0.0481	0.0755	0.0846
MgO	4.0079	3.9463	4.0995	3.9288	4	3.1696	3.8523	3.9435	3.9532	3.9356	3.6156	3.9203	3.8747	3.9593
CaO	1.6703	1.7034	1.5258	1.6689	1.6909	0.9932	1.5963	1.6991	1.6821	1.6863	1.5961	1.6946	1.7108	1.6968
MnO	2.5936	2.5915	2.5636	2.5956	2.6288	1.8579	2.563	2.6447	2.6405	2.674	2.5226	2.6923	2.7056	2.7161
FeO	33.5458	33.5458	32.8981	33.5718	33.6878	22.1274	33.8447	33.5655	33.6875	33.6114	31.3691	33.4421	33.4696	33.5629
Na2O	0.0036	0.0145	0.0104	0.0033	0.0141	0.029	0.0084	0.0141	0.0051	0.0134	0.0175	0.0141	0	0.0109
Total	100.4377	100.2889	102.1986	100.0214	100.5048	79.0198	95.8344	100.1149	100.2426	100.3351	99.1183	100.0985	100.2708	100.2246
Cation based on 12														
Si	2.98	2.983	3.001	2.966	2.986	2.91	2.902	2.975	2.971	2.972	3.021	2.979	2.977	2.979
Ti	0.002	0.002	0.001	0.001	0.001	0.001	0.001	0.002	0.001	0.001	0	0.001	0.001	0.001
Al	2.001	1.996	2.057	2.012	1.983	2.429	1.98	1.995	1.998	2	2.081	1.998	2.003	1.987
Y	0	0	0	0.002	0	0	0.001	0.002	0.003	0.003	0.002	0.002	0.003	0.004
Mg	0.477	0.471	0.475	0.47	0.476	0.462	0.488	0.472	0.473	0.47	0.43	0.469	0.462	0.473
Ca	0.143	0.146	0.127	0.144	0.145	0.104	0.145	0.146	0.145	0.145	0.137	0.146	0.147	0.146
Mn	0.175	0.176	0.169	0.177	0.178	0.154	0.184	0.18	0.179	0.181	0.171	0.183	0.183	0.184
Fe	2.24	2.244	2.138	2.254	2.25	1.81	2.405	2.252	2.259	2.251	2.095	2.243	2.241	2.25
Na	0.001	0.002	0.002	0.001	0.002	0.006	0.001	0.002	0.001	0.002	0.003	0.002	0	0.002
Total	8.018	8.019	7.97	8.026	8.022	7.877	8.107	8.026	8.028	8.026	7.939	8.022	8.018	8.026

Microprobe Analysis of F-1236 - Mica in or near Garnet-B

Oxide Wt. %	BtNGrt1	BtNGrt2	BtNGrt3	BtNGrt4	BtNGrt5	BtNGrt6	BtNGrt7	BtNGrt8	BteOGrt1	BteOGrt2	BteOGrt3	BteOGrt4	BteOGrt5	BteNGrtRim1
SiO_2	35.2599	35.356	34.4615	35.1253	35.1799	35.5011	35.2983	35.0211	35.4713	35.6045	35.3775	35.7166	35.3108	35.0032
TiO_2	3.6585	3.5129	3.8045	3.687	3.3425	4.5209	4.5899	4.8281	4.4204	4.4933	4.4153	4.3857	4.627	2.1461
Al_2O_3	17.9716	18.0744	17.5066	17.9601	18.2247	18.0514	17.9278	18.1294	18.5273	18.6932	18.7148	18.9555	18.5262	18.8918
MgO	11.0507	10.8563	10.7948	10.8886	11.2861	10.496	10.3678	10.2787	9.0497	8.862	9.0857	9.2026	9.0324	9.3018
CaO	0.0256	0.0143	0.0959	0	0.0204	0.0013	0.0074	0.0256	0.0134	0.0134	0.016	0.0147	0.0268	0.0282
MnO	0.1124	0.0952	0.0939	0.0847	0.0618	0.0549	0.0823	0.0581	0.082	0.0715	0.066	0.0773	0.0799	0.0867
FeO	18.3042	18.28	18.3864	18.5858	17.8458	18.5646	18.5085	17.6302	19.1488	18.7572	18.8443	18.641	18.8479	21.6986
Na_2O	0.1535	0.1585	0.1679	0.1474	0.1595	0.1614	0.1624	0.1676	0.0707	0.0614	0.0437	0.0746	0.0559	0.0453
K_2O	9.1667	9.2936	8.6451	9.176	9.095	9.0702	9.2304	9.0469	9.4957	9.5096	9.5275	9.5117	9.3906	9.2899
Total	99.6743	99.6101	97.8523	99.6179	99.1786	100.4253	100.1612	99.1498	100.2605	100.0487	100.0699	100.5885	99.8688	100.4363
Cation based on 22														
Si	5.324	5.342	5.305	5.315	5.323	5.318	5.31	5.298	5.343	5.361	5.332	5.343	5.332	5.321
Ti	0.415	0.399	0.44	0.42	0.38	0.509	0.519	0.549	0.501	0.509	0.5	0.493	0.525	0.245
Al	3.198	3.219	3.176	3.203	3.25	3.187	3.178	3.232	3.289	3.317	3.324	3.342	3.297	3.385
Mg	2.488	2.445	2.477	2.456	2.546	2.344	2.325	2.318	2.032	1.989	2.041	2.052	2.033	2.108
Ca	0.004	0.002	0.016	0	0.003	0	0.001	0.004	0.002	0.002	0.003	0.002	0.004	0.005
Mn	0.014	0.012	0.012	0.011	0.008	0.007	0.01	0.007	0.01	0.009	0.008	0.01	0.01	0.011
Fe	2.311	2.31	2.367	2.352	2.258	2.326	2.328	2.23	2.412	2.362	2.375	2.332	2.38	2.759
Na	0.045	0.046	0.05	0.043	0.047	0.047	0.047	0.049	0.021	0.018	0.013	0.022	0.016	0.013
K	1.766	1.791	1.698	1.771	1.756	1.733	1.771	1.746	1.825	1.827	1.832	1.815	1.809	1.802
Total	19.566	19.568	19.541	19.571	19.572	19.47	19.491	19.434	19.435	19.394	19.428	19.411	19.407	19.649

Microprobe Analysis of F-1236 - Mica in or near Garnet-B

Oxide Wt. %	BteNGrtRim2	BteNGrtRim3	BteNGrtRim4	BteNGrtRim5	BteNGrtRim6	BteNGrtRim7
SiO_2	34.5742	35.649	35.5184	34.9814	35.6936	35.2406
TiO_2	2.1378	2.4299	2.4345	2.6377	2.843	2.8659
Al_2O_3	18.6765	19.2056	19.7489	18.1031	18.5555	18.1261
MgO	9.3841	8.7709	8.8052	9.1862	9.581	9.5969
CaO	0.0377	0.0148	0.0222	0.0165	0.0426	0.02
MnO	0.0992	0.0789	0.0972	0.0804	0.1148	0.1015
FeO	21.768	20.3605	19.7259	21.3453	20.0077	20.3625
Na_2O	0.0648	0.042	0.0513	0.0388	0.0754	0.0708
K_2O	9.0076	8.3163	8.4053	9.0823	9.1821	9.414
Total	99.6617	98.8049	98.7546	99.3802	100.0631	99.733
Cation based on 22						
Si	5.3	5.43	5.398	5.367	5.395	5.371
Ti	0.246	0.278	0.278	0.304	0.323	0.328
Al	3.374	3.448	3.537	3.273	3.305	3.256
Mg	2.145	1.992	1.995	2.101	2.159	2.18
Ca	0.006	0.002	0.004	0.003	0.007	0.003
Mn	0.013	0.01	0.013	0.01	0.015	0.013
Fe	2.791	2.594	2.507	2.739	2.529	2.595
Na	0.019	0.012	0.015	0.012	0.022	0.021
K	1.762	1.616	1.63	1.778	1.771	1.83
Total	19.657	19.382	19.377	19.587	19.526	19.598

Microprobe Analysis
of F-1236 - plagioclase
in or near Garnet-B

Oxide Wt. %	PlgNBte1	PlgNBte2	PlgNBte3	PlgNBte4	PlgNBte5	Plg2-1	Plg2-2	Plg2-3	Plg2-4
SiO_2	60.7905	61.3071	60.6329	61.8982	61.5166	61.8068	61.5467	61.7684	61.568
Al_2O_3	24.1523	24.1909	23.9408	24.0319	24.2108	24.4144	24.5403	24.3618	24.5727
CaO	5.5707	5.4205	5.4451	5.5798	5.4185	5.5403	5.2708	5.4861	5.4652
FeO	0.3631	0.3585	0.372	0.2898	0.2896	0.1662	0.2246	0.1605	0.0869
Na_2O	8.239	8.1427	8.595	8.2992	8.2125	8.3494	8.4661	8.1922	8.3304
K_2O	0.1581	0.1775	0.1526	0.1796	0.1903	0.2151	0.1727	0.2013	0.2161
Total	99.2736	99.5971	99.1385	100.2785	99.8384	100.4922	100.2213	100.1702	100.2394
Cation based on 8									
Si	2.722	2.732	2.723	2.741	2.735	2.731	2.726	2.735	2.725
Al	1.275	1.271	1.267	1.254	1.268	1.271	1.281	1.271	1.282
Ca	0.267	0.259	0.262	0.265	0.258	0.262	0.25	0.26	0.259
Fe	0.014	0.013	0.014	0.011	0.011	0.006	0.008	0.006	0.003
Na	0.715	0.704	0.748	0.713	0.708	0.715	0.727	0.703	0.715
K	0.009	0.01	0.009	0.01	0.011	0.012	0.01	0.011	0.012
Total	5.002	4.989	5.022	4.993	4.99	4.997	5.002	4.987	4.997

Microprobe Analysis
of F-1236 - Garnet-A

Oxide Wt. %	GrtNBte1	GrtNBte2	GrtNBte3	GrtNBte4	GrtNBte5	GrtNBte6	GrtNBte7	GrtNBte2-1	GrtNBte2-2	GrtNBte2-3	GrtNBte2-4	GrtNBte2-5
SiO_2	37.3099	37.5013	37.4545	37.3848	37.5287	37.4108	37.3744	37.489	37.5381	37.4737	37.3889	37.4111
TiO_2	0.0239	0.0265	0.0056	0.0058	0.0068	0	0	0.0634	0.0423	0.0468	0.0556	0.0225
Al_2O_3	21.3563	21.4839	21.5591	21.5531	21.618	21.5424	21.6782	21.5183	21.5741	21.5423	21.6205	21.4396
Y_2O_3	0.0178	0.0633	0.0511	0.0744	0.0951	0.0323	0.0662	0.0366	0.0292	0.0562	0.0432	0.0491
MgO	3.6617	3.9343	4.003	4.1085	4.1826	4.2305	4.2679	3.868	4.113	4.1797	4.234	4.2463
CaO	1.5077	1.5473	1.5297	1.5087	1.5124	1.5378	1.5376	1.5499	1.5071	1.5301	1.5776	1.511
MnO	2.6969	2.7518	2.7899	2.7539	2.7424	2.7396	2.7425	2.708	2.6747	2.7142	2.6551	2.6388
FeO	33.8672	33.592	33.5011	33.3896	33.1412	32.8396	33.1208	33.8242	33.4047	33.2086	33.1914	33.0646
Na_2O	0.0065	0.0022	0.024	0.0014	0.01	0.0171	0.0096	0.0018	0.0072	0.01	0.0121	0.0175
Total	100.4478	100.9026	100.9181	100.7801	100.8372	100.3502	100.7973	101.0592	100.8903	100.7617	100.7783	100.4004
Cation based on 12												
Si	2.983	2.98	2.975	2.972	2.977	2.979	2.967	2.976	2.978	2.976	2.969	2.98
Ti	0.001	0.002	0	0	0	0	0	0.004	0.003	0.003	0.003	0.001
Al	2.012	2.012	2.018	2.02	2.021	2.022	2.028	2.013	2.017	2.016	2.023	2.013
Y	0.001	0.003	0.002	0.003	0.004	0.001	0.003	0.002	0.001	0.002	0.002	0.002
Mg	0.436	0.466	0.474	0.487	0.495	0.502	0.505	0.458	0.486	0.495	0.501	0.504
Ca	0.129	0.132	0.13	0.129	0.129	0.131	0.131	0.132	0.128	0.13	0.134	0.129
Mn	0.183	0.185	0.188	0.185	0.184	0.185	0.184	0.182	0.18	0.183	0.179	0.178
Fe	2.264	2.232	2.225	2.22	2.199	2.187	2.199	2.246	2.216	2.206	2.204	2.203
Na	0.001	0	0.004	0	0.002	0.003	0.001	0	0.001	0.002	0.002	0.003
Total	8.01	8.011	8.016	8.016	8.011	8.01	8.018	8.013	8.011	8.012	8.017	8.013

Microprobe Analysis
of F-1236 - Mica near
or in garnet-A

Oxide Wt. %	BteNGrt1	BteNGrt2	BteNGrt3	BteNGrt4	BteNGrt5	BteNGrt2-1	BteNGrt2-2	BteNGrt2-3	BteNGrt2-4	BteNGrt2-5	BteOGrt1	BteOGrt2	BteOGrt3	BteOGrt4	BteOGrt5
SiO_2															
TiO_2	36.1737	36.0447	36.1211	36.1249	36.1907	36.2829	36.2965	36.1586	36.306	36.3435	34.8492	35.6942	35.5107	35.8	35.5851
Al_2O_3	4.7991	4.8985	4.8561	4.8354	4.7209	3.528	3.5412	3.5218	3.5652	3.5966	3.7569	4.0584	4.0399	4.0824	4.1133
Cr_2O_3	18.4598	18.5574	18.7028	18.8215	18.8876	19.1289	19.3294	19.3139	19.3203	19.2882	19.6904	19.1089	19.0437	18.8981	18.7545
MgO	11.2284	11.2059	11.2023	11.281	11.388	11.996	11.9424	11.9871	12.0077	12.0999	9.5158	9.5231	9.6589	9.4668	9.4022
CaO	0.0065	0.0082	0.0147	0.0078	0.0174	0.0109	0	0	0.0126	0.0117	0.0471	0.0056	0.0091	0.0078	0
MnO	0.0683	0.0712	0.0652	0.0747	0.0945	0.0684	0.0417	0.0494	0.0507	0.0576	0.1417	0.0827	0.0832	0.084	0.0716
FeO	15.9817	16.0738	15.874	15.791	15.5516	14.7348	14.6004	14.5787	14.6495	14.5927	17.6078	17.4174	17.6148	17.816	17.9068
Na_2O	0.1708	0.1726	0.2097	0.1965	0.1926	0.137	0.1289	0.1397	0.1331	0.1466	0.0588	0.0723	0.0613	0.0563	0.0641
K_2O	9.5513	9.6005	9.5604	9.5293	9.6362	9.5687	9.67	9.7535	9.722	9.6339	9.4893	9.8238	9.8054	9.7939	9.969
Total	100.4908	100.688	100.6666	100.7279	100.7488	99.4951	99.5965	99.5428	99.8194	99.8263	99.1189	99.7784	99.8146	99.9997	99.8459
Cation based on 22															
Si	5.354	5.33	5.335	5.328	5.333	5.386	5.38	5.367	5.373	5.374	5.275	5.362	5.34	5.375	5.363
Ti	0.534	0.545	0.539	0.536	0.523	0.394	0.395	0.393	0.397	0.4	0.428	0.458	0.457	0.461	0.466
Al	3.22	3.234	3.256	3.272	3.28	3.347	3.377	3.379	3.37	3.361	3.513	3.383	3.375	3.344	3.331
Mg	2.478	2.47	2.466	2.48	2.502	2.655	2.639	2.652	2.649	2.667	2.147	2.133	2.165	2.119	2.112
Ca	0.001	0.001	0.002	0.001	0.003	0.002	0	0	0.002	0.002	0.008	0.001	0.001	0.001	0
Mn	0.009	0.009	0.008	0.009	0.012	0.009	0.005	0.006	0.006	0.007	0.018	0.011	0.011	0.011	0.009
Fe	1.978	1.988	1.961	1.948	1.917	1.829	1.81	1.81	1.813	1.804	2.229	2.188	2.215	2.237	2.257
Na	0.049	0.049	0.06	0.056	0.055	0.039	0.037	0.04	0.038	0.042	0.017	0.021	0.018	0.016	0.019
K	1.804	1.811	1.801	1.793	1.812	1.812	1.828	1.847	1.835	1.817	1.832	1.883	1.881	1.876	1.917
Total	19.427	19.438	19.429	19.424	19.437	19.473	19.47	19.494	19.483	19.475	19.466	19.44	19.465	19.439	19.473

Microprobe Analysis
of F-1296- Garnet-B

Oxide Wt. %	GrtNAmpInc1	GrtNAmpInc2	GrtNAmpInc3	GrtNAmpInc4	GrtNAmpInc5	GrtNAmpInc6	GrtNAmpInc7	GrtNAmpInc8	GrtNAmpInc9	GrtNPlgInc1	GrtNPlgInc2	GrtNPlgInc3	GrtNPlgInc4	GrtNPlgInc5
SiO_2	37.72	37.65	37.49	38.54	37.90	37.63	37.76	38.08	37.71	37.83	38.12	38.11	37.95	37.98
TiO_2	0.05	0.05	0.04	0.02	0.03	0.03	0.02	0.04	0.02	0.03	0.03	0.02	0.03	0.04
Al_2O_3	20.97	21.16	21.28	21.88	21.74	21.41	21.38	21.61	21.34	21.38	21.67	21.57	21.71	21.70
Cr_2O_3	0.03	0.04	0.03	0.01	0.02	0.03	0.04	0.03	0.01	0.02	0.01	0.02	0.02	0.01
MgO	3.65	4.03	4.04	3.93	3.77	4.87	4.72	4.77	4.79	4.67	4.68	4.70	4.78	4.73
CaO	8.06	7.95	7.97	7.83	7.58	7.52	7.68	7.36	7.41	7.67	7.73	7.89	7.99	8.12
MnO	1.10	0.96	0.92	1.03	1.21	0.91	0.88	0.89	0.91	0.86	0.88	0.86	0.82	0.83
FeO	28.37	27.90	28.06	27.90	28.45	27.45	27.37	27.57	27.53	27.35	27.26	27.21	27.34	27.11
Na_2O	0.00	0.00	0.00	0.01	0.01	0.00	0.01	0.01	0.00	0.00	0.00	0.00	0.00	0.02
Total	99.95	99.74	99.83	101.15	100.71	99.85	99.85	100.33	99.74	99.79	100.39	100.39	100.65	100.55
Total	99.95	99.74	99.83	101.15	100.71	99.85	99.85	100.33	99.74	99.79	100.39	100.39	100.65	100.55
Cations based on 12 oxygens														
Si	2.99	2.98	2.97	3.00	2.98	2.97	2.98	2.98	2.98	2.98	2.98	2.98	2.97	2.97
Ti	0.00	0.00	0.00	0.00	0.00	0.00	0.00	0.00	0.00	0.00	0.00	0.00	0.00	0.00
Al	1.96	1.98	1.99	2.01	2.01	1.99	1.99	1.99	1.99	1.99	2.00	1.99	2.00	2.00
Cr	0.00	0.00	0.00	0.00	0.00	0.00	0.00	0.00	0.00	0.00	0.00	0.00	0.00	0.00
Mg	0.43	0.48	0.48	0.46	0.44	0.57	0.55	0.56	0.56	0.55	0.55	0.55	0.56	0.55
Ca	0.69	0.68	0.68	0.65	0.64	0.64	0.65	0.62	0.63	0.65	0.65	0.66	0.67	0.68
Mn	0.07	0.06	0.06	0.07	0.08	0.06	0.06	0.06	0.06	0.06	0.06	0.06	0.05	0.06
Fe	1.88	1.85	1.86	1.82	1.87	1.81	1.80	1.81	1.82	1.80	1.78	1.78	1.79	1.77
Na	0.00	0.00	0.00	0.00	0.00	0.00	0.00	0.00	0.00	0.00	0.00	0.00	0.00	0.00
Total	8.03	8.03	8.03	8.00	8.02	8.04	8.03	8.02	8.03	8.02	8.02	8.02	8.03	8.03

Microprobe Analysis
of F-1296- Garnet-B

Oxide Wt. %	GrtNPlgInc6	GrtNPlgInc7	GrtNPlgInc8	GrtNPlgInc9	GrtNPlgInc10	GrtNPlgInc2-1	GrtNPlgInc2-2	GrtNPlgInc2-3	GrtNPlgInc3-1	GrtNPlgInc3-2	GrtNPlgInc3-3	GrtNPlgInc3-4	GrtNPlgInc3-5	GrtNPlgInc3-6
SiO_2	38.20	38.07	38.12	38.06	38.12	38.29	38.22	38.54	37.11	37.82	37.98	37.88	37.89	37.89
TiO_2	0.02	0.03	0.03	0.03	0.02	0.02	0.02	0.03	0.03	0.03	0.03	0.02	0.03	0.04
Al_2O_3	21.76	21.78	21.75	21.77	21.64	21.61	21.60	21.81	20.97	21.30	21.30	21.27	21.36	21.39
Cr_2O_3	0.00	0.01	0.01	0.00	0.01	0.02	0.00	0.01	0.04	0.01	0.01	0.00	0.01	0.03
MgO	4.77	4.80	4.76	4.78	4.77	4.60	4.67	4.70	4.59	4.67	4.69	4.70	4.79	4.74
CaO	8.09	8.11	8.11	8.19	8.19	7.55	7.63	7.66	7.79	7.76	7.72	7.75	7.90	7.80
MnO	0.84	0.83	0.81	0.83	0.82	0.94	0.90	0.89	0.89	0.90	0.88	0.90	0.88	0.87
FeO	26.80	26.92	27.12	26.95	26.78	27.76	27.41	27.48	27.23	27.56	27.69	27.43	27.49	27.36
Na_2O	0.00	0.01	0.00	0.00	0.01	0.01	0.01	0.00	0.01	0.00	0.00	0.00	0.00	0.01
Total	100.48	100.58	100.70	100.62	100.37	100.80	100.45	101.13	98.65	100.06	100.29	99.95	100.35	100.12
Total	100.48	100.58	100.70	100.62	100.37	100.80	100.45	101.13	98.65	100.06	100.29	99.95	100.35	100.12
Cations based on 12 oxygens														
Si	2.98	2.97	2.97	2.97	2.98	2.99	2.99	2.99	2.97	2.98	2.98	2.98	2.97	2.98
Ti	0.00	0.00	0.00	0.00	0.00	0.00	0.00	0.00	0.00	0.00	0.00	0.00	0.00	0.00
Al	2.00	2.00	2.00	2.00	1.99	1.99	1.99	1.99	1.98	1.98	1.97	1.97	1.98	1.98
Cr	0.00	0.00	0.00	0.00	0.00	0.00	0.00	0.00	0.00	0.00	0.00	0.00	0.00	0.00
Mg	0.56	0.56	0.55	0.56	0.56	0.54	0.54	0.54	0.55	0.55	0.55	0.55	0.56	0.56
Ca	0.68	0.68	0.68	0.69	0.69	0.63	0.64	0.64	0.67	0.66	0.65	0.65	0.66	0.66
Mn	0.06	0.06	0.05	0.06	0.06	0.06	0.06	0.06	0.06	0.06	0.06	0.06	0.06	0.06
Fe	1.75	1.76	1.77	1.76	1.75	1.81	1.79	1.78	1.82	1.82	1.82	1.81	1.80	1.80
Na	0.00	0.00	0.00	0.00	0.00	0.00	0.00	0.00	0.00	0.00	0.00	0.00	0.00	0.00
Total	8.02	8.03	8.03	8.03	8.02	8.02	8.02	8.01	8.04	8.03	8.03	8.03	8.04	8.03

Microprobe Analysis
of F-1296- Garnet-B

Oxide Wt. %	GrtNPlgInc3-7	GrtNPlgInc3-8	GrtNPlgInc3-9	GrtNPlgInc3-10	GrtNIlmInc1	GrtNIlmInc2	GrtNIlmInc3	GrtNIlmInc4	GrtNIlmInc5	GrtNIlmInc6	GrtNIlmInc7	GrtNIlmInc8	GrtNIlmInc9	GrtNIlmInc10
SiO_2	37.84	38.29	37.97	38.16	0.06	0.04	0.03	0.03	37.78	37.71	37.01	0.06	0.04	38.11
TiO_2	0.07	0.03	0.04	0.04	52.47	52.58	52.29	52.54	0.25	0.26	0.61	52.83	52.98	0.01
Al_2O_3	21.32	21.50	21.36	21.37	0.02	0.02	0.00	0.01	21.26	21.18	20.77	0.01	0.02	21.57
Cr_2O_3	0.03	0.02	0.03	0.01	0.02	0.01	0.00	0.00	0.03	0.05	0.04	0.01	0.02	0.11
MgO	4.67	4.75	4.74	4.73	0.02	0.02	0.02	0.03	4.59	4.61	4.61	0.03	0.01	4.03
CaO	7.87	7.93	7.98	7.95	0.04	0.02	0.05	0.04	8.12	7.94	7.87	0.06	0.05	7.17
MnO	0.86	0.86	0.88	0.88	0.51	0.50	0.50	0.50	0.84	0.87	0.86	0.47	0.45	1.13
FeO	27.40	27.20	27.52	27.31	46.26	45.67	45.99	46.00	27.04	27.23	27.38	45.18	45.23	28.95
Na_2O	0.00	0.01	0.00	0.00	0.00	0.00	0.00	0.00	0.00	0.00	0.02	0.00	0.01	0.01
Total	100.06	100.60	100.53	100.47	99.39	98.86	98.88	99.15	99.92	99.85	99.17	98.66	98.81	101.08
Total	100.06	100.60	100.53	100.47	99.39	98.86	98.88	99.15	99.92	99.85	99.17	98.66	98.81	101.08
Cations based on 12 oxygens														
Si	2.98	2.99	2.97	2.99	0.01	0.00	0.00	0.00	2.97	2.97	2.95	0.01	0.00	2.98
Ti	0.00	0.00	0.00	0.00	4.00	4.03	4.01	4.02	0.02	0.02	0.04	4.04	4.05	0.00
Al	1.98	1.98	1.97	1.97	0.00	0.00	0.00	0.00	1.97	1.97	1.95	0.00	0.00	1.99
Cr	0.00	0.00	0.00	0.00	0.00	0.00	0.00	0.00	0.00	0.00	0.00	0.00	0.00	0.01
Mg	0.55	0.55	0.55	0.55	0.00	0.00	0.00	0.01	0.54	0.54	0.55	0.01	0.00	0.47
Ca	0.66	0.66	0.67	0.67	0.00	0.00	0.01	0.01	0.69	0.67	0.67	0.01	0.01	0.60
Mn	0.06	0.06	0.06	0.06	0.04	0.04	0.04	0.04	0.06	0.06	0.06	0.04	0.04	0.08
Fe	1.80	1.78	1.80	1.79	3.93	3.89	3.92	3.91	1.78	1.80	1.82	3.85	3.84	1.90
Na	0.00	0.00	0.00	0.00	0.00	0.00	0.00	0.00	0.00	0.00	0.00	0.00	0.00	0.00
Total	8.03	8.02	8.04	8.03	7.99	7.97	7.99	7.98	8.02	8.03	8.04	7.95	7.95	8.02

Microprobe Analysis
of F-1296- Garnet-B

Oxide Wt. %	GrtNIlmInc11	GrtNOAmp1	GrtNOAmp2	GrtNOAmp3	GrtNOAmp4	GrtNOAmp5	GrtNOAmp6	GrtNOAmp7	GrtNOAmp8	GrtNOAmp9	GrtNOAmp10	GrtNOAmp11	GrtNIlmInc2-1	GrtNIlmInc2-2
SiO_2	37.99	37.99	37.51	37.58	37.96	37.79	37.90	38.05	37.92	38.03	38.16	38.22	38.24	38.26
TiO_2	0.03	0.03	0.03	0.02	0.01	0.02	0.03	0.01	0.02	0.02	0.03	0.01	0.15	0.18
Al_2O_3	21.66	21.64	21.22	21.34	21.40	21.63	21.56	21.60	21.60	21.71	21.48	21.67	21.62	21.71
Cr_2O_3	0.03	0.05	0.07	0.05	0.06	0.05	0.07	0.06	0.06	0.06	0.04	0.04	0.08	0.07
MgO	3.95	4.00	3.84	4.08	4.35	4.41	4.47	4.55	4.55	4.58	4.55	4.57	4.88	4.88
CaO	7.37	7.04	7.21	7.34	7.50	7.60	7.69	7.63	7.39	7.75	7.86	7.84	8.04	7.99
MnO	1.13	1.10	1.13	1.09	1.02	1.00	1.00	0.97	0.93	0.96	0.92	0.92	0.84	0.84
FeO	28.59	28.97	28.85	28.52	28.09	27.96	27.91	27.74	27.77	27.52	27.65	27.52	27.20	26.90
Na_2O	0.00	0.00	0.00	0.01	0.00	0.02	0.02	0.00	0.00	0.00	0.01	0.00	0.00	0.00
Total	100.76	100.82	99.87	100.04	100.39	100.49	100.65	100.60	100.24	100.62	100.71	100.78	101.05	100.83
Total	100.76	100.82	99.87	100.04	100.39	100.49	100.65	100.60	100.24	100.62	100.71	100.78	101.05	100.83
Cations based on 12 oxygens														
Si	2.98	2.98	2.98	2.97	2.98	2.97	2.97	2.98	2.98	2.97	2.98	2.98	2.97	2.98
Ti	0.00	0.00	0.00	0.00	0.00	0.00	0.00	0.00	0.00	0.00	0.00	0.00	0.01	0.01
Al	2.00	2.00	1.99	1.99	1.98	2.00	1.99	1.99	2.00	2.00	1.98	1.99	1.98	1.99
Cr	0.00	0.00	0.00	0.00	0.00	0.00	0.00	0.00	0.00	0.00	0.00	0.00	0.01	0.00
Mg	0.46	0.47	0.45	0.48	0.51	0.52	0.52	0.53	0.53	0.53	0.53	0.53	0.57	0.57
Ca	0.62	0.59	0.61	0.62	0.63	0.64	0.65	0.64	0.62	0.65	0.66	0.66	0.67	0.67
Mn	0.08	0.07	0.08	0.07	0.07	0.07	0.07	0.06	0.06	0.06	0.06	0.06	0.06	0.06
Fe	1.88	1.90	1.92	1.89	1.85	1.84	1.83	1.82	1.82	1.80	1.81	1.80	1.77	1.75
Na	0.00	0.00	0.00	0.00	0.00	0.00	0.00	0.00	0.00	0.00	0.00	0.00	0.00	0.00
Total	8.02	8.02	8.03	8.03	8.02	8.03	8.03	8.02	8.02	8.02	8.03	8.02	8.03	8.02

Microprobe Analysis
of F-1296- Garnet-B

Oxide Wt. %	GrtNIlmInc2-3	GrtNIlmInc2-4	GrtNIlmInc2-5	GrtNIlmInc2-6	GrtNIlmInc2-7	GrtNIlmInc2-8	GrtNIlmInc2-9	GrtNIlmInc2-10	GrtBTraverse	GrtBTraverse	GrtBTraverse	GrtBTraverse	GrtBTraverse	GrtBTraverse
SiO_2	38.34	38.48	38.85	0.54	0.05	0.07	0.06	0.06	37.38	39.39	37.91	38.06	37.90	38.08
TiO_2	0.22	0.32	0.59	52.30	53.01	53.18	53.34	53.42	0.03	0.02	0.03	0.04	0.04	0.04
Al_2O_3	21.97	21.82	22.14	0.24	0.02	0.02	0.03	0.01	21.39	22.27	21.45	21.37	21.38	21.43
Cr_2O_3	0.04	0.02	0.01	0.03	0.01	0.02	0.04	0.03	0.00	0.00	0.01	0.00	0.00	0.00
MgO	4.88	4.91	4.96	0.15	0.17	0.16	0.14	0.16	3.99	4.60	4.48	4.49	4.52	4.64
CaO	7.86	7.90	7.60	0.16	0.07	0.06	0.03	0.01	6.91	7.39	7.62	7.88	7.99	8.17
MnO	0.84	0.82	0.85	0.35	0.39	0.39	0.37	0.36	1.12	1.00	0.97	0.93	0.90	0.86
FeO	26.97	26.88	27.08	44.80	44.99	45.05	44.93	45.27	28.76	27.82	27.98	27.51	27.27	27.27
Na_2O	0.00	0.00	0.00	0.00	0.01	0.01	0.00	0.03	0.02	0.01	0.00	0.01	0.02	0.01
Total	101.13	101.17	102.08	98.57	98.72	98.95	98.95	99.33	99.59	102.49	100.45	100.30	100.01	100.49
Total	101.13	101.17	102.08	98.57	98.72	98.95	98.95	99.33	99.59	102.49	100.45	100.30	100.01	100.49

Cations based on 12 oxygens														
Si	2.97	2.98	2.98	0.05	0.01	0.01	0.01	0.01	2.97	3.01	2.98	2.99	2.98	2.98
Ti	0.01	0.02	0.03	3.99	4.05	4.05	4.06	4.05	0.00	0.00	0.00	0.00	0.00	0.00
Al	2.01	1.99	2.00	0.03	0.00	0.00	0.00	0.00	2.00	2.01	1.99	1.98	1.98	1.98
Cr	0.00	0.00	0.00	0.00	0.00	0.00	0.00	0.00	0.00	0.00	0.00	0.00	0.00	0.00
Mg	0.56	0.57	0.57	0.02	0.03	0.02	0.02	0.02	0.47	0.52	0.53	0.53	0.53	0.54
Ca	0.65	0.66	0.62	0.02	0.01	0.01	0.00	0.00	0.59	0.61	0.64	0.66	0.67	0.69
Mn	0.06	0.05	0.06	0.03	0.03	0.03	0.03	0.03	0.08	0.07	0.06	0.06	0.06	0.06
Fe	1.75	1.74	1.74	3.80	3.82	3.82	3.80	3.82	1.91	1.78	1.84	1.81	1.79	1.79
Na	0.00	0.00	0.00	0.00	0.00	0.00	0.00	0.01	0.00	0.00	0.00	0.00	0.00	0.00
Total	8.01	8.01	7.99	7.94	7.95	7.94	7.93	7.94	8.03	7.99	8.03	8.02	8.03	8.03

Microprobe Analysis
of F-1296- Garnet-B

Oxide Wt. %	GrtBTraverse	GrtBTraverse	GrtBTraverse	GrtBTraverse	GrtBTraverse	GrtBTraverse	GrtBTraverse	GrtBTraverse	GrtBTraverse	GrtBTraverse	GrtBTraverse	GrtBTraverse	GrtBTraverse	GrtBTraverse
SiO_2	38.21	38.33	38.38	38.11	38.31	38.14	38.18	38.14	37.72	38.09	29.67	38.05	38.17	38.04
TiO_2	0.04	0.04	0.05	0.05	0.04	0.07	0.05	0.04	0.06	0.03	0.09	0.04	0.05	0.04
Al_2O_3	21.44	21.44	21.73	21.52	21.41	21.27	21.36	21.50	21.28	21.47	20.06	21.38	21.39	21.35
Cr_2O_3	0.00	0.00	0.00	0.00	0.00	0.00	0.02	0.00	0.00	0.00	0.00	0.00	0.00	0.00
MgO	4.65	4.70	4.66	4.65	4.67	4.73	4.68	4.69	4.59	4.80	3.06	4.61	4.70	4.69
CaO	8.20	8.13	8.09	8.23	8.10	8.16	8.18	8.11	7.91	8.06	4.51	7.94	7.93	7.96
MnO	0.88	0.84	0.85	0.83	0.86	0.87	0.87	0.85	0.87	0.83	0.52	0.88	0.90	0.87
FeO	27.07	27.23	26.88	27.17	27.18	27.35	27.24	27.04	27.40	27.31	29.27	27.28	27.47	27.34
Na_2O	0.01	0.00	0.00	0.00	0.00	0.00	0.01	0.01	0.03	0.01	0.02	0.00	0.01	0.00
Total	100.50	100.71	100.64	100.58	100.56	100.59	100.59	100.38	99.87	100.61	87.20	100.19	100.62	100.29
Total	100.50	100.71	100.64	100.58	100.56	100.59	100.59	100.38	99.87	100.61	87.20	100.19	100.62	100.29

Cations based on 12 oxygens														
Si	2.99	2.99	2.99	2.98	2.99	2.98	2.99	2.98	2.98	2.98	2.75	2.99	2.98	2.98
Ti	0.00	0.00	0.00	0.00	0.00	0.00	0.00	0.00	0.00	0.00	0.01	0.00	0.00	0.00
Al	1.98	1.97	2.00	1.98	1.97	1.96	1.97	1.98	1.98	1.98	2.20	1.98	1.97	1.97
Cr	0.00	0.00	0.00	0.00	0.00	0.00	0.00	0.00	0.00	0.00	0.00	0.00	0.00	0.00
Mg	0.54	0.55	0.54	0.54	0.54	0.55	0.55	0.55	0.54	0.56	0.42	0.54	0.55	0.55
Ca	0.69	0.68	0.68	0.69	0.68	0.68	0.69	0.68	0.67	0.68	0.45	0.67	0.66	0.67
Mn	0.06	0.06	0.06	0.06	0.06	0.06	0.06	0.06	0.06	0.06	0.04	0.06	0.06	0.06
Fe	1.77	1.78	1.75	1.78	1.78	1.79	1.78	1.77	1.81	1.79	2.27	1.79	1.80	1.79
Na	0.00	0.00	0.00	0.00	0.00	0.00	0.00	0.00	0.01	0.00	0.00	0.00	0.00	0.00
Total	8.02	8.02	8.01	8.03	8.02	8.03	8.03	8.02	8.04	8.03	8.14	8.02	8.03	8.03

Microprobe Analysis
of F-1296- Garnet-B

Oxide Wt. %	GrtBTraverse	GrtBTraverse	GrtBTraverse	GrtBTraverse	GrtBTraverse	GrtBTraverse	GrtBTraverse	GrtBTraverse	GrtBTraverse	GrtBTraverse	GrtBTraverse	GrtBTraverse	GrtBTraverse	GrtBTraverse
SiO_2	38.21	38.07	38.30	38.17	38.07	35.57	38.18	38.14	37.95	38.07	38.03	38.14	38.18	38.07
TiO_2	0.06	0.04	0.03	0.02	0.03	0.05	0.05	0.05	0.05	0.05	0.04	0.06	0.05	0.06
Al_2O_3	21.39	21.37	21.59	21.60	21.25	19.79	21.50	21.35	21.23	21.24	21.45	21.37	21.45	21.32
Cr_2O_3	0.00	0.00	0.00	0.00	0.00	0.00	0.00	0.00	0.00	0.02	0.00	0.02	0.00	0.00
MgO	4.62	4.66	4.67	4.65	4.62	4.19	4.61	4.58	4.53	4.61	4.65	4.63	4.58	4.64
CaO	7.81	7.81	7.75	7.82	7.74	7.79	7.88	7.87	7.87	7.79	7.89	7.77	7.92	7.86
MnO	0.87	0.91	0.88	0.88	0.86	0.89	0.88	0.92	0.91	0.89	0.91	0.90	0.89	0.89
FeO	27.57	27.59	27.36	27.40	27.62	27.20	27.39	27.65	27.56	27.61	27.47	27.58	27.56	27.49
Na_2O	0.02	0.00	0.00	0.01	0.00	0.01	0.00	0.00	0.00	0.01	0.01	0.00	0.01	0.01
Total	100.53	100.46	100.58	100.56	100.19	95.50	100.48	100.55	100.11	100.31	100.45	100.46	100.64	100.33
Total	100.53	100.46	100.58	100.56	100.19	95.50	100.48	100.55	100.11	100.31	100.45	100.46	100.64	100.33
Cations based on 12 oxygens														
Si	2.99	2.98	2.99	2.98	2.99	2.96	2.99	2.99	2.99	2.99	2.98	2.99	2.99	2.99
Ti	0.00	0.00	0.00	0.00	0.00	0.00	0.00	0.00	0.00	0.00	0.00	0.00	0.00	0.00
Al	1.97	1.97	1.99	1.99	1.97	1.94	1.98	1.97	1.97	1.97	1.98	1.97	1.98	1.97
Cr	0.00	0.00	0.00	0.00	0.00	0.00	0.00	0.00	0.00	0.00	0.00	0.00	0.00	0.00
Mg	0.54	0.55	0.54	0.54	0.54	0.52	0.54	0.54	0.53	0.54	0.54	0.54	0.53	0.54
Ca	0.66	0.66	0.65	0.66	0.65	0.69	0.66	0.66	0.66	0.66	0.66	0.65	0.66	0.66
Mn	0.06	0.06	0.06	0.06	0.06	0.06	0.06	0.06	0.06	0.06	0.06	0.06	0.06	0.06
Fe	1.80	1.81	1.79	1.79	1.82	1.89	1.79	1.81	1.81	1.81	1.80	1.81	1.80	1.80
Na	0.00	0.00	0.00	0.00	0.00	0.00	0.00	0.00	0.00	0.00	0.00	0.00	0.00	0.00
Total	8.02	8.03	8.02	8.02	8.02	8.07	8.02	8.03	8.03	8.03	8.03	8.02	8.03	8.03

Microprobe Analysis
of F-1296- Garnet-B

Oxide Wt. %	GrtBTraverse	GrtBTraverse	GrtBTraverse	GrtBTraverse	GrtBTraverse	GrtBTraverse	GrtBTraverse	GrtBTraverse	GrtBTraverse	GrtBTraverse	GrtBTraverse	GrtBTraverse	GrtBTraverse	GrtBTraverse
SiO_2	38.14	29.83	37.96	37.83	38.25	38.10	38.43	38.36	37.98	38.21	37.92	32.75	37.97	38.12
TiO_2	0.02	0.05	0.06	0.07	0.07	0.05	0.05	0.11	0.06	0.04	0.05	0.06	0.06	0.06
Al_2O_3	22.86	17.49	21.51	21.30	21.14	21.47	21.35	23.33	21.26	21.66	21.40	21.51	21.39	21.33
Cr_2O_3	0.00	0.00	0.00	0.00	0.00	0.00	0.00	0.00	0.00	0.00	0.00	0.00	0.00	0.00
MgO	3.91	3.29	4.42	4.58	4.62	4.66	4.66	4.17	4.62	4.76	4.59	3.62	4.59	4.73
CaO	4.29	6.39	7.59	7.79	7.84	7.98	7.97	5.51	8.01	7.90	8.03	6.14	8.17	8.12
MnO	0.55	0.74	0.86	0.87	0.88	0.86	0.87	0.65	0.85	0.87	0.87	0.64	0.85	0.86
FeO	22.72	27.26	27.28	27.56	27.64	27.42	27.41	25.51	27.38	27.23	27.51	28.99	27.19	27.25
Na_2O	1.51	0.01	0.01	0.00	0.01	0.01	0.00	0.02	0.00	0.00	0.02	0.02	0.01	0.01
Total	94.00	85.05	99.69	99.99	100.45	100.55	100.73	97.66	100.17	100.66	100.40	93.72	100.21	100.49
Total	94.00	85.05	99.69	99.99	100.45	100.55	100.73	97.66	100.17	100.66	100.40	93.72	100.21	100.49
Cations based on 12 oxygens														
Si	3.09	2.84	2.99	2.98	3.00	2.98	3.00	3.03	2.98	2.98	2.98	2.80	2.98	2.98
Ti	0.00	0.00	0.00	0.00	0.00	0.00	0.00	0.01	0.00	0.00	0.00	0.00	0.00	0.00
Al	2.18	1.97	2.00	1.98	1.95	1.98	1.96	2.17	1.97	1.99	1.98	2.17	1.98	1.97
Cr	0.00	0.00	0.00	0.00	0.00	0.00	0.00	0.00	0.00	0.00	0.00	0.00	0.00	0.00
Mg	0.47	0.47	0.52	0.54	0.54	0.54	0.54	0.49	0.54	0.55	0.54	0.46	0.54	0.55
Ca	0.37	0.65	0.64	0.66	0.66	0.67	0.67	0.47	0.68	0.66	0.68	0.56	0.69	0.68
Mn	0.04	0.06	0.06	0.06	0.06	0.06	0.06	0.04	0.06	0.06	0.06	0.05	0.06	0.06
Fe	1.54	2.17	1.80	1.82	1.81	1.79	1.79	1.68	1.80	1.78	1.81	2.07	1.79	1.78
Na	0.24	0.00	0.00	0.00	0.00	0.00	0.00	0.00	0.00	0.00	0.00	0.00	0.00	0.00
Total	7.93	8.17	8.01	8.03	8.02	8.03	8.02	7.89	8.03	8.02	8.03	8.12	8.03	8.03

Microprobe Analysis
of F-1296- Garnet-B

Oxide Wt. %	GrtBTraverse	GrtBTraverse	GrtBTraverse	GrtBTraverse	GrtBTraverse	GrtBTraverse	GrtBTraverse	GrtBTraverse	GrtBTraverse	GrtBTraverse	GrtBTraverse	GrtBTraverse	GrtBTraverse	GrtBTraverse
SiO_2	38.25	38.09	38.14	38.21	38.35	38.16	38.08	38.24	38.04	37.89	37.98	38.24	38.24	38.24
TiO_2	0.06	0.04	0.02	0.05	0.01	0.03	0.04	0.05	0.04	0.06	0.06	0.06	0.03	0.04
Al_2O_3	21.52	21.46	21.42	21.41	21.56	21.69	21.71	21.56	21.42	21.45	21.29	21.47	21.44	21.41
Cr_2O_3	0.00	0.00	0.00	0.02	0.00	0.00	0.00	0.00	0.00	0.00	0.00	0.00	0.00	0.00
MgO	4.68	4.64	4.72	4.73	4.75	4.67	4.71	4.73	4.75	4.78	4.62	4.69	4.72	4.72
CaO	8.09	7.97	7.93	7.77	7.63	7.62	7.93	8.08	8.06	7.98	8.01	8.06	8.01	7.98
MnO	0.84	0.89	0.90	0.88	0.90	0.87	0.86	0.88	0.85	0.88	0.87	0.88	0.88	0.89
FeO	27.37	27.47	27.28	27.46	27.69	27.75	27.17	27.27	27.40	27.23	27.34	27.28	27.19	27.31
Na_2O	0.01	0.00	0.02	0.00	0.01	0.00	0.01	0.00	0.01	0.01	0.01	0.00	0.01	0.02
Total	100.81	100.57	100.43	100.51	100.89	100.80	100.51	100.81	100.57	100.29	100.17	100.66	100.50	100.60
Total	100.81	100.57	100.43	100.51	100.89	100.80	100.51	100.81	100.57	100.29	100.17	100.66	100.50	100.60
Cations based on 12 oxygens														
Si	2.98	2.98	2.99	2.99	2.99	2.98	2.98	2.98	2.98	2.97	2.98	2.99	2.99	2.99
Ti	0.00	0.00	0.00	0.00	0.00	0.00	0.00	0.00	0.00	0.00	0.00	0.00	0.00	0.00
Al	1.98	1.98	1.98	1.97	1.98	2.00	2.00	1.98	1.98	1.98	1.97	1.98	1.98	1.97
Cr	0.00	0.00	0.00	0.00	0.00	0.00	0.00	0.00	0.00	0.00	0.00	0.00	0.00	0.00
Mg	0.54	0.54	0.55	0.55	0.55	0.54	0.55	0.55	0.55	0.56	0.54	0.55	0.55	0.55
Ca	0.68	0.67	0.67	0.65	0.64	0.64	0.66	0.68	0.68	0.67	0.67	0.67	0.67	0.67
Mn	0.06	0.06	0.06	0.06	0.06	0.06	0.06	0.06	0.06	0.06	0.06	0.06	0.06	0.06
Fe	1.79	1.80	1.79	1.80	1.81	1.81	1.78	1.78	1.79	1.79	1.80	1.78	1.78	1.78
Na	0.00	0.00	0.00	0.00	0.00	0.00	0.00	0.00	0.00	0.00	0.00	0.00	0.00	0.00
Total	8.03	8.03	8.03	8.02	8.02	8.02	8.02	8.03	8.04	8.03	8.03	8.02	8.02	8.03

Microprobe Analysis
of F-1296- Garnet-B

Oxide Wt. %	GrtBTraverse	GrtBTraverse	GrtBTraverse	GrtBTraverse	GrtBTraverse	GrtBTraverse	GrtBTraverse	GrtBTraverse	GrtBTraverse	GrtBTraverse	GrtBTraverse	GrtBTraverse	GrtBTraverse	GrtBTraverse
SiO_2	38.10	41.90	37.95	38.20	37.98	37.84	38.17	38.05	38.18	38.26	37.92	38.19	38.09	38.06
TiO_2	0.05	0.09	0.07	0.05	0.05	0.05	0.02	0.04	0.04	0.04	0.06	0.04	0.05	0.05
Al_2O_3	21.48	29.01	21.49	21.41	21.35	21.60	21.43	21.37	21.52	21.30	21.45	21.47	21.45	21.43
Cr_2O_3	0.00	0.00	0.01	0.00	0.00	0.00	0.00	0.02	0.00	0.00	0.00	0.00	0.01	0.00
MgO	4.73	5.12	4.68	4.70	4.63	4.74	4.70	4.69	4.72	4.65	4.70	4.74	4.72	4.77
CaO	8.00	0.65	7.93	7.91	7.78	7.78	7.76	7.75	7.67	7.76	7.72	7.77	7.66	7.65
MnO	0.86	0.06	0.90	0.87	0.87	0.89	0.87	0.87	0.91	0.91	0.91	0.87	0.88	0.90
FeO	27.41	12.86	27.37	27.46	27.48	27.40	27.70	27.52	27.69	27.53	27.71	27.50	27.65	27.64
Na_2O	0.01	0.04	0.01	0.01	0.01	0.00	0.01	0.00	0.01	0.00	0.01	0.01	0.00	0.01
Total	100.63	89.74	100.39	100.61	100.16	100.30	100.67	100.32	100.75	100.47	100.47	100.59	100.51	100.51
Total	100.63	89.74	100.39	100.61	100.16	100.30	100.67	100.32	100.75	100.47	100.47	100.59	100.51	100.51
Cations based on 12 oxygens														
Si	2.98	3.26	2.97	2.99	2.98	2.97	2.98	2.98	2.98	3.00	2.97	2.99	2.98	2.98
Ti	0.00	0.01	0.00	0.00	0.00	0.00	0.00	0.00	0.00	0.00	0.00	0.00	0.00	0.00
Al	1.98	2.66	1.99	1.97	1.98	2.00	1.98	1.98	1.98	1.97	1.98	1.98	1.98	1.98
Cr	0.00	0.00	0.00	0.00	0.00	0.00	0.00	0.00	0.00	0.00	0.00	0.00	0.00	0.00
Mg	0.55	0.59	0.55	0.55	0.54	0.55	0.55	0.55	0.55	0.54	0.55	0.55	0.55	0.56
Ca	0.67	0.05	0.67	0.66	0.66	0.65	0.65	0.65	0.64	0.65	0.65	0.65	0.64	0.64
Mn	0.06	0.00	0.06	0.06	0.06	0.06	0.06	0.06	0.06	0.06	0.06	0.06	0.06	0.06
Fe	1.79	0.84	1.79	1.80	1.81	1.80	1.81	1.81	1.81	1.80	1.82	1.80	1.81	1.81
Na	0.00	0.01	0.00	0.00	0.00	0.00	0.00	0.00	0.00	0.00	0.00	0.00	0.00	0.00
Total	8.03	7.41	8.03	8.03	8.03	8.03	8.03	8.03	8.03	8.02	8.03	8.02	8.03	8.03

Microprobe Analysis
of F-1296- Garnet-B

Oxide Wt. %	GrtBTraverse	GrtBTraverse	GrtBTraverse	GrtBTraverse	GrtBTraverse	GrtBTraverse	GrtBTraverse	GrtBTraverse	GrtBTraverse	GrtBTraverse	GrtBTraverse	GrtBTraverse	GrtBTraverse	GrtBTraverse
SiO_2	38.30	38.06	38.01	38.12	38.17	38.12	42.17	37.93	38.10	37.96	38.15	37.98	38.14	38.18
TiO_2	0.04	0.05	0.04	0.07	0.03	0.05	0.01	0.03	0.04	0.05	0.03	0.04	0.04	0.05
Al_2O_3	21.61	21.46	21.46	21.53	21.58	21.51	19.93	21.49	21.53	21.66	21.57	21.73	21.72	21.51
Cr_2O_3	0.00	0.00	0.00	0.00	0.00	0.01	0.00	0.00	0.01	0.00	0.02	0.00	0.00	0.00
MgO	4.75	4.71	4.71	4.79	4.75	4.35	3.60	4.02	4.70	4.76	4.67	4.76	4.69	4.70
CaO	7.65	7.81	7.91	7.93	7.96	7.91	7.47	7.80	8.07	7.87	8.07	7.98	8.18	8.23
MnO	0.89	0.91	0.87	0.87	0.85	0.87	0.80	0.88	0.85	0.86	0.84	0.87	0.85	0.85
FeO	27.61	27.70	27.42	27.58	27.53	27.53	26.54	28.22	27.26	27.17	27.12	27.05	26.83	26.93
Na_2O	0.02	0.00	0.00	0.00	0.00	0.00	0.00	0.00	0.00	0.01	0.00	0.01	0.00	0.00
Total	100.87	100.68	100.43	100.90	100.86	100.35	100.51	100.38	100.56	100.33	100.47	100.40	100.44	100.45
Total	100.87	100.68	100.43	100.90	100.86	100.35	100.51	100.38	100.56	100.33	100.47	100.40	100.44	100.45
Cations based on 12 oxygens														
Si	2.98	2.98	2.98	2.97	2.98	2.99	3.25	2.98	2.98	2.97	2.98	2.97	2.98	2.98
Ti	0.00	0.00	0.00	0.00	0.00	0.00	0.00	0.00	0.00	0.00	0.00	0.00	0.00	0.00
Al	1.99	1.98	1.98	1.98	1.98	1.99	1.81	1.99	1.98	2.00	1.99	2.00	2.00	1.98
Cr	0.00	0.00	0.00	0.00	0.00	0.00	0.00	0.00	0.00	0.00	0.00	0.00	0.00	0.00
Mg	0.55	0.55	0.55	0.56	0.55	0.51	0.41	0.47	0.55	0.56	0.54	0.56	0.55	0.55
Ca	0.64	0.65	0.66	0.66	0.67	0.66	0.62	0.66	0.68	0.66	0.68	0.67	0.68	0.69
Mn	0.06	0.06	0.06	0.06	0.06	0.06	0.05	0.06	0.06	0.06	0.06	0.06	0.06	0.06
Fe	1.80	1.81	1.80	1.80	1.80	1.81	1.71	1.86	1.78	1.78	1.77	1.77	1.75	1.76
Na	0.00	0.00	0.00	0.00	0.00	0.00	0.00	0.00	0.00	0.00	0.00	0.00	0.00	0.00
Total	8.02	8.03	8.03	8.03	8.03	8.02	7.85	8.02	8.03	8.03	8.02	8.03	8.02	8.02

Microprobe Analysis
of F-1296- Garnet-B

Oxide Wt. %	GrtBTraverse	GrtBTraverse	GrtBTraverse	GrtBTraverse	GrtBTraverse	GrtBTraverse	GrtBTraverse
SiO_2	38.14	38.03	38.16	38.31	38.21	38.18	38.18
TiO_2	0.04	0.02	0.04	0.04	0.04	0.01	0.02
Al_2O_3	21.62	21.45	21.50	21.57	21.51	21.60	21.49
Cr_2O_3	0.00	0.01	0.00	0.00	0.00	0.00	0.04
MgO	4.70	4.60	4.57	4.50	4.53	4.33	4.10
CaO	8.29	8.15	8.02	7.89	7.59	7.55	7.14
MnO	0.87	0.88	0.90	0.93	0.96	0.98	1.12
FeO	26.97	27.12	27.19	27.41	28.00	27.95	29.10
Na_2O	0.01	0.00	0.01	0.01	0.01	0.01	0.00
Total	100.64	100.27	100.39	100.66	100.85	100.61	101.19
Total	100.64	100.27	100.39	100.66	100.85	100.61	101.19
Cations based on 12 oxygens							
Si	2.98	2.98	2.99	2.99	2.99	2.99	2.99
Ti	0.00	0.00	0.00	0.00	0.00	0.00	0.00
Al	1.99	1.98	1.98	1.99	1.98	1.99	1.98
Cr	0.00	0.00	0.00	0.00	0.00	0.00	0.00
Mg	0.55	0.54	0.53	0.52	0.53	0.51	0.48
Ca	0.69	0.69	0.67	0.66	0.64	0.63	0.60
Mn	0.06	0.06	0.06	0.06	0.06	0.07	0.07
Fe	1.76	1.78	1.78	1.79	1.83	1.83	1.90
Na	0.00	0.00	0.00	0.00	0.00	0.00	0.00
Total	8.03	8.03	8.02	8.02	8.02	8.02	8.02

Microprobe Analysis
of F-1296- Amphibole
in or near garnet-B

Oxide Wt. %	AmpInc1	AmpInc2	AmpInc3	AmpInc4	AmpInc5	AmpInc6	AmpO1	AmpO2	AmpO3	AmpO4	AmpO5	AmpO6	AmpO7	AmpO8
SiO_2	39.9289	39.8163	39.5608	39.2487	38.8067	25.336	44.6087	44.5724	44.6747	44.729	44.7159	44.8172	45.0397	44.0653
TiO_2	1.4047	1.1835	1.0785	0.6214	0.7127	0.0168	1.0085	0.9776	0.9562	0.9302	0.9617	0.9587	0.8902	1.5771
Al_2O_3	19.049	19.7061	19.8366	20.2679	20.2816	22.0305	12.566	12.4644	12.4845	12.5235	12.6048	12.248	12.5147	12.4436
Cr_2O_3	0.012	0.0047	0.006	0.0188	0.0345	0.0702	0.0608	0.0374	0.0472	0.0485	0.0498	0.0399	0.0559	0.0283
MgO	6.9777	6.922	6.7855	6.408	6.4715	12.7282	11.2264	11.3117	11.2805	11.3447	11.3538	11.2932	11.4676	11.0528
CaO	11.322	11.271	11.371	11.3636	11.3516	0.0438	11.172	11.2232	11.2316	11.3897	11.4456	11.4086	11.4912	11.2862
MnO	0.1376	0.1178	0.0955	0.1206	0.1008	0.1295	0.1072	0.0982	0.09	0.0747	0.0771	0.0937	0.0964	0.0943
FeO	16.2908	16.6024	16.5654	16.7585	16.6357	27.4268	14.9685	14.9631	14.9997	14.706	14.8599	14.572	14.7117	15.0842
H_2O	2.0017	2.011	2.0045	1.9912	1.982	1.7181	2.0333	2.0316	2.0332	2.0342	2.04	2.0284	2.0456	2.0271
Na_2O	1.3217	1.2958	1.3641	1.2255	1.2222	0	1.3544	1.3582	1.2897	1.2176	1.3025	1.2064	1.2198	1.3865
K_2O	0.5268	0.5832	0.6036	0.6644	0.7254	0.0013	0.5088	0.5422	0.5107	0.5192	0.5053	0.5095	0.5166	0.5575
Total	98.9729	99.5138	99.2715	98.6885	98.3247	89.5013	99.6145	99.58	99.5978	99.5172	99.9163	99.1756	100.0495	99.6029
Total	98.9729	99.5138	99.2715	98.6885	98.3247	89.5013	99.6145	99.58	99.5978	99.5172	99.9163	99.1756	100.0495	99.6029
Cations based on 23														
Si	5.981	5.936	5.918	5.91	5.871	4.421	6.578	6.578	6.588	6.593	6.572	6.625	6.602	6.518
Ti	0.158	0.133	0.121	0.07	0.081	0.002	0.112	0.108	0.106	0.103	0.106	0.107	0.098	0.175
Al	3.363	3.463	3.497	3.597	3.616	4.531	2.184	2.168	2.17	2.176	2.183	2.134	2.162	2.169
Cr	0.001	0.001	0.001	0.002	0.004	0.01	0.007	0.004	0.005	0.006	0.006	0.005	0.006	0.003
Mg	1.558	1.539	1.513	1.438	1.459	3.311	2.468	2.489	2.48	2.493	2.488	2.489	2.506	2.437
Ca	1.817	1.8	1.822	1.833	1.84	0.008	1.765	1.775	1.775	1.799	1.802	1.807	1.805	1.789
Mn	0.017	0.015	0.012	0.015	0.013	0.019	0.013	0.012	0.011	0.009	0.01	0.012	0.012	0.012
Fe	2.041	2.07	2.072	2.11	2.105	4.003	1.846	1.847	1.85	1.813	1.827	1.801	1.803	1.866
Na	0.384	0.375	0.396	0.358	0.358	0	0.387	0.389	0.369	0.348	0.371	0.346	0.347	0.398
K	0.101	0.111	0.115	0.128	0.14	0	0.096	0.102	0.096	0.098	0.095	0.096	0.097	0.105
Total	17.421	17.442	17.468	17.463	17.487	18.306	17.456	17.472	17.45	17.436	17.46	17.42	17.437	17.472

Microprobe Analysis
of F-1296- Amphibole
in or near garnet-B

Oxide Wt. %	AmpO9	AmpO10	AmpO11	AmpO12
SiO_2	43.4962	44.264	44.4454	44.1279
TiO_2	1.6531	1.5231	1.4494	1.563
Al_2O_3	12.6955	12.2483	11.9243	12.4276
Cr_2O_3	0.0341	0.0022	0.0329	0.0354
MgO	10.8013	10.9418	11.2071	10.8536
CaO	11.2917	11.238	11.2	11.2607
MnO	0.0885	0.0986	0.0934	0.0889
FeO	15.1956	15.2383	15.149	15.4191
H_2O	2.0163	2.0248	2.0235	2.0277
Na_2O	1.4061	1.3883	1.2903	1.3896
K_2O	0.5561	0.4992	0.5072	0.5697
Total	99.2345	99.4668	99.3225	99.7633
Total	99.2345	99.4668	99.3225	99.7633
Cations based on 23				
Si	6.468	6.555	6.586	6.525
Ti	0.185	0.17	0.162	0.174
Al	2.225	2.138	2.082	2.166
Cr	0.004	0	0.004	0.004
Mg	2.395	2.415	2.476	2.393
Ca	1.799	1.783	1.778	1.784
Mn	0.011	0.012	0.012	0.011
Fe	1.89	1.887	1.877	1.907
Na	0.405	0.399	0.371	0.398
K	0.106	0.094	0.096	0.107
Total	17.488	17.453	17.443	17.469

Microprobe Analysis
of F-1296- Feldpar in
or near garnet-B

Oxide Wt. %	PlgInc1	PlgInc2	PlgInc3	PlgInc4	PlgInc5	PlgInc6	PlgInc7	PlgInc8	PlgInc9	PlgInc10	PlgInc2-1	PlgInc2-2	PlgInc2-3	PlgInc2-4
SiO_2	57.8713	57.759	58.0777	58.5276	58.4288	58.8751	58.8596	58.5671	57.6201	56.4926	57.5446	57.3987	57.9934	58.1552
Al_2O_3	27.5081	27.1783	26.6157	26.0478	26.165	26.1601	26.1896	26.4744	26.55	27.073	27.1915	26.9692	27.0729	26.9391
CaO	8.907	8.5074	8.097	7.8337	7.7705	7.6905	7.5342	8.0228	8.3444	8.9327	9.0423	8.8401	8.6558	8.6103
FeO	0.1169	0.0771	0.0831	0.0481	0.0478	0.0618	0.0481	0.0723	0.0434	0.0611	0.0871	0.0592	0.0701	0.0772
Na_2O	6.4761	6.4088	6.7166	6.9539	7.0212	6.9323	6.8314	6.9282	6.5599	6.2105	6.2634	6.1941	6.5622	6.443
K_2O	0.1386	0.1513	0.1451	0.1606	0.1325	0.1853	0.1644	0.1688	0.1351	0.1393	0.2517	0.238	0.2455	0.2094
Total	101.0179	100.0819	99.7351	99.5716	99.5659	99.9051	99.6272	100.2336	99.253	98.9093	100.3805	99.6993	100.5999	100.4342
Total	101.0179	100.0819	99.7351	99.5716	99.5659	99.9051	99.6272	100.2336	99.253	98.9093	100.3805	99.6993	100.5999	100.4342
Cations based on 8														
Si	2.567	2.581	2.602	2.625	2.621	2.629	2.633	2.611	2.596	2.559	2.57	2.578	2.582	2.59
Al	1.438	1.431	1.405	1.377	1.383	1.377	1.381	1.391	1.41	1.446	1.431	1.427	1.42	1.414
Ca	0.423	0.407	0.389	0.376	0.373	0.368	0.361	0.383	0.403	0.434	0.433	0.425	0.413	0.411
Fe	0.004	0.003	0.003	0.002	0.002	0.002	0.002	0.003	0.002	0.002	0.003	0.002	0.003	0.003
Na	0.557	0.555	0.583	0.605	0.611	0.6	0.592	0.599	0.573	0.546	0.542	0.539	0.566	0.556
K	0.008	0.009	0.008	0.009	0.008	0.011	0.009	0.01	0.008	0.008	0.014	0.014	0.014	0.012
Total	4.997	4.986	4.991	4.994	4.997	4.988	4.978	4.997	4.99	4.995	4.993	4.985	4.998	4.987

Microprobe Analysis
of F-1296- Feldpar in
or near garnet-B

Oxide Wt. %	PlgInc2-5	PlgInc2-6	PlgInc3-1	PlgInc4-1
SiO_2	57.4971	57.8149	57.5412	57.6498
Al_2O_3	26.6741	27.1489	27.1971	27.1967
CaO	8.5468	8.5637	9.0363	8.7256
FeO	0.0711	0.0918	0.1228	0.0984
Na_2O	6.3664	6.4168	6.306	6.417
K_2O	0.2428	0.2464	0.2222	0.2119
Total	99.3983	100.2825	100.4256	100.2995
Total	99.3983	100.2825	100.4256	100.2995
Cations based on 8				
Si	2.589	2.58	2.569	2.574
Al	1.415	1.428	1.431	1.431
Ca	0.412	0.409	0.432	0.417
Fe	0.003	0.003	0.005	0.004
Na	0.556	0.555	0.546	0.556
K	0.014	0.014	0.013	0.012
Total	4.989	4.99	4.995	4.994

Microprobe Analysis
of F-1296- Amphibole
in or near garnet-E

Oxide Wt. %	AmpInc1	AmpInc2	AmpInc3	AmpInc4	AmpInc5	AmpInc6	AmpInc7	AmpInc8	AmpOGrt1	AmpOGrt2	AmpOGrt3	AmpOGrt4	AmpOGrt5	AmpOGrt6
SiO_2	23.89	23.90	23.82	23.88	23.86	24.14	23.73	23.72	44.38	44.08	44.14	44.35	44.68	44.53
TiO_2	0.04	0.03	0.07	0.04	0.06	0.06	0.08	0.06	1.19	1.23	1.18	1.17	1.22	1.18
Al_2O_3	22.19	22.14	22.40	22.39	22.17	22.51	22.44	22.36	12.67	12.49	12.39	12.23	12.27	12.34
Cr_2O_3	0.04	0.03	0.04	0.02	0.03	0.03	0.04	0.03	0.10	0.07	0.08	0.06	0.08	0.06
MgO	11.14	11.15	11.13	11.24	11.17	10.78	10.98	10.86	11.20	11.07	11.08	11.11	11.10	11.06
CaO	0.01	0.01	0.03	0.02	0.02	0.04	0.01	0.04	11.11	11.19	11.16	11.15	11.05	11.21
MnO	0.09	0.08	0.09	0.08	0.08	0.08	0.10	0.10	0.10	0.08	0.09	0.07	0.09	0.08
FeO	30.64	30.52	30.41	30.56	30.58	30.27	30.66	30.71	15.00	15.20	15.08	14.91	14.96	14.99
Na_2O	0.03	0.00	0.01	0.01	0.00	0.00	0.00	0.00	1.38	1.35	1.31	1.35	1.35	1.31
K_2O	0.01	0.00	0.00	0.00	0.00	0.01	0.01	0.01	0.48	0.50	0.49	0.51	0.48	0.48
Total	89.74	89.55	89.69	89.94	89.67	89.61	89.73	89.56	99.65	99.29	99.00	98.93	99.31	99.28
Total	89.74	89.55	89.69	89.94	89.67	89.61	89.73	89.56	99.65	99.29	99.00	98.93	99.31	99.28
Cations based on 23 Oxygens														
Si	4.25	4.25	4.23	4.23	4.24	4.28	4.22	4.23	6.55	6.54	6.56	6.59	6.61	6.59
Ti	0.01	0.00	0.01	0.01	0.01	0.01	0.01	0.01	0.13	0.14	0.13	0.13	0.14	0.13
Al	4.65	4.64	4.69	4.68	4.65	4.71	4.70	4.70	2.20	2.18	2.17	2.14	2.14	2.15
Cr	0.01	0.01	0.01	0.00	0.01	0.00	0.01	0.01	0.01	0.01	0.01	0.01	0.01	0.01
Mg	2.95	2.96	2.95	2.97	2.96	2.85	2.91	2.88	2.46	2.45	2.45	2.46	2.45	2.44
Ca	0.00	0.00	0.01	0.01	0.00	0.01	0.00	0.01	1.76	1.78	1.78	1.78	1.75	1.78
Mn	0.01	0.01	0.01	0.01	0.01	0.01	0.01	0.02	0.01	0.01	0.01	0.01	0.01	0.01
Fe	4.55	4.54	4.52	4.53	4.55	4.49	4.56	4.58	1.85	1.89	1.87	1.85	1.85	1.86
OH	2.00	2.00	2.00	2.00	2.00	2.00	2.00	2.00	2.00	2.00	2.00	2.00	2.00	2.00
Na	0.01	0.00	0.00	0.00	0.00	0.00	0.00	0.00	0.40	0.39	0.38	0.39	0.39	0.38
K	0.00	0.00	0.00	0.00	0.00	0.00	0.00	0.00	0.09	0.10	0.09	0.10	0.09	0.09
Total	18.43	18.42	18.42	18.43	18.42	18.36	18.42	18.42	17.46	17.47	17.45	17.45	17.42	17.43

Microprobe Analysis
of F-1296- Amphibole
in or near garnet-E

Oxide Wt. %	AmpOGrt7	AmpOGrt8	AmpOGrt2-1	AmpOGrt2-2	AmpOGrt2-3	AmpOGrt2-4	AmpOGrt2-5	AmpOGrt2-6	AmpOGrt2-7	AmpOGrt2-8	AmpOGrt2-9	AmpOGrt2-10	AmpOGrt2-11	AmpOGrt2-12
SiO_2	44.53	44.26	43.90	44.04	44.01	44.13	43.78	43.95	44.33	44.27	44.29	43.39	44.40	44.33
TiO_2	1.19	1.16	1.27	1.24	1.39	1.42	1.36	1.41	1.49	1.53	1.54	1.52	1.41	1.43
Al_2O_3	12.35	12.28	12.76	13.76	12.79	12.45	12.36	12.25	12.05	11.96	11.97	12.88	12.13	12.18
Cr_2O_3	0.08	0.05	0.04	0.03	0.05	0.03	0.04	0.03	0.03	0.06	0.04	0.02	0.01	0.03
MgO	11.05	10.89	10.73	9.92	10.61	10.69	10.92	10.87	10.91	10.86	10.92	10.53	10.91	10.93
CaO	11.03	11.13	11.18	10.46	11.14	11.30	10.89	11.25	11.28	11.13	11.12	10.56	11.15	11.14
MnO	0.09	0.08	0.07	0.10	0.08	0.08	0.10	0.07	0.11	0.08	0.09	0.10	0.10	0.08
FeO	14.98	15.01	15.25	14.89	15.43	15.28	15.52	15.42	15.31	15.58	15.47	16.03	15.21	15.42
Na_2O	1.31	1.29	1.30	1.21	1.39	1.35	1.30	1.30	1.35	1.34	1.28	1.24	1.30	1.29
K_2O	0.49	0.50	0.54	0.51	0.52	0.53	0.50	0.54	0.56	0.52	0.51	0.49	0.50	0.50
Total	99.13	98.65	99.05	98.17	99.42	99.28	98.77	99.10	99.44	99.36	99.25	98.76	99.13	99.35
Total	99.13	98.65	99.05	98.17	99.42	99.28	98.77	99.10	99.44	99.36	99.25	98.76	99.13	99.35
Cations based on 23 Oxygens														
Si	6.60	6.59	6.53	6.56	6.52	6.55	6.54	6.54	6.57	6.57	6.58	6.49	6.59	6.57
Ti	0.13	0.13	0.14	0.14	0.16	0.16	0.15	0.16	0.17	0.17	0.17	0.17	0.16	0.16
Al	2.16	2.16	2.24	2.42	2.23	2.18	2.17	2.15	2.11	2.09	2.10	2.27	2.12	2.13
Cr	0.01	0.01	0.00	0.00	0.01	0.00	0.00	0.00	0.00	0.01	0.00	0.00	0.00	0.00
Mg	2.44	2.42	2.38	2.21	2.35	2.37	2.43	2.41	2.41	2.40	2.42	2.35	2.41	2.42
Ca	1.75	1.78	1.78	1.67	1.77	1.80	1.74	1.79	1.79	1.77	1.77	1.69	1.77	1.77
Mn	0.01	0.01	0.01	0.01	0.01	0.01	0.01	0.01	0.01	0.01	0.01	0.01	0.01	0.01
Fe	1.86	1.87	1.90	1.86	1.91	1.90	1.94	1.92	1.90	1.94	1.92	2.00	1.89	1.91
OH	2.00	2.00	2.00	2.00	2.00	2.00	2.00	2.00	2.00	2.00	2.00	2.00	2.00	2.00
Na	0.38	0.37	0.38	0.35	0.40	0.39	0.38	0.38	0.39	0.39	0.37	0.36	0.37	0.37
K	0.09	0.10	0.10	0.10	0.10	0.10	0.10	0.10	0.11	0.10	0.10	0.09	0.10	0.09
Total	17.42	17.43	17.45	17.31	17.45	17.45	17.46	17.46	17.46	17.45	17.44	17.43	17.43	17.44

Microprobe Analysis
of F-1296- garnet-E

Oxide Wt. %	GrtNPlg1	GrtNPlg2	GrtNPlg3	GrtNPlg4	GrtNPlg5	GrtNPlg6	GrtNPlg7	GrtNPlg2-1	GrtNPlg2-2	GrtNPlg2-3	GrtNPlg2-4	GrtNPlg2-5	GrtNPlg2-6	GrtNPlg2-7
SiO_2	38.1577	38.2932	38.1659	38.1146	38.0686	38.244	37.8355	37.9536	37.977	38.0978	38.0123	38.0781	37.9592	38.056
TiO_2	0.0171	0.0164	0.0282	0.0108	0.0156	0.0026	0.0129	0.0278	0.0288	0.0069	0.019	0.0431	0.0489	0.0565
Al_2O_3	21.564	21.5151	21.3876	21.6428	21.2794	21.7625	21.5215	21.3843	21.6988	21.578	21.243	21.2771	21.3302	21.3265
Cr_2O_3	0.0216	0.0966	0.0804	0.0588	0.1002	0.0504	0.0621	0.0133	0.0115	0.0558	0.0296	0.0622	0.0492	0.0565
MgO	4.2363	4.2206	4.3227	4.3368	4.2604	4.3575	4.2985	4.3893	4.3698	4.3977	4.3431	4.2977	4.3376	4.3598
CaO	7.5475	7.6561	7.6593	7.4596	7.6256	7.4221	7.5085	7.8709	7.9907	7.9407	8.1439	8.2339	8.3176	8.2725
MnO	0.9072	0.8896	0.936	0.9052	0.9281	0.9338	0.9221	0.8856	0.9147	0.8543	0.8494	0.837	0.8417	0.8639
FeO	28.1029	28.2113	28.1096	28.2298	28.0503	28.1695	28.1968	27.5732	27.5218	27.5624	27.8408	27.4334	27.5047	27.6543
Na_2O	0.0035	0.0007	0.0067	0.0051	0.006	0	0	0.0085	0.0104	0	0.0083	0.0007	0.0108	0.0088
Total	100.5579	100.8996	100.6963	100.7636	100.3341	100.9423	100.3579	100.1064	100.5235	100.4936	100.4894	100.2633	100.4	100.6546
Cation based on 12 oxygens														
Si	2.99	2.992	2.989	2.981	2.992	2.984	2.975	2.985	2.974	2.983	2.984	2.991	2.98	2.981
Ti	0.001	0.001	0.002	0.001	0.001	0	0.001	0.002	0.002	0	0.001	0.003	0.003	0.003
Al	1.991	1.981	1.974	1.995	1.971	2.001	1.994	1.982	2.003	1.991	1.966	1.969	1.973	1.969
Cr	0.001	0.006	0.005	0.004	0.006	0.003	0.004	0.001	0.001	0.003	0.002	0.004	0.003	0.003
Mg	0.495	0.492	0.505	0.506	0.499	0.507	0.504	0.515	0.51	0.513	0.508	0.503	0.508	0.509
Ca	0.634	0.641	0.643	0.625	0.642	0.62	0.633	0.663	0.67	0.666	0.685	0.693	0.7	0.694
Mn	0.06	0.059	0.062	0.06	0.062	0.062	0.061	0.059	0.061	0.057	0.056	0.056	0.056	0.057
Fe	1.841	1.843	1.841	1.847	1.844	1.838	1.854	1.814	1.802	1.805	1.828	1.802	1.806	1.812
Na	0.001	0	0.001	0.001	0.001	0	0	0.001	0.002	0	0.001	0	0.002	0.001
Total	8.013	8.014	8.021	8.019	8.019	8.014	8.025	8.022	8.024	8.019	8.032	8.02	8.03	8.03

Microprobe Analysis
of F-1296- garnet-E

Oxide Wt. %	GrttoAmp1	GrttoAmp2	GrttoAmp3	GrttoAmp4	GrttoAmp5	GrttoAmp6	GrttoAmp7	GrttoAmp8	GrttoAmp9	GrttoAmp10	GrttoAmp11	GrtCPlgInc1	GrtCPlgInc2	GrtCPlgInc3
SiO_2	37.9934	37.8732	37.936	37.9322	38.1033	37.9929	37.7875	37.8771	38.1287	37.9489	37.8167	38.0927	38.0577	37.7489
TiO_2	0.0473	0.0353	0.0389	0.0486	0.0327	0.0337	0.0308	0.0427	0.034	0.0081	0.0187	0.0284	0.0182	0.0362
Al_2O_3	21.458	21.3938	21.4128	21.4764	21.6658	21.4693	21.4989	21.3911	21.4491	21.5049	21.3722	21.4752	21.6843	21.3444
Cr_2O_3	0.0455	0.0386	0.051	0.0447	0.0634	0.0362	0.0561	0.0416	0.0632	0.045	0.042	0.0021	0.0084	0.0492
MgO	4.5754	4.6417	4.7344	4.6465	4.668	4.6281	4.6402	4.6411	4.6075	4.5508	4.2666	4.5267	4.6607	4.6616
CaO	7.8618	7.8549	7.848	7.938	7.8195	7.6587	7.6428	7.4476	7.1178	6.8017	6.649	7.1358	7.0964	7.1972
MnO	0.7562	0.7461	0.8165	0.824	0.792	0.8662	0.8882	0.9222	0.9549	1.0107	1.0862	0.9387	0.9684	0.983
FeO	27.8505	27.8118	27.5304	27.5809	27.3245	27.7415	27.6283	27.8967	28.2937	28.4926	28.9768	27.9914	28.1435	28.2298
Na_2O	0	0	0.0122	0.0152	0.0018	0	0.0067	0.0085	0.0173	0	0.0049	0.0048	0	0.0037
Total	100.5881	100.3954	100.3801	100.5065	100.471	100.4266	100.1793	100.2686	100.6663	100.3626	100.2331	100.1958	100.6375	100.254
Cation based on 12 oxygens														
Si	2.976	2.973	2.975	2.972	2.979	2.978	2.97	2.977	2.985	2.982	2.983	2.992	2.977	2.971
Ti	0.003	0.002	0.002	0.003	0.002	0.002	0.002	0.003	0.002	0	0.001	0.002	0.001	0.002
Al	1.981	1.979	1.979	1.983	1.996	1.984	1.992	1.981	1.979	1.991	1.987	1.988	1.999	1.98
Cr	0.003	0.002	0.003	0.003	0.004	0.002	0.003	0.003	0.004	0.003	0.003	0	0.001	0.003
Mg	0.534	0.543	0.553	0.543	0.544	0.541	0.544	0.544	0.538	0.533	0.502	0.53	0.544	0.547
Ca	0.66	0.661	0.659	0.666	0.655	0.643	0.644	0.627	0.597	0.573	0.562	0.6	0.595	0.607
Mn	0.05	0.05	0.054	0.055	0.052	0.058	0.059	0.061	0.063	0.067	0.073	0.062	0.064	0.066
Fe	1.824	1.826	1.805	1.807	1.787	1.819	1.816	1.833	1.852	1.872	1.911	1.838	1.841	1.858
Na	0	0	0.002	0.002	0	0	0.001	0.001	0.003	0	0.001	0.001	0	0.001
Total	8.03	8.035	8.033	8.034	8.019	8.027	8.031	8.03	8.023	8.021	8.022	8.013	8.022	8.035

Microprobe Analysis
of F-1296- garnet-E

Oxide Wt. %	GrtCPlgInc4	GrtCPlgInc5	GrtCPlgInc6	GrtCPlgInc7	GrtCPlgInc8	GrtCPlgInc9	GrtCPlgInc10	PlgNGrt1	PlgNGrt2	PlgNGrt3	PlgNGrt4	PlgNGrt5	PlgNGrt6	PlgNGrt7
SiO_2	38.1106	34.195	38.2368	38.1773	38.1972	38.2162	38.2921	38.092	38.0536	37.962	37.9153	38.1719	38.227	38.0971
TiO_2	0.0608	0.0592	0.0329	0.0334	0.018	0.0207	0.0193	0.0323	0.0309	0.0422	0.035	0.0655	0.038	0.0574
Al_2O_3	21.4157	20.2947	21.5765	21.5926	21.6103	21.5694	21.748	21.5519	21.3002	21.3992	21.3853	21.2615	21.3517	21.3918
Cr_2O_3	0.043	0.0332	0.0388	0.0339	0.0258	0.0234	0.0541	0.056	0.0615	0.0273	0.0394	0.0339	0.0457	0.0342
MgO	4.5979	3.7972	4.6081	4.5966	4.6256	4.665	4.685	4.3831	4.3749	4.387	4.4181	4.3144	4.3551	4.303
CaO	7.442	6.2761	7.4721	7.4172	7.1699	7.2522	7.0963	7.7934	8.1321	8.2595	8.2582	8.2819	8.2166	8.2372
MnO	0.9417	0.7625	0.9596	0.9355	0.91	0.9583	0.9388	0.9088	0.9173	0.8688	0.8519	0.8253	0.793	0.786
FeO	27.9754	29.9143	27.9857	28.1836	28.205	27.9943	28.0022	27.7721	27.8182	27.5409	27.6815	27.8135	27.6529	27.7808
Na_2O	0.0002	0	0	0.003	0.0097	0	0.0048	0.0106	0.0116	0.0134	0.0146	0.0081	0.0028	0.009
Total	100.5872	95.3322	100.9105	100.9732	100.7715	100.6994	100.8405	100.6002	100.7001	100.5003	100.5992	100.7759	100.6827	100.6965
Cation based on 12 oxygens														
Si	2.984	2.881	2.983	2.979	2.984	2.986	2.985	2.982	2.981	2.977	2.973	2.987	2.99	2.982
Ti	0.004	0.004	0.002	0.002	0.001	0.001	0.001	0.002	0.002	0.002	0.002	0.004	0.002	0.003
Al	1.976	2.015	1.984	1.986	1.99	1.986	1.998	1.988	1.967	1.978	1.976	1.961	1.968	1.974
Cr	0.003	0.002	0.002	0.002	0.002	0.001	0.003	0.003	0.004	0.002	0.002	0.002	0.003	0.002
Mg	0.537	0.477	0.536	0.535	0.539	0.543	0.544	0.512	0.511	0.513	0.516	0.503	0.508	0.502
Ca	0.624	0.566	0.625	0.62	0.6	0.607	0.593	0.654	0.683	0.694	0.694	0.694	0.689	0.691
Mn	0.062	0.054	0.063	0.062	0.06	0.063	0.062	0.06	0.061	0.058	0.057	0.055	0.053	0.052
Fe	1.832	2.108	1.826	1.839	1.843	1.829	1.826	1.818	1.823	1.806	1.815	1.82	1.809	1.819
Na	0	0	0	0	0.001	0	0.001	0.002	0.002	0.002	0.002	0.001	0	0.001
Total	8.023	8.107	8.022	8.025	8.02	8.019	8.013	8.021	8.032	8.032	8.037	8.028	8.022	8.027

Microprobe Analysis
of F-1296- garnet-E

Oxide Wt. %	PlgNGrt8	PlgNGrt9	PlgNGrt10	GrtCtraverse1	GrtCtraverse2	GrtCtraverse3	GrtCtraverse4	GrtCtraverse5	GrtCtraverse6	GrtCtraverse7	GrtCtraverse8	GrtCtraverse9	GrtCtraverse10	GrtCtraverse11
SiO_2	37.839	37.9339	37.8601	38.1444	38.2836	38.2729	38.0048	38.2701	37.9007	38.1564	37.8447	38.2898	37.9565	37.9711
TiO_2	0.0519	0.0508	0.0524	0.024	0.0212	0.045	0.0543	0.1129	0.0587	0.0658	0.1946	0.0713	0.0477	0.0316
Al_2O_3	21.348	21.3933	21.4229	21.6378	21.664	21.5477	21.643	21.4715	21.3851	21.4972	21.5723	21.352	21.3838	21.426
Cr_2O_3	0.0415	0.0445	0.036	0	0	0	0	0	0	0	0	0	0	0
MgO	4.3606	4.3515	4.3664	4.1347	4.5939	4.6445	4.7235	4.6629	4.5581	4.5962	4.5359	4.4893	4.3219	4.3334
CaO	8.2233	8.0621	8.0485	7.0429	7.5655	7.7547	7.8844	7.8472	7.867	7.7431	7.73	7.8081	7.7354	7.6079
MnO	0.8074	0.7575	0.7963	1.0323	0.905	0.84	0.8252	0.8121	0.7845	0.7635	0.7572	0.6976	0.7102	0.6939
FeO	27.9395	27.7484	27.8255	28.6748	27.9802	27.6066	27.5865	27.701	27.8064	27.792	28.0713	28.134	28.2327	28.2794
Na_2O	0.0097	0.0141	0.0069	0.0108	0.0028	0.0083	0.008	0.0055	0.0014	0	0	0	0.0164	0
Total	100.621	100.3562	100.4152	100.7016	101.0162	100.7199	100.7297	100.8831	100.3619	100.6141	100.7059	100.8421	100.4045	100.3433
Cation based on 12 oxygens														
Si	2.969	2.979	2.973	2.989	2.983	2.987	2.969	2.984	2.976	2.984	2.963	2.991	2.982	2.984
Ti	0.003	0.003	0.003	0.001	0.001	0.003	0.003	0.007	0.003	0.004	0.011	0.004	0.003	0.002
Al	1.974	1.98	1.983	1.998	1.989	1.982	1.993	1.973	1.979	1.981	1.99	1.966	1.98	1.984
Cr	0.003	0.003	0.002	0	0	0	0	0	0	0	0	0	0	0
Mg	0.51	0.509	0.511	0.483	0.534	0.54	0.55	0.542	0.534	0.536	0.529	0.523	0.506	0.508
Ca	0.691	0.678	0.677	0.591	0.632	0.648	0.66	0.656	0.662	0.649	0.648	0.654	0.651	0.64
Mn	0.054	0.05	0.053	0.069	0.06	0.056	0.055	0.054	0.052	0.051	0.05	0.046	0.047	0.046
Fe	1.834	1.822	1.828	1.879	1.823	1.802	1.802	1.806	1.826	1.818	1.838	1.838	1.855	1.858
Na	0.001	0.002	0.001	0.002	0	0.001	0.001	0.001	0	0	0	0	0.002	0
Total	8.04	8.028	8.032	8.012	8.022	8.02	8.032	8.023	8.031	8.022	8.031	8.022	8.027	8.022

Microprobe Analysis
of F-1296- garnet-E

Oxide Wt. %	GrtCtraverse12	GrtCtraverse13	GrtCtraverse14	GrtCtraverse15	GrtCtraverse16	GrtCtraverse17	GrtCtraverse18	GrtCtraverse19	GrtCtraverse20	GrtCtraverse21	GrtCtraverse22	GrtCtraverse23	GrtCtraverse24	GrtCtraverse25
SiO_2	37.9154	37.973	37.8108	37.8409	38.0015	38.0408	37.572	37.9913	37.751	35.8378	37.8254	37.9801	37.8463	38.0037
TiO_2	0.0732	0.0423	0.0447	0.0383	0.0346	0.0606	0.6342	0.1046	0.0344	0.3055	0.0524	0.0507	0.0189	0.0145
Al_2O_3	21.2173	21.2844	21.2031	21.1835	21.3384	21.0559	21.2177	21.2132	21.2194	21.0213	21.3226	21.298	21.0489	21.2503
Cr_2O_3	0	0.0188	0	0	0.0006	0	0	0	0	0	0.0064	0	0.0292	0
MgO	4.2694	4.3275	4.1883	4.1449	4.1117	4.0685	3.9601	4.0992	4.0391	3.8038	4.0812	3.922	3.9112	3.8948
CaO	7.601	7.5904	7.6657	7.6584	7.6154	7.6476	7.4807	7.7007	7.7458	7.2426	7.6639	7.6682	7.7427	7.6141
MnO	0.6517	0.6249	0.6466	0.5865	0.615	0.5843	0.5654	0.6032	0.5722	0.5143	0.5586	0.5665	0.5318	0.5249
FeO	28.5374	28.6323	28.6918	28.9634	28.9612	28.7849	28.7938	29.0782	28.8767	29.9562	29.2125	28.9151	29.231	29.1216
Na_2O	0.0091	0.0084	0.0024	0	0.0154	0.0063	0.0039	0.0224	0.0052	0.0071	0.0137	0	0.0035	0
Total	100.2744	100.5019	100.2535	100.4159	100.6937	100.2488	100.2278	100.8128	100.2439	98.6886	100.7367	100.4005	100.3636	100.4239
Cation based on 12 oxygens														
Si	2.986	2.984	2.982	2.982	2.984	2.999	2.964	2.983	2.98	2.901	2.974	2.99	2.988	2.993
Ti	0.004	0.003	0.003	0.002	0.002	0.004	0.038	0.006	0.002	0.019	0.003	0.003	0.001	0.001
Al	1.969	1.971	1.971	1.967	1.975	1.956	1.973	1.963	1.974	2.006	1.976	1.976	1.959	1.973
Cr	0	0.001	0	0	0	0	0	0	0	0	0	0	0.001	0
Mg	0.501	0.507	0.492	0.487	0.481	0.478	0.466	0.48	0.475	0.459	0.478	0.46	0.46	0.457
Ca	0.641	0.639	0.648	0.647	0.641	0.646	0.632	0.648	0.655	0.628	0.646	0.647	0.655	0.643
Mn	0.043	0.042	0.043	0.039	0.041	0.039	0.038	0.04	0.038	0.035	0.037	0.038	0.036	0.035
Fe	1.879	1.882	1.892	1.909	1.902	1.898	1.9	1.909	1.906	2.028	1.921	1.904	1.93	1.918
Na	0.001	0.001	0	0	0.002	0.001	0.001	0.003	0.001	0.001	0.002	0	0.001	0
Total	8.026	8.028	8.031	8.032	8.028	8.02	8.012	8.032	8.032	8.078	8.036	8.019	8.031	8.02

Microprobe Analysis
of F-1296- garnet-E

Oxide Wt. %	GrtCtraverse26	GrtCtraverse27	GrtCtraverse28	GrtCtraverse29	GrtCtraverse30	GrtCtraverse31	GrtCtraverse32	GrtCtraverse33	GrtCtraverse34	GrtCtraverse35	GrtCtraverse36	GrtCtraverse37	GrtCtraverse38	GrtCtraverse39
SiO_2	37.6316	36.2915	37.8663	37.9905	37.7361	37.6923	37.7217	37.0298	37.6823	37.7615	38.0589	37.6725	38.1278	38.0216
TiO_2	0.0392	0.0555	0.0648	0.0624	0.0474	0.0793	0.0348	0.0378	0.0313	0.0494	0.0309	0.0176	0.0514	0.054
Al_2O_3	21.1551	21.1113	21.2787	21.1796	21.222	21.2611	21.3616	21.377	21.0372	21.2407	21.486	21.2529	21.3006	21.2409
Cr_2O_3	0	0	0.0095	0	0.007	0	0.0027	0	0	0	0	0	0	0.023
MgO	3.865	3.7073	3.947	3.8885	3.8277	3.7782	3.8986	3.5642	3.843	3.8024	3.7961	3.8163	3.8107	3.8284
CaO	7.8313	7.1236	7.6763	7.8384	7.8164	7.818	7.8621	7.1321	7.8381	7.8332	7.8564	7.8321	7.9012	7.726
MnO	0.5383	0.4954	0.5016	0.5067	0.5004	0.5053	0.4789	0.4581	0.4841	0.4516	0.5126	0.4906	0.4936	0.4921
FeO	29.165	30.239	29.353	29.1056	29.0379	29.1785	29.2561	29.5349	29.0788	29.2571	29.289	29.2931	29.212	29.3806
Na_2O	0.0074	0.0028	0.02	0.0102	0.0014	0.0102	0.0119	0.006	0.0137	0	0	0.0018	0.014	0.0084
Total	100.2329	99.0265	100.7172	100.5818	100.1963	100.3229	100.6283	99.1399	100.0085	100.3959	101.0298	100.3769	100.9113	100.775
Cation based on 12 oxygens														
Si	2.976	2.926	2.979	2.99	2.982	2.977	2.971	2.963	2.985	2.98	2.982	2.975	2.99	2.988
Ti	0.002	0.003	0.004	0.004	0.003	0.005	0.002	0.002	0.002	0.003	0.002	0.001	0.003	0.003
Al	1.972	2.006	1.973	1.964	1.976	1.979	1.983	2.016	1.964	1.976	1.984	1.978	1.969	1.968
Cr	0	0	0	0	0	0	0	0	0	0	0	0	0	0.001
Mg	0.456	0.446	0.463	0.456	0.451	0.445	0.458	0.425	0.454	0.447	0.443	0.449	0.446	0.449
Ca	0.664	0.615	0.647	0.661	0.662	0.662	0.663	0.611	0.665	0.662	0.66	0.663	0.664	0.651
Mn	0.036	0.034	0.033	0.034	0.033	0.034	0.032	0.031	0.032	0.03	0.034	0.033	0.033	0.033
Fe	1.929	2.039	1.931	1.915	1.919	1.927	1.927	1.977	1.927	1.931	1.919	1.935	1.916	1.931
Na	0.001	0	0.003	0.002	0	0.002	0.002	0.001	0.002	0	0	0	0.002	0.001
Total	8.036	8.068	8.033	8.025	8.027	8.03	8.037	8.027	8.032	8.029	8.024	8.035	8.023	8.025

Microprobe Analysis
of F-1296- garnet-E

Oxide Wt. %	GrtCtraverse40	GrtCtraverse41	GrtCtraverse42	GrtCtraverse43	GrtCtraverse44	GrtCtraverse45	GrtCtraverse46	GrtCtraverse47	GrtCtraverse48	GrtCtraverse49	GrtCtraverse50	GrtCtraverse51	GrtCtraverse52	GrtCtraverse53
SiO_2	37.9324	38.0794	37.6127	37.8275	37.8958	37.8443	37.9048	37.8488	37.9391	37.9071	38.007	37.8163	37.7718	38.1082
TiO_2	0.0489	0.0315	0.0505	0.0461	0.0353	0.0613	0.0492	0.0571	0.051	0.1859	0.1351	0.0572	0.0477	0.0501
Al_2O_3	21.2249	21.3257	21.2589	20.9773	21.2528	21.216	21.2313	21.2768	21.3316	21.5147	21.5353	21.2182	21.2203	21.4452
Cr_2O_3	0.0127	0.0072	0.0089	0	0.0144	0.0087	0.0358	0	0	0	0	0	0	0
MgO	3.808	3.8235	3.8734	3.9573	3.8402	4.0101	4.0036	4.0666	3.952	4.0593	4.0583	4.1499	4.0673	4.1608
CaO	7.9471	7.8851	7.8271	7.8531	7.8108	7.8455	7.8816	7.7747	7.8424	7.8071	7.9028	8.0657	8.1317	8.2353
MnO	0.5014	0.4895	0.514	0.52	0.5554	0.5722	0.5629	0.5601	0.5938	0.6128	0.595	0.6159	0.6868	0.7618
FeO	29.0967	29.2795	29.3702	29.2174	28.9165	29.0763	29.0461	28.8124	28.6517	28.8358	28.445	28.7386	28.3385	28.0519
Na_2O	0.0007	0.0119	0.0021	0	0.0098	0.0014	0.0004	0.0007	0	0.0031	0.0014	0.0262	0.0003	0
Total	100.5728	100.9332	100.5177	100.3986	100.3311	100.6357	100.7155	100.3971	100.3615	100.9258	100.68	100.6879	100.2643	100.8132
Cation based on 12 oxygens														
Si	2.986	2.987	2.968	2.986	2.988	2.978	2.98	2.981	2.987	2.97	2.979	2.973	2.978	2.982
Ti	0.003	0.002	0.003	0.003	0.002	0.004	0.003	0.003	0.003	0.011	0.008	0.003	0.003	0.003
Al	1.969	1.972	1.977	1.952	1.975	1.968	1.967	1.975	1.979	1.986	1.989	1.966	1.972	1.978
Cr	0.001	0	0	0	0.001	0	0.001	0	0	0	0	0	0	0
Mg	0.447	0.447	0.456	0.466	0.451	0.47	0.469	0.477	0.464	0.474	0.474	0.486	0.478	0.485
Ca	0.67	0.663	0.662	0.664	0.66	0.662	0.664	0.656	0.662	0.655	0.664	0.679	0.687	0.691
Mn	0.033	0.033	0.034	0.035	0.037	0.038	0.037	0.037	0.04	0.041	0.04	0.041	0.046	0.05
Fe	1.916	1.921	1.938	1.929	1.907	1.914	1.91	1.898	1.886	1.889	1.865	1.889	1.869	1.836
Na	0	0.002	0	0	0.001	0	0	0	0	0	0	0.004	0	0
Total	8.026	8.026	8.04	8.035	8.023	8.034	8.033	8.028	8.02	8.027	8.018	8.043	8.033	8.026

Microprobe Analysis
of F-1296- garnet-E

Oxide Wt. %	GrtCtraverse54	GrtCtraverse55	Grttraverse2-1	Grttraverse2-2	Grttraverse2-3	Grttraverse2-4	Grttraverse2-5	Grttraverse2-6	Grttraverse2-7	Grttraverse2-8	Grttraverse2-9	Grttraverse2-10	Grttraverse2-11	Grttraverse2-12
SiO_2	37.9589	37.8966	37.8182	38.0333	37.9937	38.1756	37.8629	37.8394	37.9521	38.0316	38.2066	37.9312	37.972	38.0342
TiO_2	0.0371	0.0435	0.0558	0.0404	0.0479	0.0701	0.0558	0.0426	0.1163	0.0703	0.034	0.0549	0.0538	0.0625
Al_2O_3	21.3019	21.1901	21.4116	21.3011	21.3015	21.378	21.4713	21.3528	21.2793	21.3712	21.3875	21.2239	21.2455	21.3547
Cr_2O_3	0.0048	0.031	0	0	0	0	0	0	0.0095	0.0108	0	0.0078	0	0
MgO	4.2611	4.2615	4.2881	4.3776	4.3121	4.4338	4.4293	4.4748	4.3829	4.463	4.4382	4.4001	4.412	4.4278
CaO	8.2925	8.068	8.205	8.2551	8.1968	8.1255	8.176	8.0156	8.0263	7.8939	7.9768	7.8473	7.7728	7.7789
MnO	0.842	0.876	0.8884	0.8641	0.8349	0.7983	0.7622	0.7865	0.7808	0.762	0.7635	0.7785	0.7794	0.775
FeO	27.6185	27.7783	27.6206	27.3734	27.4804	27.9047	27.6785	27.7695	27.4932	27.6715	27.9554	28.1274	27.95	28.2697
Na_2O	0	0.0014	0.0041	0	0.0031	0.0142	0	0	0.0079	0.0069	0	0	0.0035	0
Total	100.3168	100.1463	100.2918	100.2451	100.1703	100.9001	100.4361	100.2813	100.0484	100.2811	100.7619	100.3711	100.1888	100.7028
Cation based on 12 oxygens														
Si	2.983	2.986	2.974	2.987	2.987	2.983	2.971	2.975	2.986	2.986	2.988	2.982	2.987	2.98
Ti	0.002	0.003	0.003	0.002	0.003	0.004	0.003	0.003	0.007	0.004	0.002	0.003	0.003	0.004
Al	1.973	1.968	1.984	1.972	1.974	1.969	1.986	1.978	1.973	1.977	1.971	1.967	1.97	1.972
Cr	0	0.001	0	0	0	0	0	0	0	0	0	0	0	0
Mg	0.499	0.501	0.503	0.513	0.505	0.516	0.518	0.524	0.514	0.522	0.517	0.516	0.517	0.517
Ca	0.698	0.681	0.691	0.695	0.691	0.68	0.687	0.675	0.677	0.664	0.668	0.661	0.655	0.653
Mn	0.056	0.058	0.059	0.057	0.056	0.053	0.051	0.052	0.052	0.051	0.051	0.052	0.052	0.051
Fe	1.815	1.83	1.816	1.798	1.807	1.823	1.816	1.826	1.809	1.817	1.828	1.849	1.839	1.852
Na	0	0	0.001	0	0	0.002	0	0	0.001	0.001	0	0	0.001	0
Total	8.028	8.027	8.031	8.024	8.023	8.03	8.033	8.033	8.02	8.022	8.025	8.031	8.025	8.03

Microprobe Analysis
of F-1296- garnet-E

Oxide Wt. %	Grttraverse2-13	Grttraverse2-14	Grttraverse2-15	Grttraverse2-16	Grttraverse2-17	Grttraverse2-18	Grttraverse2-19	Grttraverse2-20	Grttraverse2-21	Grttraverse2-22	Grttraverse2-23	Grttraverse2-24	Grttraverse2-25	Grttraverse2-26
SiO_2	38.1198	37.8483	37.8483	38.1007	38.0387	37.8468	38.0509	38.066	37.7973	37.9275	38.2046	38.0145	38.1821	38.0902
TiO_2	0.0566	0.0542	0.0632	0.0617	0.0222	0.0526	0.0533	0.0505	0.0484	0.0671	0.0489	0.0476	0.0355	0.0481
Al_2O_3	21.4531	21.3124	21.339	21.2471	21.4978	21.416	21.2933	21.2636	21.47	21.3987	21.2922	21.3317	21.163	21.3128
Cr_2O_3	0	0	0	0	0	0	0	0.0096	0	0	0	0	0	0
MgO	4.5078	4.451	4.407	4.4517	4.5145	4.4906	4.4741	4.4512	4.396	4.4488	4.4942	4.4313	4.4505	4.4542
CaO	7.8013	7.7668	7.6581	7.6667	7.6714	7.5594	7.6058	7.5498	7.4619	7.5536	7.5001	7.497	7.5838	7.5961
MnO	0.7864	0.7743	0.811	0.7701	0.7906	0.7882	0.7676	0.7503	0.7852	0.7644	0.7583	0.7584	0.741	0.7837
FeO	28.3972	28.243	28.3249	28.1472	28.1979	28.2686	28.2498	28.2813	28.5568	28.4743	28.2391	28.2798	28.3777	28.2982
Na_2O	0.0132	0.0028	0.0073	0.0035	0.001	0	0.0107	0.0128	0	0.0052	0.0132	0.0128	0	0.0003
Total	101.1353	100.4528	100.4586	100.4487	100.734	100.4223	100.5057	100.435	100.5156	100.6396	100.5506	100.373	100.5337	100.5836
Cation based on 12 oxygens														
Si	2.975	2.975	2.975	2.99	2.977	2.974	2.986	2.989	2.97	2.975	2.994	2.986	2.996	2.987
Ti	0.003	0.003	0.004	0.004	0.001	0.003	0.003	0.003	0.003	0.004	0.003	0.003	0.002	0.003
Al	1.973	1.974	1.977	1.965	1.983	1.983	1.969	1.968	1.988	1.978	1.966	1.975	1.957	1.97
Cr	0	0	0	0	0	0	0	0	0	0	0	0	0	0
Mg	0.524	0.521	0.516	0.521	0.527	0.526	0.523	0.521	0.515	0.52	0.525	0.519	0.521	0.521
Ca	0.652	0.654	0.645	0.645	0.643	0.636	0.639	0.635	0.628	0.635	0.63	0.631	0.637	0.638
Mn	0.052	0.052	0.054	0.051	0.052	0.052	0.051	0.05	0.052	0.051	0.05	0.05	0.049	0.052
Fe	1.853	1.856	1.862	1.847	1.846	1.857	1.854	1.857	1.877	1.868	1.851	1.858	1.862	1.856
Na	0.002	0	0.001	0.001	0	0	0.002	0.002	0	0.001	0.002	0.002	0	0
Total	8.036	8.035	8.034	8.024	8.03	8.032	8.027	8.025	8.033	8.032	8.021	8.024	8.024	8.026

Microprobe Analysis
of F-1296- garnet-E

Oxide Wt. %	Grttraverse2-27	Grttraverse2-28	Grttraverse2-29	Grttraverse2-30	Grttraverse2-31	Grttraverse2-32	Grttraverse2-33	Grttraverse2-34	Grttraverse2-35	Grttraverse2-36	Grttraverse2-37	Grttraverse2-38	Grttraverse2-39	Grttraverse2-40
SiO_2	38.1223	37.9474	38.1423	38.115	38.0407	37.9563	38.1549	37.9348	38.263	38.0863	38.1923	35.9877	38.2573	38.1393
TiO_2	0.0582	0.0726	0.0342	0.0549	0.0755	0.0371	0.1669	0.1076	0.037	0.0347	0.038	0.4115	0.0574	0.0582
Al_2O_3	21.518	21.4917	21.3013	21.4219	21.3721	21.5329	21.808	21.382	19.433	21.368	21.2344	21.5601	21.3681	21.3225
Cr_2O_3	0	0	0	0	0	0	0	0	0	0	0	0.0039	0	0.0044
MgO	4.4379	4.5184	4.526	4.4984	4.5199	4.5784	4.657	4.5511	4.0816	4.5266	4.4799	3.9729	4.6127	4.6027
CaO	7.5209	7.4864	7.5258	7.5656	7.6038	7.455	7.4529	7.7376	7.0615	7.8286	7.8096	6.6833	7.7871	7.9272
MnO	0.7695	0.7846	0.7726	0.7768	0.7546	0.768	0.7895	0.7978	0.7118	0.7765	0.8199	0.744	0.855	0.8027
FeO	28.337	28.2245	28.3017	28.3736	28.3208	28.2553	28.0713	28.394	25.5183	27.9326	27.767	28.7079	27.7765	27.9258
Na_2O	0.0066	0.008	0.0232	0.0066	0.0031	0	0.0121	0	0	0.0059	0.0131	0.014	0.0121	0.0235
Total	100.7704	100.5336	100.6271	100.8127	100.6904	100.583	101.1126	100.9048	95.1063	100.5592	100.3542	98.0853	100.7261	100.8061
Cation based on 12 oxygens														
Si	2.982	2.976	2.989	2.982	2.98	2.974	2.969	2.969	3.134	2.984	2.996	2.909	2.99	2.982
Ti	0.003	0.004	0.002	0.003	0.004	0.002	0.01	0.006	0.002	0.002	0.002	0.025	0.003	0.003
Al	1.984	1.986	1.967	1.975	1.973	1.989	2	1.972	1.876	1.973	1.963	2.054	1.968	1.965
Cr	0	0	0	0	0	0	0	0	0	0	0	0	0	0
Mg	0.518	0.528	0.529	0.525	0.528	0.535	0.54	0.531	0.498	0.529	0.524	0.479	0.537	0.536
Ca	0.63	0.629	0.632	0.634	0.638	0.626	0.621	0.649	0.62	0.657	0.656	0.579	0.652	0.664
Mn	0.051	0.052	0.051	0.051	0.05	0.051	0.052	0.053	0.049	0.052	0.054	0.051	0.057	0.053
Fe	1.854	1.851	1.855	1.856	1.855	1.852	1.827	1.858	1.748	1.83	1.822	1.941	1.815	1.826
Na	0.001	0.001	0.004	0.001	0	0	0.002	0	0	0.001	0.002	0.002	0.002	0.004
Total	8.023	8.028	8.028	8.028	8.029	8.029	8.022	8.039	7.926	8.028	8.021	8.04	8.024	8.034

Microprobe Analysis
of F-1296- garnet-E

Oxide Wt. %	Grttraverse2-41	Grttraverse2-42	Grttraverse2-43	Grttraverse2-44	Grttraverse2-45	Grttraverse2-46	Grttraverse2-47	Grttraverse2-48	Grttraverse2-49	Grttraverse2-50	Grttraverse2-51	Grttraverse2-52	Grttraverse2-53	Grttraverse2-54
SiO_2	38.0564	38.1827	38.0313	38.2337	38.2118	38.1713	33.9695	38.1781	38.0767	33.4809	38.0379	38.2358	38.0489	38.1354
TiO_2	0.0482	0.0385	0.0411	0.0607	0.0215	0.0605	0.1473	0.0425	0.0451	0.0896	0.0783	0.0493	0.094	0.0599
Al_2O_3	21.3876	21.2297	21.329	21.3026	21.5849	21.3647	20.356	21.439	21.3108	22.2104	21.4313	21.4458	21.2923	21.4413
Cr_2O_3	0	0.0029	0	0	0	0	0.014	0	0	0	0	0	0	0
MgO	4.6256	4.5256	4.5988	4.6296	4.6099	4.6278	4.5279	4.661	4.6037	3.8629	4.7438	4.6129	4.7118	4.6841
CaO	7.8919	7.9817	7.9442	7.8355	7.6846	7.9036	5.6131	8.1299	8.0894	6.7084	8.0306	8.1925	8.2013	8.1589
MnO	0.7805	0.8369	0.8172	0.8634	0.8125	0.8191	0.604	0.8302	0.8207	0.6598	0.8175	0.8006	0.8063	0.8447
FeO	27.6566	27.6677	27.5868	27.7069	27.6718	27.7076	26.5195	27.6142	27.2296	29.905	27.3105	27.154	27.2172	27.1086
Na_2O	0.0204	0.0093	0.0097	0.0014	0.0024	0.0145	0.0309	0.0066	0.0045	0.0046	0.0059	0.0083	0	0
Total	100.4672	100.4749	100.3581	100.6338	100.5996	100.6689	91.7821	100.9014	100.1805	96.9217	100.4558	100.4991	100.3719	100.433
Cation based on 12 oxygens														
Si	2.982	2.993	2.983	2.991	2.986	2.985	2.919	2.979	2.988	2.773	2.978	2.989	2.982	2.984
Ti	0.003	0.002	0.002	0.004	0.001	0.004	0.01	0.002	0.003	0.006	0.005	0.003	0.006	0.004
Al	1.975	1.961	1.972	1.964	1.988	1.969	2.062	1.972	1.971	2.168	1.977	1.976	1.966	1.977
Cr	0	0	0	0	0	0	0.001	0	0	0	0	0	0	0
Mg	0.54	0.529	0.538	0.54	0.537	0.54	0.58	0.542	0.539	0.477	0.554	0.538	0.55	0.546
Ca	0.663	0.67	0.668	0.657	0.643	0.662	0.517	0.68	0.68	0.595	0.674	0.686	0.689	0.684
Mn	0.052	0.056	0.054	0.057	0.054	0.054	0.044	0.055	0.055	0.046	0.054	0.053	0.054	0.056
Fe	1.812	1.813	1.81	1.812	1.809	1.812	1.906	1.802	1.787	2.071	1.788	1.775	1.784	1.774
Na	0.003	0.001	0.001	0	0	0.002	0.005	0.001	0.001	0.001	0.001	0.001	0	0
Total	8.029	8.025	8.029	8.024	8.019	8.028	8.043	8.033	8.024	8.138	8.03	8.021	8.03	8.024

Microprobe Analysis
of F-1296- garnet-E

Oxide Wt. %	Grttraverse2-55	Grttraverse2-56	Grttraverse2-57	Grttraverse2-58	Grttraverse2-59	Grttraverse2-60	Grttraverse2-61	Grttraverse2-62
SiO_2	37.9773	38.2051	37.9948	37.7988	38.0598	37.886	37.7172	37.6378
TiO_2	0.0482	0.0504	0.0477	0.0349	0.0351	0.0156	0.0454	0.0375
Al_2O_3	21.3142	21.3515	21.0762	21.3556	21.3109	21.3922	21.4169	21.356
Cr_2O_3	0.0156	0	0	0	0	0	0	0.0108
MgO	4.5738	4.6464	4.5566	4.4246	4.3131	4.3145	4.2468	4.2935
CaO	8.1133	8.0578	7.831	7.5032	7.2498	7.4136	7.4893	7.5591
MnO	0.8343	0.8794	0.892	0.9876	1.0232	1.0049	1.0179	1.0113
FeO	27.3407	27.6104	27.7878	28.2049	28.4479	28.108	28.3049	28.2726
Na_2O	0	0.0052	0.0062	0.0094	0.0052	0	0	0.009
Total	100.2174	100.8062	100.1922	100.319	100.445	100.1349	100.2385	100.1876
Cation based on 12 oxygens								
Si	2.982	2.984	2.99	2.975	2.991	2.984	2.973	2.969
Ti	0.003	0.003	0.003	0.002	0.002	0.001	0.003	0.002
Al	1.973	1.966	1.955	1.981	1.974	1.986	1.989	1.986
Cr	0.001	0	0	0	0	0	0	0
Mg	0.535	0.541	0.535	0.519	0.505	0.507	0.499	0.505
Ca	0.683	0.674	0.66	0.633	0.61	0.626	0.632	0.639
Mn	0.055	0.058	0.059	0.066	0.068	0.067	0.068	0.068
Fe	1.796	1.804	1.829	1.856	1.87	1.852	1.866	1.865
Na	0	0.001	0.001	0.001	0.001	0	0	0.001
Total	8.028	8.031	8.031	8.033	8.021	8.022	8.03	8.036

Microprobe Analysis
of F-1296- Feldspar in
or near garnet-C

Oxide Wt. %	PlgNGrt	PlgNGrt	PlgNGrt	PlgNGrt	PlgNGrt	PlgNGrt	PlgNGrt	PlgNGrt	PlgNGrt	PlgNGrt	PlgNGrt	PlgNGrt	PlgNGrt2-1	PlgNGrt2-2
SiO_2	55.1948	54.9681	55.9809	55.6664	55.6673	55.7181	55.8832	55.5512	55.4912	55.7501	55.0713	54.8946	57.9611	58.0554
Al_2O_3	28.6956	28.6981	28.369	28.1828	28.0668	28.2982	28.3824	28.1573	28.1183	28.344	28.0913	28.101	26.9234	26.7286
CaO	10.6029	10.3901	10.1427	9.8882	10.0176	9.9387	9.9974	10.0604	10.0535	10.0002	10.3278	10.2422	8.5353	8.3706
FeO	0.0807	0.0537	0.0218	0.0321	0.0184	0.0264	0.0538	0.0283	0.0486	0.0611	0.0934	0.1792	0.041	0.0158
Na_2O	5.3834	5.2913	5.3889	5.663	5.6283	5.775	5.6606	5.4933	5.7131	5.6899	5.4795	5.5	6.5238	6.5565
K_2O	0.0915	0.0878	0.0949	0.1008	0.0801	0.0949	0.0998	0.1028	0.0948	0.1136	0.0878	0.0927	0.1392	0.1365
Total	100.0489	99.4891	99.9981	99.5335	99.4784	99.8512	100.0772	99.3934	99.5196	99.9589	99.1511	99.0098	100.1239	99.8633
Total	100.0489	99.4891	99.9981	99.5335	99.4784	99.8512	100.0772	99.3934	99.5196	99.9589	99.1511	99.0098	100.1239	99.8633
Cations based on 8 Oxygens														
Si	2.483	2.484	2.512	2.511	2.513	2.507	2.508	2.51	2.507	2.506	2.499	2.495	2.589	2.598
Al	1.521	1.528	1.5	1.498	1.493	1.501	1.501	1.499	1.497	1.502	1.502	1.506	1.417	1.41
Ca	0.511	0.503	0.488	0.478	0.485	0.479	0.481	0.487	0.487	0.482	0.502	0.499	0.408	0.401
Fe	0.003	0.002	0.001	0.001	0.001	0.001	0.002	0.001	0.002	0.002	0.004	0.007	0.002	0.001
Na	0.47	0.464	0.469	0.495	0.493	0.504	0.493	0.481	0.5	0.496	0.482	0.485	0.565	0.569
K	0.005	0.005	0.005	0.006	0.005	0.005	0.006	0.006	0.005	0.007	0.005	0.005	0.008	0.008
Total	4.994	4.986	4.975	4.99	4.989	4.997	4.99	4.984	4.998	4.994	4.994	4.997	4.989	4.986

Microprobe Analysis
of F-1296- Feldspar in
or near garnet-C

Oxide Wt. %	PlgNGrt2-3	PlgNGrt2-4	PlgNGrt2-5	PlgNGrt2-6	PlgGGrt3-1	PlgGGrt3-2	PlgGGrt3-3	PlgGGrt3-4	PlgGGrt3-5	PlgGGrt3-6	PlgGGrt3-7	PlgGGrt3-8	PlgGGrt3-9	PlgGGrt3-10
SiO_2	58.8783	58.979	58.0771	56.8652	56.1948	56.269	55.9625	55.5598	56.0751	55.9739	56.3619	56.4108	56.24	56.4214
Al_2O_3	26.4261	26.0814	26.4853	27.1675	28.1726	28.1839	28.5461	28.3012	28.3592	27.8392	27.8947	27.7698	27.8276	27.7188
CaO	7.8811	7.601	8.5011	8.9909	10.0446	9.9107	10.2344	10.1871	9.9083	9.715	9.8555	9.6701	9.8386	9.8791
FeO	0.0455	0.038	0.0487	0.0428	0.081	0.0763	0.1146	0.0979	0.1294	0.0529	0.0826	0.1222	0.0762	0.0781
Na_2O	6.8348	7.0187	6.5244	6.279	5.7081	5.7736	5.5353	5.5726	5.7444	5.8854	5.9692	5.9904	5.857	5.8577
K_2O	0.1601	0.1575	0.122	0.1299	0.1018	0.0955	0.0981	0.1096	0.1348	0.115	0.1204	0.1259	0.098	0.1348
Total	100.226	99.8756	99.7586	99.4753	100.3029	100.3089	100.4911	99.8283	100.3511	99.5813	100.2843	100.0892	99.9373	100.0898
Total	100.226	99.8756	99.7586	99.4753	100.3029	100.3089	100.4911	99.8283	100.3511	99.5813	100.2843	100.0892	99.9373	100.0898
Cations based on 8 Oxygens														
Si	2.621	2.634	2.602	2.562	2.517	2.519	2.503	2.502	2.511	2.524	2.526	2.532	2.527	2.532
Al	1.387	1.373	1.399	1.442	1.487	1.487	1.505	1.502	1.497	1.48	1.473	1.469	1.474	1.466
Ca	0.376	0.364	0.408	0.434	0.482	0.475	0.49	0.492	0.475	0.469	0.473	0.465	0.474	0.475
Fe	0.002	0.001	0.002	0.002	0.003	0.003	0.004	0.004	0.005	0.002	0.003	0.005	0.003	0.003
Na	0.59	0.608	0.567	0.548	0.496	0.501	0.48	0.487	0.499	0.515	0.519	0.521	0.51	0.51
K	0.009	0.009	0.007	0.007	0.006	0.005	0.006	0.006	0.008	0.007	0.007	0.007	0.006	0.008
Total	4.985	4.988	4.985	4.995	4.99	4.991	4.988	4.993	4.994	4.997	5.001	4.998	4.994	4.994

Microprobe Analysis
of F-1296- Feldspar in
or near garnet-C

Oxide Wt. %	GrtNPlg2-1	GrtNPlg2-2	GrtNPlg2-3	GrtNPlg2-4	GrtNPlg2-5	GrtNPlg2-6	GrtNPlg2-7	GrtNPlg2-8	GrtNPlg2-9	GrtNPlg3-1	GrtNPlg3-2	GrtNPlg3-3	GrtNPlg3-4	GrtNPlg3-5
SiO_2	55.7596	51.4099	54.4392	54.0909	53.2218	52.882	52.5325	53.041	52.1342	57.0729	57.7272	57.9358	57.9057	57.6668
Al_2O_3	28.2004	31.1006	29.408	29.3578	30.285	30.0172	30.5025	30.4511	30.5772	27.0724	26.7864	26.8361	26.8879	26.8245
CaO	10.1367	13.3015	11.301	11.4454	12.3083	12.3053	12.6149	12.6781	12.8425	8.6682	8.6376	8.636	8.627	8.7046
FeO	0.0935	0.0994	0.0627	0.0783	0.0602	0.0741	0.079	0.0942	0.138	0.0279	0.0331	0.0132	0	0.001
Na_2O	5.5914	3.6978	5.0562	5.1122	4.422	4.5226	4.3726	4.4607	4.2282	6.3785	6.781	6.7075	6.5127	6.6193
K_2O	0.1024	0.0823	0.0701	0.097	0.1076	0.0771	0.0528	0.0699	0.0627	0.1015	0.1269	0.1015	0.1188	0.1405
Total	99.884	99.6915	100.3372	100.1817	100.4049	99.8781	100.1543	100.795	99.9829	99.3214	100.0922	100.2301	100.052	99.9566
Total	99.884	99.6915	100.3372	100.1817	100.4049	99.8781	100.1543	100.795	99.9829	99.3214	100.0922	100.2301	100.052	99.9566
Cations based on 8 Oxygens														
Si	2.509	2.34	2.447	2.439	2.398	2.397	2.376	2.385	2.365	2.571	2.584	2.587	2.588	2.583
Al	1.495	1.668	1.558	1.56	1.608	1.603	1.626	1.613	1.635	1.438	1.413	1.412	1.416	1.416
Ca	0.489	0.649	0.544	0.553	0.594	0.598	0.611	0.611	0.624	0.418	0.414	0.413	0.413	0.418
Fe	0.004	0.004	0.002	0.003	0.002	0.003	0.003	0.004	0.005	0.001	0.001	0	0	0
Na	0.488	0.326	0.441	0.447	0.386	0.397	0.384	0.389	0.372	0.557	0.588	0.581	0.564	0.575
K	0.006	0.005	0.004	0.006	0.006	0.004	0.003	0.004	0.004	0.006	0.007	0.006	0.007	0.008
Total	4.99	4.992	4.996	5.007	4.995	5.002	5.004	5.005	5.005	4.991	5.008	5	4.989	5

Microprobe Analysis
of F-1296- Feldspar in
or near garnet-C

Oxide Wt. %	GrtNPlg3-6	GrtNPlg3-7	GrtNPlg3-8	GrtNPlg4-1	GrtNPlg4-2	GrtNPlg4-3	GrtNPlg4-4	GrtNPlg4-5	GrtNPlg5-1	GrtNPlg5-2	GrtNPlg5-3	GrtNPlg5-4	GrtNPlg5-5	GrtNPlg5-6
SiO_2	57.9636	57.7069	57.8143	54.6713	55.3615	55.1543	55.5809	55.3776	54.8493	55.7816	55.5515	55.6147	55.4707	55.3806
Al_2O_3	26.9219	27.1406	27.2581	28.6547	28.6155	28.6954	28.5277	28.6008	28.3581	28.3493	28.1746	27.9883	28.3148	28.2456
CaO	8.6647	8.8131	8.7297	10.6995	10.6186	10.5259	10.6123	10.3888	10.4548	10.0776	10.1006	10.0424	10.1602	10.2953
FeO	0.0086	0.0354	0.0118	0.0269	0.0389	0.0109	0.0424	0.0164	0.0427	0.0352	0.0165	0.0199	0.0158	0.0235
Na_2O	6.617	6.7178	6.6348	5.399	5.5848	5.6028	5.6654	5.5109	5.6496	5.6305	5.76	5.7057	5.6656	5.6229
K_2O	0.0907	0.1341	0.1469	0.1002	0.0867	0.0966	0.0848	0.103	0.0767	0.0804	0.1075	0.0895	0.1021	0.0632
Total	100.2665	100.5479	100.5955	99.5517	100.306	100.0858	100.5136	99.9975	99.4311	99.9545	99.7107	99.4605	99.7292	99.631
Total	100.2665	100.5479	100.5955	99.5517	100.306	100.0858	100.5136	99.9975	99.4311	99.9545	99.7107	99.4605	99.7292	99.631
Cations based on 8 Oxygens														
Si	2.586	2.572	2.574	2.474	2.486	2.481	2.49	2.491	2.485	2.507	2.505	2.513	2.501	2.5
Al	1.416	1.426	1.43	1.528	1.514	1.522	1.506	1.516	1.514	1.502	1.497	1.49	1.504	1.503
Ca	0.414	0.421	0.416	0.519	0.511	0.507	0.509	0.501	0.507	0.485	0.488	0.486	0.491	0.498
Fe	0	0.001	0	0.001	0.001	0	0.002	0.001	0.002	0.001	0.001	0.001	0.001	0.001
Na	0.572	0.581	0.573	0.474	0.486	0.489	0.492	0.481	0.496	0.491	0.504	0.5	0.495	0.492
K	0.005	0.008	0.008	0.006	0.005	0.006	0.005	0.006	0.004	0.005	0.006	0.005	0.006	0.004
Total	4.994	5.009	5.002	5.002	5.003	5.005	5.005	4.995	5.009	4.99	5.001	4.995	4.998	4.997

Microprobe Analysis
of F-1296- Amphibole
in or near garnet-C

Oxide Wt. %	AmpNPlgNGrt1	AmpNPlgNGrt2	AmpNPlgNGrt3	AmpNPlgNGrt4	AmpNPlgNGrt5	AmpNPlgNGrt6	AmpNPlgNGrt7	AmpNPlgNGrt8	AmpNPlgNGrt9	AmpNPlgNGrt10	AmpNPlgNGrt11	AmpNGrt1	AmpNGrt2
SiO_2	45.2058	45.1652	44.981	45.2084	45.1834	45.3155	45.361	45.459	45.1664	45.2152	45.3709	44.0324	44.2102
TiO_2	0.9054	0.9747	1.0771	1.0914	1.0961	1.1021	1.0972	1.126	1.1091	1.0855	1.0749	1.6489	1.5341
Al_2O_3	12.4427	12.3372	12.1479	12.0618	11.8974	11.9023	11.7565	11.8861	12.0294	12.0427	12.1199	12.0995	12.2962
Cr_2O_3	0.0592	0.0633	0.0403	0.0476	0.0337	0.0305	0.0368	0.0422	0.0416	0.0454	0.0604	0.0601	0.0372
MgO	12.1136	12.117	11.9455	11.9235	11.96	11.901	11.7875	11.9929	11.8778	11.8216	11.8991	11.428	11.3051
CaO	11.7172	11.6466	11.635	11.5157	11.3563	11.4836	11.4268	11.3848	11.4975	11.5185	11.4241	11.4678	11.2984
MnO	0.0412	0.05	0.0614	0.0704	0.0553	0.0678	0.0731	0.0672	0.08	0.0681	0.059	0.0714	0.0798
FeO	13.2173	13.5621	13.6374	13.7567	13.803	13.8928	13.7842	13.8064	13.7658	13.679	13.5701	14.3896	14.4164
H_2O	2.0468	2.0485	2.0387	2.0424	2.0365	2.0421	2.0347	2.0449	2.0396	2.0385	2.0435	2.0199	2.023
Na_2O	1.1842	1.2548	1.2694	1.2862	1.2851	1.2883	1.2048	1.2253	1.2641	1.2307	1.2402	1.2174	1.3095
K_2O	0.4983	0.4848	0.4961	0.4761	0.4632	0.4813	0.4846	0.5026	0.4767	0.4868	0.498	0.5358	0.4972
Total	99.4319	99.7042	99.3298	99.4804	99.1701	99.5071	99.0472	99.5374	99.3478	99.2319	99.3602	98.9709	99.007
Cations based on 23 Oxygens													
Si	6.622	6.611	6.616	6.637	6.652	6.654	6.684	6.665	6.64	6.65	6.657	6.536	6.553
Ti	0.1	0.107	0.119	0.12	0.121	0.122	0.122	0.124	0.123	0.12	0.119	0.184	0.171
Al	2.148	2.128	2.106	2.087	2.064	2.06	2.042	2.054	2.084	2.088	2.096	2.117	2.148
Cr	0.007	0.007	0.005	0.006	0.004	0.004	0.004	0.005	0.005	0.005	0.007	0.007	0.004
Mg	2.645	2.644	2.619	2.61	2.625	2.605	2.589	2.621	2.603	2.592	2.603	2.529	2.498
Ca	1.839	1.826	1.833	1.811	1.791	1.807	1.804	1.789	1.811	1.815	1.796	1.824	1.794
Mn	0.005	0.006	0.008	0.009	0.007	0.008	0.009	0.008	0.01	0.008	0.007	0.009	0.01
Fe	1.619	1.66	1.677	1.689	1.7	1.706	1.699	1.693	1.692	1.683	1.665	1.786	1.787
OH	2	2	2	2	2	2	2	2	2	2	2	2	2
Na	0.336	0.356	0.362	0.366	0.367	0.367	0.344	0.348	0.36	0.351	0.353	0.35	0.376
K	0.093	0.091	0.093	0.089	0.087	0.09	0.091	0.094	0.089	0.091	0.093	0.101	0.094
Total	17.415	17.437	17.438	17.424	17.419	17.421	17.389	17.402	17.418	17.404	17.396	17.444	17.435

Microprobe Analysis
of F-1296- Amphibole
in or near garnet-C

Oxide Wt. %	AmpNGrt3	AmpNGrt4	AmpNGrt5	AmpNGrt6	AmpNGrt2-1	AmpNGrt2-2	AmpNGrt2-3	AmpNGrt2-4	AmpNGrt2-5	AmpNGrt2-6	AmpNGrt2-7	AmpNGrt2-8	AmpNGrt2-9
SiO_2	44.2684	44.4045	44.4371	44.2995	42.8093	44.1281	44.6074	44.4363	44.5988	44.2168	43.8905	44.3171	44.0189
TiO_2	1.515	1.4749	1.519	1.448	0.0278	1.4906	1.438	1.4588	1.4425	1.5	1.4423	1.4544	1.392
Al_2O_3	12.3109	12.244	12.3706	12.4036	31.1559	12.4731	12.4821	12.0417	11.9248	12.2354	11.5994	12.2872	12.3195
Cr_2O_3	0.0486	0.0565	0.0492	0.0606	0	0.0405	0.0401	0.0468	0.0439	0.0439	0.014	0.0283	0.0446
MgO	11.4412	11.4027	11.177	11.144	0.4368	10.9977	11.1939	11.0986	11.2058	11.1153	11.0904	10.9837	11.0814
CaO	11.3763	11.253	11.3613	11.1231	0.1479	11.1035	10.9614	11.2667	11.0139	11.2085	11.1496	11.2585	11.1857
MnO	0.0897	0.0795	0.0865	0.088	0.0485	0.0895	0.0964	0.0897	0.1095	0.1023	0.0766	0.1034	0.0903
FeO	14.7763	14.8312	14.7602	14.9026	11.0557	15.0063	15.0088	15.1229	15.1554	15.2502	15.0829	15.1925	15.0726
H_2O	2.0329	2.0309	2.0331	2.0262	1.9681	2.0217	2.0351	2.0254	2.0257	2.0265	1.9969	2.0257	2.0176
Na_2O	1.3265	1.2192	1.3069	1.2855	0.0468	1.2555	1.2613	1.3351	1.3195	1.363	1.294	1.2965	1.3034
K_2O	0.5296	0.5319	0.5495	0.5279	0.1363	0.5488	0.5121	0.5028	0.5316	0.5322	0.4618	0.5064	0.558
Total	99.7154	99.5283	99.6504	99.3091	87.833	99.1551	99.6366	99.4246	99.3714	99.5941	98.0983	99.4536	99.084
Cations based on 23 Oxygens													
Si	6.529	6.556	6.553	6.555	6.522	6.545	6.572	6.578	6.601	6.542	6.59	6.56	6.542
Ti	0.168	0.164	0.168	0.161	0.003	0.166	0.159	0.162	0.161	0.167	0.163	0.162	0.156
Al	2.14	2.13	2.15	2.163	5.594	2.18	2.167	2.101	2.08	2.134	2.053	2.143	2.158
Cr	0.006	0.007	0.006	0.007	0	0.005	0.005	0.005	0.005	0.005	0.002	0.003	0.005
Mg	2.516	2.51	2.457	2.458	0.099	2.432	2.459	2.449	2.473	2.452	2.482	2.424	2.455
Ca	1.798	1.78	1.795	1.764	0.024	1.764	1.73	1.787	1.747	1.777	1.794	1.785	1.781
Mn	0.011	0.01	0.011	0.011	0.006	0.011	0.012	0.011	0.014	0.013	0.01	0.013	0.011
Fe	1.823	1.831	1.82	1.844	1.409	1.861	1.849	1.872	1.876	1.887	1.894	1.881	1.873
OH	2	2	2	2	2	2	2	2	2	2	2	2	2
Na	0.379	0.349	0.374	0.369	0.014	0.361	0.36	0.383	0.379	0.391	0.377	0.372	0.376
K	0.1	0.1	0.103	0.1	0.026	0.104	0.096	0.095	0.1	0.1	0.088	0.096	0.106
Total	17.469	17.437	17.439	17.433	15.698	17.429	17.411	17.445	17.435	17.467	17.452	17.439	17.462

Appendix 2

Abbreviations

Biotite Gneiss – BG
Calc-Silicate – CS
Quartz Vein – QV
Granitic Orthogneiss – GO
Diabase dike – Dd
Murder Creek granite – MCg
Dow's Pulpit granodiorite – DPg
Schist – S
Rocky Creek granodiorite – RCg
Amphibolite – Amp
Pegmatite – Peg
Si Cataclasite – Si-C

					Foliation		Lineation		Fold Axis		Axial Surface		IL Angle	Vergen	Joint	
Quad	Station	Lithology	Minerals	Grain Size	Strike	Dip	Trend	Plunge	Trend	Plunge	Strike	Dip			Strike	Dip
FR	38	BG	bt,plg	Medium	5	45									340	65
FR	39	BG	bt,plg	Medium	75	10										
FR	40	BG	bt,plg	Medium	75	10										
FR	41	BG	bt,plg	Medium												
FR	42	BG	bt,plg	Medium	330	10										
FR	43	BG	bt,plg	Med-Coarse	320	10									349	71
FR	44	BG	bt,plg	Med-Coarse	310	15										
FR	45	BG	bt,plg	Med-Coarse												
FR	46	BG	plg,bt	Med-Coarse												
FR	47	BG	bt,plg	Medium	50	10										
FR	48	CS	qtz,grt	Fine	65	35										
FR	49	BG	bt,plg	Medium												
FR	50	CS	qtz,grt	Fine	65	10									240	85
FR	51	BG	bt,plg	Medium	45	35									150	76
FR	52	BG	bt,plg	Medium	65	15										
FR	53	BG	bt,plg	Medium												
FR	54	BG	bt,plg	Medium	80	15										
FR	55	BG	bt,plg	Medium	300	15										
FR	56	BG	bt,plg	Med-Coarse	80	25	25	25								
FR	57	BG	bt,plg	Medium	10	15										
FR	58	BG	bt,plg	Med-Coarse	50	25									86	79
FR	59	BG	bt,plg	Med-Coarse	30	15									184	82
FR	60	BG	bt,plg	Med-Coarse	40	15										
FR	61	BG	bt,plg	Med-Coarse	30	15	23	19								
FR	62	BG	bt,plg	Med-Fine												
FR	63	BG	bt,plg	Med-Coarse	40	20										
FR	64	QV	qtz	Coarse												
FR	65	BG	bt,plg	Medium												
FR	66	BG	bt,plg	Med-Coarse	70	45										
FR	67	BG	bt,grt	Med-Coarse	45	25										
FR	68	BG	bt,plg	Medium	20	15	20	15	1	12	246	24	15	NE		
FR	69	BG	bt,plg	Med-Coarse	80	25										
FR	70	BG	bt,plg	Med-Coarse	320	15										
FR	71	BG	bt,plg	Medium	80	15										
FR	72	BG	bt,plg	Med-Coarse	80	15										
FR	73	BG	bt,plg	Medium												
FR	74	BG	bt,plg	Medium	80	15										
FR	75	BG	bt,plg	Medium	80	15										
FR	76	BG	bt,plg	Med-Coarse	80	15										
FR	77	BG	bt,plg	Medium	70	10										
FR	78	BG	bt,plg	Med-Coarse	85	15										
FR	79	BG	grt,bt	Med-Coarse											90	78
FR	80	GO	qtz,bt	Medium											154	82
FR	81	BG	bt	Med-Coarse												
FR	82	BG	plg,bt	Medium												
FR	83	BG	bt,plg	Med-Fine												
FR	84	BG	bt,plg	Medium	70	15										
FR	85	BG	bt,plg	Medium	310	10										
FR	86	BG	bt,plg	Medium	340	10										
FR	87	BG	bt,plg	Medium	40	10			9	157	56	322	30	NW		
FR	88	BG	bt,plg	Medium												
FR	89	BG	bt,plg	Medium	20	10										
FR	90	BG	bt,plg	Medium	20	10										
FR	91	QV	qtz	Coarse												
FR	92	QV	qtz	Coarse	255	15										
FR	93	BG	bt,plg	Medium	5	10										
FR	94	BG	bt,plg	Medium	5	10										
FR	95	BG	bt,plg	Med-Coarse	10	10										
FR	96	BG	bt,plg	Medium	10	10										
FR	97	BG	bt,plg	Medium	15	10										
FR	98	BG	bt,plg	Medium	15	10										

					Foliation		Lineation		Fold Axis		Axial Surface		IL Angle	Vergen	Joint	
Quad	Station	Lithology	Minerals	Grain Size	Strike	Dip	Trend	Plunge	Trend	Plunge	Strike	Dip			Strike	Dip
FR	99	BG	bt,plg	Med-Fine	327	31										
FR	100	BG	bt,plg	Medium	327	10										
FR	101	BG	bt,plg	Medium	40	45										
FR	102	BG	bt,plg	Medium	35	25	21	11	5	10	236	76	11	NE		
FR	103	BG	bt,plg	Medium	40	5										
FR	104	BG	bt,plg	Med-Fine	40	5										
FR	105	BG	bt,plg	Med-Fine	30	15										
FR	106	BG	bt,plg	Med-Fine	40	15										
FR	107	BG	bt,plg	Med-Fine	35	15										
FR	108	BG	bt,plg	Med-Fine	45	15										
FR	109	BG	bt,plg	Med-Fine	45	15										
FR	110	BG	bt,plg	Med-Fine	45	25										
FR	111	BG	bt,plg	Med-Fine	130	11										
FR	112	QV	bt,plg	Med-Fine	80	26									157	80
FR	113	BG	bt,plg	Med-Fine	50	25									88	80
FR	114	BG	bt,plg	Med-Fine	0	0										
FR	115	BG	plg,bt	Med-Fine	40	19									160	91
FR	116	BG	plg,bt	Med-Fine	0	0										
FR	117	GO	plg,qtz	Med-Fine	0	0										
FR	118	BG	bt,grt	Med-Fine	290	10									90	81
FR	119	BG	bt,ms	Med-Fine	320	25									350	76
FR	120	BG	bt,ms	Med-Fine	315	5										
FR	121	BG	bt,plg	Medium	300	5										
FR	122	BG	plg,bt	Medium	305	10										
FR	123	BG	bt,plg	Medium	60	15										
FR	124	BG	bt,plg	Medium	320	10										
FR	125	BG	bt,plg	Medium	128	11										
FR	126	BG	bt,plg	Medium	0	0										
FR	127	BG	bt,plg	Med-Fine	20	15	31	10								
FR	128	BG	bt,plg	Med-Fine	45	45										
FR	129	BG	bt,plg	Med-Fine	45	35										
FR	130	BG	bt,plg	Med-Fine	45	35										
FR	131	BG	bt,plg	Med-Fine	60	5										
FR	132	BG	bt,plg	Medium	15	55										
FR	133	BG	bt,plg	Medium	20	15										
FR	134	BG	bt,plg	Medium	45	10										
FR	135	BG	bt,plg	Medium	85	24										
FR	136	BG	bt,plg	Medium	20	22										
FR	137	BG	bt,plg	Medium	50	25										
FR	138	BG	bt,plg	Medium	100	25										
FR	139	BG	bt,plg	Medium	50	26										
FR	140	BG	bt,plg	Medium												
FR	141	BG	bt,plg	Medium	65	30										
FR	142	Dd	prx	Fine												
FR	143	Dd	qtz	Fine												
FR	144	Dd	qtz	Fine												
FR	145	BG	bt,plg	Medium	25	13										
FR	146	BG	bt,plg	Medium	55	12										
FR	147	BG	bt,plg	Medium	340	25										
FR	148	CS	qtz,grt	Fine	105	5										
FR	149	Dd	prx,amp	Fine												
FR	150	Dd	prx,amp	Fine												
FR	151	Dd	prx,amp	Fine												
FR	152	Dd	prx,amp	Fine												
FR	153	Dd	prx,amp	Fine												
FR	154	Dd	prx,amp	Fine												
FR	155	Dd	prx,amp	Fine												
FR	156	Dd	prx,amp	Fine												
FR	157	BG	plg,bt	Med-Coarse	275	5										
FR	158	BG	plg,bt	Med-Coarse	285	10										
FR	159	CS	qtz,grt	Fine												

					Foliation		Lineation		Fold Axis		Axial Surface		IL Angle	Vergen	Joint	
Quad	Station	Lithology	Minerals	Grain Size	Strike	Dip	Trend	Plunge	Trend	Plunge	Strike	Dip			Strike	Dip
FR	160	BG	bt,plg	Medium	40	10										
FR	161	BG	bt,plg	Medium	22	19										
FR	162	BG	bt,plg	Medium	340	15			60	30	275	80	25	NE		
FR	164	BG	bt,plg	Med-Fine	275	15										
FR	165	BG	bt,plg	Med-Fine	230	36										
FR	166	BG	bt,plg	Medium	340	5										
FR	167	BG	bt,plg	Medium	50	45										
FR	168	QV	qtz	Coarse	170	15										
FR	169	CS	qtz,grt	Fine												
FR	170	CS	qtz,grt	Fine												
FR	171	BG	bt,plg	Med-Coarse												
FR	172	BG	bt,plg	Med-Coarse												
FR	173	BG	bt,plg	Med-Coarse												
FR	174	BG	bt,plg	Medium												
FR	175	CS	qtz,grt	Fine												
FR	176	CS	qtz,grt	Fine												
FR	177	CS	qtz,grt	Fine												
FR	178	BG	bt,plg	Med-Coarse	231	36										
FR	179	BG	bt,plg	Med-Coarse	61	46										
FR	180	BG	bt,plg	Med-Coarse	20	8										
FR	181	BG	bt,plg	Medium	30	15										
FR	182	BG	bt,plg	Medium	35	5										
FR	183	BG	bt,plg	Medium	40	5										
FR	184	BG	bt,plg	Medium												
FR	185	BG	bt,plg	Medium	35	13										
FR	186	BG	bt,plg	Medium	40	15										
FR	187	BG	bt,plg	Medium	50	8										
FR	188	BG	bt,plg	Med-Fine	50	8	110	8	55	34	270	76	21	NE		
FR	189	BG	bt,plg	Med-Fine	20	20										
FR	190	MCg	plg, qtz	Medium												
FR	191	BG	bt,plg	Medium												
FR	192	BG	plg,bt	Med-Coarse												
FR	193	BG	plg,bt	Med-Coarse												
FR	194	BG	plg,bt	Med-Fine	225	8										
FR	195	BG	plg,bt	Med-Coarse	240	5										
FR	196	BG	plg,bt	Med-Coarse	230	12										
FR	197	BG	plg,bt	Med-Coarse	230	12										
FR	198	BG	plg,bt	Med-Coarse	235	16										
FR	199	BG	plg,bt	Med-Coarse	225	16										
FR	200	BG	plg,bt	Med-Coarse	190	6										
FR	201	BG	plg,bt	Med-Coarse	200	14										
FR	202	CS	qtz,grt	Med-Coarse	215	10										
FR	203	DPg	plg, qtz	Medium												
FR	204	DPg	plg, qtz	Medium	315	40										
FR	205	DPg	plg, qtz	Medium	325	15										
FR	206	DPg	plg, qtz	Medium												
FR	207	DPg	plg, qtz	Medium												
FR	208	DPg	plg, qtz	Medium												
FR	209	BG	plg, qtz	Medium	315	35										
FR	210	DPg	plg, gtz	Medium	305	43										
FR	211	S	sil,ms	Medium	225	85										
FR	212	DPg	plg,qtz,grt	Medium	185	20										
FR	213	DPg	plg,qtz,grt	Medium												
FR	214	DPg	plg,qtz,grt	Medium												
FR	215	DPg	plg,qtz,grt	Medium												
FR	216	DPg	plg,qtz,grt	Medium												
FR	217	DPg	plg,qtz,grt	Medium												
FR	218	DPg	plg,qtz,grt	Medium												
FR	219	DPg	plg,qtz,grt	Medium												
FR	220	DPg	plg,qtz,grt	Medium												
FR	221	DPg	plg,qtz,grt	Medium												

					Foliation		Lineation		Fold Axis		Axial Surface		IL Angle	Vergen	Joint	
Quad	Station	Lithology	Minerals	Grain Size	Strike	Dip	Trend	Plunge	Trend	Plunge	Strike	Dip			Strike	Dip
FR	222	DPg	plg,qtz,grt	Medium												
FR	223	DPg	plg,qtz,grt	Medium												
FR	224	DPg	plg,qtz,grt	Medium	220	42										
FR	225	DPg	plg,qtz,grt	Medium												
FR	226	DPg	plg,qtz,grt	Medium	220	65										
FR	227	DPg	plg,qtz,grt	Medium												
FR	228	S	grt,ms	Medium												
FR	229	MCg	plg, qtz	Med-Coarse												
FR	230	MCg	plg, qtz	Med-Coarse												
FR	231	MCg	plg, qtz	Med-Coarse												
FR	232	MCg	plg, qtz	Med-Coarse												
FR	233	MCg	plg, qtz	Med-Coarse												
FR	234	MCg	plg, qtz	Med-Coarse												
FR	235	MCg	plg, qtz	Med-Coarse												
FR	236	MCg	plg, qtz	Med-Coarse												
FR	237	MCg	plg, qtz	Med-Coarse												
FR	238	MCg	plg, qtz	Med-Coarse	230	23										
FR	239	MCg	plg, qtz	Med-Coarse												
FR	240	S	grt,ms	Medium												
FR	241	RCg	qtz,plg	Fine	40	7										
FR	242	RCg	qtz,plg	Fine												
FR	243	RCg	qtz,plg	Fine	95	35										
FR	244	RCg	qtz,plg	Fine	75	24										
FR	245	RCg	qtz,plg	Fine												
FR	246	RCg	qtz,plg	Fine												
FR	247	RCg	qtz,plg	Fine	40	42										
FR	248	BG	bt,plg	Medium	55	14										
FR	249	BG	bt,plg	Medium	54	14										
FR	250	BG	bt,plg	Medium	40	21										
FR	251	BG	bt,plg	Medium	26	31										
FR	252	BG	bt,plg	Medium	26	31										
FR	253	S	sil,ms	Medium	41	23										
FR	254	S	sil,ms	Medium	41	23										
FR	255	S	sil,ms	Medium	41	24										
FR	256	BG	bt,plg	Medium	41	24										
FR	257	S	sil,ms	Medium	43	24										
FR	258	Dd	qtz,grt	Fine												
FR	259	Dd	qtz,grt	Fine												
FR	260	BG	bt,plg	Medium	43	26										
FR	261	BG	bt,plg	Medium	46	43	25	13								
FR	262	BG	bt,plg	Medium	72	43										
FR	263	BG	bt,plg	Medium	72	26										
FR	264	QV	qtz	Medium	35	29										
FR	265	BG	bt,plg	Med-Coarse	24	29										
FR	266	BG	bt,plg	Med-Coarse	29	29	140	14								
FR	267	BG	bt,plg	Med-Coarse	34	9										
FR	267	BG	bt,plg	Med-Coarse	330	12										
FR	267	BG	bt,plg	Med-Coarse	34	9										
FR	268	BG	bt,plg	Med-Coarse	65	11										
FR	269	BG	bt,plg	Med-Coarse	65	11										
FR	270	MCg	qtz,plg	Med-Coarse												
FR	271	BG	bt,plg	Med-Coarse	65	11										
FR	272	BG	bt,plg	Med-Coarse	65	16										
FR	273	BG	bt,plg	Med-Coarse	55	12										
FR	274	BG	bt,plg	Med-Coarse	56	14										
FR	275	Amp	grt,amp	Med-Coarse	26	16										
FR	276	Amp	grt,amp	Med-Coarse	55	24										
FR	277	Amp	grt,amp	Med-Coarse	35	22										
FR	278	Amp	grt,amp	Med-Coarse	25	26										
FR	279	Amp	grt,amp	Med-Coarse	25	32										
FR	280	Amp	grt,amp	Med-Coarse	14	12										

					Foliation		Lineation		Fold Axis		Axial Surface		IL Angle	Vergen	Joint	
Quad	Station	Lithology	Minerals	Grain Size	Strike	Dip	Trend	Plunge	Trend	Plunge	Strike	Dip			Strike	Dip
FR	281	Amp	amp,grt	Med-Coarse	34	32										
FR	282	Amp	amp,grt	Med-Coarse	19	29										
FR	283	Amp	amp,grt	Med-Coarse	32	19										
FR	284	Amp	amp,grt	Med-Coarse	21	13										
FR	285	Amp	amp,grt	Med-Coarse	33	23										
FR	286	Amp	amp,grt	Med-Coarse	34	36										
FR	287	Amp	amp,grt	Med-Coarse	34	32										
FR	288	BG	bt,plg	Med-Coarse	17	59										
FR	289	BG	bt,plg	Med-Coarse	34	56										
FR	290	BG	bt,plg	Med-Coarse	37	15										
FR	291	BG	bt,plg	Med-Coarse	37	24										
FR	292	BG	bt,plg	Med-Coarse	19	23										
FR	293	BG	bt,plg	Med-Coarse	35	33										
FR	294	BG	bt,plg	Med-Coarse	36	34										
FR	295	BG	bt,plg	Med-Coarse	23	19										
FR	296	BG	bt,plg	Med-Coarse	29	32										
FR	297	BG	bt,plg	Med-Coarse	28	29	11	29								
FR	298	BG	bt,plg	Med-Coarse	34	39										
FR	299	BG	bt,plg	Med-Coarse	9	63										
FR	300	BG	bt,plg	Med-Coarse	11	52										
FR	301	BG	bt,plg	Med-Coarse	35	23										
FR	302	BG	bt,plg	Med-Coarse	32	21										
FR	303	BG	bt,plg	Med-Coarse	21	11										
FR	304	BG	bt,plg	Med-Coarse	23	16										
FR	305	BG	bt,plg	Med-Coarse	9	11										
FR	306	BG	bt,plg	Med-Coarse	26	49										
FR	307	BG	bt,plg	Med-Coarse	45	11										
FR	308	BG	plg,bt	Med-Coarse	14	44										
FR	309	BG	plg,bt	Med-Coarse	59	24										
FR	310	BG	plg,bt	Med-Coarse	39	24										
FR	311	BG	bt,plg	Med-Coarse	19	39										
FR	312	BG	plg,bt	Med-Coarse	19	39										
FR	313	BG	plg,bt	Med-Coarse	43	26										
FR	314	BG	plg,bt	Med-Coarse	41	23										
FR	315	BG	plg,bt	Med-Coarse	56	15										
FR	316	BG	plg,bt	Med-Coarse	36	29										
FR	317	BG	plg,bt	Med-Coarse	34	26										
FR	318	BG	plg,bt	Med-Coarse	34	19										
FR	319	BG	plg,bt	Med-Coarse	51	11										
FR	320	BG	plg,bt	Med-Coarse	19	29										
FR	321	BG	plg,bt	Med-Coarse	24	35	75	35								
FR	322	GO	qtz,plg	Med-Coarse	36	19										
FR	323	BG	plg,bt	Med-Coarse	21	24										
FR	324	BG	plg,bt	Med-Coarse	21	21										
FR	325	BG	plg,bt	Med-Coarse	36	26										
FR	326	BG	plg,bt	Med-Coarse	0	0										
FR	327	BG	plg,bt	Med-Coarse	29	49										
FR	328	BG	plg,bt	Med-Coarse	54	24										
FR	329	BG	plg,bt	Med-Coarse	41	31										
FR	330	BG	plg,bt	Med-Coarse	47	49										
FR	331	BG	bt,plg	Med-Fine	51	61										
FR	331	BG	bt,plg	Med-Fine	40	52										
FR	332	BG	bt,plg	Med-Fine	45	34										
FR	333	GO	qtz,plg	Med-Fine	41	14										
FR	334	BG	bt,plg,grt	Med-Fine	29	45	345	45								
FR	335	BG	bt,plg,grt	Med-Fine	32	29										
FR	336	BG	bt,plg,grt	Med-Fine	28	43										
FR	337	BG	bt,plg,grt	Med-Fine	22	37										
FR	338	BG	bt,plg,grt	Med-Fine	22	25										
FR	339	BG	bt,plg,grt	Med-Fine	39	20										
FR	340	BG	bt,plg,grt	Med-Fine	29	41										

					Foliation		Lineation		Fold Axis		Axial Surface		IL Angle	Vergen	Joint	
Quad	Station	Lithology	Minerals	Grain Size	Strike	Dip	Trend	Plunge	Trend	Plunge	Strike	Dip			Strike	Dip
FR	341	BG	bt,plg,grt	Med-Fine	49	32										
FR	342	BG	bt,plg,grt	Med-Fine	42	23	350	11	0	4	160	4	5	NE		
FR	345	BG	plg,bt	Med-Fine	39	38										
FR	346	BG	plg,bt	Med-Fine	45	41										
FR	347	BG	plg,bt	Med-Fine	49	41										
FR	348	BG	plg,bt	Med-Fine	31	55										
FR	349	BG	bt,plg,grt	Med-Fine	27	16										
FR	350	BG	bt,plg,grt	Med-Fine	11	46										
FR	351	BG	bt,plg,grt	Med-Fine	4	13										
FR	352	BG	bt,plg,grt	Med-Fine	20	54										
FR	353	BG	bt,plg,grt	Med-Fine	19	43										
FR	354	MCg	qtz,plg	Med-Coarse												
FR	355	MCg	qtz,plg	Med-Coarse												
FR	356	MCg	qtz,plg	Med-Coarse												
FR	357	MCg	qtz,plg	Med-Coarse												
FR	358	MCg	qtz,plg	Med-Coarse												
FR	359	BG	plg,bt	Med-Coarse	39	41										
FR	360	BG	plg,bt	Med-Coarse	9	49										
FR	361	BG	bt,plg	Fine	31	36										
FR	362	MCg	plg,bt	Med-Coarse												
FR	363	GO	kspr,bt	Med-Coarse												
FR	364	GO	kspr,bt	Med-Coarse	5	45										
FR	365	MCg	kspr,bt	Med-Coarse	1	59										
FR	366	BG	plg,bt	Medium												
FR	367	MCg	bt,plg	Med-Coarse												
FR	368	BG	bt,plg	Med-Coarse	53	31										
FR	369	BG	bt,plg	Med-Coarse	29	23										
FR	370	BG	bt,plg	Med-Coarse	51	34										
FR	371	BG	bt,plg	Med-Coarse	59	32										
FR	372	BG	bt,plg	Med-Coarse	52	34										
FR	373	BG	bt,plg	Med-Coarse	62	32										
FR	374	BG	bt,plg	Medium	49	32										
FR	375	BG	bt,plg	Medium	56	19										
FR	376	BG	bt,plg	Medium	355	74										
FR	377	MCg	plg,bt	Med-Coarse	56	62										
FR	378	BG	plg,bt	Med-Coarse	43	23										
FR	379	BG	plg,bt	Med-Coarse	31	44										
FR	380	BG	plg,bt	Med-Coarse	45	34										
FR	381	BG	plg,bt	Med-Coarse	25	32	355	32								
FR	383	BG	plg,bt	Med-Coarse	22	28										
FR	384	BG	plg,bt	Med-Coarse	43	32										
FR	385	BG	plg,bt	Med-Coarse	31	23										
FR	386	BG	plg,bt	Med-Coarse	31	23										
FR	387	BG	plg,bt	Fine	0	0										
FR	388	BG	plg,bt	Med-Coarse	14	45										
FR	389	BG	plg,bt	Med-Coarse	18	28	10	25								
FR	390	BG	plg,bt	Med-Coarse	43	24										
FR	391	BG	plg,bt	Med-Coarse	330	14										
FR	392	BG	plg,bt	Med-Coarse	34	35	55	35								
FR	393	BG	plg,bt	Med-Coarse	40	18										
FR	394	BG	plg,bt	Medium	21	40										
FR	395	BG	plg,bt	Med-Coarse	63	19										
FR	396	BG	plg,bt	Med-Coarse	26	34										
FR	397	BG	plg,bt	Med-Coarse	39	22										
FR	398	BG	plg,bt	Med-Coarse	23	33										
FR	399	BG	plg,bt	Med-Coarse	37	47										
FR	400	BG	plg,bt	Med-Coarse	37	43										
FR	401	BG	plg,bt	Med-Coarse	32	40										
FR	402	BG	plg,bt	Med-Coarse	45	42										
FR	403	BG	plg,bt	Med-Coarse	43	41										
FR	404	BG	plg,bt	Med-Coarse	20	18										

					Foliation		Lineation		Fold Axis		Axial Surface		IL Angle	Vergen	Joint	
Quad	Station	Lithology	Minerals	Grain Size	Strike	Dip	Trend	Plunge	Trend	Plunge	Strike	Dip			Strike	Dip
FR	405	BG	plg,bt	Med-Coarse	17	11										
FR	406	BG	plg,bt	Med-Coarse	23	24										
FR	407	BG	plg,bt	Med-Coarse	33	15										
FR	408	BG	plg,bt	Med-Coarse	24	21										
FR	409	BG	plg,bt	Med-Coarse	21	18										
FR	410	BG	plg,bt	Med-Coarse	21	24										
FR	411	BG	plg,bt	Med-Coarse	51	35										
FR	412	BG	plg,bt	Med-Coarse	49	38										
FR	413	BG	plg,bt	Med-Coarse	23	32										
FR	414	BG	plg,bt	Med-Coarse	43	23										
FR	415	BG	plg,bt	Med-Coarse	45	29										
FR	416	BG	plg,bt	Med-Coarse	45	23										
FR	417	BG	plg,bt	Med-Coarse	43	26										
FR	418	BG	plg,bt	Med-Coarse	24	46										
FR	419	MCg	qtz,plg	Coarse	195	21										
FR	420	MCg	qtz,plg	Coarse	300	32										
FR	421	MCg	qtz,plg	Coarse												
FR	422	MCg	qtz,plg	Coarse												
FR	423	Dd	qtz,grt	Fine												
FR	424	MCg	qtz,plg	Coarse												
FR	425	MCg	qtz,plg	Coarse												
FR	426	MCg	qtz,plg	Coarse												
FR	427	Amp Gneiss	amp,plg	Fine	315	29										
FR	428	RCg	qtz,plg	Fine												
FR	429	RCg	qtz,plg	Fine												
FR	430	RCg	qtz,plg	Fine												
FR	431	RCg	qtz,plg	Fine	185	42										
FR	432	RCg	qtz,plg	Fine	245	56										
FR	433	RCg	qtz,plg	Fine												
FR	434	RCg	qtz,plg	Fine												
FR	435	RCg	qtz,plg	Fine												
FR	436	RCg	qtz,plg	Fine												
FR	437	RCg	qtz,plg	Fine												
FR	438	RCg	qtz,plg	Fine												
FR	439	RCg	qtz,plg	Fine												
FR	440	RCg	qtz,plg	Fine	185	70										
FR	441	BG, MS-BT S	bt,plg	Fine	20	25										
FR	442	BG, MS-BT S	bt,plg	Fine	15	21										
FR	443	BG, Amp	bt,plg	Fine	21	28										
FR	444	BG, Amp	bt,plg	Fine	21	24										
FR	445	BG, Amp	bt,plg	Fine	27	26										
FR	446	BG	bt,plg	Fine	14	45										
FR	447	BG	bt,plg	Med-Coarse	3	30										
FR	448	BG	bt,plg	Med-Coarse	30	23										
FR	449	BG	bt,plg	Med-Coarse	342	43										
FR	450	BG	bt,plg	Med-Coarse	14	24										
FR	451	BG	bt,plg	Med-Coarse	15	34										
FR	452	BG	bt,plg	Med-Coarse	44	54										
FR	453	Peg	plg,qtz	Coarse												
FR	454	BG	plg,bt	Medium	345	43										
FR	455	Amp	amp,bt	Med-Fine												
FR	456	BG	bt,plg	Medium	25	31										
FR	457	BG	bt,plg	Medium	346	26										
FR	458	BG	plg,qtz	Med-Coarse												
FR	459	BG	plg,qtz	Med-Coarse	3	35										
FR	460	BG	plg,qtz	Med-Coarse	8	24										
FR	461	BG	plg,qtz	Med-Coarse	10	32										
FR	462	BG	plg,qtz	Med-Coarse	339	14										
FR	463	BG	plg,qtz	Med-Coarse												
FR	464	BG	plg,qtz	Med-Coarse	7	30										
FR	465	Amp	amp	Medium												

					Foliation		Lineation		Fold Axis		Axial Surface		IL Angle	Vergen	Joint	
Quad	Station	Lithology	Minerals	Grain Size	Strike	Dip	Trend	Plunge	Trend	Plunge	Strike	Dip			Strike	Dip
FR	466	BG	plg,qtz	Fine	25	44										
FR	467	BG	plg,qtz	Medium	12	20										
FR	468	BG	bt,plg	Medium	32	37										
FR	469	BG	bt,plg	Medium	16	31										
FR	470	BG	bt,plg	Medium	23	21			42	40	51	30	13	SW		
FR	471	BG	bt,plg	Medium	22	21										
FR	472	BG	bt,plg	Medium	6	34										
FR	473	BG	bt,plg	Medium	23	31										
FR	474	Amp	amp,bt	Med-Fine												
FR	475	BG	plg,qtz	Med-Coarse												
FR	476	BG	plg,qtz	Med-Coarse	21	54										
FR	477	BG	plg,bt	Med-Coarse	23	31										
FR	478	BG	plg,qtz	Med-Coarse	14	19										
FR	479	BG	plg,qtz	Med-Coarse	8	34										
FR	480	BG	plg,qtz	Med-Coarse	330	24										
FR	481	BG	plg,qtz	Med-Coarse	7	21										
FR	482	BG	plg,qtz	Medium	14	0										
FR	483	BG	plg,qtz	Medium	14	21										
FR	484	MCg	plg,qtz	Coarse	355	40										
FR	485	MCg	plg,qtz	Coarse												
FR	486	MCg	plg,qtz	Coarse												
FR	487	MCg	plg,qtz	Coarse												
FR	488	Amp	amp,plg	Med-Fine												
FR	489	MCg	plg,qtz	Coarse												
FR	490	MCg	plg,qtz	Coarse												
FR	491	MCg	plg,qtz	Coarse	34	21	39	21								
FR	492	S	sil,ms	Med-Coarse												
FR	493	MCg	plg,qtz	Coarse	44	21										
FR	494	RCg	plg,qtz	Fine	0	0										
FR	495	RCg	plg,qtz	Fine	0	0										
FR	496	MCg	plg,qtz	Coarse	71	45										
FR	497	DPg	plg,qtz	Medium	0	0									305	86
FR	499	MCg	plg,qtz	Coarse	349	23										
FR	500	MCg	plg,qtz	Coarse	69	24										
FR	501	MCg	plg,qtz	Coarse	71	23										
FR	502	DPg	plg,qtz	Medium	57	65										
FR	503	S	sil,ms	Med-Fine												
FR	504	RCg	plg,qtz	Med-Fine	239	36										
FR	505	MS S	ms	Medium												
FR	506	MCg	plg,qtz	Coarse	71	34										
FR	507	DPg	plg,qtz	Medium												
FR	508	DPg	plg,qtz	Medium												
FR	509	S	sil,bt	Medium	7	70										
FR	510	S	sil,grt	Med-Fine	23	42			46	41	51	36	12	SW		
FR	512	S	sil,grt	Med-Fine	17	30										
FR	513	S	sil,grt	Med-Fine	13	29										
FR	514	S	sil,grt	Med-Fine	17	22										
FR	515	S	sil,grt	Med-Fine	17	26										
FR	516	S	sil,grt	Med-Fine	11	31										
FR	517	S	sil,grt	Med-Fine	245	81									340	65
FR	518	S	sil,grt	Med-Fine	12	11										
FR	519	BG	bt,plg	Medium	9	6										
FR	520	BG	bt,plg	Medium	75	41										
FR	521	BG	plg,qtz	Medium	284	18										
FR	522	Amp	amp,plg	Med-Fine	19	16										
FR	523	MG	plg,bt	Coarse	0	19										
FR	524	BG	bt,plg	Medium	9	33										
FR	525	BG	bt,plg	Medium	9	21										
FR	526	MCg	plg,qtz	Coarse	36	30										
FR	527	MCg	plg,qtz	Coarse												
FR	528	MCg	plg,qtz	Coarse												

					Foliation		Lineation		Fold Axis		Axial Surface		IL Angle	Vergen	Joint	
Quad	Station	Lithology	Minerals	Grain Size	Strike	Dip	Trend	Plunge	Trend	Plunge	Strike	Dip			Strike	Dip
FR	529	Amp	amp,grt	Medium												
FR	530	Amp	amp,grt	Medium												
FR	531	Amp	amp,grt	Medium												
FR	532	MCg	plg,qtz	Med-Coarse												
FR	533	MCg	plg,qtz	Med-Coarse												
FR	534	Amp	amp,grt	Medium												
FR	535	MCg	qtz,plg	Med-Coarse												
FR	536	MCg	qtz,plg	Med-Coarse	15	42										
FR	537	BG	bt,plg	Med-Fine												
FR	538	RCg	qtz,plg	Med-Fine												
FR	539	RCg	qtz,plg	Med-Fine												
FR	540	S	sil,grt	Med-Fine												
FR	541	BG	plg,grt	Med-Fine	9	21										
FR	542	S	sil,grt	Med-Fine	11	21										
FR	543	S	sil,grt	Med-Fine												
FR	544	S	sil,grt	Med-Fine	12	21										
FR	545	MCg	qtz,plg	Coarse												
FR	546	MCg	plg,qtz	Coarse												
FR	547	MCg	plg,qtz	Coarse												
FR	548	MCg	plg,qtz	Med-Coarse	25	36										
FR	549	S	plg,qtz	Med-Fine	25	45										
FR	550	Amp	amp,bt	Med-Fine												
FR	551	BG	bt,plg	Med-Fine	339	21										
FR	552	RCg	qtz,plg	Med-Fine												
FR	553	RCg	qtz,plg	Med-Fine												
FR	554	RCg	qtz,plg	Med-Fine												
FR	555	Peg	ms	Med-Coarse												
FR	556	RCg	qtz,plg	Fine												
FR	557	RCg	qtz,plg	Fine												
FR	558	RCg	qtz,plg	Fine												
FR	559	MS S	ms	Medium												
FR	560	S	ms,sil	Medium	85	65										
FR	561	S	ms,sil	Medium	25	18										
FR	562	S, BG	ms,sil	Medium	32	19										
FR	563	DPg	plg,qtz	Med-Coarse												
FR	564	DPg	plg,qtz	Medium												
FR	565	MCg	plg,qtz	Med-Coarse												
FR	566	MCg	plg,qtz	Med-Coarse												
FR	567	MCg	plg,qtz	Med-Coarse												
FR	568	MCg	plg,qtz	Med-Coarse												
FR	569	MCg	plg,qtz	Med-Coarse	52	40										
FR	570	MCg	plg,qtz	Med-Coarse												
FR	571	MCg	plg,qtz	Med-Coarse												
FR	572	MCg	plg,qtz	Med-Coarse												
FR	573	MCg	plg,qtz	Med-Coarse												
FR	574	MCg	plg,qtz	Med-Coarse												
FR	575	QV	qtz	Coarse												
FR	576	CS	qtz,grt	Fine												
FR	577	MCg	plg,qtz	Med-Coarse												
FR	578	BG	bt,plg	Med-Fine	31	35										
FR	579	BG	bt,plg	Med-Fine	51	23										
FR	580	BG	bt,plg	Medium												
FR	581	BG	bt,plg	Medium												
FR	582	BG	bt,plg	Med-Fine												
FR	583	BG	bt,plg	Med-Coarse												
FR	584	BG	bt,plg	Med-Coarse												
FR	585	S	sil,ms	Med-Fine	3	21										
FR	586	BG	bt,plg	Med-Fine												
FR	587	BG	bt,plg	Med-Fine												
FR	588	MCg	plg,qtz	Med-Coarse												
FR	589	Amp	amp,grt	Fine												

					Foliation		Lineation		Fold Axis		Axial Surface		IL Angle	Vergen	Joint	
Quad	Station	Lithology	Minerals	Grain Size	Strike	Dip	Trend	Plunge	Trend	Plunge	Strike	Dip			Strike	Dip
FR	590	S	sil,ms	Fine	5	14										
FR	591	S	sil,ms	Fine	7	14										
FR	592	S	sil,ms	Fine	7	12										
FR	593	BG	bt,plg	Med-Fine												
FR	594	BG	bt,plg	Med-Fine												
FR	595	BG	bt,plg	Med-Fine	210	54										
FR	596	BG	bt,plg	Med-Fine	26	34										
FR	597	BG	bt,plg	Med-Fine	26	21										
FR	598	BG	bt,plg	Med-Fine												
FR	599	BG	bt,plg	Med-Fine	29	17										
FR	600	BG	bt,plg	Med-Fine	23	13										
FR	601	BG	bt,plg	Med-Fine	45	10										
FR	602	BG	bt,plg	Med-Fine	42	11										
FR	603	BG	bt,plg	Med-Fine	41	13										
FR	604	BG	bt,plg	Med-Fine	49	16										
FR	605	BG	bt,plg	Med-Fine												
FR	606	S	sil,ms	Med-Fine	34	19										
FR	607	S	sil,ms	Med-Fine	44	12										
FR	608	S	sil,ms	Med-Fine	42	11										
FR	609	S	sil,ms	Med-Fine	41	11										
FR	610	S	sil,ms	Med-Fine	41	12										
FR	611	S	sil,ms	Med-Fine	29	23										
FR	612	S	sil,ms	Med-Fine	25	35										
FR	613	S	sil,ms	Med-Fine	29	21										
FR	614	S	sil,ms	Med-Fine	54	41										
FR	615	BG	bt,plg	Med-Fine												
FR	616	GO	plg,bt	Med-Fine	23	31										
FR	617	Amp	amp,plg	Coarse	0	0										
FR	618	GO	plg,bt	Med-Fine	24	41										
FR	619	BG	bt,plg	Med-Fine												
FR	620	GO	plg,bt	Med-Fine	29	31										
FR	621	GO	plg,bt	Med-Fine	31	32										
FR	622	GO	plg,bt	Med-Fine	26	35										
FR	623	GO	plg,bt	Med-Fine	100	60										
FR	624	BG	bt,plg	Med-Fine	12	23										
FR	625	BG	bt,plg	Med-Fine	349	12										
FR	626	BG	bt,plg	Med-Fine	24	31										
FR	627	BG	bt,plg	Med-Fine												
FR	628	BG	bt,plg	Med-Fine												
FR	629	BG	bt,plg	Med-Fine	22	31										
FR	630	BG	bt,plg	Med-Fine	21	30										
FR	631	BG	bt,plg	Med-Fine	26	9										
FR	632	BG	bt,plg	Med-Fine	21	9										
FR	633	BG	bt,plg	Medium	49	30										
FR	634	BG	bt,plg	Med-Fine	54	22										
FR	635	BG	bt,plg	Med-Fine	26	21										
FR	636	BG	bt,plg	Med-Fine	28	29										
FR	637	BG	bt,plg	Med-Fine												
FR	638	BG	bt,plg	Med-Fine	41	33										
FR	639	BG	bt,plg	Med-Fine	54	24										
FR	640	BG	bt,plg	Med-Fine	51	23										
FR	641	BG	bt,plg	Med-Fine	50	20										
FR	642	BG	bt,plg	Med-Fine	73	33										
FR	643	BG	bt,plg	Medium	56	13										
FR	644	BG	bt,plg	Medium	61	10										
FR	645	BG	bt,plg	Medium	46	10										
FR	646	BG	bt,plg	Medium	55	13										
FR	647	BG	bt,plg	Medium	46	17										
FR	648	BG	bt,plg	Medium	39	23										
FR	649	BG	bt,plg	Medium	41	26										
FR	650	Amp	amp,plg	Med-Coarse												

					Foliation		Lineation		Fold Axis		Axial Surface		IL Angle	Vergen	Joint	
Quad	Station	Lithology	Minerals	Grain Size	Strike	Dip	Trend	Plunge	Trend	Plunge	Strike	Dip			Strike	Dip
FR	651	BG	bt,plg	Med-Fine	86	44										
FR	652	BG	bt,plg	Med-Fine	84	42										
FR	653	BG	bt,plg	Med-Fine	44	26										
FR	654	MS S	ms,grt	Fine	49	39										
FR	655	BG	bt,plg	Med-Coarse	14	4										
FR	656	BG	bt,plg	Med-Coarse												
FR	657	BG	bt,plg	Med-Coarse	17	23										
FR	658	BG	bt,plg	Med-Coarse	17	21										
FR	659	BG	bt,plg	Med-Coarse	19	35										
FR	660	Amp	amp,plg	Med-Fine												
FR	661	MS S	ms	Fine	41	20										
FR	662	BG	bt,plg	Med-Fine	18	30										
FR	663	BG	plg,qtz	Med-Fine	20	30										
FR	664	BG	plg,qtz	Med-Fine	17	28										
FR	665	BG	qtz,bt	Med-Coarse												
FR	666	BG	qtz,bt	Med-Coarse												
FR	667	BG	bt,plg	Med-Coarse												
FR	668	BG	bt,plg	Med-Coarse	44	16										
FR	669	BG	qtz,bt	Med-Fine												
FR	670	BG	qtz,bt	Med-Fine	41	22										
FR	671	GO	plg,qtz	Med-Coarse	31	65										
FR	672	GO	plg,qtz	Med-Coarse	34	22										
FR	673	BG	plg,bt	Med-Coarse												
FR	674	GO	plg,qtz	Med-Coarse	39	21										
FR	675	GO	plg,qtz	Med-Coarse	37	25										
FR	676	S	ms,sil	Med-Fine	34	35										
FR	677	BG	bt,plg	Med-Coarse	46	41										
FR	678	BG	bt,plg	Med-Coarse	42	45										
FR	679	BG	bt,plg	Med-Coarse	29	36										
FR	680	BG	bt,plg	Med-Coarse	39	34										
FR	681	S	ms,sil	Med-Fine	27	19										
FR	682	S	ms,sil	Med-Fine	39	25										
FR	683	S	ms,sil	Med-Fine	29	19										
FR	684	S	ms,sil	Med-Fine	21	21										
FR	685	BG	bt,plg	Medium	29	16										
FR	686	BG	plg,bt	Med-Fine												
FR	687	BG	plg,bt	Med-Fine	343	31										
FR	688	BG	plg,bt	Med-Fine	66	70										
FR	689	BG	plg,bt	Med-Fine	27	40										
FR	690	BG	plg,bt	Med-Fine	29	49										
FR	691	BG	plg,bt	Med-Fine	29	49										
FR	692	BG	plg,bt	Med-Fine	34	43										
FR	693	BG	plg,bt	Med-Fine	29	43										
FR	694	BG	plg,bt	Med-Fine												
FR	695	BG	plg,bt	Med-Fine	25	41										
FR	696	BG	plg,bt	Med-Fine	29	31										
FR	697	BG	plg,bt	Med-Fine	25	28										
FR	698	BG	plg,bt	Med-Fine	26	19										
FR	699	BG	plg,bt	Med-Fine	22	35										
FR	700	GO	plg,qtz	Med-Fine	120	21										
FR	701	BG	plg,bt	Med-Fine	29	41										
FR	702	BG	plg,bt	Med-Fine	26	18										
FR	703	GO	plg,qtz	Med-Fine	23	21										
FR	704	BG	plg,bt	Med-Fine	19	12										
FR	705	BG	plg,bt	Med-Fine	21	15										
FR	706	BG	plg,bt	Med-Fine												
FR	707	BG	plg,bt	Med-Fine	350	42										
FR	708	S	ms,sil	Med-Fine	335	30										
FR	709	GO	plg,qtz	Medium	25	34										
FR	710	GO	plg,qtz	Med-Coarse	22	34										
FR	711	GO	plg,qtz	Med-Coarse	21	33										

					Foliation		Lineation		Fold Axis		Axial Surface		IL Angle	Vergen	Joint	
Quad	Station	Lithology	Minerals	Grain Size	Strike	Dip	Trend	Plunge	Trend	Plunge	Strike	Dip			Strike	Dip
FR	712	BG	bt,plg	Med-Fine	10	12										
FR	713	BG	bt,plg	Med-Fine	12	16										
FR	714	BG	bt,plg	Med-Fine	12	17										
FR	715	BG	bt,plg	Med-Fine	296	36										
FR	716	BG	bt,plg	Med-Fine	326	56										
FR	717	BG	bt,plg	Med-Fine	330	43										
FR	718	BG	bt,plg	Med-Fine	30	30									350	46
FR	720	BG	bt,plg	Med-Fine	310	54										
FR	721	BG	bt,plg	Med-Fine	30	50										
FR	722	BG	bt,plg	Med-Fine	31	30										
FR	723	BG	bt,plg	Med-Fine	30	28										
FR	724	BG	bt,plg	Med-Fine	27	32										
FR	725	BG	bt,plg	Med-Fine	24	46										
FR	726	BG	bt,plg	Med-Fine	25	27										
FR	727	BG	bt,plg	Med-Fine	27	23										
FR	728	BG	bt,plg	Med-Fine	23	21										
FR	729	BG	bt,plg	Med-Fine	29	42										
FR	730	BG	bt,plg	Med-Fine	14	36										
FR	731	BG	bt,plg	Med-Fine	24	17										
FR	732	BG	bt,plg	Med-Fine	25	26										
FR	733	BG	bt,plg	Med-Fine	13	32										
FR	734	GO	plg,qtz	Med-Coarse	26	23										
FR	735	BG	qtz,bt	Medium	349	24									86	79
															184	82
FR	737	BG	qtz,bt	Medium	346	26										
FR	738	BG	bt,plg	Med-Fine	356	19										
FR	739	BG	bt,plg	Med-Fine	275	17										
FR	740	BG	bt,plg	Med-Fine	354	12										
FR	741	BG	bt,plg	Med-Fine	2	14										
FR	742	BG	bt,plg	Med-Fine	4	5										
FR	743	BG	bt,plg	Med-Fine	352	32										
FR	744	BG	bt,plg	Med-Fine	2	32										
FR	745	CS	qtz,grt	Fine												
FR	746	GO	plg,qtz	Medium	349	9										
FR	747	BG	bt,plg	Med-Fine	3	16										
FR	748	BG	bt,plg	Med-Fine												
FR	749	BG	bt,plg	Med-Fine	345	12										
FR	750	BG	plg,bt	Med-Fine	356	10										
FR	751	BG	bt,plg	Med-Fine	9	19										
FR	752	MS S	ms,grt	Med-Fine	1	20										
FR	753	S	sil,ms	Med-Fine												
FR	754	BG	bt,plg	Med-Fine												
FR	755	BG	bt,plg	Med-Fine												
FR	756	BG	bt,plg	Medium	26	35										
FR	757	BG	bt,plg	Medium	25	32										
FR	758	BG	bt,plg	Medium	27	36										
FR	759	S	sil,ms	Fine	41	45										
FR	760	BG	bt,plg	Medium	39	67										
FR	761	BG	bt,plg	Med-Fine												
FR	762	BG	bt,plg	Med-Fine												
FR	763	BG	bt,plg	Med-Fine												
FR	764	BG	bt,plg	Med-Fine												
FR	765	BG	bt,plg	Med-Fine												
FR	766	CS	qtz,grt	Fine												
FR	767	GO	plg,qtz	Med-Coarse												
FR	768	BG	bt,plg	Med-Coarse												
FR	769	BG	bt,plg	Med-Coarse												
FR	770	BG	bt,plg	Med-Fine												
FR	771	BG	bt,plg	Med-Fine												
FR	772	BG	bt,plg	Med-Fine												
FR	773	BG	bt,plg	Med-Fine												

					Foliation		Lineation		Fold Axis		Axial Surface		IL Angle	Vergen	Joint	
Quad	Station	Lithology	Minerals	Grain Size	Strike	Dip	Trend	Plunge	Trend	Plunge	Strike	Dip			Strike	Dip
FR	774	BG	bt,plg	Med-Fine												
FR	775	BG	bt,plg	Med-Fine												
FR	776	BG	bt,plg	Med-Fine												
FR	777	BG	bt,plg	Medium												
FR	778	BG	bt,plg	Medium												
FR	779	S	sil,ms	Fine	170	54										
FR	780	BG	bt,plg	Med-Coarse	134	11										
FR	781	BG	bt,plg	Med-Coarse												
FR	782	Peg	plg,ms	Coarse	250	0										
FR	783	BG	bt,plg	Med-Fine	144	35										
FR	784	BG	bt,plg	Med-Fine	89	20										
FR	785	BG	bt,plg	Med-Fine												
FR	786	BG	qtz	Fine												
FR	787	BG	qtz	Fine					200	12	349	24	15	NE		
FR	789	BG	bt,plg	Med-Fine	49	14										
FR	790	BG	bt,plg	Med-Fine												
FR	791	BG	bt,plg	Med-Fine												
FR	792	BG	bt,plg	Med-Fine	48	18										
FR	793	S	sil,ms	Med-Fine	349	31										
FR	794	S	sil,ms	Med-Fine	355	27										
FR	795	S	sil,ms	Med-Fine	359	15										
FR	796	BG	bt,plg	Fine	355	71										
FR	797	BG	plg,bt	Coarse	341	40										
FR	798	BG	bt,plg	Fine	15	13										
FR	799	GO	bt,plg	Fine	331	19										
FR	800	BG	bt,plg	Fine	330	9									240	85
															150	76
FR	801	S	ms,grt	Fine												
FR	802	BG	bt,plg	Fine	341	7										
FR	803	BG	bt,plg	Fine	31	29										
FR	804	BG	bt,plg	Fine	62	28										
FR	805	S	ms	Med-Fine	170	12										
FR	806	S	sil,ms	Med-Fine	7	34										
FR	807	BG	bt,plg	Med-Fine												
FR	808	BG	bt,plg	Med-Fine												
FR	809	GO	plg,qtz	Fine	32	5										
FR	810	GO	plg,qtz	Fine	21	27										
FR	811	GO	plg,qtz	Fine	28	2										
FR	812	GO	plg,qtz	Fine												
FR	813	S	sil,ms	Fine	352	14										
FR	814	S	sil,ms	Fine	210	6										
FR	815	S	sil,ms	Fine	54	12										
FR	816	S	sil,ms	Fine	31	19										
FR	817	S	sil,ms	Fine	29	46										
FR	818	BG	bt,plg	Medium	29	50										
FR	819	BG	bt,plg	Medium												
FR	820	BG	bt,plg	Medium	29	12										
FR	821	BG	bt,plg	Medium	31	11										
FR	822	BG	bt,plg	Medium	29	17										
FR	823	BG	bt,plg	Medium	25	42										
FR	824	BG	bt,plg	Medium	31	20										
FR	825	BG	bt,plg	Medium	40	48										
FR	826	BG	bt,plg	Medium	41	37										
FR	827	S	sil,ms	Med-Fine												
FR	828	GO	plg,qtz	Med-Fine	36	31										
FR	829	BG	bt,plg	Med-Fine	60	22										
FR	830	BG	plg,qtz	Med-Fine	0	0										
FR	831	BG	plg,qtz	Med-Fine	60	28										
FR	832	BG	plg,qtz	Med-Fine	61	29										
FR	833	S	ms,sil	Med-Fine												
FR	834	GO	plg,qtz	Medium	12	4										

					Foliation		Lineation		Fold Axis		Axial Surface		IL Angle	Vergen	Joint	
Quad	Station	Lithology	Minerals	Grain Size	Strike	Dip	Trend	Plunge	Trend	Plunge	Strike	Dip			Strike	Dip
FR	835	S	sil,ms	Fine	0	0										
FR	836	GO	plg,qtz	Med-Fine	59	21										
FR	837	GO	plg,qtz	Med-Fine												
FR	838	BG	plg,bt	Med-Coarse	358	15										
FR	839	BG	bt,plg	Med-Coarse	304	18										
FR	840	BG	bt,plg	Medium	93	12										
FR	841	BG	plg,bt	Med-Coarse	125	13										
FR	842	GO	plg,qtz	Med-Fine	21	8										
FR	843	BG	plg,bt	Med-Coarse	30	26										
FR	844	BG	plg,bt	Med-Coarse	32	17										
FR	845	GO	plg,qtz	Med-Fine	350	11										
FR	846	MCg	plg,qtz	Med-Coarse												
FR	847	MCg	plg,qtz	Med-Coarse	25	12										
FR	848	RCg	plg,qtz	Med-Fine	56	21										
FR	849	MCg	plg,qtz	Med-Coarse												
FR	850	RCg	plg,qtz	Med-Fine	210	21										
FR	851	MCg	plg,qtz	Med-Coarse												
FR	852	MCg	plg,qtz	Med-Coarse												
FR	853	RCg	plg,qtz	Med-Fine	175	75										
FR	854	MCg	plg,qtz	Med-Coarse												
FR	855	MCg	plg,qtz	Med-Coarse												
FR	856	MCg	plg,qtz	Med-Coarse												
FR	857	MS S	ms	Med-Fine												
FR	858	MS S	ms	Med-Fine												
FR	859	MCg	plg,qtz	Coarse	60	50										
FR	860	MCg	plg,qtz	Med-Coarse												
FR	861	MCg	plg,qtz	Coarse												
FR	862	MCg	plg,qtz	Med-Coarse												
FR	863	S	sil,ms	Med-Fine	71	23										
FR	864	S	sil,ms	Med-Fine	61	26										
FR	866	MCg	plg,qtz	Med-Coarse	210	42			20	10	220	41	65	NW		
FR	867	MCg	plg,qtz	Med-Coarse	42	31										
FR	868	MCg	plg,qtz	Med-Coarse												
FR	869	MCg	plg,qtz	Med-Coarse												
FR	870	MCg	plg,qtz	Med-Coarse	43	41										
FR	871	BG	bt,plg	Med-Fine												
FR	872	BG	plg,bt	Fine												
FR	873	BG	plg,bt	Fine												
FR	874	BG	plg,bt	Fine												
FR	875	BG	plg,bt	Fine												
FR	876	BG	bt,plg	Med-Fine												
FR	877	BG	bt,plg	Med-Fine	32	23										
FR	878	BG	bt,plg	Med-Fine	35	22										
FR	879	Dd		Fine												
FR	880	Dd		Fine												
FR	881	S	sil,ms	Med-Fine												
FR	882	BG	bt,plg	Med-Fine												
FR	883	BG	bt,plg	Med-Fine												
FR	884	BG	bt,plg	Med-Fine												
FR	885	BG	bt,plg	Med-Fine	23	17										
FR	886	GO	plg,qtz	Med-Fine	46	17										
FR	887	GO	plg,qtz	Med-Fine	46	18										
FR	888	S	sil,ms	Med-Fine	49	29										
FR	889	BG	bt,plg	Med-Fine												
FR	890	BG	bt,plg	Medium	54	24										
FR	891	BG	bt,plg	Medium	60	37										
FR	892	BG	bt,plg	Medium	56	21										
FR	893	BG	bt,plg	Medium	57	20										
FR	894	Amp	amp,grt	Med-Fine												
FR	895	BG	bt,plg	Med-Fine												
FR	896	BG	bt,plg	Med-Fine	55	19										

					Foliation		Lineation		Fold Axis		Axial Surface		IL Angle	Vergen	Joint	
Quad	Station	Lithology	Minerals	Grain Size	Strike	Dip	Trend	Plunge	Trend	Plunge	Strike	Dip			Strike	Dip
FR	897	BG	bt,plg	Med-Fine												
FR	898	BG	bt,plg	Med-Fine	52	25										
FR	899	BG	bt,plg	Med-Fine	50	40										
FR	900	BG	bt,plg	Med-Fine	54	21										
FR	901	BG	bt,plg	Med-Fine	70	42										
FR	902	BG	bt,plg	Med-Fine												
FR	903	BG	bt,plg	Med-Fine												
FR	904	BG	bt,plg	Med-Fine												
FR	905	BG	bt,plg	Med-Fine	51	39										
FR	906	BG	bt,plg	Med-Fine												
FR	907	BG	bt,plg	Med-Fine	50	17										
FR	908	BG	bt,plg	Med-Fine												
FR	909	S	ms,sil	Med-Fine												
FR	910	S	ms,sil	Med-Fine	69	10										
FR	911	BG	bt,plg	Medium	11	18										
FR	912	BG	bt,plg	Med-Fine	51	14										
FR	913	BG	bt,plg	Med-Fine	52	9										
FR	914	BG	bt,plg	Med-Fine	56	39										
FR	915	BG	bt,plg	Med-Fine	49	19										
FR	916	BG	qtz,plg	Med-Coarse	52	32										
FR	917	BG	plg,bt	Medium	59	56										
FR	918	BG	bt,plg	Fine												
FR	919	BG	bt,plg	Fine	51	27										
FR	920	BG	bt,plg	Fine	50	54										
FR	921	BG	bt,plg	Fine												
FR	922	Amp	amp	Fine												
FR	923	BG	plg,bt	Medium												
FR	924	BG	plg,bt	Med-Coarse	36	50										
FR	925	BG	plg,bt	Med-Coarse	37	20										
FR	926	BG	plg,bt	Med-Coarse												
FR	927	BG	plg,bt	Med-Coarse												
FR	928	BG	plg,bt	Med-Coarse												
FR	929	Peg	ms,plg	Coarse												
FR	930	BG	bt,plg	Med-Fine												
FR	931	GO	plg,qtz	Med-Fine	345	35										
FR	932	GO	plg,qtz	Med-Fine												
FR	933	GO	plg,qtz	Med-Fine												
FR	934	GO	plg,qtz	Med-Fine												
FR	935	GO	plg,qtz	Med-Fine	290	9										
FR	936	BG	plg,qtz	Med-Fine	341	19										
FR	937	BG	plg,qtz	Med-Fine	16	34										
FR	938	GO	qtz,plg	Coarse	10	20										
FR	939	BG	bt,plg	Medium	39	36			200	9	95	13	24	SW		
FR	941	BG	plg,bt	Medium	16	17										
FR	942	BG	plg,bt	Medium	15	15										
FR	943	BG	plg,bt	Medium												
FR	944	BG	plg,bt	Medium	12	4										
FR	945	BG	plg,bt	Medium												
FR	946	BG	plg,bt	Medium												
FR	947	BG	plg,bt	Medium	16	5										
FR	948	BG	plg,bt	Medium												
FR	949	BG	plg,bt	Medium	20	16										
FR	950	BG	plg,bt	Medium												
FR	951	BG	plg,bt	Medium	356	22										
FR	952	BG	plg,bt	Medium												
FR	953	BG	plg,bt	Medium	356	35										
FR	954	BG	plg,bt	Med-Coarse	5	36										
FR	955	BG	plg,bt	Med-Coarse	13	32									359	85
															269	78
FR	956	BG	plg,bt	Med-Coarse												
FR	957	BG	plg,bt	Med-Coarse												

					Foliation		Lineation		Fold Axis		Axial Surface		IL Angle	Vergen	Joint	
Quad	Station	Lithology	Minerals	Grain Size	Strike	Dip	Trend	Plunge	Trend	Plunge	Strike	Dip			Strike	Dip
FR	958	BG	plg,bt	Med-Coarse												
FR	959	BG	plg,bt	Med-Coarse												
FR	960	BG	plg,bt	Med-Coarse	7	4										
FR	961	BG	plg,bt	Med-Coarse	10	32										
FR	962	S	bt	Med-Fine	20	17										
FR	963	BG	amp,plg	Med-Fine	327	42										
FR	964	S	sil,ms	Med-Fine	34	36										
FR	964	S	sil,ms	Med-Fine	191	16										
FR	965	BG	bt,plg	Med-Fine	44	34										
FR	966	BG	bt,plg	Med-Fine	41	38										
FR	967	BG	bt,plg	Med-Fine	12	51										
FR	968	BG	bt,plg	Med-Fine	34	19										
FR	969	BG	bt,plg	Med-Fine	46	28										
FR	970	BG	bt,plg	Med-Fine												
FR	971	BG	bt,plg	Med-Fine	48	32										
FR	972	BG	bt,plg	Med-Fine	40	23										
FR	973	BG	bt,plg	Med-Fine	27	24										
FR	974	BG	bt,plg	Med-Fine												
FR	975	BG	bt,plg	Med-Fine	355	32										
FR	976	BG	bt,plg	Med-Fine	28	24										
FR	977	BG	bt,plg	Med-Fine	32	26										
FR	978	BG	bt,plg	Med-Fine	28	20										
FR	979	BG	bt,plg	Med-Fine	48	42										
FR	980	BG	bt,plg	Med-Fine	40	49										
FR	981	BG	bt,plg	Med-Fine	38	21										
FR	982	BG	bt,plg	Med-Fine	356	16	125	16								
FR	983	BG	bt,plg	Med-Fine	1	40										
FR	984	BG	bt,plg	Med-Fine	16	24										
FR	985	BG	bt,plg	Med-Fine	44	42										
FR	1-b	BG	bt,plg	Med-Coarse	55	10										
FR	2-b	BG	bt,plg	Med-Coarse	40	8										
FR	3-b	BG	bt,plg	Med-Coarse	50	8										
FR	4-b	BG	bt,plg	Med-Coarse	20	10										
FR	5-b	BG	bt,plg	Med-Coarse	0	11										
FR	7-b	BG	bt,plg	Med-Coarse	250	5										
FR	8-b	BG	bt,plg	Med-Coarse	85	14										
FR	9-b	BG	bt,plg	Med-Coarse	70	16										
FR	10-b	BG	bt,plg	Med-Coarse	65	16										
FR	11-b	BG	bt,plg	Med-Coarse	72	20										
FR	12-b	BG	bt,plg	Med-Coarse	30	30										
FR	13-b	BG	bt,plg	Med-Coarse	10	12										
FR	14-b	BG	bt,plg	Med-Coarse	45	10										
FR	16-b	BG	bt,plg	Medium	15	25										
FR	17-b	BG	bt,plg	Medium	50	10										
FR	18-b	BG	bt,plg	Medium	15	15										
FR	19-b	BG	bt,plg	Med-Coarse	55	10										
FR	23-b	BG	bt,plg	Med-Coarse	60	15										
FR	24-b	BG	bt,plg	Med-Coarse	60	11										
FR	25-b	BG	bt,plg	Med-Coarse	40	35	15	6								
FR	27-b	BG	bt,plg	Medium	25	30										
FR	28-b	BG	bt,plg	Medium	20	10										
FR	29-b	BG	bt,plg	Medium	40	8										
FR	30-b	BG	bt,plg	Medium	30	9										
FR	31-b	BG	bt,plg	Med-Coarse	35	18										
FR	32-b	BG	bt,plg	Med-Coarse	10	12										
FR	33-b	BG	bt,plg	Med-Coarse	45	15										
FR	34-b	BG	bt,plg	Med-Coarse	20	15										
FR	35-b	BG	bt,plg	Med-Coarse	50	14										
FR	36-b	BG	bt,plg	Med-Coarse	12	21										
FR	37-b	BG	bt,plg	Medium	70	14										
FR	6-b	BG	bt,plg	Med-Coarse												

					Foliation		Lineation		Fold Axis		Axial Surface		IL Angle	Vergen	Joint	
Quad	Station	Lithology	Minerals	Grain Size	Strike	Dip	Trend	Plunge	Trend	Plunge	Strike	Dip			Strike	Dip
FR	15-b	BG	bt,plg	Medium												
FR	20-b	BG	bt,plg	Medium												
FR	21-b	BG	bt,plg	Medium												
FR	22-b	BG	bt,plg	Medium												
FR	986	DPg														
FR	987	DPg	plg,qtz	Med-Coarse	20	15										
FR	988	DPg	plg,qtz	Med-Coarse												
FR	989	DPg	plg,qtz	Med-Coarse												
FR	990	MCg	plg,qtz	Coarse												
FR	991	MCg	plg,qtz	Coarse												
FR	992	CS	qtz	Fine												
FR	993	DPg	plg,qtz	Med-Coarse												
FR	994	MCg	plg,bt	Med-Coarse	60	21										
FR	995	MCg	plg,bt	Med-Coarse	111	70										
FR	996	MCg	plg,bt	Med-Coarse	89	51	60	11								
FR	997	MCg	plg,bt	Med-Coarse												
FR	998	RCg	plg,qtz	Med-Fine												
FR	999	MCg	plg,qtz	Coarse												
FR	1000	MCg	plg,qtz	Coarse	30	71										
FR	1001	MCg	plg,qtz	Coarse	30	71										
FR	1002	MCg	plg,qtz	Coarse	54	56	90	25								
FR	1003	MCg	plg,qtz	Coarse												
FR	1004	RCg														
FR	1005	MCg	plg,qtz	Med-Coarse	71	65										
FR	1006	MCg	plg,qtz	Med-Coarse	46	30										
FR	1007	MCg	plg,qtz	Med-Coarse												
FR	1008	MCg	plg,qtz	Med-Coarse	51	59										
FR	1009	DPg	plg,qtz	Med-Coarse												
FR	1010	DPg	plg,qtz	Med-Coarse												
FR	1011	MCg	plg,qtz	Med-Coarse	50	45										
FR	1012	MCg	plg,qtz	Med-Coarse												
FR	1013	MCg	plg,qtz	Med-Coarse	50	45										
FR	1014	MCg	plg,qtz	Med-Coarse												
FR	1015	MCg	plg,qtz	Med-Coarse												
FR	1016	MCg	plg,qtz	Med-Coarse												
FR	1017	DPg	plg,qtz	Medium												
FR	1018	CS														
FR	1019	BG, S	plg,qtz	Med-Fine												
FR	1020	BG, S	plg,qtz	Med-Fine												
FR	1021	BG, S	plg,qtz	Med-Fine												
FR	1022	BG	plg,qtz	Med-Fine												
FR	1023	RCg	plg,qtz	Med-Fine												
FR	1024	GO	plg,ms	Medium	10	68										
FR	1025	MCg	plg,qtz	Med-Coarse	61	56										
FR	1026	MCg	plg,qtz	Med-Coarse	13	25										
FR	1027	DPg	plg,qtz	Med-Coarse	60	34										
FR	1028	DPg	plg,qtz	Medium	70	17										
FR	1029	DPg	plg,qtz	Med-Fine												
FR	1030	DPg	plg,qtz	Med-Fine												
FR	1031	DPg	plg,qtz	Med-Fine												
FR	1032	S	sil,plg	Fine	101	12										
FR	1033	S	sil,plg	Fine	63	75										
FR	1034	DPg	plg,qtz	Medium												
FR	1035	DPg	plg,qtz	Medium	54	26										
FR	1036	DPg	plg,qtz	Medium												
FR	1037	S	plg,sil	Med-Fine												
FR	1038	S	plg,sil	Med-Fine												
FR	1039	S	plg,sil	Med-Fine												
FR	1040	S	plg,sil	Med-Fine												
FR	1041	S	plg,sil	Med-Fine												
FR	1042	S	plg,sil	Med-Fine												

					Foliation		Lineation		Fold Axis		Axial Surface		IL Angle	Vergen	Joint	
Quad	Station	Lithology	Minerals	Grain Size	Strike	Dip	Trend	Plunge	Trend	Plunge	Strike	Dip			Strike	Dip
FR	1043	S	plg,sil	Med-Fine												
FR	1044	S, mylonite	plg,sil	Med-Fine												
FR	1045	DPg	qtz,plg	Med-Coarse												
FR	1046	CS														
FR	1047	S	sil,plg	Med-Fine												
FR	1048	S	sil,plg	Med-Fine												
FR	1049	DPg														
FR	1050	DPg	plg,qtz	Fine												
FR	1051	S	sil,plg	Med-Fine												
FR	1052	BG	bt,plg	Medium												
FR	1053	BG	bt,plg	Medium												
FR	1054	BG	plg,qtz	Med-Coarse												
FR	1055	DPg	plg,qtz	Medium												
FR	1056	DPg	plg,qtz	Medium	111	71										
FR	1057	S	sil,plg	Med-Fine												
FR	1058	S	sil,plg	Med-Fine	190	26										
FR	1059	CS														
FR	1060	DPg	qtz,plg	Medium												
FR	1061	DPg	plg,qtz	Med-Coarse												
FR	1062	DPg	plg,qtz	Med-Coarse												
FR	1063	DPg	plg,qtz	Med-Coarse												
FR	1064	S	sil,plg	Med-Fine												
FR	1065	S	sil,plg	Med-Fine												
FR	1066	S	sil,plg	Med-Fine	85	16										
FR	1067	S	sil,plg	Med-Fine	161	12										
FR	1068	S	sil,plg	Med-Fine	88	16										
FR	1069	S	sil,plg	Med-Fine												
FR	1070	S	sil,plg	Med-Fine												
FR	1071	S	sil,plg	Med-Fine												
FR	1072	S	sil,plg	Med-Fine												
FR	1073	S	sil,plg	Med-Fine												
FR	1074	S	sil,plg	Med-Fine												
FR	1075	DPg														
FR	1076	S	sil,plg	Med-Fine	45	41										
FR	1077	S	sil,plg	Med-Fine	51	7										
FR	1078	S	sil,plg	Med-Fine	50	32										
FR	1079	DPg	plg,bt	Med-Coarse	56	17										
FR	1080	DPg	plg,bt	Med-Coarse												
FR	1081	Peg														
FR	1082	BG, S	plg,qtz	Med-Fine												
FR	1083	RCg														
FR	1084	RCg														
FR	1085	RCg														
FR	1086	RCg														
FR	1087	RCg			46	35										
FR	1088	DPg														
FR	1089	DPg			76	64										
FR	1090	DPg			71	32										
FR	1091	BG	bt,plg	Medium	140	79	135	5								
FR	1092	MCg														
FR	1093	MCg			135	26										
FR	1094	MCg														
FR	1095	MCg			200	34										
FR	1096	MCg			111	16										
FR	1097	MCg			121	34										
FR	1098	MCg														
FR	1099	MCg														
FR	1100	MCg													1	88
FR	1100	MCg													89	79
FR	1101	MCg														
FR	1102	MCg														

					Foliation		Lineation		Fold Axis		Axial Surface		IL Angle	Vergen	Joint	
Quad	Station	Lithology	Minerals	Grain Size	Strike	Dip	Trend	Plunge	Trend	Plunge	Strike	Dip			Strike	Dip
FR	1103	MCg														
FR	1104	MCg														
FR	1105	MCg														
FR	1106	MCg														
FR	1107	MCg														
FR	1108	MCg														
FR	1109	MCg			79	23										
FR	1110	MCg			65	12										
FR	1111	MCg														
FR	1112	RCg														
FR	1113	DPg														
FR	1114	DPg			46	18										
FR	1115	MCg														
FR	1116	MCg														
FR	1117	MCg														
FR	1118	MCg			330	8										
FR	1119	MCg			46	12										
FR	1120	MCg			54	16										
FR	1121	MCg			64	8									89	89
															170	79
FR	1122	MCg			98	24										
FR	1123	MCg														
FR	1124	MCg			190	41										
FR	1125	RCg														
FR	1126	DPg														
FR	1127	MCg														
FR	1128	MCg			51	11										
FR	1129	MCg			21	14										
FR	1130	MCg	bt,plg	Med-Coarse	54	16										
FR	1131	MCg	bt,plg	Med-Coarse												
FR	1132	MCg	bt,plg	Med-Coarse												
FR	1133	Si-C														
FR	1134	Si-C														
FR	1135	Si-C														
FR	1136	Si-C														
FR	1137	Si-C														
FR	1138	Si-C														
FR	1139	DPg	plg,qtz	Med-Coarse												
FR	1140	Si-C														
FR	1141	Si-C														
FR	1142	Si-C														
FR	1143	Si-C														
FR	1144	Si-C														
FR	1145	MCg														
FR	1146	MCg														
FR	1147	MCg														
FR	1148	MCg														
FR	1149	MCg														
FR	1150	MCg			101	24										
FR	1151	Si-C														
FR	1152	Si-C														
FR	1153	Si-C														
FR	1154	Si-C														
FR	1155	Si-C														
FR	1156	Si-C														
FR	1157	Gneiss	bt,plg	Med-Fine												
FR	1158	Gneiss	bt,plg	Med-Fine												
FR	1159	Gneiss	bt,plg	Med-Fine	36	23										
FR	1160	BG	bt,plg	Fine	346	30										
FR	1161	BG	bt,plg	Fine	346	30										
FR	1162	BG- S	bt,plg	Fine	344	14										

					Foliation		Lineation		Fold Axis		Axial Surface		IL Angle	Vergen	Joint	
Quad	Station	Lithology	Minerals	Grain Size	Strike	Dip	Trend	Plunge	Trend	Plunge	Strike	Dip			Strike	Dip
FR	1163	BG- S	bt,plg	Fine	5	21										
FR	1164	BG- S	bt,plg	Fine	29	22										
FR	1165	BG- S	bt,plg	Fine	21	17										
FR	1166	Dd														
FR	1167	Amp	amp,plg	Fine												
FR	1168	BG	bt,plg	Med-Fine												
FR	1169	BG- S	bt,plg	Med-Fine	19	5										
FR	1170	BG- S	bt,plg	Med-Fine	39	17										
FR	1171	BG- S	bt,plg	Med-Fine												
FR	1172	BG- S	bt,plg	Med-Fine												
FR	1173	BG- S	bt,plg	Med-Fine												
FR	1174	BG- S	bt,plg	Med-Fine												
FR	1175	BG- S	bt,plg	Med-Fine												
FR	1176	RCg														
FR	1177	BG	bt,plg	Fine												
FR	1178	BG	bt,plg	Fine	28	30										
FR	1179	BG	bt,plg	Fine	29	35										
FR	1180	BG	bt,plg	Med-Coarse												
FR	1181	BG	bt,plg	Med-Coarse												
FR	1180	BG	bt,plg	Med-Coarse												
FR	1181	BG	bt,plg	Med-Coarse												
FR	1182	Si-C														
FR	1183	Si-C														
FR	1184	Si-C														
FR	1185	Si-C														
FR	1186	Si-C														
FR	1187	BG	plg,bt	Med-Coarse												
FR	1188	BG	plg,bt	Med-Coarse												
FR	1189	Si-C														
FR	1190	S	sil,ms	Fine	27	65										
FR	1191	Amp	amp,grt	Medium												
FR	1192	S	sil,ms	Fine	332	52									139	77
															29	80
FR	1193	Amp	amp,grt	Medium												
FR	1194	S	sil,plg	Med-Fine	356	34										
FR	1195	Amp	amp,plg	Medium												
FR	1196	BG	bt,plg	Fine												
FR	1197	Amp	amp,plg	Medium												
FR	1198	BG	bt,plg	Medium	54	32										
FR	1199	BG	bt,plg	Med-Fine	35	30										
FR	1200	BG	bt,plg	Med-Fine	6	12			6	12	201	49	25	SE		
FR	1201	Amp	amp,plg	Medium												
FR	1202	Amp	amp,plg	Medium	24	51			172	38	201	46	10	NE		
FR	1203	Amp	amp,plg	Medium	29	41									142	88
FR	1204	BG, Amp	bt,plg	Med-Fine	29	23										
FR	1205	BG, Amp	bt,plg	Med-Fine	32	41										
FR	1206	BG, Amp	bt,plg	Med-Fine	56	24										
FR	1207	BG, Amp	bt,plg	Med-Fine	49	9										
FR	1208	S, Amp	sil,ms	Fine	49	12										
FR	1209	S, Amp	sil,ms	Fine	45	27										
FR	1210	S, Amp	sil,ms	Med-Fine	0	0										
FR	1211	S, Amp	sil,ms	Med-Fine	45	31										
FR	1212	Amp	amp,plg	Medium	41	25										
FR	1213	BG	bt,plg	Med-Fine												
FR	1214	BG	bt,plg	Med-Fine	32	30										
FR	1215	BG	bt,plg	Med-Fine												
FR	1216	BG	bt,plg	Med-Fine												
FR	1217	BG	bt,plg	Med-Fine												
FR	1218	BG	bt,plg	Fine												
FR	1219	Gondite	grt	Fine	271	68										
FR	1220	S, Amp	sil,ms	Fine	49	25										

					Foliation		Lineation		Fold Axis		Axial Surface		IL Angle	Vergen	Joint	
Quad	Station	Lithology	Minerals	Grain Size	Strike	Dip	Trend	Plunge	Trend	Plunge	Strike	Dip			Strike	Dip
FR	1221	S, Amp	sil,ms	Fine	43	27										
FR	1222	Amp	amp,plg	Medium												
FR	1223	Amp	amp,plg	Medium												
FR	1224	BG	bt,plg	Fine	23	47	23	16								
FR	1225	BG	bt,plg	Fine	25	37										
FR	1226	BG, Amp	bt,plg	Fine	20	34										
FR	1227	BG	bt,plg	Fine	9	20										
FR	1228	BG	bt,plg	Fine	9	27	8	11								
FR	1229	BG	bt,plg	Fine	9	32										
FR	1230	BG	bt,plg	Fine	27	55										
FR	1231	BG	bt,plg	Fine	9	38	10	11								
FR	1232	BG	bt,plg	Fine	11	34										
FR	1233	BG	bt,plg	Fine	59	34										
FR	1234	BG	bt,plg	Medium	11	23										
FR	1235	RCg														
FR	1236	BG	bt,plg	Med-Fine	11	20										
FR	1237	BG	bt,plg	Coarse	12	50										
FR	1238	BG	bt,plg	Med-Coarse	11	50										
FR	1239	BG	bt,plg	Med-Coarse	12	44										
FR	1240	BG	bt,plg	Med-Coarse	15	49										
FR	1241	BG	bt,plg	Med-Coarse	11	34	10	12								
FR	1242	BG	bt,plg	Med-Coarse												
FR	1243	BG	bt,plg	Medium	0	23										
FR	1244	BG	bt,plg	Medium												
FR	1245	BG	bt,plg	Medium												
FR	1246	GO	plg,qtz	Medium	12	40										
FR	1247	BG	bt,plg	Med-Fine	24	20										
FR	1248	QV														
FR	1249	BG, Amp	bt,plg	Medium	13	40										
FR	1250	BG, Amp	bt,plg	Medium	31	51										
FR	1251	BG, Amp	bt,plg	Medium	31	24										
FR	1252	Amp	amp,plg	Med-Fine												
FR	1253	Amp	amp,plg	Med-Fine												
FR	1254	RCg														
FR	1255	RCg														
FR	1256	RCg														
FR	1257	S	sil,ms	Med-Fine	29	54										
FR	1258	S	sil,ms	Med-Fine												
FR	1259	S	sil,ms	Med-Fine												
FR	1260	S	sil,ms	Med-Fine												
FR	1261	DPg														
FR	1262	S	sil,ms	Med-Fine												
FR	1263	DPg														
FR	1264	DPg														
FR	1265	RCg														
FR	1266	DPg														
FR	1267	DPg														
FR	1268	DPg														
FR	1269	RCg														
FR	1270	DPg														
FR	1271	DPg														
FR	1272	DPg														
FR	1273	DPg														
FR	1274	QV	qtz	Fine												
FR	1275	DPg	plg,qtz	Med-Coarse												
FR	1276	DPg	plg,qtz	Med-Coarse												
FR	1277	DPg	plg,qtz	Med-Coarse												
FR	1278	DPg	plg,qtz	Med-Coarse												
FR	1279	MCg	bt,kspr	Coarse	46	34										
FR	1280	DPg														
FR	1281	RCg	plg,qtz	Fine												

					Foliation		Lineation		Fold Axis		Axial Surface		IL Angle	Vergen	Joint	
Quad	Station	Lithology	Minerals	Grain Size	Strike	Dip	Trend	Plunge	Trend	Plunge	Strike	Dip			Strike	Dip
FR	1282	DPg	plg,qtz	Med-Coarse												
FR	1283	DPg	plg,qtz	Med-Coarse												
FR	1284	DPg	plg,qtz	Med-Coarse												
FR	1285	DPg	plg,qtz	Med-Coarse												
FR	1286	DPg	plg,qtz	Med-Coarse												
FR	1287	MCg	bt,kspr	Coarse												
FR	1288	DPg	plg,qtz	Med-Coarse												
FR	1289	DPg	plg,qtz	Med-Coarse												
FR	1290	RCg	plg,qtz	Fine												
FR	1291	DPg	plg,qtz	Med-Coarse												
FR	1292	RCg														
FR	1293	DPg														
FR	1294	RCg														
FR	1295	RCg														
FR	1296	RCg														
FR	1297	DPg														
FR	1298	DPg														
FR	1299	DPg	plg,qtz	Med-Coarse	1	34										
FR	1300	RCg		Fine												
FR	1301	DPg														
FR	1302	RCg														
FR	1303	RCg														
FR	1304	S	sil,ms	Med-Fine												
FR	1305	DPg	plg,plg	Med-Coarse												
FR	1306	S	sil,ms	Fine	331	46										
FR	1307	S	sil,ms	Fine												
FR	1308	S	sil,ms	Fine												
FR	1309	DPg														
FR	1310	DPg														
FR	1311	S	sil,ms	Med-Fine												
FR	1312	DPg														
FR	1313	S	sil,ms	Med-Fine												
FR	1314	DPg														
FR	1315	RCg														
FR	1316	RCg														
FR	1317	S	sil,ms	Med-Fine												
FR	1318	S	sil,ms	Med-Fine												
FR	1319	S	sil,ms	Med-Fine												
FR	1320	S	sil,ms	Med-Fine												
FR	1321	S	sil,ms	Med-Fine												
FR	1322	DPg														
FR	1323	S	sil,ms	Fine												
FR	1324	S	sil,ms	Fine												
FR	1325	QV														
FR	1326	DPg														
FR	1327	DPg														
FR	1328	DPg	plg,qtz	Med-Coarse	67	64										
FR	1329	S	sil,ms	Fine												
FR	1330	RCg														
FR	1331	RCg			66	37										
FR	1332	RCg														
FR	1333	DPg														
FR	1334	DPg														
FR	1335	S	sil,ms	Med-Fine												
FR	1336	DPg														
FR	1337	DPg	plg,qtz	Med-Coarse												
FR	1338	RCg	plg,qtz	Fine												
FR	1339	DPg	plg,ms	Med-Coarse	153	54										
FR	1340	DPg	plg,ms	Med-Coarse	153	54										
FR	1341	DPg	plg,qtz	Med-Coarse												
FR	1342	S	ms,plg	Medium												

					Foliation		Lineation		Fold Axis		Axial Surface		IL Angle	Vergen	Joint	
Quad	Station	Lithology	Minerals	Grain Size	Strike	Dip	Trend	Plunge	Trend	Plunge	Strike	Dip			Strike	Dip
FR	1343	DPg	plg,qtz	Med-Coarse												
FR	1344	DPg	plg,qtz	Med-Coarse												
FR	1345	RCg	plg,qtz	Med-Fine												
FR	1346	DPg	plg,qtz	Med-Coarse												
FR	1347	DPg	plg,qtz	Med-Coarse												
FR	1348	DPg														
FR	1349	DPg														
FR	1350	DPg														
FR	1351	DPg, MCg	plg,qtz	Med-Coarse	80	20										
FR	1352	DPg	plg,qtz	Med-Coarse												
FR	1353	DPg														
FR	1354	DPg	plg,qtz	Med-Coarse											85	87
FR	1354	DPg	plg,qtz	Med-Coarse												
FR	1355	DPg	plg,qtz	Med-Coarse												
FR	1356	DPg	plg,qtz	Med-Coarse												
FR	1357	MCg	kspr,qtz	Coarse												
FR	1358	DPg														
FR	1359	MCg														
FR	1360	DPg														
FR	1361	DPg														
FR	1362	MCg	kspr,qtz	Coarse											101	78
FR	1363	DPg														
FR	1364	MCg	kspr,qtz	Coarse	15	20	15	2								
MF	1	CS														
MF	2	DPg	plg,qtz	Med-Coarse	49	23										
MF	3	DPg	plg,qtz	Med-Coarse	45	22										
MF	4	BG, S	plg,qtz	Med-Coarse	145	16										
MF	5	BG, S	plg,qtz	Med-Coarse	41	32	132	6								
MF	6	BG, S	plg,qtz	Med-Coarse												
MF	7	Gneiss	bt,plg	Med-Fine												
MF	8	BG, S	plg,qtz	Med-Fine	160	11									130	81
															40	79
MF	9	BG, S	plg,qtz	Med-Fine	160	11	11	1								
MF	10	Gneiss	plg,qtz	Med-Coarse	98	14										
MF	11	Gneiss	plg,qtz	Med-Coarse	56	12										
MF	12	Gneiss	plg,qtz	Med-Coarse	16	46										
MF	13	MCg		Med-Coarse												
MF	14	Gneiss	bt,plg	Med-Fine	46	16										
MF	15	MCg	bt,plg	Med-Coarse	46	14										
MF	16	S	sil,ms	Med-Fine	31	43										
MF	17	S	sil,ms	Med-Fine												
MF	18	S	sil,ms	Med-Fine	43	14										
MF	19	S	sil,ms	Med-Fine	59	12										
MF	20	S	sil,ms	Med-Fine												
MF	21	S	sil,ms	Med-Fine												
MF	22	S	sil,ms	Med-Fine	333	16										
MF	23	S	sil,ms	Med-Fine	74	18										
MF	24	S	ms	Med-Coarse	54	25										
MF	25	S	ms	Med-Coarse	98	34										
MF	26	S	ms	Med-Coarse												
MF	27	DPg														
MF	28	S	sil,ms	Med-Coarse	42	12										
MF	29	S	sil,ms	Med-Coarse	56	14										
MF	30	S	sil,ms	Med-Coarse	181	59										
MF	31	S	sil,ms	Med-Coarse	59	51			220	3	61	65				
MF	33	S	sil,ms	Med-Coarse	31	17										
MF	34	S	sil,ms	Med-Coarse												
MF	35	S	sil,ms	Med-Coarse	54	26									315	88
MF	36	S	sil,ms	Med-Coarse											240	85
MF	37	S	sil,ms	Med-Coarse												

					Foliation		Lineation		Fold Axis		Axial Surface		IL Angle	Vergen	Joint	
Quad	Station	Lithology	Minerals	Grain Size	Strike	Dip	Trend	Plunge	Trend	Plunge	Strike	Dip			Strike	Dip
MF	38	DPg														
MF	39	BG	plg,bt	Med-Coarse												
MF	385	BG	bt,plg	Fine	1	20			356	20	350	70				
MF	40	BG	plg,bt	Med-Coarse												
MF	41	BG	plg,bt	Med-Coarse												
MF	42	BG	plg,bt	Med-Coarse	24	46									280	78
															30	88
MF	43	BG	plg,bt	Med-Coarse												
MF	44	BG	plg,bt	Med-Coarse												
MF	45	BG	plg,bt	Med-Coarse	26	23										
MF	46	BG	plg,bt	Med-Coarse	25	32										
MF	47	BG	plg,bt	Med-Coarse												
MF	48	BG	plg,bt	Med-Coarse												
MF	49	BG	plg,bt	Med-Coarse												
MF	50	BG	plg,bt	Med-Coarse												
MF	51	BG	plg,bt	Med-Coarse	25	34										
MF	52	BG	plg,bt	Med-Coarse	56	15										
MF	53	BG	plg,bt	Med-Coarse	58	34										
MF	54	BG	plg,bt	Med-Coarse	65	37										
MF	55	BG	plg,bt	Med-Coarse												
MF	56	BG	plg,bt	Med-Coarse												
MF	57	BG	plg,bt	Med-Coarse												
MF	58	BG	plg,bt	Med-Coarse												
MF	59	BG	plg,bt	Med-Coarse												
MF	60	BG	plg,bt	Med-Coarse												
MF	61	BG	plg,bt	Med-Coarse	54	26										
MF	62	BG	plg,bt	Med-Coarse	55	34										
MF	63	BG	plg,bt	Med-Coarse												
MF	64	BG	plg,bt	Med-Coarse												
MF	65	DPg	qtz,plg	Med-Coarse												
MF	66	DPg	qtz,plg	Med-Coarse												
MF	67	DPg	qtz,plg	Med-Coarse												
MF	68	DPg	qtz,plg	Med-Coarse												
MF	69	DPg	qtz,plg	Med-Coarse												
MF	70	DPg	qtz,plg	Med-Coarse												
MF	71	DPg	qtz,plg	Med-Coarse												
MF	72	DPg	qtz,plg	Med-Coarse												
MF	73	DPg	qtz,plg	Med-Coarse	46	17										
MF	74	DPg	qtz,plg	Med-Coarse												
MF	75	MCg	bt,plg	Med-Coarse												
MF	76	BG	bt,plg	Med-Coarse												
MF	77	BG	bt,plg	Med-Coarse												
MF	78	BG	bt,plg	Med-Coarse												
MF	79	BG	bt,plg	Med-Coarse	38	12										
MF	80	BG	bt,plg	Med-Coarse	345	21										
MF	81	BG	bt,plg	Med-Coarse	46	20										
MF	82	BG	bt,plg	Med-Coarse	29	6										
MF	83	BG	bt,plg	Med-Coarse	9	61			61	58	55	49	23	SW		
MF	84	BG	bt,plg	Med-Coarse	52	26										
MF	86	BG	bt,plg	Med-Coarse	29	35			63	23	63	89	35	upright		
MF	87	BG	plg,bt	Coarse	56	35										
MF	88	BG	plg,bt	Coarse	52	30										
MF	89	BG	plg,bt	Coarse	52	34										
MF	90	BG	plg,bt	Coarse	53	66										
MF	91	BG	plg,bt	Coarse	51	55										
MF	92	BG	plg,bt	Coarse	48	42										
MF	93	BG	plg,bt	Coarse	51	36										
MF	94	S	ms,sil	Medium												
MF	95	S	ms,sil	Medium	67	16										
MF	96	S	ms,sil	Medium												
MF	97	S	ms,sil	Medium												

					Foliation		Lineation		Fold Axis		Axial Surface		IL Angle	Vergen	Joint	
Quad	Station	Lithology	Minerals	Grain Size	Strike	Dip	Trend	Plunge	Trend	Plunge	Strike	Dip			Strike	Dip
MF	98	BG	plg,bt	Coarse	59	12										
MF	99	BG	plg,bt	Coarse												
MF	100	Si-C														
MF	101	Si-C														
MF	102	Si-C														
MF	103	BG	plg,bt	Med-Fine												
MF	104	BG	plg,bt	Med-Fine												
MF	105	Amp														
MF	106	Si-C														
MF	107	Si-C														
MF	108	Amp														
MF	109	Amp														
MF	110	BG	plg,bt	Med-Fine												
MF	111	BG	plg,bt	Med-Fine	66	24										
MF	112	BG	plg,bt	Med-Fine												
MF	113	Si-C														
MF	114	BG	plg,bt	Medium	53	12										
MF	115	BG	plg,bt	Medium	46	85										
MF	116	BG	plg,bt	Medium	46	23										
MF	117	BG	plg,bt	Medium												
MF	118	BG	plg,bt	Medium	53	57										
MF	119	BG	plg,bt	Medium	250	70										
MF	120	S	bt,grt	Medium												
MF	121	S	bt,grt	Medium	239	79										
MF	122	S	bt,grt	Medium	241	70										
MF	123	S	bt,grt	Medium												
MF	124	S	bt,sil	Medium												
MF	125	S	bt,sil	Medium	251	27										
MF	126	S	bt,sil	Medium												
MF	127	Granite	plg,qtz	Fine												
MF	128	BG	plg,bt	Med-Coarse												
MF	129	BG	plg,bt	Med-Coarse												
MF	130	BG	plg,bt	Med-Coarse											306	76
MF	130	BG	plg,bt	Med-Coarse											219	80
MF	131	BG	plg,bt	Med-Coarse												
MF	132	BG	plg,bt	Med-Coarse												
MF	133	BG	plg,bt	Med-Coarse												
MF	134	BG	plg,bt	Med-Coarse												
MF	135	BG	plg,bt	Med-Coarse	49	39										
MF	136	BG	plg,bt	Med-Coarse	54	75										
MF	137	BG	plg,bt	Med-Coarse	54	27										
MF	138	BG	plg,bt	Med-Coarse	44	46										
MF	139	BG	plg,bt	Med-Coarse												
MF	140	BG	plg,bt	Med-Coarse												
MF	141	BG	plg,bt	Med-Coarse	54	34										
MF	142	BG	bt,plg	Medium												
MF	143	BG	bt,plg	Medium	245	81										
MF	144	BG	bt,plg	Medium												
MF	145	BG	bt,plg	Med-Fine	221	60										
MF	146	BG	bt,plg	Med-Fine	51	41										
MF	147	BG	bt,plg	Med-Fine												
MF	148	Peg														
MF	149	BG	plg,bt	Med-Coarse	24	51										
MF	150	BG	plg,bt	Med-Coarse												
MF	151	BG	plg,bt	Med-Coarse	14	41										
MF	152	BG	plg,bt	Med-Coarse												
MF	153	BG	plg,bt	Med-Coarse												
MF	154	BG	plg,bt	Med-Coarse												
MF	155	BG	plg,bt	Med-Coarse												
MF	156	BG	plg,bt	Med-Coarse												
MF	157	BG	plg,bt	Med-Coarse	47	21										

					Foliation		Lineation		Fold Axis		Axial Surface		IL Angle	Vergen	Joint	
Quad	Station	Lithology	Minerals	Grain Size	Strike	Dip	Trend	Plunge	Trend	Plunge	Strike	Dip			Strike	Dip
MF	158	BG	plg,bt	Med-Coarse												
MF	159	BG	plg,bt	Med-Coarse												
MF	160	BG	plg,bt	Med-Coarse	98	14	210	14								
MF	161	BG	plg,bt	Med-Coarse												
MF	162	BG	plg,bt	Med-Coarse	21	21										
MF	163	BG	plg,bt	Med-Coarse												
MF	164	BG	plg,bt	Med-Coarse	49	31										
MF	165	BG	plg,bt	Med-Coarse	57	80										
MF	166	BG	plg,bt	Med-Coarse	197	75										
MF	167	BG	plg,bt	Med-Coarse	45	76										
MF	168	BG	plg,bt	Med-Coarse	10	79										
MF	169	BG	plg,bt	Med-Coarse	46	74										
MF	170	BG	plg,bt	Med-Coarse	28	79										
MF	171	BG	plg,bt	Med-Coarse												
MF	172	BG	plg,bt	Med-Coarse	45	78										
MF	173	BG	plg,bt	Med-Coarse												
MF	174	BG	plg,bt	Med-Coarse												
MF	175	BG	bt,plg	Med-Fine												
MF	176	BG	bt,plg	Med-Fine												
MF	177	BG	bt,plg	Med-Fine												
MF	178	BG	bt,plg	Med-Fine												
MF	179	BG	bt,plg	Med-Fine												
MF	180	BG	bt,plg	Med-Fine												
MF	181	BG	bt,plg	Med-Fine												
MF	182	BG	bt,plg	Med-Fine												
MF	183	BG	plg,bt	Med-Coarse												
MF	184	BG	plg,bt	Med-Coarse												
MF	185	BG	plg,bt	Coarse												
MF	186	BG	plg,bt	Coarse												
MF	187	BG	plg,bt	Coarse												
MF	188	BG	plg,bt	Coarse												
MF	189	BG	plg,bt	Coarse												
MF	190	BG	bt,plg	Med-Fine												
MF	191	BG	bt,plg	Med-Fine												
MF	192	Amp	amp	Fine												
MF	193	BG	bt,plg	Med-Fine	46	79										
MF	194	BG	bt,plg	Med-Fine	45	64										
MF	195	BG	bt,plg	Coarse	42	61										
MF	196	S	bt	Med-Fine												
MF	197	BG	bt,plg	Med-Coarse												
MF	198	BG	bt,plg	Med-Fine												
MF	199	BG	bt,plg	Med-Fine												
MF	200	BG	bt,plg	Med-Fine												
MF	201	BG	bt,plg	Med-Fine												
MF	202	BG	bt,plg	Med-Fine												
MF	203	BG	bt,plg	Med-Fine	216	61										
MF	204	BG	bt,plg	Med-Fine	44	61										
MF	205	BG	bt,plg	Med-Fine												
MF	206	BG	bt,plg	Med-Fine	45	65										
MF	207	BG	bt,plg	Med-Fine												
MF	208	BG	bt,plg	Med-Fine	51	39										
MF	209	BG	bt,plg	Med-Fine												
MF	210	BG	bt,plg	Med-Fine												
MF	211	BG	bt,plg	Med-Fine												
MF	212	BG	bt,plg	Med-Fine												
MF	213	BG	bt,plg	Med-Fine												
MF	214	BG	bt,plg	Med-Fine												
MF	215	BG	bt,plg	Med-Fine	46	61										
MF	216	BG	bt,plg	Med-Fine	94	51										
MF	217	BG	bt,plg	Med-Fine	158	29										
MF	218	BG	bt,plg	Med-Fine	86	34			220	46	70	46	25	NE		

					Foliation		Lineation		Fold Axis		Axial Surface		IL Angle	Vergen	Joint	
Quad	Station	Lithology	Minerals	Grain Size	Strike	Dip	Trend	Plunge	Trend	Plunge	Strike	Dip			Strike	Dip
MF	219	BG	bt,plg	Med-Fine	69	81										
MF	220	BG	bt,plg	Med-Fine	59	26										
MF	221	BG	bt,plg	Med-Coarse												
MF	222	BG	bt,plg	Med-Coarse	59	74			50	75	30	64	40	upright		
MF	223	BG	bt,plg	Med-Coarse	51	65										
MF	224	BG	bt,plg	Med-Coarse	66	49										
MF	225	BG	bt,plg	Med-Coarse	74	76										
MF	226	BG	bt,plg	Med-Coarse	49	54										
MF	227	BG	bt,plg	Med-Coarse												
MF	228	BG	bt,plg	Med-Coarse												
MF	229	BG	bt,plg	Med-Coarse												
MF	230	BG	bt,plg	Med-Coarse	60	49										
MF	231	BG	bt,plg	Med-Coarse	225	49									324	87
															215	85
MF	232	BG	bt,plg	Med-Coarse												
MF	233	BG	bt,plg	Med-Coarse												
MF	234	BG	bt,plg	Med-Fine												
MF	235	S	bt,plg	Med-Fine												
MF	236	Amp														
MF	237	Amp														
MF	238	Amp	amp,plg													
MF	239	Amp	amp,plg													
MF	240	Amp	amp,plg													
MF	241	BG	bt,plg	Med-Coarse	51	60										
MF	242	BG	bt,plg	Med-Coarse												
MF	243	BG	bt,plg	Coarse												
MF	244	Amp	amp,plg	Fine												
MF	245	BG	bt,plg	Medium												
MF	246	S	sil,bt	Med-Fine												
MF	247	S	sil,bt	Med-Fine												
MF	248	Amp	amp,plg	Med-Fine												
MF	249	BG	bt,plg	Med-Coarse												
MF	250	S	bt,sil	Medium												
MF	251	S	bt,sil	Med-Fine												
MF	252	BG	bt,plg	Med-Coarse	51	64										
MF	253	BG	bt,plg	Med-Coarse	150	21	4	5								
MF	254	BG	bt,plg	Med-Coarse	49	36										
MF	255	BG	bt,plg	Med-Coarse	54	63										
MF	256	BG	bt,plg	Med-Coarse	46	31	308	31								
MF	257	BG	bt,plg	Med-Coarse	74	66										
MF	258	BG	bt,plg	Med-Coarse	46	76										
MF	259	BG	bt,plg	Med-Fine	56	61										
MF	260	BG	bt,plg	Med-Fine												
MF	261	BG	bt,plg	Med-Fine												
MF	262	BG	bt,plg	Med-Coarse												
MF	263	BG	bt,plg	Med-Coarse	16	32										
MF	264	BG	bt,plg	Med-Coarse	12	84										
MF	265	BG	bt,plg	Med-Coarse	15	67									130	78
															215	81
MF	266	BG	bt,plg	Med-Coarse	31	71			350	30	351	46	41	NW		
MF	268	BG	bt,plg	Med-Coarse	31	84										
MF	269	BG	bt,plg	Med-Coarse	11	20										
MF	270	BG	bt,plg	Med-Coarse	59	30										
MF	271	BG	bt,plg	Med-Coarse	78	76										
MF	272	BG	bt,plg	Med-Coarse	34	49										
MF	273	BG	bt,plg	Med-Coarse	34	38			70	46	73	46	96	NW		
MF	274	BG	bt,plg	Med-Coarse												
MF	275	BG	bt,plg	Med-Coarse	50	61										
MF	276	BG	bt,plg	Med-Fine												
MF	277	BG	plg,bt	Medium												
MF	278	BG	plg,bt	Medium												

					Foliation		Lineation		Fold Axis		Axial Surface		IL Angle	Vergen	Joint	
Quad	Station	Lithology	Minerals	Grain Size	Strike	Dip	Trend	Plunge	Trend	Plunge	Strike	Dip			Strike	Dip
MF	279	BG	plg,bt	Med-Fine												
MF	280	BG	plg,bt	Med-Coarse												
MF	281	BG	plg,bt	Med-Fine												
MF	282	BG	plg,bt	Coarse												
MF	283	BG	plg,bt	Med-Fine												
MF	284	BG	plg,bt	Med-Fine												
MF	285	BG	plg,bt	Med-Fine												
MF	286	BG	plg,bt	Fine												
MF	287	Amp	amp,plg	Fine												
MF	288	BG	bt,plg	Med-Fine												
MF	289	BG	bt,plg	Med-Coarse												
MF	290	BG	plg,bt	Med-Coarse												
MF	291	BG	plg,bt	Med-Coarse												
MF	292	BG	plg,bt	Med-Coarse												
MF	293	BG	plg,bt	Med-Coarse												
MF	294	BG	plg,bt	Med-Coarse												
MF	295	S	bt,sil	Med-Fine												
MF	296	S	bt,sil	Med-Fine												
MF	297	S	bt,sil	Med-Fine												
MF	298	BG	bt,plg	Med-Fine												
MF	299	BG	bt,plg	Med-Fine												
MF	300	BG	bt,plg	Med-Coarse												
MF	301	BG	bt,plg	Med-Coarse												
MF	302	BG	bt,plg	Med-Coarse	40	31										
MF	303	BG	bt,plg	Med-Coarse												
MF	304	BG	bt,plg	Med-Coarse												
MF	305	BG	bt,plg	Fine												
MF	306	BG	bt,plg	Fine												
MF	307	BG	bt,plg	Fine												
MF	308	BG	bt,plg	Fine	46	73										
MF	309	S	bt,sil	Med-Fine												
MF	310	S	bt,sil	Med-Fine												
MF	311	S	bt,sil	Med-Fine												
MF	312	S	bt,sil	Med-Fine	69	46	339	10							221	84
															137	65
MF	313	S	bt,sil	Med-Fine	54	34										
MF	314	S	bt,sil	Med-Fine												
MF	315	S	bt,sil	Med-Fine												
MF	316	S	bt,sil	Med-Fine												
MF	317	S	bt,sil	Med-Fine	123	28										
MF	318	BG	bt,plg	Med-Coarse												
MF	319	BG	bt,plg	Med-Coarse												
MF	320	BG	bt,plg	Med-Coarse												
MF	321	BG	bt,plg	Med-Coarse	63	30										
MF	322	BG	bt,plg	Med-Coarse												
MF	323	BG	bt,plg	Med-Coarse												
MF	324	BG	bt,plg	Med-Coarse	45	73										
MF	325	BG	bt,plg	Med-Coarse												
MF	326	S	bt,sil	Medium												
MF	327	BG	plg,bt	Med-Fine												
MF	328	BG	plg,bt	Med-Fine												
MF	329	BG	plg,bt	Med-Fine												
MF	330	BG	plg,bt	Medium	45	36										
MF	331	BG	plg,bt	Med-Coarse												
MF	332	BG	plg,bt	Med-Coarse												
MF	333	BG	plg,bt	Med-Fine												
MF	334	BG	plg,bt	Med-Fine												
MF	335	BG	plg,bt	Fine												
MF	336	BG	plg,bt	Coarse												
MF	337	BG	plg,bt	Coarse												
MF	338	BG	plg,bt	Coarse												

					Foliation		Lineation		Fold Axis		Axial Surface		IL Angle	Vergen	Joint	
Quad	Station	Lithology	Minerals	Grain Size	Strike	Dip	Trend	Plunge	Trend	Plunge	Strike	Dip			Strike	Dip
MF	339	BG	plg,bt	Coarse	45	76										
MF	340	BG	plg,bt	Fine												
MF	341	BG	plg,bt	Fine	49	39	211	13								
MF	342	BG	plg,bt	Med-Coarse												
MF	343	BG	plg,bt	Med-Coarse	49	79										
MF	344	BG	plg,bt	Med-Coarse	44	30										
MF	345	BG	plg,bt	Med-Coarse	41	81										
MF	346	BG	bt,plg	Med-Coarse	59	74										
MF	347	BG	bt,plg	Med-Coarse	42	71										
MF	348	BG	bt,plg	Med-Coarse	44	71										
MF	349	BG	bt,plg	Med-Coarse	42	69										
MF	350	BG	bt,plg	Med-Coarse	32	30										
MF	351	BG	bt,plg	Med-Coarse												
MF	352	BG	bt,plg	Med-Coarse	39	42										
MF	353	BG	bt,plg	Med-Coarse	35	64										
MF	354	BG	bt,plg	Med-Coarse	32	65										
MF	355	Amp	amp,plg	Med-Fine												
MF	356	BG	bt,plg	Med-Fine												
MF	357	BG	bt,plg	Fine	52	42										
MF	358	Amp	amp,plg	Fine												
MF	359	BG	bt,plg	Med-Fine												
MF	360	BG	bt,plg	Med-Fine												
MF	361	BG	bt,plg	Med-Fine												
MF	362	BG	bt,plg	Med-Fine												
MF	363	BG	bt,plg	Med-Fine												
MF	364	BG	bt,plg	Med-Fine												
MF	365	BG	bt,plg	Coarse												
MF	366	BG	bt,plg	Coarse												
MF	367	BG	bt,plg	Fine	46	56										
MF	368	BG	bt,plg	Fine												
MF	369	BG	bt,plg	Fine												
MF	370	BG	bt,plg	Fine												
MF	371	BG	bt,plg	Med-Coarse	88	39	178	21	78	12	88	86	80	NW		
MF	372	BG	bt,plg	Coarse	46	70										
MF	373	BG	bt,plg	Coarse	52	79										
MF	374	BG	bt,plg	Fine												
MF	375	BG	bt,plg	Med-Fine												
MF	376	BG	bt,plg	Med-Coarse	82	76										
MF	377	BG	bt,plg	Med-Coarse												
MF	378	BG	bt,plg	Coarse	52	35										
MF	379	BG	bt,plg	Coarse												
MF	380	BG	bt,plg	Fine												
MF	381	Amp	amp,plg	Fine												
MF	382	BG	bt,plg	Med-Fine	44	76										
MF	383	BG	bt,plg	Med-Fine	46	77										
MF	384	BG	bt,plg	Med-Fine	46	65										
MF	385	BG	bt,plg	Fine	3	70										
MF	387	DPg	plg,qtz	Med-Coarse												
MF	388	Dd		Fine												
MF	389	DPg														
MF	390	Si-C														
MF	391	QV														
MF	392	QV														
MF	393	QV			14	71										
MF	394	S	sil,ms	Fine	76	16										
MF	395	QV														
MF	396	QV			45	32										
MF	397	BG	qtz,bt	Medium	111	12										
MF	398	S	sil,ms	Med-Fine	111	23										
MF	399	BG	bt,qtz	Fine												
MF	400	QV														

					Foliation		Lineation		Fold Axis		Axial Surface		IL Angle	Vergen	Joint	
Quad	Station	Lithology	Minerals	Grain Size	Strike	Dip	Trend	Plunge	Trend	Plunge	Strike	Dip			Strike	Dip
MF	401	QV														
MF	402	BG	bt,plg	Med-Coarse	114	21			350	5	114	21	5	NW		
MF	403	GO	plg,qtz	Med-Coarse	98	23										
MF	404	BG	bt,plg	Med-Coarse	87	23										
MF	405	Amp														
MF	406	QV														
MF	407															
MF	408	Si-C		Fine												
MF	409	Si-C		Fine												
MF	410	Si-C		Fine												
MF	411	Si-C		Fine												
MF	412	Si-C		Fine												
MF	413	Si-C		Fine												
MF	414	QV														
MF	415	QV														
MF	416	QV														
MF	417	MCg	plg,kspr	Coarse												
MF	418	MCg	plg,kspr	Coarse												
MF	419	DPg	plg,qtz	Medium												
MF	420	MCg	plg,kspr	Coarse												
MF	421	MCg	plg,kspr	Coarse												
MF	422	BG	bt,plg	Medium												
MF	423	Si-C														
MF	424	Si-C														
MF	425	DPg														
MF	426	DPg														
MF	427	DPg														
MF	428	MCg														
MF	429	DPg														
MF	430	MCg														
MF	431	DPg														
MF	432	DPg														
MF	433	DPg														
MF	434	DPg														
MF	435	DPg														
MF	436	DPg														
MF	437	DPg														
MF	438	DPg														
MF	439	DPg														
MF	440	DPg														
MF	441	DPg														
MF	442	DPg														
MF	443	DPg														
MF	444	DPg														
MF	445	DPg														
MF	446	Si-C														
MF	447	Si-C														
MF	448	BG	bt,qtz	Med-Coarse	44	36	42	10	161	29	56	325	150	NE		
MF	449	S	sil,ms	Med-Fine	24	20										
MF	450	Gneiss	bt,qtz	Med-Fine	320	21										
MF	451	S	sil,ms	Med-Fine	18	17										
MF	452	S	sil,ms	Med-Fine	15	40										
MF	453	Amp														
MF	454	Amp			12	35										
MF	455	Gneiss	bt,plg	Medium	32	31										
MF	456	S	sil,ms	Med-Fine	18	34										
MF	457	S	sil,ms	Med-Fine	14	43										

VITA

Brittany Allison Davis was born June 10, 1983 in Knoxville, Tennessee to Philip D. Davis and Iris G. Tollett. Brittany was raised just outside of Lenoir City, TN, in the Valley and Ridge of Tennessee. She moved to Powell, Tennessee with her mother when she was 6 years old. Her father still lived in Lenoir City. Brittany visited her father every weekend, when they would take trips to the Clinch River to locate and collect native American artifacts. Brittany graduated the top 10% of her high school class at the age of 17, and went on to attend Pellissippi Community college where she earned a full 2-year scholarship in mechanical engineering. After taking a Geology 101 class, and becoming friends with the professor, and with some encouragement, she changed my major to Geology. After 2 ½ years attending Pellissippi, Brittany transferred to the University of Tennessee, Knoxville. While at UT she had many opportunities to participate in scientific debates with fellow students, and learn the many spectra of geology. She particularly took interest in her structural geology class with Dr. Caleb Holyoke. After attending UT for 2 ½ years Brittany graduated, and that following January she moved to Atlanta, GA to work for Terracon Consulting Firm, an environmental geology and engineering firm. After working for Terracon for nine months, Brittany was itching to get back in school. She decided to contact Bob Hatcher to pursue her love of structural geology. Brittany began working with Dr. Hatcher that following fall term, and went on to work in the southern Appalachian Inner Piedmont mapping a little over a quadrangle in central Georgia.

Plate 1: Geologic map of portions of the Farrar and Mansfield quadrangles, Jasper, Morgan, and Newton counties, Georgia

Geologic Map of portions of the 7.5-Minute Farrar and Mansfield Quadrangles, Georgia

Mapping by Brittany A. Davis, University of Tennessee-Knoxville

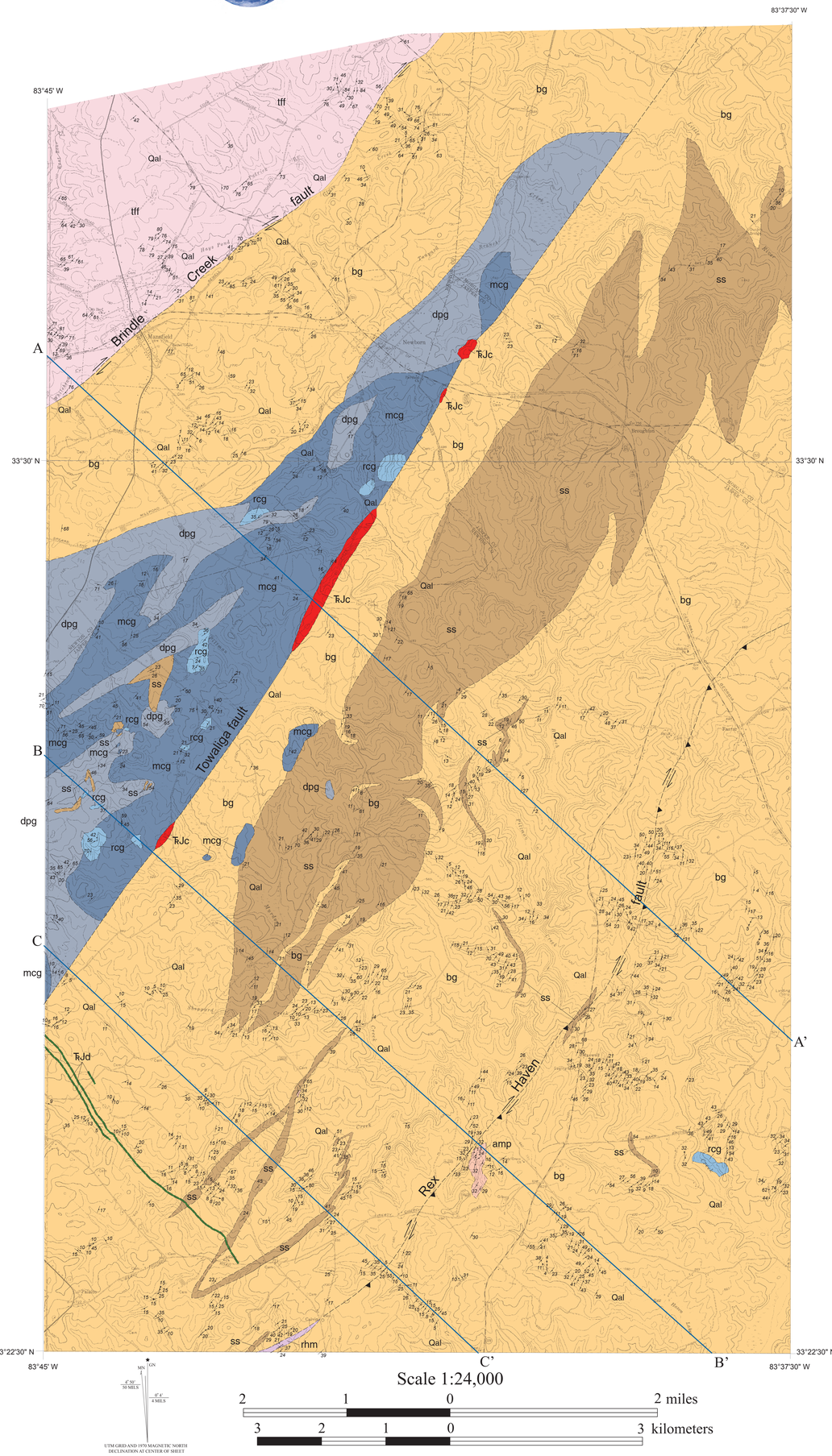

Detailed Geologic Map Explanation

Linear Structures—Origin at point of observation
(May be combined with planar structures)

- 27 — trend and plunge of tight to open mesoscopic fold
  - Antiform
  - Synform
- 7 — trend and plunge of mineral lineation
- 50 / 48 — linear structure combined with planar structure
  Intersection marks observation point
- 44 — inclined fold hinge

Planar Structures—Centered on point of observation (May be combined with linear structures)

- 48 — strike and dip of foliation
  Inclined
- 48 — strike and dip of schistosity
  Inclined
- fold axial surface

Contacts—Solid-observed. Long-dash-located within 15 m. Dotted-concealed.

Ductile fault—Solid-observed. Long dash-located within 15 m. Dotted-concealed. Arrows indicate movement direction along fault. Teeth located on upper plate

2009 - Field Review

Georgia State Survey
John Costello

Clemson University
Ralph Crawford

U.S.G.S.
Aruthur Merschat

University of Tenessee-Knoxville
Robert D. Hatcher, Jr.
Matthew Huebner

Rock Unit Descriptions

Quaternary

Qal Alluvium

Poorly sorted, unconsolidated alluvial and colluvial deposited sediment ranging from clay to silt to boulders.

Mesozoic rocks

TrJc Siliceous cataclasite

White to tan, brecciated, cohesive, predominantly quartz, strongly jointed, and fine- to medium-grained. Generally have several generations of jointing in outcrop. Multiple episodes of fracturing are apparent from crosscutting quartz-filled veins. Some sericitic alteration of feldspar is evident in thin section. Accessory minerals include feldspar, sericite, and opaques.

TrJd Diabase dikes

Fine-grained, dark gray on a fresh surface. Weathers to spheroidal orange-brown boulders. Composed predominantly of plagioclase and augite with characteristic ophitic texture, along with minor olivine.

Tugaloo terrane

tff Tallulah Falls Formation

Metagraywacke-biotite gneiss, light to dark gray, medium- to fine-grained, generally thick layered, strongly foliated, commonly porphyroblastic. Major mineralogy is quartz, alkali feldspars, plagioclase, biotite, and muscovite. Minor constituents are epidote, chlorite, zircon, and opaque minerals. Porphyroclasts are plagioclase and microcline. Layer thickness varies from a few millimeters to several meters. Foliation is defined by quartzofeld-spathic material and micas in the metagraywacke, locally interlayered with abundant amphibolite. Probably derived from a feldspathic sandstone.

Cat Square terrane (?)

Metasedimentary Rocks

bg Biotite gneiss/metagraywacke

Gray to dark gray, thin- to thick-layered, fine- to coarse-grained, biotite- quartz-feldspar gneiss, in part garnetiferous. Mineral assemblage includes: quartz, plagioclase, microcline, biotite, muscovite, garnet, opaques, and apatite. Accessory minerals include epidote and zircon. Locally inequigranular and porphyroblastic. Migmatization increases in proximity of the BCF and localized shear zones, with frequent local quartzo-feldspathic leucosomes. Contains interlayers and boudins of fine-grained calc-silicate. Gradational into and interlayered with sillimanite-mica schist.

ss Sillimanite-mica schist

Thin- to thick-layered sillimanite-mica schist, variably garnetiferous, locally pyritic. Blocky muscovite commonly occurs as pseudomorphs after sillimanite, and sericitic alteration is abundant. Weathers to a light brown to reddish brown or silvery blue-gray saprolite.

rhm Rex Haven mylonite

Wide variations in lithologies exist for the Rex Haven mylonite including a reduced mylonitic biotite gneiss with porphyroclasts of K-feldspar and plagioclase. Mineral assemblage include quartz, plagioclase, microcline, biotite, garnet, muscovite, and accessory minerals of: epidote and zircon. It also consists of an ultramylonitic sillimanite schist. Mineral assemblage includes quartz, plagioclase, garnet, and sillimanite.

Igneous Rocks

amp Amphibolite

Dark-gray, fine- to medium-grained, predominantly composed of hornblende, plagioclase, with smaller amounts of garnet,diopside, epidote, and quartz. Amphibolite is generally present as boudins within the metasedimentary units.

rcg Rocky Creek granodiorite

Fine-grained equigranular granitoid, light gray, non- to weakly foliated. Outcrops appear as small to large boulders exhibiting exfoliation surfaces. Composed of alkali feldspars, quartz, plagioclase, biotite. Accessory minerals include epidote-clinozoisite, sphene, apatite, and zircon.

dpg Dows Pulpit granodiorite

Light gray, medium- to coarse-grained, equigranular, granoblastic, weakly- to nonfoliated. Major minerals include plagioclase, quartz, microcline, biotite, and muscovite. Accessory minerals include garnet, apatite, sphene, zircon, and opaque minerals. Weathers to white and tan saprolite, and contains xenoliths of biotite gneiss.

mcg Murder Creek granite

Bitoite-rich, megacrystic, light to dark-gray, weakly to strongly foliated. Megacrysts consist of microcline and plagioclase, microcline often contains myrmekitic rims. Matrix is composed of fine- to medium-grained quartz, plagioclase, microcline, biotite, and muscovite. Accessory minerals include garnet, zircon, apatite, epidote, and opaques.

Age
Relative

Cross Sections

Plate 2: Geologic map of portions of the Berner, Indian Springs, Farrar, Covington, Mansfield, Worthville, Stewart, Lloyd Shoals, and Jackson quadrangles, Newton, Morgan, Georgia.

Brittany A. Davis, Matthew T. Huebner, Robert D. Hatcher, Jr., and Robert J. Hooper

Department of Earth and Planetary Sciences and Science Alliance Center of Excellence, University of Tennessee-Knoxville

Aeromagnetic Map - Grayscale

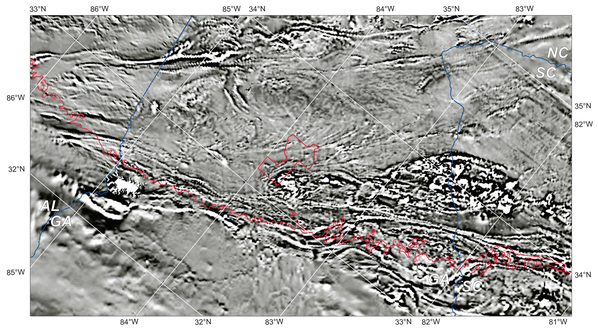

Grayscale aeromagnetic map with the area of interest highlighted in red. Note the prominent lineament that extends through the northwestern portion of the field area, and the curved anomalies that are truncated against said lineament.

Aeromagnetic Map - Terrane Overlay

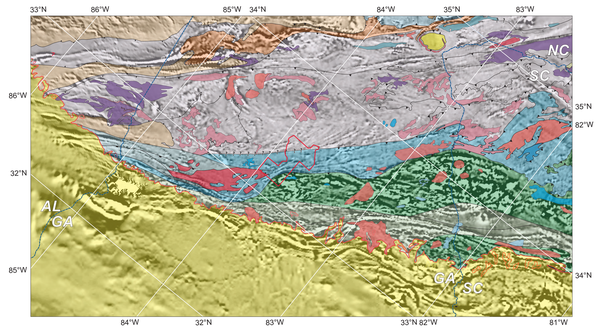

Grayscale aeromagnetic map with current tectonic map overlay. The prominent lineament that extends through the northwestern portion of the field area is the extension of the Brindle Creek fault, and the curved anomalies may be representative of channel flow in the Inner Piedmont. The lineament in the southeastern portion of the Farrar quadrangle is the Rex Haven fault. The gabbroic body in the southeastern portion of the field area defines the central Piedmont suture.

Explanation of Map Symbols

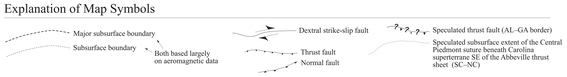

Rock Unit Descriptions

Quaternary

Qal Alluvium

Poorly sorted, unconsolidated alluvial and colluvial deposited sediment ranging from clay to silt to boulders.

Mesozoic rocks

MJc Siliceous cataclasite

White to tan, brecciated, cohesive, predominantly quartz, strongly jointed, and fine- to medium-grained. Generally have several generations of jointing in outcrop. Multiple episodes of fracturing are apparent from crosscutting quartz-filled veins. Some sericitic alteration of feldspar is evident in thin section. Accessory minerals include feldspar, sericite, and opaques.

MJd Diabase dikes

Fine-grained, dark gray on a fresh surface. Weathers to spheroidal orange-brown boulders. Composed predominantly of plagioclase and augite with characteristic ophitic texture, along with minor olivine.

Pine Mountain Window

Ywo Woodland Gneiss

Felsic augen gneiss with augen of microcline (up to 10 cm). The matrix is composed primarily of microcline, plagioclase, quartz, and biotite. Minor amounts of charnokite are present. Varies from a strongly foliated augen gneiss with definable S-C fabric to a weakly foliated coarse-grained megacrystic gneiss with megacrysts up to 10 cm.

Tugaloo terrane

Igneous Rocks

rpg Rocky Plains granitoid

Fine-grained equigranular granitoid, light gray, non to weakly foliated, generally fine-grained granite. Outcrops appear as small to large boulders exhibiting exfoliation surfaces. Composed of alkali feldspar, quartz, plagioclase, biotite. Similar to Rocky Creek in appearance.

ccg Cedar Rock granodiorite

Coarse-grained, strongly foliated granite to granodiorite. Mineralogy is predominantly quartz, biotite, alkali feldspars and plagioclase, along with minor garnet. Occurs as large pavement outcrops.

Metasedimentary Rocks

gt Gondite

Medium- to fine- grained foliated rock predominantly composed of quartz and garnet, often exhibiting a dark purple iridescent sheen as a result of the high manganese content. Occurs as a <1 m thick layer.

ttf Tallulah Falls Formation

Metagraywacke-biotite gneiss, light to dark gray, medium- to fine-grained, generally thick layered, strongly foliated, commonly porphyroblastic. Major mineralogy is quartz, alkali feldspars, plagioclase, biotite, and muscovite. Minor constituents are epidote, chlorite, zircon, and opaque minerals. Porphyroclasts are plagioclase and microcline. Layer thickness varies from a few millimeters to several meters. Foliation is defined by quartzofeld-spathic material and micas in the metagraywacke, locally interlayered with abundant amphibolite. Probably derived from a feldspathic sandstone.

Cat Square terrane (?)

Metasedimentary Rocks

bg Biotite gneiss/metagraywacke

Gray to dark gray, thin- to thick-layered, fine- to coarse-grained, biotite- quartz-feldspar gneiss, in part garnetiferous. Mineral assemblage includes: quartz, plagioclase, microcline, biotite, muscovite, garnet, opaques, and apatite. Accessory minerals include epidote and zircon. Locally inequigranular and porphyroblastic. Migmatization increases in proximity of the BCF and localized shear zones, with frequent local quartzo-feldspathic leucosomes. Contains interlayers and boudins of fine-grained calc-silicate. Gradational into and interlayered with sillimanite-mica schist.

ss Sillimanite-mica schist

Thin- to thick-layered sillimanite-mica schist, variably garnetiferous, locally pyritic. Blocky muscovite commonly occurs as pseudomorphs after sillimanite, and sericitic alteration is abundant. Weathers to a light brown to reddish brown or silvery blue-gray saprolite.

tm Towaliga mylonite

Wide variations in lithologies exist for the Towaliga mylonite including a mylonitic augen gneiss that contains a biotite-rich matrix, and grades into finer-grained mylonite; and phyllonite consisting of muscovite, biotite, garnet, chlorite, and quartz. The Towaliga mylonite occasionally displays a well-developed S-C fabric and mineral lineation.

rhm Rex Haven mylonite

Wide variations in lithologies exist for the Rex Haven mylonite including a reduced mylonitic biotite gneiss with porphyroclasts of K-feldspar and plagioclase. Mineral assemblage include quartz, plagioclase, microcline, biotite, garnet, muscovite, and accessory minerals of: epidote and zircon. It also consists of an ultramylonitic sillimanite schist. Mineral assemblage includes quartz, plagioclase, garnet, and sillimanite.

Igneous Rocks

ncg Rocky Creek granodiorite

Fine-grained equigranular granitoid, light gray, non- to weakly foliated. Outcrops appear as small to large boulders exhibiting exfoliation surfaces. Composed of alkali feldspars, quartz, plagioclase, biotite. Accessory minerals include epidote-clinozoisite, sphene, apatite, and zircon.

dpg Dows Pulpit granodiorite

Light gray, medium- to coarse-grained, equigranular, granoblastic, weakly- to nonfoliated. Major minerals include plagioclase, quartz, microcline, biotite, and muscovite. Accessory minerals include garnet, apatite, sphene, zircon, and opaque minerals. Weathers to white and tan saprolite, and contains xenoliths of biotite gneiss.

mcg Murder Creek granite

Biteite-rich, meagcrystic, light to dark-gray, weakly to strongly foliated. Megacrysts consist of microcline and plagioclase, microcline often contains myrmekitic rims. Matrix is composed of fine- to medium-grained quartz, plagioclase, microcline, biotite, and muscovite. Accessory minerals include garnet, zircon, apatite, epidote, and opaques.

amp Amphibolite

Dark-gray, fine- to medium-grained, predominantly composed of hornblende, plagioclase, with smaller amounts of garnet,diopside, epidote, and quartz. Amphibolite is generally present as boudins within the metasedimentary units.

Age

Relative

bg Layered biotite gneiss (metavolcanic?)

Layered medium-coarse inequigranular to fine-grained feldspathic biotite gneiss, interlayered with a thinly layered fine-grained sulfidic tonalite. Inequigranular biotite gneiss contains ~1 cm alkali feldspar megacrysts.

Carolina Superterrane

Layered Gneiss Series

lfgn Layered felsic gneisses

Layered quartz, two-feldspar, two-mica gneiss, locally garnetiferous, and locally schistose when the mica content becomes sufficiently high. Subordinate volumes of mafic and intermediate gneiss occur as layers and boudins throughout the unit. Small plutons (plugs?) of granitic to granodioritic composition locally form pavement outcrops.

lign Layered intermediate gneisses

Layered biotite-rich and/or hornblende-rich gneiss. Equal proportions of felsic gneiss are locally interlayered with the intermediate gneiss. Subordinate volumes of mafic gneiss are interlayered throughout the unit.

lmgn Layered mafic gneisses

Amphibolite and amphibole gneiss with localized epidote-rich zones. Subordinate volumes of felsic and biotite gneiss are interlayered throughout the unit. Layering is defined predominantly by varying proportions of mafic phases between layers, though locally enhanced by grain-size variation.

aag Amygdaloidal amphibole gneiss

Medium-grained amphibole gneiss that contains ellipsoidal packets of quartz interpreted to be strained amygdules.

Metaplutonic Series

mgd Metagabbroic-dioritic rocks

Olivine gabbro to a less leucodioritic. Individual intrusions are structurally of various ages; plutons contain strong foliations as well as plutons that are essentially free of deformation with well-defined contact aureoles.

mum Metaultramafic rocks

Metapyroxenite and chlorite/chlorite-actinolite schist. Occur either as boudins or thin layers within the layered mafic gneisses or are associated with mafic plutonic rocks.

gg Gladesville gabbro

Composite pluton composed of two distinct intrusions. Rocks range in composition from medium-grained, olivine-bearing, two-pyroxnc gabbro, to coarse-grained, non-olivine bearing, two-pyroxene gabbro, to fine-grained, granular, two-pyroxene gabbro.

Tectonic Map Explanation

Terranes

Dahlonega gold belt
Neoproterozoic/Cambrian–Middle Ordovician clastic deposition & MORB/arc volcanism, minor 1.15 Ga(?) basement. Sedimentary component >>> volcanic. Contains detrital zircons of possible Gondwanan or Penokean affinity.

Cowrock terrane
Neoproterozoic/Cambrian clastic deposition, ophiolite, & volcanism, minor 1.15 Ga(?) basement. Sedimentary component >>> volcanic. Middle Ordovician tonalite pluton.

Cartoogechaye terrane
Neoproterozoic/Cambrian(?) clastic deposition, ophiolite (mafic-ultramafic complexes), & MORB/arc volcanism, minor 1.15 Ga basement. Sedimentary component >volcanic.

Cat Square terrane
Mixed Laurentian & Avalonian affinity,
post-430 Ma deposition, arc-to-MORB volcanics.

Tugaloo terrane
Distal Laurentian; Neoproterozoic/Cambrian–Middle Ordovician deposition & volcanism, minor 1.15 Ga basement; arc-to-MORB volcanics; mélanges. Abundant Ordovician plutons. Sedimentary component >> volcanic.

Carolina superterrane (peri–Gondwanan)

Carolina terrane
Supracrustal (low grade) components
Neoproterozoic deposition and arc volcanism
to Ordovician (?) deposition.

Charlotte terrane
Infracrustal (high grade) components
Neoproterozoic deposition and arc volcanism.

Igneous Rocks

325–285 Ma granitoid plutons (Modern age dates)
350–325 Ma granitoid plutons (Modern age dates)
380–355 Ma granitoid plutons (Modern age dates)
410–80 Ma plutons
Likely Ordovician plutons (no age dates)
Ordovician plutons (Modern age dates)

Platform Rocks

Cambrian–Ordovician clastic to carbonate

Rifted Margin Rocks

Neoproterozoic–Early Cambrian clastic & volcanic rocks. Includes Baltimore terrane.

Quartzite of unknown affinity in windows in Cartoogechaye terrane, Tugaloo terrane, and Sauratown Mountains window.

Pine Mountain Window Rocks

Metamorphosed Paleozoic platform(?) cover
1.0–1.1 GA basement rocks

Mapping Responsibilities

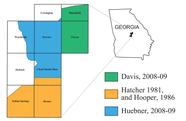

Detailed Geologic Map Explanation

Linear Structures—Origin at point of observation (May be combined with planar structures)

- 27 Antiform / 27 Synform — trend and plunge of tight to open mesoscopic fold
- 7 — trend and plunge of mineral lineation
- 50 / 48 — linear structure combined with planar structure
- Intersection marks observation point
- 44 — inclined fold hinge

Planar Structures—Centered on point of observation (May be combined with linear structures)

- 45 — strike and dip of foliation: Inclined
- 48 — strike and dip of schistosity: Inclined
- fold axial surface

Contacts—Solid-observed. Long-dash-located within 15 m. Dotted-concealed.

Ductile fault—Solid-observed. Long dash-located within 15 m. Dotted-concealed. Arrows indicate movement direction along fault. Teeth located on upper plate

Cross Sections

Structural Domains

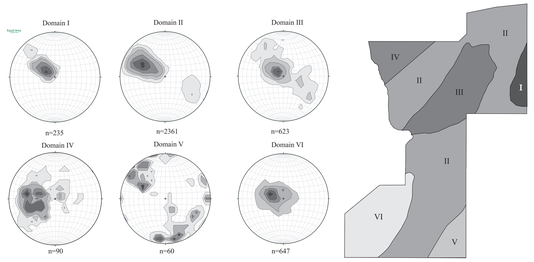

Brindle Creek fault



Mylonitic Murder Creek granite with porphyroclasts displaying a dextral shear sense, consistent with the Brindle Creek fault. Porphyroclasts are K-feldspar and plagioclase.



Sheared biotite gneiss / metagraywacke displaying porphyroclasts and a well-developed S-C fabric indicating dextral shear sense.



Sheared biotite gneiss / metagraywacke displaying feldspar porphyroclasts and S-C fabric indicating dextral shear sense.

Towaliga fault



Sheared biotite gneiss / metagraywacke displaying a dextral shear sense.



Brittle reactivation of the Towaliga fault. Siliceous cataclasite displaying multiple sets of joints.

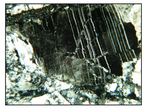

The Towaliga fault transitions from a garnet-grade fault to a brittly reactivated fault along its northeastern extent. It tends to form step overs in its displacement, represented by rhombs of siliceous cataclasite.

Photomicrograph of microfractures offsetting twins in a plagioclase crystal.

Rex Haven fault



Mylonitic hornblende gneiss from the Rex Haven Mylonite with feldspar porphyroclasts and a well-developed S-C fabric indicating a dextral shear sense.



Plagioclase-quartz-microcline-biotite-garnet mylonite, of the Rex Haven fault. The Rex Haven fault generally displays a well-developed S-C fabric and well-defined shear sense from tailed porphyroclasts.



Tailed feldspar porphyroclast with a dextral shear sense.

References

Hooper, R. J., 1986, Geologic Studies at the East end of the Pine Mountain window and adjacent Piedmont, Central Georgia. [Ph D. disseration]: University of South Carolina, 74 p.

Davis, B. A., Huebner, M. T., and Hatcher, R. D. Jr., 2009, Detailed geologic mapping and structural analysis of a portion of the Central Georgia Inner Piedmont, and a possible fault identified with aeromagnetic data: Geological Society of America Abstracts with Programs, v. 41, No. 3, p. 29.

D. L. Daniels, unpub aeromagnetic data.

Acknowledgements

U. S. Geological Survey National Cooperative Geologic Mapping Program
EDMAP Component
Tectonics and Structural Geology Group, UTK
University of Tennessee - Science Alliance Center of Excellence
University of Tennessee - Department of Earth and Planetary Sciences
A special thanks to Iris Tollett, Phillip Davis, and Chuck Beckmann for field assistance, and Andrew Wunderlich for cartographic and GIS assistance.